THE ANATOMICAL AND MOLECULAR CHARACTERISATION OF VASCULAR INGRESSION IN THE EMBRYONIC VERTEBRATE BRAIN

UNIVERSITY of PORTSMOUTH

The thesis is submitted in partial fulfilment of the requirements
for the award of the degree of Doctor of Philosophy of the
University of Portsmouth

Amanda Rose Corla

School of Biological Sciences

May 2017

SUMMARY

The vascularisation of the embryonic brain is a dynamic process governed by an intricate network of regulatory pathways. The process of vascularisation has been studied in the spinal cord of avian embryos but very little work has been conducted in the rostral brain. The present study therefore aimed to characterise the major events involved in the vascularisation of the *Gallus gallus* brain, with supporting work conducted in *Xenopus laevis*. Endothelial cells migrated from the mesoderm towards the brain, leading to the formation of the perineural vascular plexus. Endothelial sprouts invaded the brain, which then branched and fused to form the intraneural vascular plexus. Cell replication was also detected throughout the process. A similar sequence of events have previously been described in quail and mouse, providing support for an evolutionarily conserved process throughout vertebrate evolution.

Matrix metalloproteinases play a major role in remodelling the extracellular matrix, which is an essential aspect in angiogenesis. MMPs -1, -2 and -9 were expressed within the perineural vascular plexus, differentially within the invading sprouts and also in the intraneural vascular plexus. Gelatinase activity was also detected in specific cells within the perineural vascular plexus and in the invading sprouts. Altering the level of MMP activity lead to the formation of endothelial cell clusters, which may have resulted from defective proliferation and migration. The results provide a novel contribution to the role of MMPs in brain vascularisation.

The brain plays an important role in organising its vasculature, therefore the influence of neural tube patterning on ingression was investigated. The ectopic expression of the ventralising signal, sonic hedgehog, expanded the perineural vascular plexus and disrupted sprout formation. Lowering Notch activity lead to a significant increase in the number of endothelial cells within the brain. Endothelial cell clusters were formed, suggesting that Notch may also play a role in maintaining the structural integrity of vessel sprouts. The arrangement of the sprout, with a leading tip cell and follower stalk cells, is reminiscent of invasion by certain cancers. The process of endothelial ingression may therefore share similarities with tumour angiogenesis and could aid in developing novel strategies for reducing tumourigenesis and for stroke recovery.

ACKNOWLEDGEMENTS

I would first like to express my deepest gratitude to the Anatomical Society for funding my PhD and providing me with the freedom to seize the opportunities that in abundance have been a blessing over the last few years. My sincere thanks go to my supervisor, Dr. Frank Schubert, for your continued support and guidance throughout my research. Your relaxed nature consistently worked to plant my feet on terra firma, especially when long days and nights saw me drifting in a world where time tends to elude the analytical mind. You welcomed my enigmatic tendencies to go against the tides and accepted my nature as a purist. The experience in your lab soon grew into a fruitful journey like no other and for that, I will always be grateful.

The completion of this work could not have been done without the help and expertise of the EXRC, particularly Mr. Alan Jafkins, Dr. Anna Noble and Dr. Liliya Nazlamova. To Prof. Matt Guille, with whom we embraced the call of the sea, a special thanks for your bountiful knowledge and encouragement that you have provided me from the very start. With great pleasure, I would also like to express my thanks to Dr. Andy Pickford, Dr. Colin Sharpe, Dr. Alan Thorne, Prof. Helen Fillmore and Dr. Susanne Dietrich for showing confidence in my research. Your feedback and unexpected generosity is truly inspiring and it has been a privilege to work with you and in most cases, more elusively, among you.

The assistance and cooperation from my fellow colleagues, friends and students have been essential for motivating and shaping my research over the years. My gratitude goes to Rob for his help with MMP-1 purification, Emily for beginning the roller culture experiments, Natalie for working with me on ISZ, Hamish for his preliminary investigation in *Xenopus* and to Matt as he continues to work on this ongoing project. To Anaïs, Charlotte and Luis, we will always have Paris, and to Bing Bing for bringing us closer together.

Endless thanks go to Jason for always being there whenever I needed you and for your unwavering resilience to my creative theatrical entertainment. Finally, I am forever thankful for the loving support of my parents and my brother - your patience has been a virtue.

DISSEMINATION

Oct 2013:	Genes and Development meeting University of Portsmouth, oral presentation
Jun 2014:	TC2N Final Meeting Gent, Belgium, poster presentation (P-19)
Jul 2014:	1st Year Postgraduate Research Degree Poster Day University of Portsmouth, poster presentation
Jul 2014:	Anatomical Society Summer Meeting University of Bradford, poster presentation (A19)
Nov 2014:	18th International Conference of the ISD & BSDB The Guoman Tower Hotel, London, poster presentation (P37)
Dec 2014:	Anatomical Society Winter Meeting University of Birmingham, poster presentation (B35)
Apr 2015:	BSCB-BCDB Joint Spring Meeting University of Warwick, poster presentation (P63)
May 2015:	Institute of Biomedical and Biomolecular Science Research Day University of Portsmouth, poster presentation
	Young Researchers in Life Science Institut Curie, Paris, France, poster presentation (P32)
Dec 2015:	Anatomical Society Winter Meeting Magdalene College, Cambridge, oral presentation
Jun 2016:	Institute of Biomedical and Biomolecular Science Research Day University of Portsmouth, oral presentation (S20)

CONTENTS

			Page
LIST OF FIGURES			9
LIST OF ABBREVIATIONS			14
1.	INTRODUCTION		15
	1.1	*Gallus gallus* embryos as a model organism for developmental biology	15
	1.2	The avian and mouse neural tube and the retina as models for CNS vascularisation	18
	1.3	CNS angiogenesis is regulated by neural-tube derived signals	23
	1.4	The recruitment of angioblasts and endothelial cells	28
	1.5	Endothelial sprouting	30
	1.6	The influence of neural tube patterning on the developing vascular network	36
	1.7	The regulation of angiogenesis by ETS and MADS box transcription factors	46
	1.8	The role of MMPs in angiogenesis	48
		1.8.1 MMP-1	51
		1.8.2 MMP-2 and MMP-9	56
		1.8.3 MT-MMPs	61
	1.9	Research aims and strategy	64
2.	MATERIALS AND METHODS		68
	2.1	Ethical statement	68
	2.2	Ets1, MMP and VEGFR PCR amplification	68
	2.3	Gateway cloning reactions for Ets1, MMPs and VEGFRs	72
	2.4	Bacterial transformation and minipreps	72
	2.5	Template DNA synthesis	72
	2.6	Antisense RNA probe synthesis for ISH	73

2.7	Incubation and preparation of *G. gallus* embryos for ISH and IHC	73
2.8	Whole-mount ISH protocol	74
2.9	Whole-mount IHC - DAB staining and fluorescence	75
2.10	Gelatin embedding and vibratome sectioning of *G. gallus* embryos	77
2.11	LHC on *X. laevis* sections	77
2.12	Bead experiments with MMP inhibitors, active MMP-1 and Notch inhibitor, followed by IHC	78
2.13	Roller culture experiments	81
2.14	Whole-mount ISZ with DQ gelatin, followed by IHC	81
2.15	VEGFA RT-PCR	83
2.16	Electroporation of Shh into the *G. gallus* mesencephalon, followed by IHC	84
2.17	Microscope analyses	86

3.	ANATOMICAL CHARACTERISATION OF VASCULAR INGRESSION INTO THE EMBRYONIC VERTEBRATE BRAIN	87
3.1	Brain vascularisation involves endothelial cell migration, PNVP formation, sprouting and INVP formation	87
3.2	Fibronectin expression occurs in close proximity to invading endothelial cells	94
3.3	The detection of Mef2c and CD34 can also be used to identify the location of endothelial cells during brain vascularisation	96
3.4	Endothelial cell migration and PNVP formation occur earlier in the brain than in the spinal cord	104
3.5	Endothelial cells proliferate throughout the process of vascularisation	106
3.6	The process of brain vascularisation is evolutionarily conserved throughout vertebrate evolution	109
3.7	Vascular ingression proceeds in correlation with the pattern of neurogenesis in the early brain	112

4. THE INFLUENCE OF MMP ACTIVITY ON ENDOTHELIAL CELL INGRESSION 115

4.1 MMPs are expressed in the PNVP and the nascent INVP, with differential expression identified within the invading sprouts 116

4.2 Gelatinase activity is present in specific cells in the PNVP and within the invading sprouts 126

4.3 Altering MMP activity leads to changes in endothelial cell ingression 130

4.4 Altering MMP activity leads to the formation of endothelial cell clusters 142

4.5 Lowering MMP-2 activity leads to reduced breakdown of fibronectin and α6 integrin 144

5. THE INFLUENCE OF NEURAL TUBE PATTERNING ON BRAIN VASCULARISATION 150

5.1 The identification of VEGFA isoforms and VEGFR expression during the vascularisation of the embryonic *G. gallus* brain 150

5.2 Ectopic expression of Shh leads to PNVP expansion, disrupted sprout formation and ectopic endothelial ingression 162

5.3 Notch activity affects endothelial cell ingression and may play a role in maintaining endothelial sprout integrity after ingression 169

REFERENCES 175

APPENDICES 230

DECLARATION

Whilst registered as a candidate for the above degree, I have not been registered for any other research award. The results and conclusions embodied in this thesis are the work of the named candidate and have not been submitted for any other academic award.

LIST OF FIGURES AND TABLES

1.	**Introduction**	
Fig. 1i	Comparison of brain development in early human and chick embryos	17
Fig. 1ii	Vascularisation of the avian neural tube	20
Fig. 1iii	VEGFs and VEGFRs	25
Fig. 1iv	VEGFA isoforms in human	27
Fig. 1v	Vessel sprouting into the embryonic *G. gallus* brain	32
Fig. 1vi	Schematic of tip and stalk cell selection and endothelial sprouting into the neural tube	33
Table 1i	Classification of MMPs	50
Fig. 1vii	Crystal structure of inactive proMMP-1	53
Fig. 1viii	Gene regulation at the initiation of angiogenesis	66
Fig. 1ix	The selection of tip and stalk cells during sprouting angiogenesis	67
2.	**Materials and Methods**	
Fig. 2i	MMP primer design and PCR-amplified sequences for ISH experiments	71
Table 2i	Primary and secondary antibodies	76
Fig. 2ii	Bead placement for bead implantation studies and method for cell counting	80
Fig. 2iii.	MC method for roller culture experiments	82
Fig. 2iv	Schematic of electroporation experiments	85
3.	**Anatomical characterisation of vascular ingression into the embryonic vertebrate brain**	
Fig. 3i	Planes of sectioning following whole-mount ISH and IHC	89
Fig. 3ii	Endothelial cell migration and PNVP formation	90
Fig 3iii	Vascularisation of the *G. gallus* mesencephalon and rhombencephalon using ISH with an Ets1 antisense probe and IHC with a TuJ1 antibody	91

Fig. 3iv	Vascularisation of the *G. gallus* prosencephalon and mesencephalon using ISH with an Ets1 antisense probe and IHC with a TuJ1 antibody	92
Fig. 3v	The arrangement of tip and stalk cells within endothelial sprouts	93
Fig. 3vi.	Time-course analysis of fibronectin production within the midbrain of stage HH19-26 *G. gallus* embryos	95
Fig. 3vii	Vascularisation of the *G. gallus* prosencephalon and mesencephalon using ISH with a Mef2c antisense probe	97
Fig. 3viii	Vascularisation of the *G. gallus* mesencephalon and rhombencephalon using ISH with a Mef2c antisense probe	98
Fig. 3ix	Ets1 and Mef2c expression in the PNVP of the mesencephalon	99
Fig. 3x	Summary of events involved in the vascularisation of the *G. gallus* brain	100
Fig. 3xi	Schematic summary showing the progression of vascularisation of the embryonic *G. gallus* brain	101
Fig. 3xii	The detection of endothelial cells using ISH and IHC methods	103
Fig. 3xiii	Comparison of spinal cord and brain vascularisation events in the avian embryo	105
Fig. 3xiv	Investigating cell replication during brain vascularisation	108
Fig. 3xv	Vascularisation of the *X. laevis* midbrain using LHC on sections	111
Fig. 3xvi	Vascularisation of the brain progresses in a similar pattern to neurogenesis in the *G. gallus* embryo	114
4.	**The influence of MMP activity on endothelial cell ingression**	
Fig. 4i	MMP expression in the ventral half of the mesencephalon of stage HH19 *G. gallus* embryos	118
Fig. 4ii	MMP expression in the dorsal half of the mesencephalon of stage HH19 *G. gallus* embryos	119
Fig. 4iii	MMP expression in the prosencephalon of stage HH21 *G. gallus* embryos	120
Fig. 4iv	MMP expression in the ventral half of the mesencephalon of stage HH21 *G. gallus* embryos	121
Fig. 4v	MMP expression in the dorsal half of the mesencephalon of stage HH21 *G. gallus* embryos	122

Fig. 4vi	MMP expression in the ventral half of the mesencephalon of stage HH24 *G. gallus* embryos	123
Fig. 4vii	MMP expression in the dorsal half of the mesencephalon of stage HH24 *G. gallus* embryos	124
Fig. 4viii	MMP expression within endothelial sprouts	125
Fig. 4ix	Whole-mount ISZ in the prosencephalon of stage HH26 embryos	128
Fig. 4x	Whole-mount ISZ in the mesencephalon of stage HH26 embryos	129
Fig. 4xi	Signalling pathways involved in angiogenesis affected by altering MMP levels	131
Fig. 4xii	Sections through the mesencephalon of embryos following the implantation of beads containing MMP inhibitors in DMSO	134
Fig. 4xiii	Sections through the mesencephalon of embryos following the implantation of beads containing MMP inhibitors in PBS	135
Fig. 4xiv	Sections through the mesencephalon of embryos following the implantation of beads containing active MMP-1 in Tris-HCl	138
Fig. 4xv	The effect of 1uM active MMP-1 on endothelial cell ingression	140
Fig. 4xvi	Preliminary investigation into the effect of MMP-2 inhibitor, ARP 100, on components of the ECM	146
Fig. 4xvii	Roller culture experiments with ARP 100 followed by neural crest cell detection using IHC with an anti-HNK-1 antibody	147
5.	**The influence of neural tube patterning on brain vascularisation**	
Fig. 5i	Nested primers used in RT-PCR for the identification of VEGFA isoforms in *G. gallus* embryos at stages HH11-28 of development	152
Fig. 5ii	VEGFA isoforms present in *G. gallus* embryos identified by RT-PCR.	153
Fig. 5iii	VEGFR1 expression in the mesencephalon of stage HH19-22 *G. gallus* embryos	156
Fig. 5iv	VEGFR1 expression in the mesencephalon of stage HH24-28 *G. gallus* embryos	157
Fig. 5v	VEGFR2 expression in the mesencephalon of stage HH19-22 *G. gallus* embryos	158

Fig. 5vi	VEGFR2 expression in the mesencephalon of stage HH24-28 *G. gallus* embryos	159
Fig. 5vii	VEGFR3 expression in the mesencephalon of stage HH19-22 *G. gallus* embryos	160
Fig. 5viii	VEGFR3 expression in the mesencephalon of stage HH24-28 *G. gallus* embryos	161
Fig. 5ix	*G. gallus* embryos following the electroporation of an expression construct for Shh into the mesencephalon	164
Fig. 5x	Sections taken from the mesencephalon of stage HH28 embryos following electroporation of a Shh expression construct compared with the GFP control	165
Fig. 5xi	Abnormal development of the mesencephalon following ectopic expression of Shh	166
Fig. 5xii	Endothelial cell detection using fluorescent IHC following the co-electroporation of Shh and GFP expression constructs into the mesencephalon	167
Fig. 5xiii	Endothelial cell detection using fluorescent IHC in the mesencephalon of control embryos	168
Fig. 5xiv	Sections through the mesencephalon of *G. gallus* embryos following the implantation of beads containing DAPT	171
Fig. 5xv	The effect of 10mM DAPT in DMSO on endothelial cell ingression	172

Appendices

Appendix A	Endothelial cell counts from bead implantation experiments with MMP inhibitors and active MMP-1	230
Appendix B	Paired t-test and histogram for DMSO control bead experiments	233
Appendix C	Paired t-test and histogram for bead experiments with 8mM ARP 100 in DMSO	234
Appendix D	Paired t-test and histogram for bead experiments with 8mM SB-3CT in DMSO	235
Appendix E	Paired t-test and histogram for bead experiments with 1mM Batimastat in DMSO	236

Appendix F	Paired t-test and histogram for PBS control bead experiments	237
Appendix G	Paired t-test and histogram for bead experiments with 8mM ARP 100 in PBS	238
Appendix H	Paired t-test and histogram for bead experiments with 1mM ARP 100 in PBS	239
Appendix I	Paired t-test and histogram for bead experiments with 8mM SB-3CT in PBS	240
Appendix J	Paired t-test and histogram for bead experiments with 1mM SB-3CT in PBS	241
Appendix K	Paired t-test and histogram for 100mM Tris-HCl pH7.5 control bead experiments	242
Appendix L	Paired t-test and histogram for bead experiments with 25nM active MMP-1 in Tris-HCl	243
Appendix M	Paired t-test and histogram for bead experiments with 250nM active MMP-1 in Tris-HCl.	244
Appendix N	Paired t-test and histogram for bead experiments with 1μM active MMP-1 in Tris-HCl	245
Appendix O	Endothelial cell counts from bead implantation experiments with DAPT	246
Appendix P	Paired t-test and histogram for DMSO control bead experiments	247
Appendix Q	Paired t-test and histogram for PBS control bead experiments	248
Appendix R	Paired t-test and histogram for bead experiments with 10mM DAPT in DMSO	249
Appendix S	Paired t-test and histogram for bead experiments with 10mM DAPT in PBS	250

LIST OF ABBREVIATIONS

ADAMs	A disintegrin and metalloprotease
BBB	Blood-brain barrier
FGF2	Fibroblast growth factor 2
BMP	Bone morphogenetic protein
CNS	Central Nervous System
Dll4	Delta-like 4
EGF	Epidermal growth factor
ETS	E-twenty six
FGF	Fibroblast growth factor
FGFR	Fibroblast growth factor receptor
GBM	Glioblastoma multiforme
GPCRs	G protein-coupled receptors
HH	Hamburger and Hamilton
IHC	Immunohistochemistry
INVP	Intraneural vascular plexus
ISH	*In situ* hybridisation
LHC	Lectin histochemistry
LEL	*Lycopersicon esculentum* (Tomato) lectin
MB1	Quail leukocyte/vascular endothelium antigen
Mef2c	Myocyte enhancing factor 2C
MMP	Matrix metalloproteinase
MT-MMP	Membrane type-matrix metalloproteinase
PNVP	Perineural vascular plexus
SEMA	Semaphorin
Shh	Sonic hedgehog
TIMP	Tissue inhibitor of metalloproteinases
uPA	Urokinase-plasminogen activator
uPAR	Urokinase-plasminogen-activated receptor
VEGF(A)	Vascular endothelial growth factor (A)
VEGFR	Vascular endothelial growth factor receptor

1. INTRODUCTION

The development of a properly patterned blood vessel network is crucial for supplying oxygen and nutrients to developing organ systems during embryogenesis. A critical step in the development of the vertebrate nervous system is the vascularisation of the neural tube. The brain in particular has a high demand for oxygen and nutrients, relying on an efficient and highly specialised network of blood vessels to meet its substantial metabolic demands. In early embryogenesis, the neuroectoderm is absent of endothelial cells and is also unable to give rise to angioblastic cells. The vascularisation of the neural tube therefore relies solely on an extraneuroectodermal origin of endothelial cells and angioblasts, which are recruited from the surrounding mesodermal tissue. A primary capillary bed, referred to as the perineural vascular plexus (PNVP), begins to form as endothelial cells aggregate around the developing neural tube (reviewed in Kurz *et al*., 1996; James & Mukouyama, 2011), which then receives its first blood vessels by the dorsal immigration of isolated angioblasts and the ventral and medial invasion of endothelial sprouts. The arrangement of the endothelial sprout, with a leading tip cell and follower stalk cells, is reminiscent of multicellular invasion by certain cancers, shown to be facilitated by matrix metalloproteinases (MMPs). The mechanisms underlying the invasive behaviour of endothelial cells in central nervous system (CNS) vascularisation may therefore share similarities with cancer biology, particularly tumour invasiveness and angiogenesis (Kurz *et al*., 1996; Gerhardt *et al*., 2003; Wolf *et al*., 2007; James *et al*., 2009). Once inside the neural tube, sprouts extend along radial glia and encounter the ependymal layer where they then branch and fuse to form the intraneural vascular plexus (INVP) (Gerhardt *et al*., 2003). In the adult, PNVP-derived vessels form the blood-brain barrier (BBB), which has a neuroprotective role by regulating the transport of substances between the blood and the brain (Risau & Wolburg, 1990; Bauer *et al*., 1993).

1.1 *Gallus gallus* embryos as a model organism for developmental biology

The embryos of *G. gallus* have been used extensively as a model organism in developmental biology and for studying the processes of disease. Chicken eggs are relatively cheap and easy to maintain compared to many other research models and

are readily accessible throughout the year. The semitransparent embryos are large enough to perform experimental manipulations inside the egg under a dissecting microscope and can also be removed from the shell for culture. The nature of *G. gallus* as amniotes is a key advantage for research and so their development of these embryos, which is described as a series of Hamburger and Hamilton (HH) stages based on morphological characteristics (Hamburger & Hamilton, 1951), is close to that of humans. The development of human embryos has been described in a morphological system of Carnegie stages based on features such as embryonic length and number of somites, covering the first 60 days of gestation (Streeter, 1942; O'Rahilly & Müller, 1987). A comparison of the developing brain in early chick and human embryos is shown in Fig. 1i. The majority of information obtained from chick embryos is also applicable to the quail and embryos of other avians, although a major limitation is that the information on genetic mutations is scarce compared to other models such as *Drosophila melanogaster* and *Danio rerio*. Information obtained across a range of research models must therefore be integrated for a thorough understanding of how the brain develops in terms of anatomy and molecular control, which is essential for the applicability to understanding human embryology and the subsequent developmental origins of disorders.

Figure 1i. Comparison of brain development in early human and chick embryos. A. The first sign of neural tube development in the human embryo is the emergence of neural ridges along the two sides of the neural plate on embryonic day (E)19, which fold over to begin the formation of the neural tube. The neural tube begins to close in the central regions on E22, proceeding in both rostral and caudal directions. The anterior and posterior neuropores are the last segments to close on E25 and E27, respectively. The shape of the cylindrical centre of the neural tube changes as the brain grows larger and more complex, expanding to form the three primary brain vesicles that are distinguished by E28: the prosencephalon is the embryonic precursor of the forebrain, the mesencephalon is the precursor of midbrain structures and the most posterior is the rhombencephalon that will become the hindbrain. The embryo bends into a 'C' shape on E28-E30 and a prominent cephalic flexure appears at the level of the mesencephalon. A cervical flexure appears at the boundary between the hindbrain and the spinal cord at the beginning of the fifth week and the primary brain vesicles further subdivide by E49 to form five secondary vesicles that establish the primary organisation of the central nervous system, which persist into adulthood. The prosencephalon differentiates into the telencephalon that ultimately forms the cerebral hemispheres and the diencephalon with optic vesicles extending from the lateral walls. The rhombencephalon differentiates into the metencephalon and a more caudal myelencephalon, whereas the mesencephalon does not further divide and remains tubular in structure. Adapted from Stiles & Jernigan (2010) and iKnowledge (2015). **B**. The chick embryo is a popular model organism and the development of the chick and human brains share various similarities, although specific regions develop at different rates. Neural folds become visible in the head region towards the end of E1 (HH7) and the neural tube begins to close at the level of the future mesencephalon on E2 (HH8). Closure of the anterior and posterior neuropores occurs between E2 and E3 (HH12-HH13). The three primary brain vesicles are established by E2 (HH10) during which the cranial and cervical flexures are first indicated. The subdivision of primary vesicles into the five secondary brain vesicles soon follows, which continue to grow in size and complexity. Adapted from Hamburger & Hamilton (1951) and www.mun.ca. The morphological similarities between a 5-week human embryo and E4 (HH22) chick embryo are shown in **C** and **D**, respectively.

A HUMAN

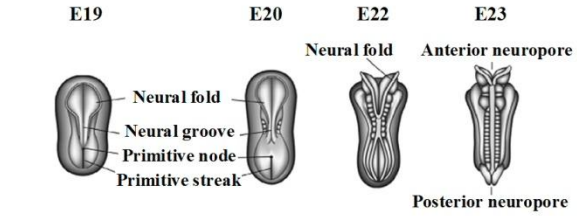

PRIMARY VESICLES

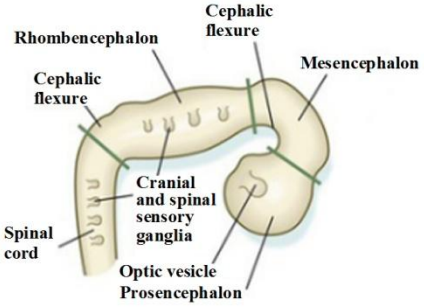

SECONDARY VESICLES

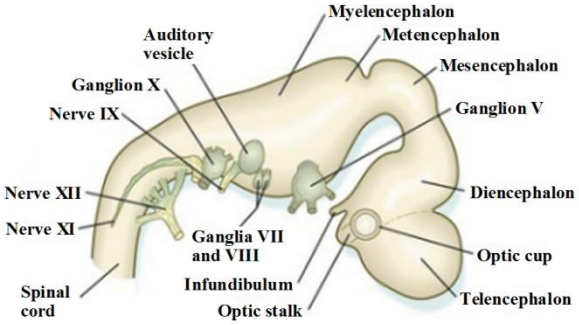

B CHICK

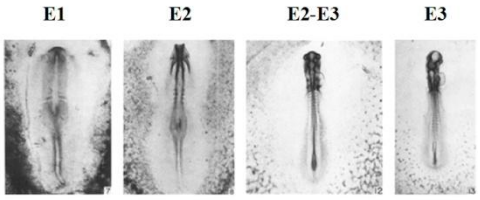

PRIMARY VESICLES

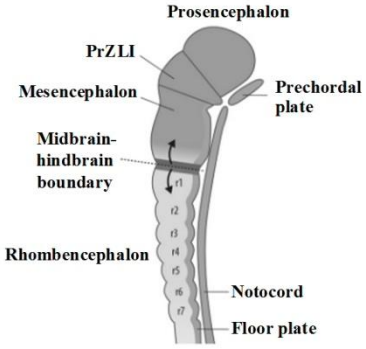

SECONDARY VESICLES

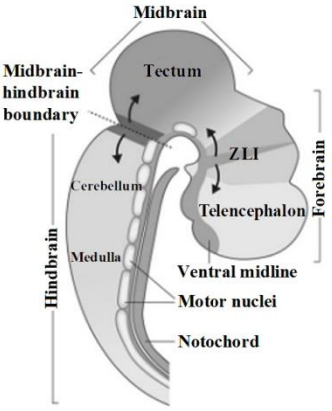

C

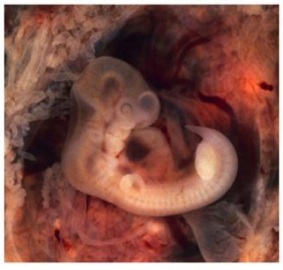

D

1.2 The avian and mouse neural tube and the retina as models for CNS vascularisation

The earliest descriptions of the vascularisation of the neural tube were achieved primarily through the use of conventional histology and India ink injections in the spinal cord of avian embryos. The formation of the PNVP was first described in the classic study by Feeney & Watterson (1946), which also documented the appearance of sixteen distinct intraneural capillaries in specific regions along the dorsoventral axis of the chick neural tube. The spatial and temporal formation of early vessels was found to give rise to a scaffold, allowing for association with subsequent vessels.

The avian embryo has been a popular model organism for developmental studies on angiogenesis, particularly since the use of anti-MB1 monoclonal antibodies (Peault *et al*., 1983) within the quail-chick chimera system. The MB1 antigen (Labastie *et al*., 1986; Peault *et al*., 1987) is expressed on the surface of hemangioblasts and all endothelial and haematopoietic cells, excluding mature erythrocytes. Throughout ontogenesis and in the adult, MB1 is used as a lineage-specific marker characteristic of endothelial cells specific to quail. Other monoclonal antibodies have been produced that have similar specificities, such as the QH1 antibody (Pardanaud *et al*., 1987). A systematic approach to investigating the origin of cephalic blood vessel endothelial cells was conducted by Couly *et al*. (1995) in early avian embryos by performing grafts of defined mesodermal territories from the 3-somite stage quail embryo into stage-matched chick embryos in a strictly isotopic manner. The tyrosine-kinase receptor Quek1 (Eichmann *et al*., 1993), which is the avian homologue of the mammalian vascular endothelial growth factor receptor 2 (VEGFR2), was used as a molecular marker to label endothelial precursors from the time of gastrulation. Quek1 positive cells later form endothelial cells of blood vessels and express the antigen MB1/QH1, specifically in quail. The monoclonal antibody, MB1/QH1, was therefore used as a second molecular marker in order to identify endothelial cells as they assemble to constitute the lining of the newly formed blood vessels. The use of two markers to label vascular endothelial cells and their precursors showed that the cephalic mesoderm has considerable angiogenic potentials, vascularising specific regions of the face and brain in a restricted and well

defined pattern. The anterior region of the cephalic paraxial mesoderm was shown to be largely recruited by the forebrain to provide its vasculature, while angiogenic cells from the more posterior mesodermal territories vascularised the corresponding levels of the brain.

The major blood vessel patterning events in the quail neural tube were observed by Kurz *et al.* (1996) and James *et al*. (2009), utilising the monoclonal antibody QH1 directed against quail endothelial cells and angioblasts. Kurz *et al.* (1996) found that the first blood vessels in the quail spinal cord at cervical level develop by a combination of two processes, the dorsal immigration of isolated migrating angioblastic cells at stage HH19 and the ventral sprouting of endothelial cells on either side of the floor plate at HH21, both of which contribute to the developing INVP. The exclusive extraectodermal origin of angioblastic cells was also demonstrated through the study of chick-quail chimeras. Replacing the quail neural tube with a chick neural tube graft resulted in the same distribution of angioblasts and sprouts observed in controls. Starting caudal to the rhombencephalic neural tube, the same pattern of vascularisation was observed in a craniocaudal sequence with sprouting cells displaying extremely long filopodia. James *et al*. (2009) characterised blood vessel ingression into the quail neural tube at the thoracic level, visualising patent vessels and non-patent sprouts with QH1 immunostaining. Neural development was also followed by staining with a TuJ1 antibody against β-tubulin III to label differentiated neurons. PNVP formation was found to initiate at stages HH16-18 along the mid-levels of the lateral surface of the neural tube and continued to develop until stages HH22-24. The dorsal migration of single QH1-positive angioblasts and ventral sprouting were first observed at stages HH22-24 followed by medial angiogenic sprouting at stages HH24-25, occurring slightly later than that of the cervical neural tube identified by Kurz *et al*. (1996). Obvious stereotypical blood vessel ingression points were exhibited by stage HH26. The number of TuJ1-positive cells were found to increase over time forming a TuJ1-positive area into which angiogenic sprouts invaded at specific ventral and medial regions. Once inside the neural tube, the angiogenic sprouts avoided the TuJ1-negative medial area containing proliferative progenitor cells, suggesting that blood vessel ingression may be influenced by the developing neural tube (Fig. 1ii).

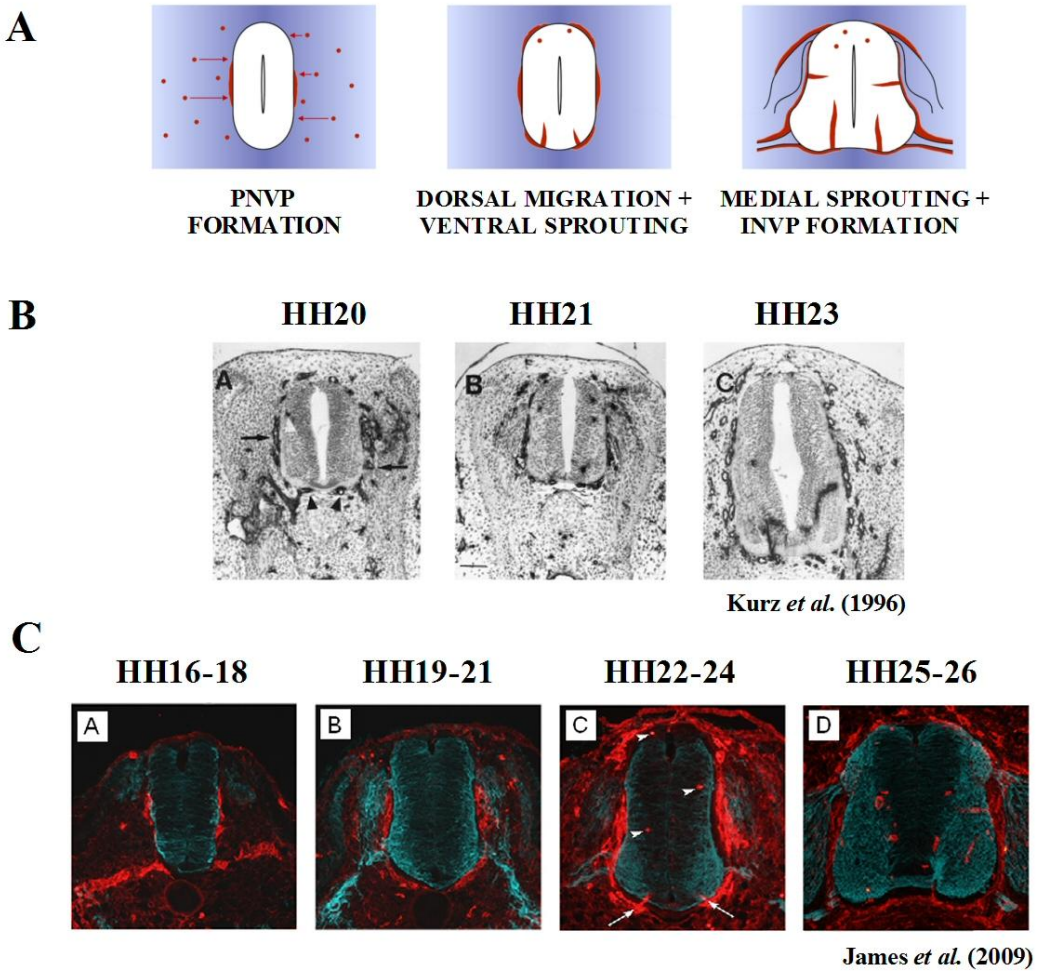

Figure 1ii. Vascularisation of the avian neural tube. A. Schematic summary of the major blood vessel patterning events in the spinal cord from the initial migration of endothelial cells towards the neural tube leading to the formation of the PNVP, dorsal migration of isolated angioblasts and ventral sprouting, followed by medial sprouting and formation of the INVP. Vascularisation of the quail neural tube by QH1 immunostaining reveals the beginning of sprouting at stage HH21 at cervical level (**B**) and stages HH22-24 at thoracic level (**C**) as endothelial cells invade the ventral spinal cord. Obvious stereotypical blood vessel ingression points were exhibited by stage HH26 (Kurz *et al*., 1996; James *et al*., 2009).

The mouse embryo hindbrain and forebrain are popular mammalian models used to study the cellular mechanisms of CNS vascularisation. In the mouse hindbrain, vascularisation initiates around embryonic (E) day 9.5 when blood vessels begin to sprout from the PNVP and grow radially towards the ventricular zone where vascular growth factors are released by neural progenitors. The radial vessels begin sprouting at near right angles from around E10.25 and extend parallel to the surface of the hindbrain. The subventricular vascular plexus (SVP) is formed by E12.5 through the anastomosis of neighbouring vessel sprouts (Ruhrberg *et al.*, 2002; Fantin *et al.*, 2010; Fantin *et al.*, 2013), which is promoted by tissue macrophages derived from the yolk sac. The macrophages interact with endothelial tip cells and bridge neighbouring vessel sprouts during the fusion process (Fantin *et al.*, 2010; Schmidt & Carmeliet, 2010). Pericytes also interact with endothelial cells as they assemble into sprouts, providing them with structural support and instructive cues (Gerhardt & Betsholtz, 2003). In the mouse forebrain, blood vessels begin to sprout from the PNVP into the ventrolateral brain at E9.5, progressing in an orderly ventrolateral to dorsomedial direction across the rostrocaudal axis. The SVP is formed in the ventral forebrain by E10, while the dorsal part remains largely avascular. Interestingly, the vasculature in the dorsal forebrain derives from the SVP of the ventral compartment rather than sprouting from the dorsal PNVP. The SVP forms in both the ventral and dorsal areas and by E11, reaching the dorsal medial wall of the forebrain (Vasudevan *et al.*, 2008).

The retina is another popular model for studying CNS angiogenesis as it originates from the developing forebrain and is easily accessible due to the position outside the brain. Vascularisation of the mouse retina begins around birth and studies in additional species including rat, cat, human, rabbit and possum, have revealed that development of the retinal vasculature is regulated by interactions between astrocytes, retinal neurons and vessel sprouts. Astrocytes make up the largest cell population of the CNS and their organisation, differentiation and migration are crucial for retinal angiogenesis. Astrocyte progenitor cells (APCs) are derived from neuroepithelial cells of the optic nerve, therefore morphogenesis of the optic stalk, which is the precursor of the optic nerve, is important for astrocyte development. Studies in zebrafish have demonstrated the importance of Nodal, a member of the transforming growth factor beta (TGFβ) family, for early proximal-distal patterning

of the eye that occurs in part through modulating the Sonic hedgehog (Shh) pathway (Take-uchi *et al*., 2003; Müller *et al*., 2000). In chick embryos, the chemical inhibition of Shh and Nodal pathways have been shown to result in optic vesicles that were lost or defective (Mercier *et al*., 2013). Optic vesicle formation was also lost in Nodal deficient mice (Lowe *et al*., 2001). The differentiation of optic stalk neuroepithelial cells into APCs at E12 to E14 is coincident with the onset of *Shh* expression from differentiating retinal ganglion cells (RGCs), which promotes the proliferation of astrocytes and may also induce the expression of the receptor tyrosine kinase (RTK), platelet-derived growth factor receptor alpha (PDGFR alpha), in APCs (Kuwabara, 1975; Xie *et al*., 2001; Dakubo *et al*., 2003; Dakubo *et al*., 2008). In rodents, fibronectin-expressing astrocytes emerge from the optic nerve head and invade the inner surface of the retina over the axons of RGCs. Genetic studies have demonstrated that the neuroretina provides the permissive extracellular matrix (ECM) for the migration of astrocytes as deletions of laminin α1, β2 and γ3 chains in the retina disrupts astrocyte migration and spatial distribution (Edwards *et al*., 2010; Gnanaguru *et al*., 2013). RGCs express platelet-derived growth factor alpha (PDGF-A), which is critical to the patterning of the retinal astrocyte network as PDGF-A stimulates the proliferation of the invading astrocytes by binding to PDGFR alpha present on the cell surface (Stone & Dreher, 1987; Watanabe & Raff, 1988*;* Ling *et al*., 1989; Fruttiger *et al*., 1996; Sandercoe *et al*., 1999; West *et al*., 2005). The network of retinal astrocytes transiently secretes vascular endothelial growth factor A (VEGFA) that promotes angiogenesis by stimulating the invasion, proliferation and migration of endothelial cells, thus guiding the radial expansion of vessel sprouts, also emerging from the optic nerve head, over the retina. The arrival of endothelial cells relieves the oxygen tension in the retina and the arrangement of blood vessels depends on the pattern of retinal astrocytes, which is determined by the factors influencing astrocyte development. Oxygen-enriched atmospheres have been shown to prevent the development of retinal blood vessels, leading to retinal hypoxia, which is associated with inhibited astrocyte differentiation and downregulated VEGFA expression. The formation of vessels therefore depends on oxygen demand and the hyperoxia-induced obliteration of newly-formed retinal vessels in premature newborn results in retinopathy of prematurity (Stone *et al*., 1995; Jiang *et al*., 1995; Alon *et al*., 1995; Pierce *et al*., 1996; Zhang & Stone, 1997; Provis *et al*., 1997; Fruttiger, 2002; West *et al*., 2005).

1.3 CNS angiogenesis is regulated by neural-tube derived signals

The stereotypical pattern of vessel ingression and the existence of a hierarchical system of intraneural blood vessel development has lead to the investigation into the regulation of neural tube angiogenesis by neural tube-derived signals (James & Mukouyama, 2011). Hogan *et al*. (2004) used mouse-quail chimeras to identify the neural tube as a midline signalling centre for vascular patterning that directs the formation of the PNVP. Mouse neural tubes, derived from *ROSA26* heterozygous embryos that ubiquitously express the *lacZ* transgene, were transplanted between the intermediate mesoderm and lateral plate in quail hosts. β-galactosidase staining and whole-mount visualisation showed the grafts to be well incorporated. QH1 staining on sections identified the recruitment of host-derived blood vessels immediately adjacent to the grafted neural tube in a structure resembling the PNVP. The grafting of acrylic beads and avian notochords did not elicit a vascular plexus, indicating that the vascular plexus surrounding the neural tube did not result from the encapsulation of a foreign body. The neural tube-derived vascular patterning signal was also demonstrated to induce target cells at a distance by grafting mouse presomitic mesoderm into a cavity made from the removal of lateral presomitic mesoderm in the quail host, thus setting up a buffer of several cell layers of quail mesoderm between the host neural tube and the graft. Graft-derived vascular cells were found to contribute to the PNVP, indicating that the signal does not require direct cell contact. VEGFA expression was then analysed in mouse embryos and correlated with PNVP formation, suggesting it as a component of the neural tube signal. A collagen gel explant model was developed in which explants of mouse presomitic mesoderm formed a robust vascular plexus when incubated with added VEGFA. Co-cultures between presomitic mesoderm and neural tube also resulted in vascular plexus formation, indicating that the neural tube was able to replace the requirement for VEGFA. Furthermore, VEGFA signalling through the VEGFR2 receptor was found to be a required component of the neural tube vascular patterning signal, identified through a combination of pharmacological and genetic perturbations. VEGFA was therefore identified to be a necessary component of the neural tube vascular patterning signal.

The VEGF family of growth factors comprises VEGFA, VEGFB, VEGFC, VEGFD and placental growth factor (PlGF), which bind to the RTKs VEGFR1 (Flt-1), VEGFR2 (Flk-1) and VEGFR3 (Flt-4), together with co-receptors neuropilin-1 (NRP1) and neuropilin-2 (NRP2), to stimulate cellular responses including vasculogenesis and angiogenesis (Fig. 1iii). VEGFA as an endothelial growth factor with unique target cell specificity for vascular endothelial cells was first isolated from the AtT-20 pituitary cell line (Plouët *et al*., 1989) and was characterised as a homodimer composed of two subunits with molecular weights of 23 kd. The potent mitogen for vascular endothelial cells *in vitro* was also found to induce angiogenesis *in vivo*, the process by which new blood vessels are formed from the remodelling of existing ones, without stimulating the growth of other cell types of the vascular system. VEGFA can also have direct effects on neuroectoderm-derived cells and has been demonstrated to promote neurogenesis and neuronal patterning. The treatment of cultured primary cortical neurons with VEGFA was shown to enhance neurite growth and maturation independently of blood vessels (reviewed by Rosenstein *et al*., 2010). VEGFs are now known to be synthesised by many different cell types including macrophages (Sunderkotter *et al.*, 1994), keratinocytes (Frank *et al*., 1995), platelets (Verheul *et al*., (1997) and tumour cells (Boocock *et al*., 1995; Itakura *et al*., 2000), playing a number of roles in normal physiological functions, development and pathology.

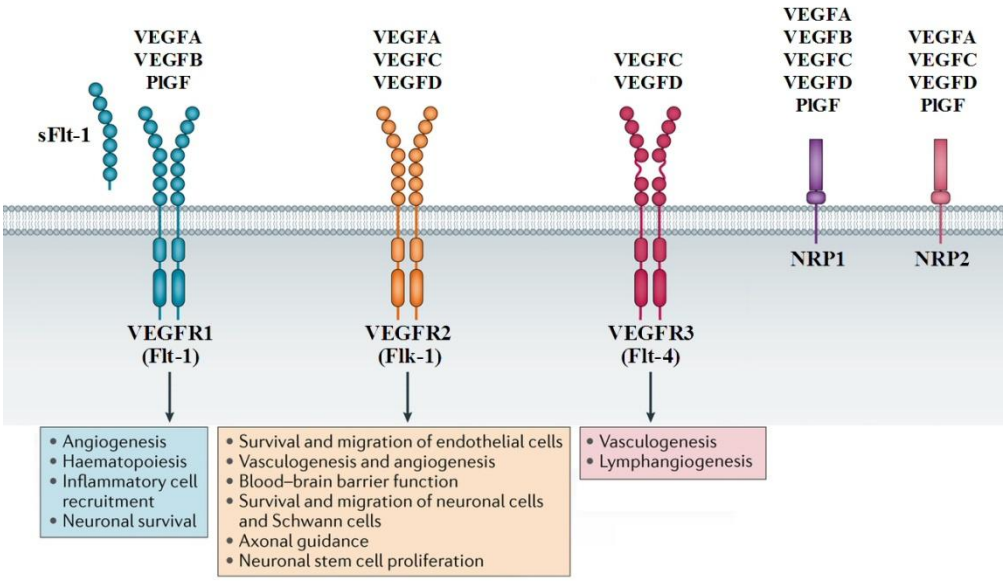

Figure 1iii. VEGFs and VEGFRs. The binding of VEGF isoforms, VEGFA, VEGFB, VEGFC, VEGFD and PlGF, to RTKs VEGFR1, VEGFR2 and VEGFR3 and co-receptors, NRP1 and NRP2, stimulates cellular responses in the vasculature and CNS. NRP1 can also act independent of VEGFA to control brain angiogenesis. The biological actions of VEGFA, VEGFB and PlGF can be reduced by binding to soluble VEGFR1 (sFlt-1) (adapted from Lange *et al*., 2016).

The alternative splicing of the VEGFA primary transcript results in multiple transcript variants that encode distinct isoforms (Fig. 1iv) that differ in receptor binding properties and have different affinities for the ECM. The three major isoforms in human are termed VEGF121, VEGF165 and VEGF189, which reflect the number of total amino acid residues present in the mature protein. The corresponding isoforms in mouse are one amino acid shorter in length and are named VEGF188, VEGF165, VEGF120 and VEGF112, respectively. VEGFA isoforms differ in biochemical properties such as the capacity to interact with the ECM, which is dependent upon the ability to bind heparin most likely through binding to heparin sulfate proteoglycans (HSPGs; Esko & Lindahl, 2001). VEGFA isoforms are differentially sequestered by HSPGs and are subject to inhibitors that are involved in establishing vascular quiescence (Ambati *et al*., 2006). The release of VEGFA from sequestration is typically proangiogenic and occurs as extracellular proteases cleave HSPG core proteins and associated ECM molecules (Flaumenhaft *et al*., 1990; Purushothaman *et al*., 2006). Proteases can also cleave VEGFA to generate new isoforms (Lee *et al*., 2005).

The presence of heparin-binding domains encoded within exons 6 and 7 allow each isoform to interact with the ECM to a different extent, resulting in the distribution of the various isoforms across the matrix that regulate sprout guidance and vessel growth. Isoforms VEGF189 and VEGF165 have the strongest matrix interactions and exhibit steep spatial gradients, whereas VEGF121 is more diffusible due to the absence of heparin-binding properties (Park *et al*., 1993; Bautch, 2012). A diffuse immunostaining pattern has been shown in the hindbrain of mice engineered to secrete only VEGF120, whereas wild-type mice that predominantly secrete VEGF164 possess a steeper gradient with a higher level of VEGFA at the midline that falls off more rapidly (Ruhrberg *et al*., 2002). The gradient does not only reflect restricted diffusion rates of VEGFA from secreting cells and the heterogeneities in the concentration of VEGFA binding partners, but also results from combined sequestration and degradation. Soluble VEGFA inhibitors including the splice form of VEGFR1, sFlt-1, play a major role in VEGFA patterning (Kappas *et al*., 2008; Chappell *et al*., 2009; Vempati *et al*., 2011; Hashambhoy *et al*., 2011). Furthermore, the VEGFA gradient in endothelial cells is shaped by the degradation of VEGFA through internalisation of the VEGFA-VEGFR complex (Greenaway *et al*., 2007).

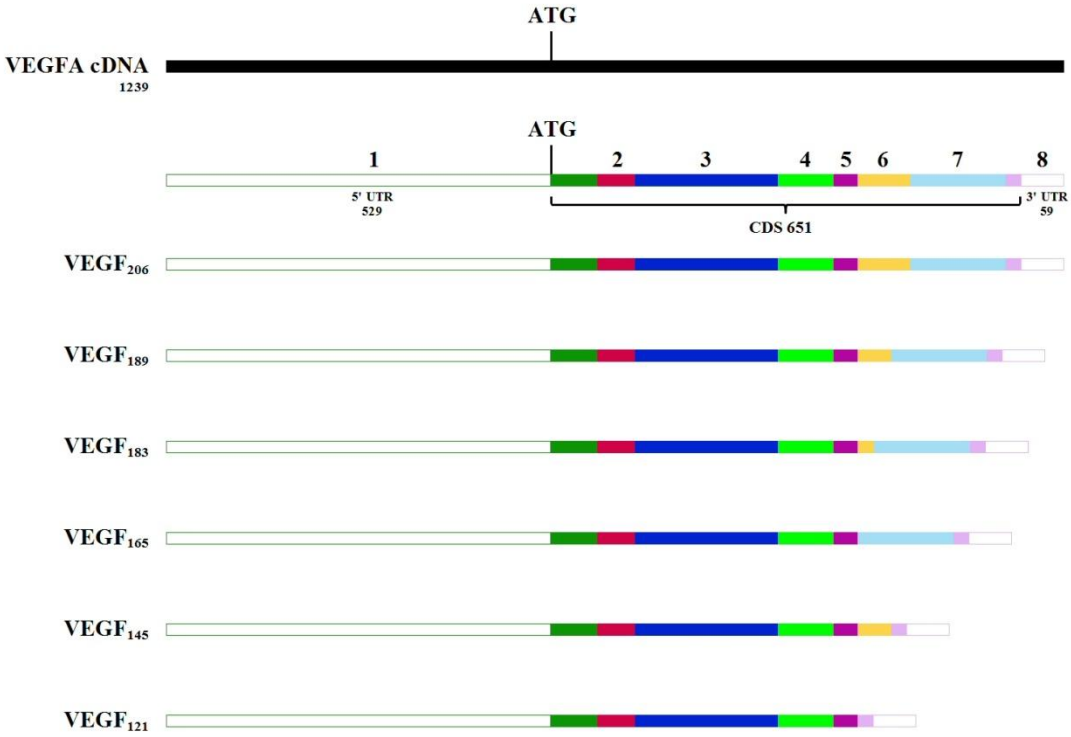

Figure 1iv. VEGFA isoforms in human. The primary transcript of VEGFA is alternatively spliced to form multiple transcript variants that encode distinct isoforms. The major isoforms in human are VEGF189, VEGF165 and VEGF121, which differ in biochemical properties including their affinity for VEGFRs and HSPGs, resulting in varied effects on the growth of blood vessels. Heparin-binding domains encoded within exons 6 and 7 confer the ability of each isoform to interact with the ECM and the extent to which they bind, resulting in the distribution of the various isoforms across the matrix. VEGF189 and VEGF165 have the strongest matrix interactions and steepest gradients. The diffusion of these isoforms is therefore more restricted compared with VEGF121, which is more diffusible due to the absence of heparin-binding properties.

1.4 The recruitment of angioblasts and endothelial cells

Ambler *et al*. (2003) analysed mouse-avian chimeras and found mammalian angioblasts could recognise, migrate and pattern in response to avian vascular patterning cues. Murine embryonic stem (ES) cell-derived embryoid bodies (EBs) labelled with Nile Blue were grafted into the host in a cavity made by the removal of presomitic mesoderm from one side of the quail neural tube. The murine endothelial cells and progenitors derived from the ES cells migrated extensively, colonised the appropriate vascular beds of the host and also formed mosaic vessels with avian endothelial cells. The requirement of the VEGFA signalling pathway for proper vascular patterning of the embryo was also demonstrated by grafting EBs either mutant for VEGFR2 (*Flk-1*$^{-/-}$) or VEGFA (*VEGFA*$^{-/-}$) into quail hosts. The *Flk-1*$^{-/-}$ EB grafts produced rare endothelial cells that neither migrated nor assembled into vessels. However, *VEGFA*$^{-/-}$ EB grafts produced endothelial cells that resembled wild-type and colonised vascular beds of the host. The *VEGFA*$^{-/-}$ graft endothelial cells also crossed the midline but at a much lower frequency compared with wild-type EB grafts, suggesting that signals derived from the host are able to partially rescue mutant graft vascular patterning.

Endothelial cells originating from the presomitic mesoderm have been shown to make a significant contribution to the PNVP of the neural tube and the migration of angioblasts towards their source has been attributed to a neural tube-derived gradient of VEGFA (Ambler *et al*., 2001; Ambler *et al*., 2003; Hogan *et al*., 2004; James *et al*., 2009; Kurz *et al*., 1996; Wilting *et al*., 1995). The distinct localisation of heparin-binding VEGFA isoforms and non-heparin binding VEGF120 was investigated in the developing hindbrain of mouse embryos. In $VEGF_{120/120}$ embryos that completely lack heparin-binding isoforms, a *VEGFA lacZ* reporter identified high levels of VEGFA gene expression near the hindbrain midline at 10.5 dpc. The immunostaining of nonpermeabilised hindbrains with an antiserum that detects all VEGFA isoforms was also performed in order to visualise the distribution of secreted VEGFA protein. A steep concentration gradient was shown in wild type embryos in which VEGFA protein accumulated in patches surrounding the sites of production that was highest near the midline and tapered off toward the front of the developing subventricular plexus. In $VEGF_{120/120}$ mouse embryos, the absence of

heparin-binding isoforms resulted in a loss of this steep gradient with VEGFA protein appearing more widely dispersed. The development of blood vessels was also examined in $VEGF_{120/120}$ mouse embryos, which exhibited a reduction in the complexity of vascular branching. $VEGF_{120/120}$ mice were not viable and displayed an altered distribution of endothelial cells resulting in capillary networks with fewer branch points and a larger luminal diameter. Endothelial cells were preferentially integrated within existing vessels rather than into additional branch points in the gut, somites and all regions of the CNS (Ruhrberg *et al*., 2002).

The role of VEGFA signalling in the spatially localised molecular communication between the neuroepithelium of the quail neural tube and embryonic blood vessels has been investigated by James *et al*. (2009), demonstrating its involvement in the ingression of angiogenic sprouts. Individual VEGFA isoforms were ectopically expressed at the thoracic level of the quail neural tube in order to determine their effects on neural tube development. The electroporation of VEGF189 or VEGF165 at stages HH16-18 of development resulted in an increase in the number of ingression points in the dorsal area of the electroporated side, which is normally avascular, compared to the non-electroporated control side. The interaction of VEGFA isoforms with the local matrix are therefore crucial for proper vessel ingression and the heparin-binding properties of VEGF189/165 enabled these isoforms to interact with the matrix and confer the ability to induce localised ectopic ingression points. The ectopic expression of the non-heparin binding isoform VEGF121, however, did not affect the number of blood vessel ingression points although ingressing vessels became dysmorphogenic. Complementary to these findings, the absence of heparin-binding isoforms in $VEGF_{120/120}$ mouse embryos showed an altered distribution of endothelial cells within the growing vasculature, which resulted in a decrease in the formation of capillary branches and an increase in vessel lumen size (Ruhrberg *et al*., 2002). The loss of endogenous VEGFA signalling, achieved by ectopically expressing sFlt-1 into the developing neural tube, dramatically blocked normal vessel ingression on the electroporated side (James *et al*., 2009). The protein sFlt-1 is a natural soluble splice form of the VEGFR1 receptor that lacks the transmembrane domain and acts as a VEGFA inhibitor by binding and sequestering VEGFA to prevent downstream signalling (Kendall & Thomas, 1993). Furthermore, the analysis of several regional markers of neural tube

patterning showed that neural tube development was not detectably perturbed by the ectopic expression of VEGFA isoforms. James *et al*. (2009) confirmed that VEGFA signalling is necessary to pattern the angiogenic blood vessels that enter the neural tube but not sufficient to explain the stereotypical pattern observed as VEGFA is broadly expressed and not localised to sites of ingression. The data supports a model in which positive signals emanating from the neural tube are balanced by neural tube-derived negative spatial cues that prevent ingression, of which semaphorins, slits and netrins are candidates, leading to ingression at specific points along the dorsoventral axis. The influence of patterning signals therefore needs to be investigated further in order to obtain a better understanding of the regulation of blood vessel ingression.

1.5 Endothelial sprouting

The arrangement of growing blood vessel sprouts into a leading tip cell and the follower stalk cells was first described in the hindbrain and retina of the mouse (Ruhrberg *et al*., 2002; Gerhardt *et al*., 2003) and has been observed in preliminary images of sprouting into the embryonic *G. gallus* brain (Fig. 1v). In addition to its involvement in attracting endothelial cells towards the neural tube, VEGFA also has a role in the selection of tip cells that initiate ingression by signalling through VEGFRs. Roberts *et al*. (2004) showed that the formation of developmental blood vessels is affected by VEGFR1, which modulates signalling of VEGFA through VEGFR2. Mice lacking the VEGFA receptor VEGFR1 died from vascular overgrowth, which was primarily caused by aberrant cell division. The upregulation of VEGFR2 signalling in the mutant was indicated by the increased phosphorylation of VEGFR2 identified in differentiated ES cell cultures in which VEGFR1 was absent.

The behaviour of endothelial cells is orchestrated by the induction of the Notch pathway by VEGFA, resulting in the emergence of tip cells that initiate new sprouts and stalk cells that proliferate and contribute to the expansion of the vessel (Gerhardt *et al*., 2003). Vascular sprouting and vessel branching is controlled by Delta-like 4 (Dll4)-Notch1 signalling between endothelial cells within the vessel sprout, which is crucial in establishing an adequate ratio of tip cells to stalk cells required for normal

sprouting patterns (Fig. 1vi). VEGFA signalling through VEGFR2 increases the expression of Dll4 on emerging tip cells. The Dll4 ligand then binds to Notch receptors on adjacent endothelial cells, resulting in an increase in VEGFR1 expression (Harrington *et al*., 2008; Funahashi *et al*., 2010) and reduced expression of both VEGFR2 and VEGFR3 (Tammela *et al*., 2008; Shawber *et al*., 2007; Suchting *et al*., 2007; Benedito *et al*., 2012) thereby reducing their sensitivity to VEGFA, preventing these cells from becoming tip cells and promoting stalk cell identity. Crosstalk between the VEGFA and Notch pathways is mediated by VEGFR1, which maintains VEGFA signalling at appropriate levels for the effective use of Notch in lateral inhibition. VEGFR1 negatively regulates vessel formation as it binds VEGFA with 10-fold higher affinity than VEGFR2, limiting the amount of VEGFA that can access the VEGFR2 receptors (Roberts *et al*., 2004; Chappell *et al*., 2013).

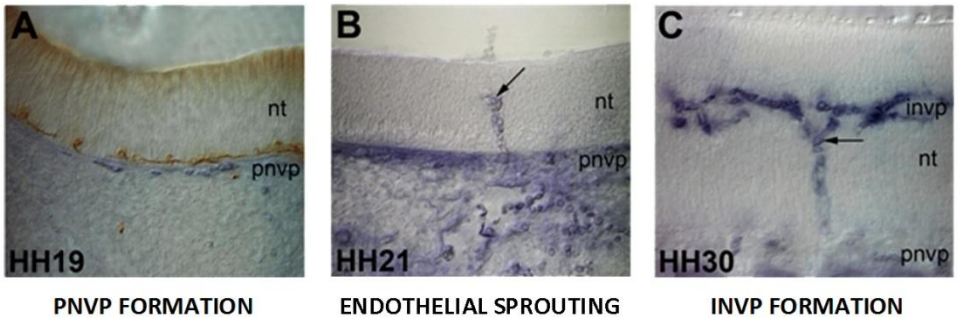

Figure 1v. Vessel sprouting into the embryonic *G. gallus* brain. Endothelial cells (blue) and neurons (brown) were detected with an antisense Ets1 probe and a TuJ1 antibody against neuron-specific Class III β-tubulin antibody, respectively. **A**. Endothelial cells line up against the basal lamina of the neural tube (nt) to form the PNVP. **B**. The first ingressing endothelial cells were detected at HH21, initiated by the tip cell (arrow). **C**. The ingressing stream of cells then begins to branch (arrow) and forms the INVP by HH30.

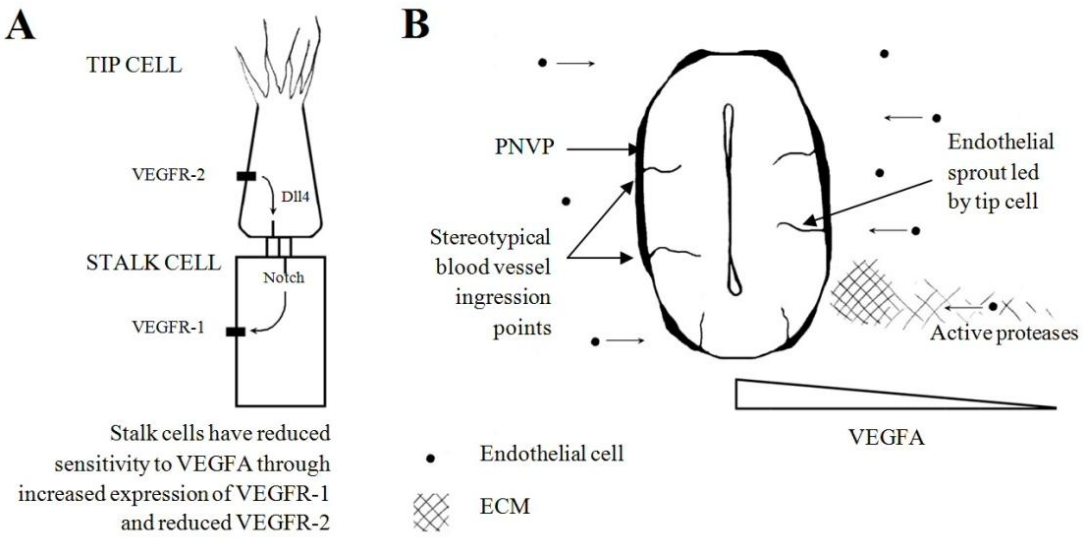

Figure 1vi. Schematic of tip and stalk cell selection and endothelial sprouting into the neural tube. **A**. The selection of tip and stalk cells depends on Notch signalling between endothelial cells within the PNVP. An endothelial cell receiving more VEGFA via the VEGFR2 receptor compared with neighbouring cells leads to an increase in the expression of the transmembrane ligand Dll4, resulting in the emergence of a tip cell. Dll4 signals to the neighbouring cells via the Notch receptor, promoting an increase in VEGFR1 that reduces the sensitivity of these cells to VEGFA signalling and prevents the formation of more tip cells. Vessel sprouting is promoted by high levels of VEGFR2 and low VEGFR1 in tip cells relative to the neighbouring stalk cells, thus establishing an adequate ratio of tip and stalk cells required for normal sprouting patterns. **B**. The process of vascularisation involves the migration of endothelial cells towards the neural tube in response to a gradient of VEGFA. The ECM is remodelled by active proteases during migration and as tip cells penetrate the basal lamina at stereotypical ingression points at the initiation of vessel sprouting.

A recent study has described a tumour suppressor function of Notch. Activating the Notch pathway has been shown to reduce tip cell numbers and branching in retina models and reduce glioma growth in the mouse forebrain. In humans, high Notch activity strongly correlates with distinct subtypes of gliomas, lower tumour grade and increased patient survival. Conversely, the inhibition of Notch signalling has been shown to promote an increase in tip cell numbers and vessel branching in the retina and also accelerates PDGF-driven glioma growth in mice (Hellstrom *et al*., 2007; Suchting *et al*., 2007; Giachino *et al*., 2015). The increase in tip cell numbers can however be useful to promote vascularisation and restore blood flow to areas of ischaemia and may also be important in the recovery of stroke.

The extension of long filopodia from endothelial cells at the tips of vascular sprouts has been revealed by isolectin B4 staining in the postnatal mouse retina, indicating an active migratory phenotype. The filopodia were of uniform thickness (approximately 100nm) and the longest that exceeded 100μm were largely restricted to the tip cell, which was revealed to be a highly polarised endothelial cell identified by isolectin B4, vascular endothelial (VE) cadherin, fibronectin and nuclei staining. Additional staining for platelet-endothelial cell adhesion molecule (PECAM)-1, endomucin and VEGFR2 further confirmed the endothelial identity of this cell. The gene expression profile of tip cells was also found to be distinct from stalk cells by their strong expression of platelet-derived growth factor B (PDGF-B) mRNA and both VEGFR2 mRNA and protein (Gerhardt *et al*., 2003). PDGF-B was previously shown to have a crucial role in attracting pericyte progenitor cells to new capillaries, thereby stabilising the nascent vessels, through the study of PDGF-B-deficient mice (Lindahl *et al*., 1997). The migration of tip cells is guided by the distribution of VEGFA in the extracellular space, whereas the proliferation of stalk cells is regulated by its concentration (Gerhardt *et al*., 2003). The directed extension of filopodia becomes impaired when the normal VEGFA gradient is disrupted, and spatially restricted stimulatory cues are suggested to be provided by heparin-binding isoforms in order to guide the initiation of branch formation by sprouting endothelial cells. In embryos that possess only a heparin-binding VEGFA isoform, excess endothelial filopodia were observed and abnormally thin branches were present in ectopic sites (Ruhrberg *et al*., 2002). VEGFA signalling via VEGFR2 has been investigated in the retina following the injection of VEGFR2-specific antibodies into

the eyes of P5 mice. The resulting retraction of tip cell filopodia and inhibition of plexus spreading shows the necessity of VEGFR2 in the extension and maintenance of filopodia (Gerhardt *et al*., 2003). Although filopodia are proposed to mediate the directional migration of tip cells and guide the formation of vascular sprouts, they are not required in the induction of tip cells or the translation of guidance cues from the extracellular environment. Filopodia do however facilitate the rapid and persistent migration of endothelial cells. Upon inhibiting the formation of filopodia during sprouting angiogenesis in zebrafish embryos using low concentrations of Latrunculin B, endothelial cells generate lamellipodia that can drive migration albeit at a reduced velocity. Furthermore, when the endothelial Notch ligand Dll4 was knocked down using a Dll4 splice morpholino, ectopic sprouting was displayed and the attraction of aberrant vessels towards VEGF165 also occurred, even when filopodia were absent. The role of filopodia in facilitating vessel anastomosis by mediating new contacts was also indicated as their absence resulted in delayed dorsal longitudinal anastomotic vessel (DLAV) formation and blocked vein plexus formation (Phng *et al*., 2013).

Urokinase-plasminogen-activated receptor (uPAR) is a glycosylphosphatidylinositol-(GPI) anchored protein that is also expressed in tip cells as well as many other cell types, which participates in degrading the ECM and facilitating the growth of sprouts in the correct direction. uPAR converts inactive urokinase-plasminogen activator (uPA) that binds to the receptor into active uPA. The active uPAR-bound uPA subsequently triggers cell migration by converting cell-bound plasminogen to plasmin, resulting in the degradation of the ECM that serves as a storage depot for numerous biologically active molecules. Furthermore, uPAR regulates cell migration by interacting with αvβ1 integrin and caveolin, which are also highly expressed in tip cells. ECM degradation leads to the localised release of matrix-immobilised enzymes and proangiogenic growth factors including fibroblast growth factor 2 (FGF2) and VEGFA. Cell proliferation and differentiation is in part regulated by FGF2, which is initially bound to heparan sulfate (HS) in the ECM. The release of active FGF2 is brought about by the sequential breakdown of HS-proteoglycans through the synergistic action of cellular heparanase and ECM-resident uPA (Quigley *et al*., 1987; Vlodavsky *et al*., 1990; Wei *et al*., 1996; Blasi & Carmeliet, 2002).

The ECM of the CNS forms a basal lamina surrounding the brain and spinal cord that contributes to the overall structural organisation and controls individual cells by various mechanisms such as regulating the distribution of growth and differentiation factors. Following the penetration of the basal lamina and invasion of the developing neural tube, the ECM provides a substrate on which endothelial cells can migrate and the composition of which differs from that of the surrounding mesenchyme. The complex expression patterns of glycoproteins, including laminins, tenascins and proteoglycans, are developmentally regulated and control the migration and positioning of neurons within the developing brain. Similar to the radial migration by endothelial sprouts towards the ventricular zone, excitatory neurons of the neocortex migrate radially from the ventricular zone into the developing cortical wall along radial glial cells that extend from the ventricular zone to the marginal zone. Radial migration is also seen in the cerebellum as Purkinje cells and granule neurons migrate along radial glial fibres and Bergman glial fibres, respectively. A disruption to the attachment of radial glial cells to the pial surface in the neocortex of β1 integrin-deficient animals have shown that although neurons are able to associate with intact radial glial cells and exhibit normal migration, ectopias occur near the marginal zone where the endfeet of radial glial cells have detached from the basal lamina. Mice that lack α6 integrin that forms a heterodimer with β1 integrin to form laminin receptors have also shown similar phenotypes (reviewed by Franco & Müller, 2011). Since ECM glycoproteins and their receptors play a critical role in the positioning of neurons that associate with radial glia, a similar function could occur in the navigation of endothelial sprouts along radial glia during extension towards the ventricular zone.

1.6 The influence of neural tube patterning on the developing vascular network

The temporal and spatial generation of defined types of neurons from multipotent neural stem (NS) and progenitor cells is a fundamental element of neurogenesis, which occurs prior to the development of the vascular network. In the embryonic mouse telencephalon, endothelial cells express region-specific homeobox transcription factors, Nkx2.1, Dlx1/2 and Pax6, which regulate angiogenesis along a ventral-to-dorsal gradient and control the development of neuroepithelial domains and postmitotic neurons. The vasculature therefore develops with the support of

angiogenesis programs that are intrinsic to the CNS (Vasudevan *et al*., 2008), and as vascularisation of the neural tube shares some of the same molecular pathways as neural development and neural tube patterning, such as those involved in axon guidance and tip cell migration, the molecular communication existing between the two processes is thus revealed.

A correlation between the initiation of PNVP formation and the start of neuronal differentiation at HH16-18 has been shown by immunostaining quail embryos with QH1 to label endothelial cells and TuJ1 to identify neurons. Angiogenic sprouts initially invade the neural tube on either side of the floor plate and although bilateral connections are subsequently formed over the roof plate, the vascular system of both sides remain separated by the floor plate and notochord for quite some time. The sprouts ingress into the TuJ1-positive area containing differentiated neurons and avoid the TuJ1-negative medial area containing proliferative neural progenitor cells (Kurz *et al.*, 1996; James *et al*., 2009; Kurz, 2009). In the guidance of tip cells, the transmembrane receptor NRP1 is required in addition to VEGFA signalling. The analysis of endothelial tip cell guidance in the mouse hindbrain has revealed a role of NRP1 in allowing tip cell filopodia to switch substrate and branch in a new direction within the subventricular zone (Gerhardt *et al*., 2004).

NRP1 and neuropilin-2 (NRP2) are single pass transmembrane proteins highly conserved in vertebrates. Neuropilins (NRPs) were first identified in the developing *Xenopus* nervous system as an epitope recognised by a monoclonal antibody that labels specific subsets of axons (Takagi *et al*., 1987; Fujisawa *et al*., 1989; Takagi *et al*., 1991) and studied as an adhesion molecule in the developing chick nervous system (Takagi *et al*., 1995). NRP1 was found to be highly expressed on the axons of neurons, acting as a receptor for semaphorins by forming a complex with plexin receptors in the control of axon guidance (He & Tessier-Lavigne, 1997; Kolodkin *et al*., 1997; Chen *et al*., 1997; Giger *et al.*, 1998; Takahashi *et al*., 1999). The mechanism of semaphorin 3 (SEMA3) proteins in the repulsion of axon growth has been well studied (Fujisawa, 2004), although a chemoattractant role was first shown for cortical pyramidal neurons in which SEMA3A acts as a chemorepellent for axons but as a chemoattractant for apical dendrites (Polleux *et al*., 2000). NRP1 was later discovered as a co-receptor for VEGF165 in endothelial cells and tumour cells by

forming a receptor complex with VEGFR2 to enhance the VEGFA-VEGFR2 interaction (Soker *et al*., 1998; Gluzman-Poltorak *et al*., 2000). In modulating endothelial cell motility *in vitro,* SEMA3A and VEGF165 compete for NRP1 binding sites as the binding of SEMA3A to NRP1 inhibits the binding of angiogenic-promoting VEGF165 to NRP1 and vice versa (Miao *et al*., 1999). However, studies conducted *in vivo* have found no evidence for competition between SEMA3A and VEGF165 for binding NRP1 during vascular or neuronal growth (Vieira *et al*., 2007). In addition to VEGF165, NRP1 also binds VEGF189 and VEGF121. Biochemical studies have shown that VEGF189 binds NRP1 at a higher affinity than VEGF165, which is likely due to the presence of exons 6, 7 and 8. The domain encoded by exon 8 carries a C-terminal arginine residue that mediates the binding of VEGF121 to NRP1, which occurs at an affinity that is ten times lower than that of VEGF165. *In vivo* studies involving *in situ* ligand-binding assays with VEGFA isoforms on mouse brain tissue have demonstrated that VEGF165, but not VEGF121, can bind NRP1-expressing axon tracts (Vieira *et al*., 2007; Pan *et al*., 2007; Vintonenko *et al*., 2011; Parker *et al*., 2012; Tillo *et al*., 2015). Further studies have also shown that NRP1 present in endothelial cells and β8 integrin in neuroepithelial cells cooperatively regulate sprouting angiogenesis by mediating adhesion and signalling events between blood vessels and the neuroepithelium through balancing TGFβ signalling during embryonic brain development (Hirota *et al*., 2015). NRP1 is now known to be essential for the vascularisation of the mouse spinal cord (Kawasaki *et al*., 1999), forebrain (Gu *et al*., 2003), hindbrain (Gerhardt *et al*., 2004) and retina (Fantin *et al*., 2014; Gelfand *et al*., 2014; Raimondi *et al*., 2014; Fantin *et al*., 2015; Aspalter *et al*., 2015) and recent evidence suggests that NRP1 can control brain angiogenesis independent of VEGFA. Mice expressing NRP1 with a homozygous mutation of tyrosine 297 (Y297A/Y297A), which is a residue important for the high affinity binding of VEGFA165, lead to a loss of VEGFA binding and attenuated NRP1 expression. The NRP1 (Y297A/Y297A) mice were born at normal Mendelian ratios although postnatal mortality was increased and mild impairment to angiogenesis of the hindbrain was exhibited (Fantin *et al*., 2014). In addition to this, the brain of $NRP1^{VEGF-}$ mice with abolished VEGFA-NRP1 binding exhibited normal developmental angiogenesis and mutants survived into adulthood (Gelfand *et al*., 2014).

The class 3 semaphorin SEMA3E is a traditional repulsive axon guidance cue that does not bind to NRP1 but instead binds directly to Plexin-D1 (Gu *et al*., 2005). SEMA3E-Plexin-D1-mediated repulsion can however be converted into axonal attraction in CNS neurons by the extracellular domain of NRP1 during brain development (Chauvet *et al*., 2007). SEMA3E-Plexin-D1 signalling is also involved in regulating angiogenesis via a VEGFA-induced feedback mechanism. In the developing mouse retina, SEMA3E is secreted by retinal neurons and is evenly distributed throughout the retina. However, SEMA3E-Plexin-D1 signalling is spatially regulated by high levels of VEGFA secreted from the avascular periphery, which induces Plexin-D1 expression in endothelial cells at the front of sprouting vessels. Gain-of-function experiments have shown that SEMA3E-Plexin-D1 signalling decreases VEGFA-induced Dll4 expression *in vitro* and *in vivo*, whereas the loss of SEMA3E-Plexin-D1 signalling has been demonstrated to upregulate Dll4 expression and Notch activity in the retina, thereby impairing the formation of tip cells (Kim *et al*., 2011).

The Hedgehog (Hh) signalling pathway is also required during CNS vascularisation and is positively regulated by NRPs. The expression of NRPs during mouse development has been shown to coordinate with active Hh signal transduction. A positive feedback circuit exists as Hh signalling induces the transcription of NRP1 and the overexpression of NRP1 results in increased activation of Hh target genes (Hillman *et al*., 2011). The three mammalian Hedgehog homologues are Shh, Desert hedgehog (Dhh) and Indian hedgehog (Ihh), of which Shh is the best studied. Shh is a secreted protein produced by the notochord and floor plate, and is involved in the dorsoventral patterning of the neural tube (Echelard *et al*., 1993). Shh is also involved in modulating angiogenic sprouting and BBB establishment during the vascularisation of the CNS. In the mouse embryo, motor neurons in the ventral neural tube in close proximity to the infiltrating vessels express the angiogenic factors VEGFA and angiopoietin-1 (Ang-1). Inhibiting the induction of motor neurons in the neural tube of cultured mouse embryos through the application of cyclopamine, a pharmacological inhibitor of Shh, dramatically impaired vessel ingression and motor neurons were almost completely lost. A reduction in the expression of Ang-1 within the neural tube was found in embryos treated with cyclopamine, leading to the suggestion that Shh signalling is indirectly required for

regulating angiogenic sprouting in the neural tube by establishing populations of Ang-1 positive motor neurons that guide ingressing vessels (Nagase *et al*., 2005). However, impaired vessel ingression may have been brought about by general patterning defects as cyclopamine not only results in defective motor neuron formation but generally impairs the patterning of the ventral neural tube. Further investigation into the effects of specific patterning molecules on vessel ingression is therefore required. The subsequent formation of the BBB is also promoted by Shh signalling. The secretion of Shh by astrocytes and the expression of Hh receptors by associated endothelial cells stabilises the nascent BBB by reducing vascular permeability. Furthermore, the Hh pathway prevents autoimmune attacks by decreasing the expression of proinflammatory mediators and also limits the secretion of chemokines from the endothelium, which reduces the migration of leukocytes (Alvarez *et al*., 2011).

The tight coordination between neurogenesis and vascularisation of the developing brain is further supported by additional factors common to both processes. Wnt signalling is a crucial stem cell regulator and plays an important role in regulating synaptic structure and function during the development of the nervous system (Ciani & Salinas, 2005; Inestrosa & Arenas, 2010; Kühl & Kühl, 2013). Neural progenitors regulate the ingression of blood vessels into the brain through VEGFA signalling and the canonical Wnt pathway, as well as stabilising nascent vessels by downregulating Wnt/β-catenin signalling (Santhosh & Huang, 2015). Whereas VEGFA signalling is ubiquitously active in sprouting angiogenesis, canonical Wnt signalling is specific for the vascularisation of the CNS and is active in endothelial cells of both the PNVP and INVP. The CNS-specific deletion of Wnt7a and Wnt7b, which are normally highly expressed by the embryonic spinal cord, or the vascular-specific loss of β-catenin in developing mice, resulted in the reduction of neural tube vascularisation and disorganisation of neural tissue. Vessels that did ingress were dilated and haemorrhagic and the distribution of INVP endothelial cells and pericytes were defective (Stenman *et al*., 2008; Daneman *et al*., 2009). Canonical Wnt signalling in endothelial cells is therefore crucial for normal formation of the PNVP and the proper ingression of blood vessels to form the INVP. The integrity of nascent brain vessels is also promoted by neural progenitors through αvβ8 integrin activation of TGFβ signalling (Santhosh & Huang, 2015).

Bone morphogenetic protein (BMP) together with Wnt signals are potent inhibitors of neurogenesis and have critical roles in the development of the telencephalon by maintaining the proliferation of NS cells (Furuta *et al*., 1997; Galceran *et al*., 1999; Shou *et al*., 1999; Lee *et al*., 2000; Caronia *et al*., 2010). BMP signalling has also been investigated as a regulator of vessel sprouting. The analysis of early vascular development in zebrafish has identified BMP as a vein-specific angiogenic cue, regulating angiogenic sprouting from the axial vein and not the dorsal aorta, independently of VEGFA signalling (Wiley *et al*., 2011). The same group found that the context-dependent proangiogenic function of BMP2 is mediated by a cargo-specific adapter protein for clathrin, disabled homolog 2 (Dab2), which functions in the internalisation of BMP receptors in endothelial cells and the phosphorylation of Sma and Mad Related Family (SMAD) 1, 5 and 8 (Kim *et al*., 2012). In mouse studies, an endothelial-specific member of the BMP/TGF-β receptor family, activin receptor-like kinase 1 (ALK1), has been shown to cooperate with the Notch pathway to inhibit angiogenesis. Blocking ALK1 resulted in hypervascularisation and arteriovenous malformations of the postnatal mouse retina, further exacerbated by the combined blockade of Notch signalling (Larrivée *et al*., 2012). The requirement of SMAD1 and SMAD5-mediated BMP signalling in the developing vasculature has also been investigated in the mouse embryo. The co-inactivation of endothelium-specific *SMAD1* and *SMAD5* resulted in impaired Dll4/Notch signalling, increased numbers of tip-cell-like cells at the expense of stalk cells, excessive sprouting and embryonic lethality. Evidence for a regulatory circuit has therefore been provided in which BMP/TGF-β-Smad1/5 synergises with Notch signalling in endothelial cells to orchestrate the selection of tip and stalk cells during sprouting angiogenesis (Moya *et al*., 2012).

FGF is also involved in angiogenesis in addition to its crucial role in the specification of mesoderm together with BMP (Yamaguchi *et al*., 1994; Deng *et al*., 1994; Tang *et al*., 1998; Saxton & Pawson, 1999; Marom *et al*., 2005) and its differentiation towards haematopoietic and endothelial cell fates (Yamaguchi *et al*., 1994; Sirard *et al*., 1998; Chang *et al*., 1999). The FGF family of proteins are highly conserved in gene structure and amino-acid sequence and are involved in diverse cellular processes during development including cell migration, differentiation, proliferation, cell adhesion and apoptosis. FGFs bind with high affinity to HSPGs

both on the cell surface and within the ECM. The release of HS-bound FGF from this reservoir ensues in a controlled manner by the action of HS-degrading enzymes, such as heparanases, thereby regulating the growth of capillary blood vessels. FGF binds to and activates RTK cell-surface FGF receptors (FGFRs), FGFR1-4, with HSPGs also acting as a co-receptor in order to modulate its biological effects (Vlodavsky *et al*., 1991; Johnson & Williams, 1993; Ornitz, 2000; Ornitz & Itoh, 2001). FGF1 and FGF2 are the best studied FGFs and are more potent angiogenic factors than VEGFs or PDGF (Cao *et al*., 2003). VEGFs, FGF and PDGF each have unique roles during angiogenesis, however, combinations of the three growth factors have been shown to have synergistic effects and increase angiogenesis *in vitro* and *in vivo* (Kim *et al*., 2015).

Crystallography studies have revealed that the low affinity binding of FGF2 to FGFR1 is stabilised by the presence of heparin or heparin sulfates, resulting in the formation of a dimer containing two FGF:FGFR1 complexes (Plotnikov *et al*., 1999). FGFR1 is required for the development and maintenance of the vasculature and has been demonstrated by infecting human umbilical vein endothelial cells (HUVECs) and injecting mouse embryos with an adenovirus expressing a dominant-negative form of FGFR1. The expression of the dominant-negative FGFR in HUVECs resulted in a reduction in endothelial cell number and the activation of mitogen-activated protein kinase (MAPK) phosphorylation by FGF2 was selectively inhibited. In embryos, expression of the dominant-negative FGFR resulted in abnormal development as neural folds did not fuse and the turning of the embryos within the yolk sac was incomplete. The vascular integrity was also disrupted as embryos displayed a poorly developed primitive intracranial vasculature and in 50% of embryos, the primary capillary plexus surrounding the forebrain was absent (Lee *et al*., 2000).

FGFR1-mediated signalling is known to activate a number of intracellular signalling cascades including the Ras pathway, Src family tyrosine kinases (SRKs) and phosphoinositide 3-kinase (PI3K). In the chicken chorioallantoic membrane (CAM), angiogenesis has been shown to be induced by FGF and VEGFA. The Ras-mitogen-activated protein kinase (MAPK) signalling cascade is important in FGF-stimulated angiogenesis. The pathway initiates as activated Ras recruits and activates Raf,

which phosphorylates the protein kinase, MEK. MEK activates the final kinase, extracellular signal-regulated protein kinase (ERK), in the Ras-Raf-MEK-ERK pathway, resulting in the expression of genes involved in the regulation of cell proliferation, growth and survival. Treatment with a specific MEK inhibitor, PD98059, which prevents its ability to phosphorylate and activate ERK, blocked FGF-induced angiogenesis (Eliceiri *et al*., 1998). FGF and VEGFA have been shown to stimulate distinct angiogenic pathways in corneal or chorioallantoic membrane models as the induction of angiogenesis by FGF depends on αvβ3 integrin, whereas initiation by VEGFA depends on αvβ5 integrin. The administration of nitric oxide (NO) synthase inhibitors have demonstrated that NO synthase lies downstream from VEGFA- but not FGF2-stimulated angiogenesis (Friedlander *et al*., 1995; Ziche *et al*., 1997). Furthermore, FGF and VEGFA can both activate Src kinase activity. However, Src activity is selectively required for endothelial cell survival during VEGFA-, but not FGF-, induced angiogenesis. CAMs were stimulated with either FGF or VEGFA and subsequently infected with a kinase-deleted Src 251-containing retrovirus. The introduction of the dominant negative Src kinase cytoplasmic tyrosine kinase was shown to inhibit angiogenesis in CAMs stimulated with VEGFA but not those stimulated with FGF (Eliceiri *et al*., 1999). In endothelial cells, PI3K has been found to regulate the expression of VEGFA and is also required for normal angiogenesis in the embryo (Jiang *et al*., 2000).

Similar to VEGFA, FGF promotes endothelial cell proliferation and stimulates the secretion of proteases and plasminogen activators from endothelial cells, leading to the degradation of the basement membrane. Endothelial cells invade the surrounding matrix, proliferate and differentiate to form a nascent vessel, the stability of which is generated through the secretion of growth factors by the endothelial cells, including PDGF, which attract supporting cells such as pericytes to the site (Carmeliet, 2000; Cross & Claesson-Welsh, 2001). CNS pericytes originate from neural crest and mesodermal cells and are located at the abluminal surface of capillary blood vessels. The specialised cells vary in morphology and express a variety of different histological markers including PDGFRB, CD13, NG2, desmin and vimentin, constituting a heterogenic cell population that performs multiple functions in vascular homeostasis during angiogenesis, vessel stabilisation and blood

flow regulation (reviewed by Trost *et al*., 2016). Pericytes induce the polarisation of astrocyte end-feet that surround CNS blood vessels and are crucial in determining the vascular permeability of the BBB during development. The interaction between pericytes and CNS endothelial cells is necessary in regulating functional aspects of the BBB by preventing the exchange of molecules across the endothelium, which complements the barrier role of the inter-endothelial tight junctions. Pericytes inhibit the expression of molecules that increase vascular permeability and studies in pericyte-deficient mouse mutants have shown an elevation in endothelial transcytosis, thus increasing BBB permeability (Armulik *et al*., 2010; Daneman *et al*., 2010). The molecular crosstalk between cells that constitute the neurovascular unit is regulated by a number of factors including Shh, BMP, PDGF, TGFβ and integrins and disruption to these signalling pathways leads to perturbation of the BBB (Armulik *et al*., 2010; Daneman *et al*., 2010; Li *et al*., 2011; Hirota *et al*., 2011; Alvarez *et al*., 2011; Arnold *et al*., 2012; Allinson *et al*., 2012).

The homeodomain-containing transcription factor, Pax6, functions in neurogenesis and also contributes to CNS angiogenesis. Radial glial cells, commonly referred to as apical progenitors, are a major NS cell population in the developing CNS that initially exist in the neural tube as neuroepithelial stem cells (Alvarez-Buylla *et al*., 2001; Anthony *et al*., 2004; Götz & Huttner, 2005; Kriegstein & Alvarez-Buylla, 2009). Pax6 is highly conserved among vertebrate and invertebrate species and plays an essential role in regulating radial glial cell neurogenesis. The expression of Pax6 has been shown to be localised in radial glial cells within the ventricular zone of the developing mouse cortex in a high rostrolateral to low caudomedial gradient, with the highest levels present at the onset of corticogenesis (Götz *et al*., 1998; Heins *et al*., 2002; Bibel *et al*., 2004; Englund *et al*., 2005; Manuel *et al*., 2015). Studies on homozygous mouse mutant embryos that lack the functional Pax6 protein showed a disruption in the dorsoventral regionalisation of the telencephalon. Mutant embryos displayed a ventralisation of the molecular patterning, thereby revealing an essential role of Pax6 in the regulation of forebrain morphogenesis (Stoykova *et al*., 2000).

Pax6 is also involved in the initiation of neurogenesis in the spinal cord. The timing of Pax6 activation in the neural tube is regulated by FGF signalling from the

presomitic mesoderm, which has been shown to exert an inhibitory effect on Pax6 expression in chick embryos. FGF8 is present in the presomitic mesoderm in a decreasing caudorostral gradient and grafting FGF8-soaked beads at the level of the neural tube inhibits the activation of Pax6. Conversely, disrupting FGF8 signalling by blocking FGFR1 transduction with the protein tyrosine kinase (PTK) inhibitor, SU5402, results in premature activation of Pax6 in the neural plate (Bertrand *et al*., 2000). Pax6 has also been identified as a downstream target of the Wnt/ß-catenin pathway and its activation by the binding of the ß-catenin/Tcf complex to the Pax6 promoter has been demonstrated *in vitro*. Furthermore, the genetic ablation of ß-catenin in mice has been shown to inhibit the formation of the neocortex by disrupting the development of radial glial cells. The level of Pax6 expression observed in the mutants had dramatically decreased in these cells and also in sphere-forming NS cells (Gan *et al*., 2014).

The quantitative levels of Pax6, VEGFA and phosphatase and tensin homolog (PTEN) expression are independent prognostic genetic markers of outcome for patients with astrocytic malignant gliomas (Zhou *et al*., 2003). A common characteristic of locally advanced solid tumours and malignant progression is hypoxia, which induces processes including angiogenesis in order to survive or escape the oxygen-deficient environment. Changes in oxygen levels lead to changes in the expression of oxygen homeostasis regulatory genes, one of which is the transcription factor hypoxia-inducible factor 1 alpha (HIF-1α). HIF-1α is degraded by the proteosome under normoxic conditions, however under hypoxic conditions, HIF-1α is stabilised and mediates the cellular responses in adapting to hypoxic stress by activating the expression of specific genes involved in both angiogenesis and tumourigenesis. HIF-1α promotes angiogenesis by inducing the expression of VEGFA, thus directing the migration of endothelial cells towards the hypoxic environment (Carmeliet *et al*., 1998; Hewitson & Schofield, 2004; Vaupel, 2004; Déry *et al*., 2005; Ziello *et al*., 2007). The HIF-1 pathway is therefore a therapeutic target with a major impact in cancer and ischaemic disease. PTEN suppresses VEGFA expression by downregulating HIF-1α which is mediated by inactivating the oncogenic PI3K/Akt signalling pathway active in malignant gliomas (Gomez-Manzano *et al*., 2003). A tumour suppressor function of Pax6 has also been identified in glioma cells in which it downregulates glioma cell expression of

VEGFA resulting in the suppression of angiogenesis, independent of the canonical pathway through PI3K/Akt-HIF-1α signalling or the von Hippel-Lindau tumour suppressor gene (VHL) (Zhou *et al*., 2005; Zhou *et al*., 2010). Pax6 has been shown to increase the susceptibility of glioma cells to detachment, an early event in tumour invasion, and to oxidative stress from both the necrotic zone and increased intracellular reactive oxygen species (ROS) following detachment (Chang *et al*., 2007). The function of Pax6 in suppressing cell invasion in glioblastoma multiforme (GBM) involves repressing the expression of proinvasive genes including MMP-2. *In vitro* Matrigel invasion assays have demonstrated that the invasiveness of GBM cells is suppressed by Pax6, which requires its DNA-binding domain. Reverse transcription-polymerase chain reaction (RT-PCR) has also indicated a significant reverse correlation between Pax6 and MMP-2 expression in 41 GBMs, 43 anaplastic astrocytomas and 7 adjacent normal tissues. The stable overexpression of Pax6 has been shown to repress MMP-2 expression in the GBM cell line U251HF grown *in vitro* and also within intracranial xenografts in nude mice. Furthermore, electrophoretic mobility shift assays have demonstrated that Pax6 binds directly to the MMP-2 promoter in a sequence specific manner and a Pax6-specific binding site in a 245 base pair (bp) region (-177 to +68) of the MMP-2 promoter has been identified (Mayes *et al*., 2006). Conversely, in studies of lung cancer tissue and cell lines, Pax6 mRNA is highly expressed and promotes cell growth by activating the MAPK pathway, resulting in faster progression into the S phase of the cell cycle (Zhao *et al*., 2014).

1.7 The regulation of angiogenesis by ETS and MADS box transcription factors

The development of the vasculature is regulated by intrinsic factors, including the E-twenty six (ETS) transcription factors and myocyte enhancing factor 2C (*Mef2c),* in addition to the extrinsic factors, such as VEGFA and FGF. The ETS transcription factors play important roles in the development of endothelial cells and are characterised by a highly conserved winged helix-turn-helix DNA binding domain that recognises the ETS DNA binding site, containing the sequence 5'-GGA(A/T)-3', present in the regulatory regions for almost all endothelial cell-specific genes. While many ETS factors act as transcriptional activators, some are associated with transcriptional repression, regulating a large number of genes involved in several

biological processes including development, migration and proliferation. *Ets1*, *Etv2*, *Erg* and *Fli-1* are among a subset of ETS family members that have important roles in angiogenesis and vasculogenesis (Sementchenko *et al*., 2000; Dejana *et al*., 2007; Randi *et al*., 2009; Heo *et al*., 2010; Marcelo *et al*., 2013).

The differentiation of endothelial cells from mesodermal progenitors involves the activity of many ETS factors and a critical evolutionarily conserved role for *Etv2* (Etsrp, ETS variant 2), which has been lost in the evolution of birds, has recently been identified. *Etv2* is highly expressed in haematopoietic and endothelial cell precursors, which targets many ETS genes during development. In differentiating ES cells, Etv2 directly activates other *Ets* genes, thereby establishing a hierarchical expression of ETS factors in which Etv2 functions at the top, followed by sequential induction of *Fli1*, *Erg*, *Elk3*, *Ets1* and *Ets2*. Initially, *Etv2* expression is widespread within the primitive streak mesoderm and subsequently becomes restricted to the developing vascular endothelial cells. Once endothelial cells begin to mature, its expression is rapidly downregulated. *Etv2* is both necessary and sufficient for initiating vasculogenesis and in newly forming endothelial cells, *Etv2* induces *VEGFR2* expression, promoting the commitment of these cells to an endothelial fate. The morpholino knockdown of Etsrp protein function or mutations within the *Etsrp* gene leads to the complete absence of circulation in developing zebrafish embryos and a significant reduction in the expression of vascular endothelial markers including *VEGFR2* and *VE cadherin*. Conversely, the overexpression of *Etv2* results in an expansion of endothelial cell differentiation *in vivo*, detected by the ectopic expression of endothelial markers in multiple cell types (Sumanas & Lin, 2006; Pham *et al*., 2007; Sumanas *et al*., 2008; Lee *et al*., 2008; De Val *et al*., 2008; Salanga *et al*., 2010; Kataoka *et al*., 2011; reviewed by Marcelo *et al*., 2013; Liu *et al*., 2015).

The *in vivo* expression of Ets1 protein by endothelial cells during angiogenesis has been demonstrated by immunohistochemical analysis using a murine model for angiogenesis. Furthermore, in the initiation of angiogenesis, growth factors including VEGFA, FGF and epidermal growth factor (EGF) have been shown to induce the expression of Ets1 in HUVECs, immortalised HUVECS and human omental microvascular endothelial cells (HOMECs), which in turn induces the

expression of the serine protease uPA, MMP-1, MMP-3 and MMP-9. Cell migration is also induced, converting these cells to an angiogenic phenotype. The importance of Ets1 as a molecular target for regulating angiogenesis is revealed through the study of these downstream mechanisms. Blocking the expression of Ets1 has been shown to significantly inhibit the expression of uPA and MMP-1. Cell migration is prevented as Ets1 also controls the expression of genes involved in cell attachment and endothelial cell migration, including αv integrins, β2 and β3 integrins, intracellular adhesion molecules (ICAMs) and VE cadherin, ultimately leading to the inhibition of angiogenesis (Iwasaka *et al*., 1996; Sato, 1998; Kita *et al*., 2001).

The gene regulatory events implicated in controlling sprouting angiogenesis also involves the specific induction of the MADS box transcription factor *Mef2c*, by VEGFA and FGF2, which also functions in muscle cell differentiation and the specification of numerous cell types. Embryonic lethality in Mef2c-/- mutant mice results from prominent heart defects and vascular malformations in which endothelial cells fail to properly arrange into a vascular plexus (Bi *et al*., 1999; Schweighofer *et al*., 2009; del Toro *et al*., 2010; Rivera *et al*., 2011). Whereas Ets1 primarily acts to promote angiogenesis, Ets1 directly activates Mef2c in endothelial cells resulting in a strong inhibitory effect on angiogenic sprouting, a response mediated by alpha-2-macroglobulin (A2M), affecting cell migration and not proliferation. The Mef2c/A2M axis is suggested to adapt sprouting activity to local oxygen concentration. Hypoxia is the initial trigger for VEGFA production and in hypoxic conditions Mef2c induction is much less pronounced and A2M upregulation is prevented when compared with normoxia. The Mef2c/A2M pathway therefore functions as a negative feedback mechanism in endothelial cells to prevent inappropriate sprouting and excess angiogenesis under normoxic conditions when sufficient levels of oxygen are reached after neovascularisation (De Val *et al*., 2004; Hickey & Simon, 2006; Sturtzel *et al*., 2014).

1.8 The role of MMPs in angiogenesis

MMPs play a crucial role in angiogenesis, vascular disease and tumour progression with research focusing on elucidating the regulatory networks involved during development, physiological conditions and various pathologies in order to identify

MMPs and inhibitors as prognostic markers and targets for therapy (Duffy & McCarthy 1998, Amin *et al*., 2016; Yang *et al*., 2016; King, 2016). The remodelling of the ECM is an integral aspect in developmental processes, liberating cells and subsequently enabling their response to a variety of signals. MMPs, also designated matrixins, are a large family of zinc-dependant endopeptidases that can be categorised into various groups (Table 1i). MMPs are involved in remodelling the ECM during normal physiological processes, such as embryonic development and tissue repair, as well as in pathological conditions including arthritis and tumour metastasis (Visse & Nagase, 2003). Thus, MMPs are likely to be implicated in the interaction between the ingressing endothelial cells and the cells and ECM of the developing brain. MMPs hydrolyse structural components present in the ECM such as collagen, elastin and gelatin, together with cell surface molecules involved in a variety of biological processes including CD44, E-cadherin and Fas-ligand (Visse & Nagase, 2003). The precise and complex regulation of MMP activity ensues at multiple levels including transcriptional control, activation of the secreted zymogens, or inactive precursors referred to as procollagenases (proMMPs), the presence and activity of endogenous inhibitors and interaction with specific components of the ECM (Nagase & Woessner, 1999; Woessner & Nagase, 2000; Hiller *et al*., 2000).

The involvement of proteases in angiogenesis is well-established (Egeblad & Werb, 2002) and extracellular proteases are essential in remodelling the ECM during CNS vascularisation for the migration of endothelial cells towards the neural tube and for the penetration of the basal lamina by tip cells during ingression (Fig. 1vi). It is also important to note that the organisation of the endothelial sprout with a leading tip cell and the follower stalk cells is similar to invasive cell migration by certain cancers, which is facilitated by pericellular proteases. Extracellular proteolysis and ECM degradation play a crucial role in tumour invasiveness and metastasis and a well-established correlation exists between metastatic potential and the expression of proteases and heparinases.

Table 1i. Classification of MMPs. Members of the MMP family can be classified into various groups based on domain architecture and functional diversity. The activity of MMPs is precisely regulated under normal physiological conditions at both transcriptional and translational level through the combination of *cis*-regulatory elements, epigenetic mechanisms, proMMP activation, interaction with ECM components and mechanisms of inhibition by endogenous inhibitors. Collagenases include MMP-1, MMP-8, MMP-13 and MMP-18 (*Xenopus*), which cleave interstitial collagens as well as other ECM and non-ECM molecules. Gelatinases, MMP-2 and MMP-9, have three repeats of a type II fibronectin domain located inside the catalytic domain, which allows the binding and processing of gelatin, collagens and laminin. MMPs -2 and -9 also degrade fibronectin, elastin, aggrecan and vitronectin as well as non-ECM molecules. Stromelysins, MMP-3, MMP-10 and MMP-11, are unable to cleave native collagen but can degrade many different ECM components and process bioactive substrates including E-cadherin and stromal-cell derived factor-1. Stromelysins can also participate in the activation of a number of proMMPs. Matrilysins, MMP-7 and MMP-26, lack a hemopexin domain and digest a number of ECM components. MMP-7 also catalyses the ectodomain shedding of cell surface molecules including Fas ligand and E-cadherin. MT-MMPs are classified into type I transmembrane proteins and GPI-anchored proteins. Type I transmembrane proteins (MT1-MMP, MT2-MMP, MT3-MMP and MT5-MMP) cleave various substrates and are major activators of proMMP-2. The second subgroup includes MT4-MMP and MT6-MMP, which are bound to the cell surface with a GPI-anchor. MT6-MMP processes gelatin, collagen IV, fibrin, fibronectin and proteoglycans, whereas MT4-MMP shows low enzymatic activity against ECM components. A third subgroup, consisting of MMP-23A and MMP-23B, are type II transmembrane MMPs that have the same amino acid sequence but are encoded by distinct genes in the human genome. These MMPs lack the cysteine switch motif, the hemopexin domain and the signal peptide that are characteristic of all MMPs, but contain cysteine-array and immunoglobulin domains in the C-terminal tail. Several MMPs are not classified in the above categories due to their divergence and substrate specificity: MMP-12 is the most potent elastolytic enzyme that also digests a number of other proteins and is essential for macrophage migration; MMP-19 is a potent enzyme against components of basement membranes including type IV collagen and tenascin, as well as gelatin and aggrecan; MMP-20 digests amelogenin and is secreted by ameloblasts and odontoblasts during the formation of tooth enamel; MMP-27 was first cloned from chicken fibroblasts and degrades gelatin and casein; and MMP-28 is mainly expressed in keratinocytes and may function in tissue hemostasis and wound repair. The functions of MMP-21 and MMP-22 are not well understood.

COLLAGENASES

MMP-1 (collagenase 1, interstitial collagenase)

MMP-8 (collagenase 2, neutrophil collagenase)

MMP-13 (collagenase 3)

MMP-18 (collagenase 4, *Xenopus*)

GELATINASES

MMP-2 (gelatinase A, 72 kDa type IV collagenase)

MMP-9 (gelatinase B, 92 kDa type IV collagenase)

STROMELYSINS

MMP-3 (stromelysin 1)

MMP-10 (stromelysin 2)

MMP-11 (stromelysin 3)

OTHER MMPs

MMP-12 (macrophage elastase, metalloelastase)

MMP-19

MMP-20

MMP-21 (XMMP, *Xenopus*)

MMP-22

MMP-27 (CMMP, *Gallus*)

MMP-28 (Epilysin)

MEMBRANE-TYPE MMPSs

Type I transmembrane:

MMP-14 (MT1-MMP)

MMP-15 (MT2-MMP)

MMP-16 (MT3-MMP)

MMP-24 (MT5-MMP)

Type II transmembrane:

MMP-23A

MMP-23B

Glycosylphosphatidylinositol (GPI) anchored:

MMP-17 (MT4-MMP)

MMP-25 (MT6-MMP)

MATRILYSINS

MMP-7 (matrilysin 1)

MMP-26 (matrilysin 2)

Pericellular proteases have an intricate role in degrading matrix proteins during endothelial cell migration and invasion in addition to controlling the activation, liberation and modification of angiogenic growth factors and cytokines (Peretz *et al*., 1990; Leto *et al*., 1992; Garbisa *et al*., 1992; Sreenath *et al*., 1992; Park *et al*., 1993; van Hinsbergh *et al*., 2006; Wolf *et al*., 2007). The major groups of matrix-degrading proteases involved in regulating angiogenesis include the MMP family (Matrisian, 1990, 1992; Nagase *et al*., 2006), the adamalysin-related membrane proteases (ADAM family) (Wolfsberg *et al*., 1995), cathepsin cysteine proteases (Turk *et al*., 2001) and serine proteases (Kraut, 1977; Yoshida & Shiosaka, 1999), which are tightly controlled at several levels by specific activation and inhibition mechanisms including tissue inhibitors of metalloproteinases (TIMPs) (Gomez *et al*., 1997; Lambert *et al*., 2004), cystatins, kininogens (Turk *et al*., 2002), and serpins (Schapira & Patston, 1991). Other matrix-degrading proteases have also been shown to cooperate with MMPs as activated plasmin can activate various MMPs, including MMP-1, -2, -3 and -9, thus contributing to vascular remodelling (Davis *et al*., 2001).

The four major subgroups of MMPs include interstitial collagenases, gelatinases, stromelysins and membrane type (MT-) MMPs. Collagens are the most abundant proteins present in the ECM and the breakdown of which is initiated by collagenolytic MMPs, which cleave types I-III collagens at specific peptide bonds. MMP-1 (collagenase 1, interstitial collagenase), MMP-2 (gelatinase A, 72 kDa type IV collagenase), MMP-8 (collagenase 2, neutrophil collagenase), MMP-13 (collagenase 3) and MMP-18 (collagenase 4, *Xenopus*) are interstitial collagenases capable of cleaving triple helical collagen by hydrolysing a single Gly-Ile/Leu bond in the collagen α chains three-fourths from the N-terminus, generating 3/4 and 1/4-length fragments that are further degraded by other proteolytic enzymes (Gross *et al*., 1974; Miller *et al*., 1976; Birkedal-Hansen *et al*., 1993; Aimes & Quigley, 1995; Visse & Nagase, 2003).

1.8.1 MMP-1

In 1962, MMP-1 was the first MMP to be discovered as the anuran tadpole was found to have strong collagenolytic activity during metamorphosis. MMP-1 was subsequently purified from tadpole tail fin and back skin (Gross & Lapiere, 1962;

Nagi *et al*., 1966). MMP-1, also termed human fibroblast collagenase, was later discovered in a form, which when incubated with trypsin, resulted in a significant increase in activity that was accompanied by a 10 kDa loss in molecular weight. Furthermore, auto-activation of the procollagenase to yield the active enzyme form also occurred without a detectable change in molecular weight (Bauer *et al*., 1975; Stricklin *et al*., 1977). MMP-1 is initially synthesised in a preproenzyme form that is co-translationally processed to form the inactive procollagenase, which is secreted from the cell. The proenzyme, termed zymogen, has a characteristic structure similar to all MMPs consisting of a pro-peptide domain (PRO) and a catalytic domain (CAT) joined via a linker region to a hemopexin domain (HPX) (Fig. 1vii). The proteolytic activation of MMP-1 results in the removal of 81 amino acid residues from the amino-terminal section of the proenzyme, generating the active collagenase (Goldberg *et al*., 1986; Visse & Nagase, 2003; Jozic *et al*., 2005).

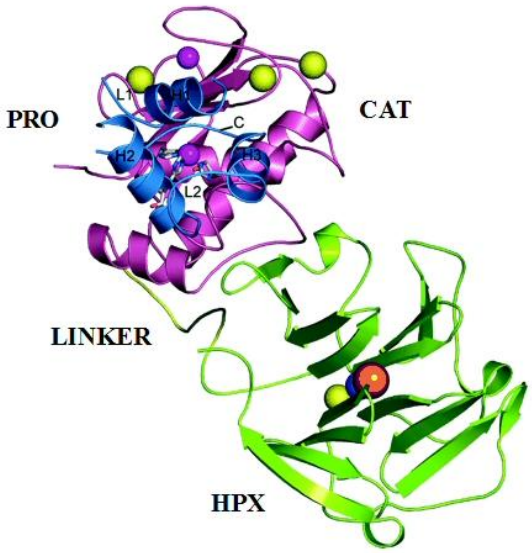

Figure 1vii. Crystal structure of inactive proMMP-1. The activity of the enzyme is inhibited by the PRO domain (blue) that maintains the MMP in zymogen form (proMMP) by binding to the CAT domain (purple), which interacts with the HPX domain (green). A water molecule essential for peptide hydrolysis is coordinated with the active site zinc present within the CAT domain. The activation of proMMPs requires disrupting the bond between the cysteine in the PRO domain and the zinc in the CAT domain, referred to as the Cys-Zn^{2+} cysteine switch. Removal of the PRO domain proceeds either by proteases or non-proteolytic agents as well as other MMPs (Nagase & Woessner Jr., 1999; Visse & Nagase, 2003; Jozic *et al*., 2005).

MMP-1 degrades interstitial collagens, types I, II and III and is ubiquitously produced by a variety of cells including stimulated fibroblasts, endothelial cells and macrophages. The expression of MMP-1 has been associated with increased angiogenesis in xenograft models of breast, melanoma and prostate cancer (Vincenti *et al*., 1996; Benbow *et al*., 1999; Boire *et al*., 2005; Blackburn *et al*., 2007; Pulukuri & Rao, 2008; Eck *et al*., 2009) and its activity has also been linked to tumour invasion, progression and poor prognosis (Murray *et al*., 1996; Murray *et al*., 1998; Nakopoulou *et al*., 1999; Airola *et al*., 1999, Inoue *et al*., 1999; Ito *et al*., 1999; Pickett *et al*., 1999; Kanamori *et al*., 1999; Korem *et al*., 1999; Nishioka *et al*., 2000; Ghilardi *et al*., 2001; Hinoda *et al*., 2002; Poola *et al*., 2005; Przybylowska *et al*., 2006). The control of angiogenesis occurs at multiple levels and several genes encoding matrix-degrading proteases are transactivated by the transcription factor Ets1. The expression of Ets1 and two of its target genes, MMP-1 and MMP-9, has been found in endothelial cells and stromal fibroblasts at the onset of stroma generation during the early stages of breast carcinogenesis, which becomes significantly upregulated in invasive ductal and lobular cancers (Behrens *et al*., 2001).

MMP-1 expression has been associated with increased angiogenesis through the activation of the protease-activated receptor (PAR), PAR1. PARs are G protein-coupled receptors (GPCRs) that are expressed by a number of cell types within the tumour microenvironment including endothelial cells, fibroblasts, macrophages and platelets (Ossovskaya & Bunnett, 2004; Boire *et al*., 2005; Blackburn & Brinckerhoff, 2008). PARs are unique as they carry their own ligand, which is masked under resting conditions. Activation of the receptor by proteolytic cleavage within the extracellular amino terminus exposes the tethered ligand domain, which binds to the body of the receptor, inducing signalling to intracellular G proteins and initiating multiple signalling cascades (Seeley *et al*., 2003), leading to changes in cellular morphology, migration, proliferation and adhesion (Hollenberg & Compton, 2002). The role of PAR1, a high-affinity thrombin receptor expressed in endothelial cells, has been investigated in breast carcinoma cells and its expression is both required and sufficient to promote the growth and invasion of xenografts in nude mice. Furthermore, MMP-1 activity derived from fibroblasts in the stromal-tumour microenvironment functions as a

protein agonist of the receptor. MMP-1 cleaves and activates PAR1, resulting in the generation of PAR1-dependent Ca^{2+} signals and the promotion of cell migration. The migration of cells is inhibited by blocking the pathway downstream of MMP-1 with cell-penetrating pepducin antagonists of PAR1, which prohibits signalling between the receptor and intracellular G proteins. Knocking down the expression of PAR1 with small interfering RNA (siRNA) also revealed that MMP-1 requires PAR1 to induce chemotaxis of cancer cells and angiogenesis (Boire *et al*., 2005). The role of MMP-1 in melanoma metastasis has been investigated in which the proangiogenic effect of tumour-derived MMP-1 was inhibited in a xenograft model using short hairpin RNAs (shRNA). The reduction of MMP-1 expression in tumour cells expressing MMP-1 shRNAs had diminished collagenase activity and significantly decreased the ability of the primary tumour to metastasize (Blackburn *et al*., 2007). Blocking PAR1 through the application of PAR1 antagonists in both *in vivo* and *in vitro* systems has shown to inhibit endothelial cell growth and proliferation as well as increase apoptosis, demonstrating that PAR1 has a key role in mediating angiogenesis. Furthermore, MMP-1 is suggested to induce cell proliferation and promote angiogenesis by activating nuclear factor-κB (NF-κB), which subsequently stimulates *VEGFR2* expression in endothelial cells (Zania *et al*., 2006; Mazor *et al*., 2013). Gene expression analysis in human microvessel endothelial cells has also revealed that the activation of PAR1 by MMP-1 results in the induction of a different subset of proangiogenic genes compared with thrombin-activated PAR1, which may better facilitate angiogenesis (Blackburn & Brinckerhoff, 2008).

Tumour-secreted proteinases are involved in breaching the BBB and MMP-1 plays a critical pathological role in brain metastasis of breast cancer. Upon examination of MMP expression in brain metastasis-free breast cancer patients and in breast cancer cell lines known to preferentially metastasise to the brain, only MMP-1 was found to be significantly upregulated in brain metastatic cell lines. Immunohistochemical analysis of tumours that metastasised in the brain of breast cancer patients revealed a strong expression of MMP-1 in both primary lesions and brain metastatic lesions in these patients. Furthermore, a weak expression of MMP-1 was found in primary tumours of patients with high grade

breast cancer that had not metastasised in the brain (Wu *et al*., 2015). Brain metastasis is promoted by MMP-1 by targeting and degrading claudin-5 and occludin, which are major components of tight junctions (Liebner *et al*., 2000; Abbott *et al*., 2010), resulting in enhanced BBB permeability. The expression of MMP-1 is promoted by cyclooxygenase COX2, a gene previously identified to mediate the passage of cancer cells through the BBB (Bos *et al*., 2009) that is highly upregulated in brain metastatic cells. COX2-induced prostaglandins directly promote MMP-1 expression and also activate tumour associated astrocytes to release chemokine ligand 7 (CCL7), which promotes the self-renewal of tumour-initiating cells within the brain (Wu *et al*., 2015).

MMP-1 has also been identified as a key factor in promoting the highly invasive behaviour of GBM cells and is regulated by epidermal growth factor receptor (EGFR). The aberrant overexpression of EGFR in GBM leads to sustained oncogenic signalling and has been shown to contribute to the induction of MMP-1 expression and glioma cell invasion in EGF-treated T98G cells, via the MAPK pathway. In addition to enhancing tumourigenicity, an increase in organised endothelial growth was detected as a consequence of MMP-1 overexpression. Tumour size was enhanced and the expression of anti-angiogenic factors, particularly TIMP-4, were inverse to the levels of MMP-1 (Anand *et al*., 2011; Pullen *et al*., 2012). A functional single nucleotide polymorphism in the MMP-1 promoter has also been identified that consists of either the presence or absence of a guanine nucleotide at position -1607, resulting in two genotypes referred to as the 2G or 1G allele, respectively. The presence of a guanine base creates a ETS DNA binding site that leads to increased MMP-1 transcription and promoter genotyping has shown that the 2G/2G genotype is more prevalent in glioblastoma tissue compared to healthy individuals (Rutter *et al*., 1998; McCready *et al*., 2005).

1.8.2 MMP-2 and MMP-9

The breakdown of the ECM is a critical event during invasion, therefore considerable attention has focussed on the gelatinases, MMP-2 (gelatinase A, 72 kDa type IV collagenase) and MMP-9 (gelatinase B, 92 kDa type IV

collagenase), due to their ability to degrade type IV collagen present in the basement membrane (Nakajima *et al*., 1987; Zeng *et al*., 1999). MMP-2 and MMP-9 are expressed as proenzymes that become activated to their 62 kDa and 82 kDa forms, respectively, once secreted into the extracellular environment. Three repeats of fibronectin type II domains are inserted in the catalytic domain, which bind to gelatin, collagens and laminin. MMP-2 and MMP-9 are key regulators of angiogenesis and analogous to the interaction of integrins with uPA/uPAR, they can be localised to the cell surface in their active form by binding to αvβ3 integrin and CD44, respectively, to promote focused proteolytic activity and cell-mediated invasion (Brooks *et al*., 1996; Brooks *et al*., 1998; Yu & Stamenkovic, 1999; Silletti *et al*., 2001; Chapman & Wei, 2001; Blasi & Carmeliet, 2002; Visse & Nagase, 2003).

The increased expression of MMP-2 and MMP-9 and the breakdown of type IV collagen in the basement membrane have been reported in various human cancers including colorectal, breast, prostate, ovarian, endometrial, bladder, skin, lung carcinomas and brain cancers (Pyke *et al*., 1992; Pyke *et al*., 1993; Brown *et al*., 1993; Rao *et al*., 1993; Davies *et al*., 1993a; Davies *et al*., 1993b; Hamdy *et al*., 1994; Sato *et al*., 1994; Tamakoshi *et al*., 1994; Liabakk *et al*., 1996; Zeng *et al*., 1999; Belotti *et al*., 2003; Qin *et al*., 2008) and has been associated with angiogenic microvessel density in pancreatic cancer (Xiang *et al*., 2016). Furthermore, a potential role has been suggested for MMP-2 and MMP-9 as biomarkers in predicting the response to treatment of high-grade gliomas. A baseline of high MMP-2 and low MMP-9 levels in the plasma prior to the administration of bevacizumab, a monoclonal antibody against VEGFA, has been associated with a high response rate, prolonged progression-free survival and overall survival in recurrent high-grade gliomas that are treated with bevacizumab (Tabouret *et al*., 2015).

Matrix-degrading proteases have a significant role in morphogenetic events and tissue remodelling during embryogenesis. The expression patterns of MMP-2 have been documented and analysed in the early avian embryo, revealing an essential role in cell motility during epithelial-mesenchymal transformations (EMTs). The distribution of MMP-2 RNA was detected using whole-mount *in*

situ hybridisation (ISH), followed by sectioning and labelling with the monoclonal antibody HNK-1 against neural crest cells; a transient, multipotent, migratory cell population unique to vertebrates that gives rise to diverse cell lineages including craniofacial cartilage and bone, smooth muscle, melanocytes, peripheral and enteric neurons and glia. Superimposition of the labelling patterns revealed that early migratory neural crest cells express MMP-2 as they detach from the neural tube during an EMT but is rapidly extinguished as the cells disperse. MMP-2 was also found to be expressed in the sclerotome and dermis at the time of EMT initiation and upon cell migration, which becomes downregulated once motility has ceased. Furthermore, MMP-2 expression was detected in mesenchyme where tissue remodelling was in progress, including the head mesenchyme, lateral plate mesoderm, limb dermis and in the developing feather germs. Inhibiting MMP activity with BB-94 and TIMP-2 prevented the EMT required to generate neural crest cells in tissue culture and *in vivo*, although the migration of cells that had already detached from the neural tube was unaffected. The acquisition of the HNK-1 epitope in cells retained in the dorsal neural tube following *in ovo* incubation with BB-94 revealed that neural crest cells do appear to be correctly specified, but were unable to detach. Similarly, the specific knockdown of MMP-2 expression by electroporating antisense morpholino oligonucleotides in the dorsal neural tube resulted in perturbation of the EMT but also did not affect the migration of neural crest cells that had already detached from the neural epithelium. The expression of MMP-2 therefore correlates with the generation of neural crest, sclerotome and dermatome, with a critical role in the transformation of epithelia to mesenchyme, together with dispersion of mesenchymal tissues later in development (Duong & Erickson, 2004).

MMP-9 is a target gene of Ets1 and has a critical role in stimulating the onset of tumour angiogenesis but subsequently also generates inhibitors including the cleavage fragment of basement membrane collagen IV, tumstatin, which suppresses angiogenesis through αvβ3 integrin expressed on pathological, but not on physiological, angiogenic blood vessels (Hamano *et al*., 2003). In supporting tumour growth, MMP-9 is supplied to the tumour microenvironment by tumour-associated macrophages (TAMs) and tumour-associated neutrophils (TANs)

(Coffelt *et al*., 2010; Deryugina *et al*., 2014). TAMs and TANs are infiltrating leukocytes implicated in regulating angiogenesis and are recruited to tumours by the release of tumour cell or stromal-derived chemoattractants (Mantovani *et al*., 2002; Fridlender *et al*., 2009; Ruffell *et al*., 2012; De Palma & Lewis, 2013; Tazzyman *et al*., 2013; Galdiero *et al*., 2013). TANs are major contributors of highly angiogenic MMP-9, supporting the intratumoural vasculature required for the development of metastasis. *In vivo,* the levels of angiogenesis mediated by neutrophil and TAN-delivered MMP-9 significantly exceed those induced by macrophages and TAMs. However, MMP-9-producing TAMs do not express its natural inhibitor, TIMP-1, but initiate only a relatively low-level production of TIMP-free MMP-9 zymogen following differentiation and polarisation compared with TANs (Deryugina *et al*., 2014).

Distinct patterns observed in the spatial distribution of MMP-9 and TIMP-1 mRNA expression had previously been demonstrated using ISH studies in human colorectal cancer (CRC) and liver metastases, suggesting distinct cellular origins and regulatory networks. The expression patterns of MMP-9 and TIMP-1 mRNA in liver metastases and primary CRCs were found to be similar and predominantly stromal in origin. MMP-9-positive cells were round in shape localised within the peritumour stroma or at the interface between the liver metastases lesion and surrounding normal liver. However, TIMP-1 mRNA was more diffuse and found throughout the tumour stroma. Immunohistochemical staining with the monoclonal antibody CD68 identified MMP-9-positive cells as macrophages, whereas TIMP-1 was detected in spindle-shaped stromal cells (Zeng *et al*., 1995).

The influence of MMP-9 on endothelial progenitor cell (EPC)-induced vascular remodelling following ischaemia has also been investigated. In response to ischaemia, EPCs are mobilised to the sites of neovascularisation where they differentiate into endothelial cells, increasing angiogenesis in the brain (Fan *et al*., 2010; Moubarik *et al*., 2011; Rosell *et al*., 2013). Mice subjected to cerebral ischaemia were treated with EPCs and after 3 weeks, an increase in the peri-infarct vessel density was observed in WT mice but not in MMP-9/KO mice, identifying MMP-9 as a key factor in stroke recovery (Morancho *et al*., 2015). Mesenchymal stem cell (MSC) treatment in a permanent model for ischaemic

stroke in rats has also been investigated, resulting in a significant increase in MMP-2 activity, vascular density and greater neurological recovery (Nam *et al*., 2015). Cell therapy involving the transplantation of EPCs and MSCs has therefore become a promising strategy for enhancing angio-vasculogenic responses in patients with ischaemic diseases. Recently, membrane-bound MMP-9 has been used as a marker for identifying and separating proangiogenic cells from early EPCs with implications in vascular regeneration (Kanayasu-Toyoda, 2016).

The effect of microRNAs (miRNAs) and small interfering RNAs (siRNAs) on angiogenesis through regulating MMP-2 and MMP-9 expression has also been investigated. miRNAs are small, non-protein-coding RNAs that negatively regulate the expression of target mRNAs by destabilising or inhibiting translation. The widely studied miRNA-21 (miR-21), is considered an oncogene involved in pro-angiogenesis (Zhao *et al*., 2013), apoptosis (Lan *et al*., 2015), proliferation (Wang *et al*., 2015), necrosis (Ma *et al*., 2015) and invasion (Li *et al*., 2015) and is significantly upregulated following spinal cord injury (SCI) in a rat model (Hu *et al*., 2013). The high expression of miR-21 in endothelial cells previously suggested a role in angiogenesis (Voellenkle *et al*., 2012). The upregulation of miR-21 has been shown to promote the survival, migration and tube formation of endothelial cells by targeting and decreasing the expression of TIMP-3, originally classified according to its ability to inhibit MMP-1, -2, -3 and -9. The expression and secretion of MMP-2 and MMP-9 are thus promoted, leading to the degradation of the ECM and endothelial cell migration (Apte *et al*., 1995; Zhang *et al*., 2011; Wang *et al*., 2013; Hu *et al*., 2016). TIMP-3 is an ECM component and a potent angiogenic inhibitor that limits the density of vessels in the vascular bed of tumours and can also curtail tumour growth by direct interaction with VEGFR2, blocking VEGFA binding and resulting in the inhibition of proliferation, migration and tube formation of endothelial cells, independent of MMP inhibition (Anand-Apte *et al*., 1996; Qi *et al*., 2003; Visse & Nagase, 2003; Cruz-Muñoz *et al*., 2006a; Cruz-Muñoz *et al*., 2006b). Further studies into miRNAs have suggested a potential therapeutic role of miRNA-195a-3p, which is highly expressed in mesenchymal stem cells (MSCs), as an inhibitor of angiogenesis. miRNA-195a-3p was found to negatively modulate angiogenesis

by targeting the transcript of MMP-2, resulting in the reduction of MSC proliferation and migration (Gao *et al*., 2016).

RNA interference technology using siRNAs has also been employed to further elucidate the roles of MMP-2 and MMP-9 in angiogenesis. The knockdown of the Annexin II receptor AXIIR in HUVECs, which is also a receptor for plasminogen (Flood & Hajjar, 2011), resulted in the significant inhibition of proliferation, migration, adhesion and tube formation *in vitro* and suppression of angiogenesis in nude mice. Cell cycle arrest was induced in the S/G2 phase by the siRNA directed against AXIIR and the expression of MMP-2 and MMP-9 was inhibited. A plausible mechanism by which AXIIR siRNA inhibits angiogenesis has been suggested in which MMPs are regulated by the PI3K and Ras/MAPK pathways. AXIIR siRNA was found to significantly suppress the phosphorylation and activation of AKT and ERK1/2, resulting in the decreased expression of MMP-2 and MMP-9 mRNA and protein, and increased expression of TIMP-2 (Song *et al*., 2015).

1.8.3 MT-MMPs

The MT-MMP family members are expressed at the cell surface rather than secreted, consisting of four type I transmembrane proteins: MMP-14, MMP-15, MMP-16, MMP-24, and two GPI-anchored proteins, MMP-17 and MMP-25, which are involved in digesting a number of ECM components including collagen, laminin-1, laminin-5, fibronectin and aggrecan, as well as releasing and modifying growth factors and cytokines. MT1-MMP (also referred to as MMP-14) has collagenolytic activity that digests types I, II and III collagens. Similar to all other MT-MMPs, except MT4-MMP, MT1-MMP is capable of locally activating the type IV collagenase, proMMP-2 (Sato *et al*., 1994; Ohuchi *et al*., 1997; Visse & Nagase, 2003; Mott & Werb, 2004), therefore proteolytic activity is focused on specific cell surface sites during degradation of the basement membrane in the initiation of invasion.

MT1-MMP has been investigated in a number of studies, elucidating its role in cell migration and angiogenesis as well as in the progression of various cancers

including breast adenocarcinoma, metastatic brain tumours and pituitary adenomas (Sounni *et al*., 2002; Liu *et al*., 2010; Kwak *et al*., 2012; Hui *et al*., 2015). In regulating migration and adhesion of tumour cells, MT1-MMP processes αvβ3 integrin and CD44, to which MMP-2 and MMP-9 respectively bind in their localisation to the cell surface, as well as tissue transglutaminase (Brooks *et al*., 1996; Yu & Stamenkovic, 1999; Belkin *et al*., 2001; Kajita *et al*., 2001; Deryugina *et al*., 2002). MT1-MMP has been shown to co-localise with β1 integrins at intercellular contacts and co-localises with αvβ3 integrin at motility-associated structures on migrating endothelial cells (Gálvez *et al*., 2002). MT1-MMP also binds CD44, which interacts with actin, via its extracellular HPX domain. CD44 therefore closely associates MT1-MMP to the cortical actin cytoskeleton within the cell and directs it towards the lamellipodia on the front of migrating cells (Mori *et al*., 2002). Furthermore, the binding of MMP-2 with TIMP-2 to MT1-MMP on the cell surface facilitates the activation of MMP-2 by an adjacent molecule of MT1-MMP and the di-/oligomerisation of MT1-MMP molecules required for MMP-2 activation is promoted by the interaction of CD44H, the dominant form in endothelial cells, with both actin and the HPX domain of MT1-MMP, resulting in the degradation of matrix proteins (Henke *et al*., 1996; Mori *et al*., 2002; Visse & Nagase, 2003). The stability of newly formed microvessels is suggested to be regulated by the selective expression of TIMPs from perivascular supporting cells as the expression of TIMP-2 and TIMP-3 from pericytes co-cultured with HUVECs can inhibit MT1-MMP activity, resulting in the suppression of pro-MMP2 activation (Lafleur *et al*., 2001). EGF receptor has been investigated in a cervical cancer cell line and is also suggested to be involved in upregulating MT1-MMP and downregulating MMP-2 synthesis via the PI3K/Akt and MAPK/ERK pathways (Zhang *et al*., 2009).

In 3D collagen matrices, MT1-MMP is indispensable for driving neovessel formation conferring endothelial cells with the ability to form invading capillary-like structures, whereas neither MMP-2, MMP-9, β3 integrin, CD44, nor plasminogen were found to be essential for invasion or neovessel formation (Chun *et al*., 2004). The regulation of MT1-MMP is involved in the initiation of endothelial sprouts in a mechanism involving vimentin, the major intermediate

filament protein present in endothelial cells, which forms a complex with MT1-MMP in a process that requires the cytoplasmic domain. Vimentin is cleaved by calpains to facilitate the translocation of MT1-MMP to the membrane, leading to sprout formation (Kwak *et al*., 2012).

Further studies into the regulatory pathways of MT1-MMP have revealed that ELK3, a member of the ETS family of transcription factors that is known to be involved in transcriptional repression, has a negative effect on VEGFA-induced angiogenesis in HUVECs and *in vivo* Matrigel plug assays by inhibiting the transcriptional activity of angiogenic Ets1 on the *MT1-MMP* promoter (Giovane *et al*., 1994; Ayadi *et al*., 2001; Heo *et al*., 2014). In both *in vitro* and *in vivo* studies of human glioma cells and breast adenocarcinoma cells, the overexpression of MT1-MMP leads to the upregulation of VEGFA gene expression as well as the activation of proMMP-2, resulting in stimulated angiogenesis and promotion of tumour growth. The specific effect on VEGFA upregulation requires functional catalytic and cytoplasmic domains of MT1-MMP and also involves Src tyrosine kinase activity, a pathway distinct to that involved in inducing cell migration involving ERK (Deryugina *et al*., 2002; Sounni *et al*., 2002; Sounni *et al*., 2004). The overexpression of MT1-MMP also induces the activation of ERK resulting in increased cell migration, which also requires the presence of the cytoplasmic domain (Gingras *et al*., 2001). An antiangiogenic effect of MT1-MMP, which does not require the catalytic domain, has however been identified in corneal angiogenesis, as knockouts of MT1-MMP in corneal cells significantly increased cell proliferation and migration. MT1-MMP also cleaves VEGFR1 leading to reduced proangiogenic effect of VEGF165 (Azar *et al*., 2010; Han *et al*., 2015). The importance of MMPs in angiogenesis is highlighted by the consequences resulting from the deletion of reversion-inducing-cysteine-rich protein with kazal motifs (RECK), a GPI-anchored glycoprotein that regulates Notch signalling and the activities of MMPs and ADAMs including MMP-2, MMP-9, MT1-MMP and ADAM-10, which disrupts vascular development likely by excessive MMP activation, resulting in the premature death of mouse embryos (Noda *et al*., 2003; Muraguchi *et al*., 2007).

1.9 Research aims and strategy

The aims of this research are to characterise the interaction of ingressing cells with the brain, test the role of MMPs in the ingression process and investigate the influence of neural tube patterning on endothelial ingression.

Anatomy:

The brain in particular has a high demand for oxygen and nutrients and therefore depends on an efficient blood supply. Endothelial cells will be visualised at the different stages involved in the initiation of brain vascularisation using *in situ* hybridisation (ISH) in *G. gallus* embryos, complemented by immunohistochemistry (IHC) for the detection of neural cells. The process of brain vascularisation in amphibians has not yet been documented, anatomically nor molecularly, therefore a method of lectin histochemistry (LHC) will also be used to characterise the ingression of endothelial cells into the brain of *Xenopus laevis* during early embryonic development.

Mechanism:

Endothelial sprouting in the brain shares similarities to tumour angiogenesis as the ectoderm is invaded by sprouts from the mesoderm, therefore it is possible that similar mechanisms are shared between both processes. We hypothesise that MMP activity influences endothelial cell ingression and the focus of this research will be on MMP-1, MMP-2 and MMP-9, which are known to have a key role in angiogenesis. The expression patterns of these MMPs will be analysed in the developing brain using ISH in comparison to staining for endothelial cells. The presence of active MMPs will be analysed using *in situ* zymography (ISZ) and the role in ingression will be tested by manipulating MMP levels through exposure to pharmacological inhibitors and active MMP-1. The resulting phenotype will be analysed by immunostaining for endothelial cells and ECM components.

Regulation:

The intricate level of molecular communication between the development of the neural tube and vasculogenesis is evident from the numerous signalling pathways that govern the two processes (Fig. 1viii-ix). The effect of the dorsoventral

patterning molecule, Shh, upon endothelial ingression will be investigated through electroporation experiments conducted in the early neural tube, followed by endothelial cell detection. A second focus will be on the inhibition of Notch signalling and analysing the effect upon ingression, specifically in the early embryonic brain.

Figure 1viii. Gene regulation at the initiation of angiogenesis. The ETS family of transcription factors have important roles in vasculogenesis and angiogenesis, regulating genes involved in cell migration and proliferation. Growth factors including VEGFA, FGF2 and EGF induce the expression of Ets1 in endothelial cells at the initiation of angiogenesis, resulting in the induction of uPA, MMP-1, MMP-3 and MMP-9, together with cell attachment and migration genes αv integrins, β2/β3 integrins, ICAMs and VE cadherin. Cell migration is triggered as the GPI-anchored uPAR activates uPA that converts plasminogen to plasmin, ultimately resulting in MMP activation and the mobilisation of proangiogenic factors following ECM degradation. Furthermore, uPA can act directly on a number of matrix proteins such as fibronectin. Endothelial cell migration is also promoted by the cleavage and activation of PAR1 by active MMP-1, together with the interaction of uPAR with α5β1 integrin and caveolin that are highly expressed in tip cells. Sprouting angiogenesis is also controlled by the transcription factor Mef2c, which is directly activated by Ets1 and mediated by A2M, resulting in a strong inhibitory effect on cell migration. The Mef2c/A2M pathway functions as a negative feedback mechanism in normoxic conditions to prevent inappropriate sprouting and excess angiogenesis when sufficient levels of oxygen are reached following neovascularisation.

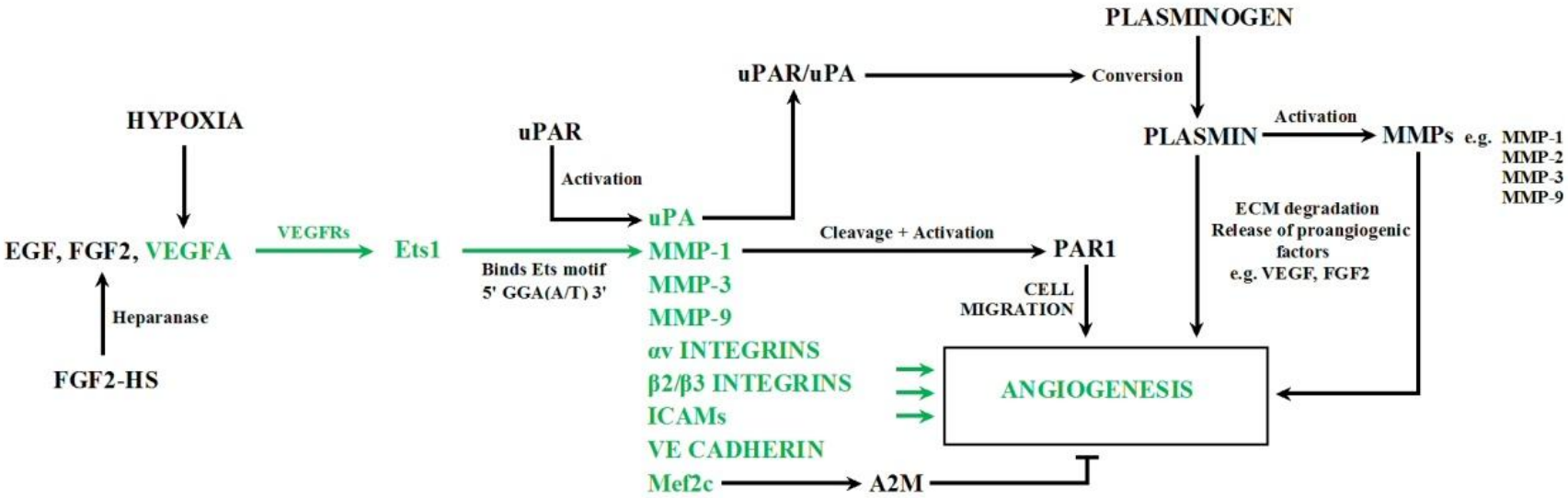
PLASMINOGEN
uPAR/uPA
Conversion
HYPOXIA
uPAR
Activation
PLASMIN
Activation
MMPs
e.g. MMP-1
MMP-2
MMP-3
MMP-9
uPA
ECM degradation
Release of proangiogenic factors
e.g. VEGF, FGF2
VEGFRs
Ets1
Cleavage + Activation
PAR1
EGF, FGF2, VEGFA
Binds Ets motif
5' GGA(A/T) 3'
MMP-1
MMP-3
MMP-9
CELL MIGRATION
Heparanase
αv INTEGRINS
β2/β3 INTEGRINS
ICAMs
VE CADHERIN
ANGIOGENESIS
FGF2-HS
Mef2c
A2M

Figure 1ix. The selection of tip and stalk cells during sprouting angiogenesis. The selection of tip and stalk cells is influenced by the interaction between endothelial cells, neuroglial cells and microglia during vascularisation of the CNS. Neuroglial cells secrete a number of factors including VEGFA, SEMA3A, SEMA3E, SEMA3F, Wnt7a, Wnt7b and Shh. Microglia, which are the resident macrophages of the CNS, synthesise VEGFA, MMP-1, MMP-9 and PARs. Vessel sprouting is regulated by VEGFA and when one endothelial cell within a group receives more VEGFA via VEGFR2 this leads to an increase in the expression of the transmembrane ligand, Dll4, resulting in the emergence of a tip cell. The Dll4 ligand binds to Notch receptors on adjacent endothelial cells leading to an increase in VEGFR1 expression and a decrease in VEGFR2 and VEGFR3, resulting in neighbouring cells emerging as stalk cells. Vessel formation is negatively regulated by VEGFR1, which binds VEGFA with 10-fold higher affinity than VEGFR2, thereby limiting the amount of VEGFA accessible to VEGFR2. Tip and stalk cells differ in genetic identity with tip cells expressing high levels of Dll4, $\alpha 5\beta 1$ integrins and caveolin, together with transmembrane proteins VEGFR1, VEGFR2, VEGFR3, PLXND1 and NRP1. The migration of tip cells is guided by NRP1 and the distribution of VEGFA in the extracellular space. NRP1 acts as a co-receptor for VEGF165 by forming a complex with VEGFR2, which enhances the VEGFA-VEGFR2 interaction. SEMA3A-NRP1 signalling on the other hand prevents VEGF165 from binding NRP1, leading to reduced cell motility. Stalk cells have high expression of VEGFR1, ALK1 and endothelium-specific Smad1 and Smad5, which cooperate with Notch to reduce tip cell numbers. The proliferation of stalk cells is regulated by the concentration of VEGFA. The Dll4-Notch signalling pathway is therefore crucial in establishing an adequate ratio of tip cells to stalk cells required for normal sprouting patterns.

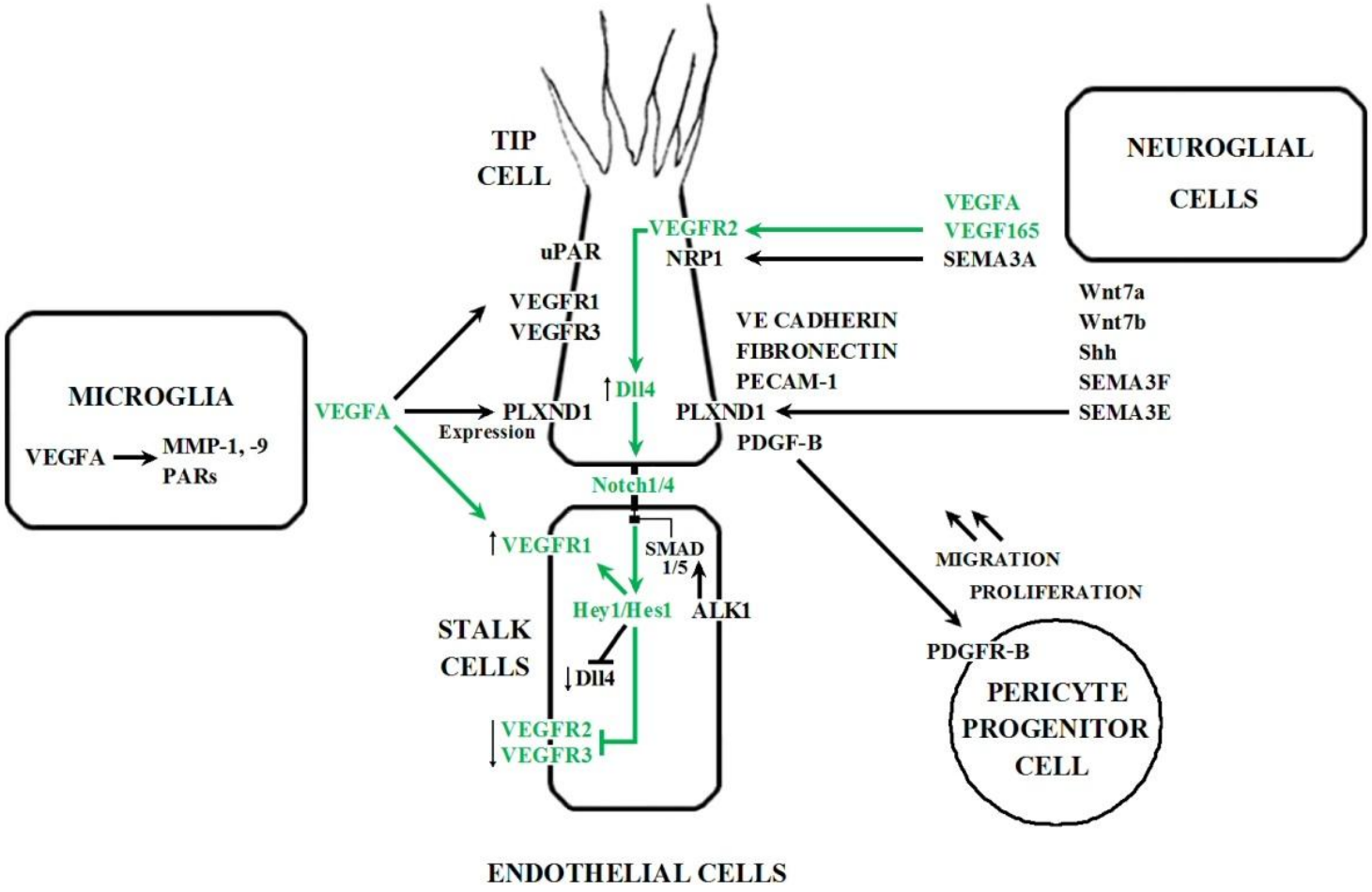
TIP
CELL
NEUROGLIAL
CELLS
VEGFA
VEGF165
SEMA3A
VEGFR2
NRP1
uPAR
VEGFR1
VEGFR3
Wnt7a
Wnt7b
Shh
SEMA3F
SEMA3E
VE CADHERIN
FIBRONECTIN
PECAM-1
MICROGLIA
VEGFA → MMP-1, -9
PARs
VEGFA
PLXND1
Expression
↑Dll4
PLXND1
PDGF-B
Notch1/4
↑VEGFR1
SMAD
1/5
Hey1/Hes1
ALK1
STALK
CELLS
↓Dll4
VEGFR2
VEGFR3
MIGRATION
PROLIFERATION
PDGFR-B
PERICYTE
PROGENITOR
CELL
ENDOTHELIAL CELLS

2. MATERIALS AND METHODS

2.1 Ethical statement

All research projects are monitored by the University's ethics committee and current work in the laboratory has been approved by the committee. *G. gallus* embryos were not used beyond half-way through gestation and hence the experiments are not subject to the Scientific Procedures Act. *X. laevis* experiments were covered by existing Home Office licences. None of the experiments involved human subjects or tissues.

2.2 Ets1, MMP and VEGFR PCR amplification

G. gallus genomic DNA was used as template to amplify regions from *Ets1*, *MMPs* and *VEGFRs* using nested primers in PCR to increase the yield and provide more specific product. A volume of 1µl genomic DNA (or cDNA for VEGFR PCR) was combined with 10.5µl H_2O, 12.5µl 2x Pwo master mix (Roche 03789403001) and 0.5µl each of the outer forward and reverse primers (100pmol/µl). The PCR was conducted with the following parameters: 1' 95^{o}C; 5x (15" 95^{o}C, 15" 58^{o}C, 2' 72^{o}C); 25x (15" 95^{o}C, 15" 52^{o}C, 2' 72^{o}C); 15' 72^{o}C. Inner primers were then used to amplify a region within the product by combining 1.0µl of PCR product with 10.5µl H_2O, 12.5µl 2x Pwo master mix and 0.5µl each of the inner forward and reverse primers (100pmol/µl) extended with the Gateway attB cloning sequence (blue) in a second reaction using the following parameters: 1' 95^{o}C; 5x (15" 95^{o}C, 15" 50^{o}C, 2' 72^{o}C); 25x (15" 95^{o}C, 15" 65^{o}C, 2' 72^{o}C); 15' 72^{o}C. The PCR2 product was gel purified using a NucleoSpin Gel and PCR Clean-up kit (Macherey-Nagel 740609.250) and stored at 4^{o}C.

Ets1 outer primers:

cEts1_F1 TGGCAGGGGATTAGTGAAAG

cEts1_R1 ATGTTGGATAGACCCCACCA

Ets1 inner primers:

B1_F_cEts1 GGGGACAAGTTTGTACAAAAAAGCAGGCTGCTGAAGTGCCTTTTTC

B2_R_cEts1 GGGGACCACTTTGTACAAGAAAGCTGGGTTTGGGAATAGGGGAAGA

MMP-1 outer primers:

cMMP1_F1 AGTTTGATCCTCGTGCCAAA

cMMP1_R1 TTTAATGCAGCAGGTAAAAGTG

MMP-1 inner primers:

B1_F_MMP1_3

GGGGACAAGTTTGTACAAAAAAGCAGGCTTCTTTTCCACATGCACACTG

B2_R_MMP1_3

GGGGACCACTTTGTACAAGAAAGCTGGGTCTGTGGAATCTAGGCAGGA

MMP-2 outer primers:

cMMP2_F1 GCGAGTTTGATCATTACTGCCA

cMMP2_R1 TTGGCATTTCATGTTTGGGAC

MMP-2 inner primers:

B1_F_MMP2_3

GGGGACAAGTTTGTACAAAAAAGCAGGCTGGTTGCCACGGGATTTGATT

B2_R_MMP2_3

GGGGACCACTTTGTACAAGAAAGCTGGGTACACCTTCTGTTGCCCAATG

MMP-9 outer primers:

CMMP9_F1 AGCCCAGGAGTGCTGTGG

CMMP9_R1 TTCCAAAGGACGGCTTTTATTAC

MMP-9 inner primers:

B1_F_MMP9_3

GGGGACAAGTTTGTACAAAAAAGCAGGCTCAGGGCTTGCAGTCTCCC

B2_R_MMP9_3

GGGGACCACTTTGTACAAGAAAGCTGGGTAGCAGGTGAAGGATGGCAT

The primer design for and PCR-amplified sequences for MMPs -1, -2 and -9 are shown in Fig. 2i.

VEGFR1 Outer Primers:

cVEGFR1_F1 TCCTGAGCTGTGAGACAACC

cVEGFR1_R1 TCACTTTCATTGGCAAGCGA

VEGFR1 Inner Primers:

B1_F_VEGFR1 GGGGACAAGTTTGTACAAAAAAGCAGGCTGTGGGCACAAGTATAGCACG

B2_R_VEGFR1 GGGGACCACTTTGTACAAGAAAGCTGGGTAGGGTCCACTCTTCACATGG

VEGFR2 Outer Primers:

cVEGFR2_F1 ACGAAATAAAGACACAGCCCTG

cVEGFR2_R1 ATTAACCCGCCCTCTCTACC

VEGFR2 Inner Primers:

B1_F_VEGFR2 GGGGACAAGTTTGTACAAAAAAGCAGGCTCTCAGAGTTATCCCGTGCC

B2_R_VEGFR2 GGGGACCACTTTGTACAAGAAAGCTGGGTGGCAGTTCAGAGGGGAATT

VEGFR3 Outer Primers:

CVEGFR3_F1 AGGCAGATCTGGTGAGCAG

CVEGFR3_R1 ACCCACGTGTTCTCCTTCTT

VEGFR3 Inner Primers:

B1_F_VEGFR3

GGGGACAAGTTTGTACAAAAAAGCAGGCTAGCATCACCGAGGAAGAACA

B2_R_VEGFR3 GGGGACCACTTTGTACAAGAAAGCTGGGTCAAAGACATAGGCGCTGACC

B. AMPLIFIED SEQUENCES

MMP-1:

GGGGACAAGTTTGTACAAAAAAGCAGGCTTCTTTTCCACATGCACACTGCATATTTTTA
AGTGTATATTTTATATGTATATTTTTTATGTGCTGAATTTTTCAGCATTTCATGACTAACA
GTTCAAAATGGATTCCTGCCTAGATTCCACAGACCCAGCTTTCTTGTACAAAGTGGTCC
CC

MMP-2:

GGGGACAAGTTTGTACAAAAAAGCAGGCTGTTGCCACGGGATTTGATTTGTATTGATGC
ATGATGGAATCATGGCAAGAAACTGTATTAAAGTATTGTTTTAAAGTACTTTCTATTTTA
AAACCTTAGTTCAACTTAGCAATTTGCTTCCTGCACTTTGTTACTACTCTATAACTTGTC
TATACAGACAGAATGACTCAGATGTTTTAAATCAATGTATTATACACAGAAGTCAAGTA
TTACTGTTTACCTTGTTTTATTTTTCTGTTCTTTATAATATTGAGTTTTTGTTTGGTTAGGC
TTTCTGCTTAGGCATTGGGCAACAGAAGGTGTACCCAGCTTTCTTGTACAAAGTGGTCC
CC

MMP-9:

GGGGACAAGTTTGTACAAAAAAGCAGGCTCAGGGCTTGCAGTCTCCCTGGCAGGATGG
GGCGTGTGCTCCCGGCCCCCACCAGGGGCTGCCCGTCTGGGGAGCGGCGACTCACGCC
AGCTTTGCTGCCCGGAGACGTTTGCCCGGCGCAAACTGCACACGGATTTGTAATGACTT
TATCTTTTCCTGAGCCAGTAACGCTGGGTCGGCCTCGCGCGGGCAGGGACACGGGGCTT
TGTGCCTCCCCCGCCTCGCCGCCGGGTGATGCCATCCTTCACCTGCTACCCAGCTTTCTT
GTACAAAGTGGTCCCC

Figure 2i. MMP primer design and PCR-amplified sequences for ISH experiments. **A**. The inner primers designed for the production of RNA probes to detect MMPs -1, -2 and -9 were used in PCR with chick genomic DNA as template and the products of which are shown on the right following gel purification. PCR products were then cloned in a Gateway pDONR^{TM}221 vector, which was used to transform competent bacteria. Template DNA was then synthesised and used to make antisense RNA probes for ISH. **B**. The amplified sequences for MMP-1, MMP-2 and MMP-9 inner primers are shown, extended with the Gateway attB cloning sequences (blue).

2.3 Gateway cloning reactions for Ets1, MMPs and VEGFRs

The purified Ets1, MMP-1, MMP-2, MMP-9 and VEGFR PCR2 products were Gateway cloned in a BP reaction by combining 2µl attB-PCR2 with 1µl Gateway® pDONR™221 vector (150ng/µl; Invitrogen 12536017), 1µl TE buffer pH8 and 1µl Gateway® BP Clonase® enzyme mix (Invitrogen 11789013) then incubating for 1 hour at room temperature (RT). The reaction was terminated by incubating with 0.5µl Proteinase K (Qiagen 19131) for 10 minutes at 37°C and samples were then stored on ice prior to transformation.

2.4 Bacterial transformation and minipreps

The transformation of α select chemically competent cells (Bioline BIO-85026) was achieved by adding 50µl α select bacteria to each cloning reaction sample and incubating on ice for 10 minutes. The cells were heat-shocked at 42°C for 30 seconds then immediately placed back on ice before adding 150µl SOC medium (Invitrogen 15544034) to each sample and shaking for 1 hour at 37°C. The samples were plated on LB agar containing the relevant antibiotic (30µg/ml kanamycin and 75µg/ml chloramphenicol for Ets1 or 30µg/ml kanamycin for MMPs and VEGFRs) and incubated for 15-18 hours at 37°C before storing at 4°C. Liquid cultures of transformed bacteria were prepared by inoculating 2 ml YT growth medium or LB broth, containing the same antibiotics used for the LB plates, with a single colony. The cultures were shaken for 17 hours at 37°C prior to plasmid purification using a High Pure Plasmid Isolation Kit (Roche 11754785001) or a NucleoSpin Plasmid QuickPure kit (Macherey-Nagel 740727.250). Purified plasmid DNA samples were sequenced and stored at 4°C.

2.5 Template DNA synthesis

Template DNA was synthesised from Ets1, MMP and VEGFR plasmid minipreps by combining 0.5µl plasmid DNA with 21.5µl H_2O, 25.0µl 2x Biomix Red (Bioline BIO-25006), 2.0µl DMSO and 0.5µl each of the M13 forward and reverse primers (5'CCAGGGTTTTCCCAGTCACG and 5'TCACACAGGAAACAGCTATG, respectively; GIBCO by Life Technologies), then conducting PCR with the

following parameters: 1' 95°C; 5x (15" 95°C, 15" 65°C, 2' 72°C); 25x (15" 95°C, 15" 50°C, 2' 72°C); 8' 72°C. Templates were then purified using a High Pure PCR Product Purification Kit (Roche 11732676001) or a NucleoSpin Gel and PCR Clean-up kit and stored at 4°C. Mef2c template DNA was gifted from Dr. Dietrich, University of Portsmouth.

2.6 Antisense RNA probe synthesis for ISH

Antisense RNA probes were synthesised from Ets1, Mef2c, MMP and VEGFR DNA templates by incubating 3.0µl template with 37.5µl H_2O, 5.0µl 10x transcription buffer (Roche), 2.0µl DIG RNA labelling mix (Roche; 11277073910), 0.5µl Protector RNase inhibitor (Roche 03335399001) and either T7 (for Ets1, MMPs, VEGFRs; Roche 10881767001) or T3 (for Mef2c; Roche 11031163001) RNA polymerase for 2 hours at 37°C. A volume of 2µl DNase I (RNase free, Roche 04716728001) was then added to each sample, which were incubated for a further 15 minutes at 37°C. RNA probes were purified using a SigmaSpin Sequencing Reaction Clean-up Kit (Sigma-Aldrich S5059) and stored at -20°C.

2.7 Incubation and preparation of *G. gallus* embryos for ISH and IHC

Chicken eggs were acquired from Henry Stewart & Co. Ltd. and incubated to the required developmental stage according to Hamburger & Hamilton (1951) at 38.5°C in a humidified incubator. Embryos were harvested in phosphate-buffered saline (PBS) and fixed in 4% paraformaldehyde/PBS (PFA/PBS) for at least 24 hours at 4°C. The embryos were prepared to allow for the diffusion of solutions through the tissues during the whole-mount ISH and IHC protocols. A small incision was made to the forebrain of the youngest embryos, up to stage HH13. Stage HH14-16 embryos were prepared by removing the left eye and opening the hindbrain, while stage HH17-22 embryos were prepared by removing both lens and the left telencephalic vesicle, piercing the heart and otic vesicles and opening the hindbrain. Embryos older than stage HH22 had both eyes and the telencephalon removed to ensure an open passage to the midbrain. A small hole was cut into the posterior midbrain to the right of the midline for the removal of air bubbles and the hindbrain

was also opened. Finally, the majority of the trunk was removed by cutting posterior to the otic vesicles.

2.8 Whole-mount ISH protocol

Whole-mount ISH was used to detect endothelial cells by identifying the spatial and temporal expression of *Ets1* and *Mef2c*, together with *MMP* and *VEGFR* expression in *G. gallus* embryos. Embryos fixed in 4% PFA/PBS were washed in PBS with 0.1% Tween-20 (PBT) and dehydrated in 25% MeOH, 50% MeOH then 75% MeOH in PBS before bleaching in 6% H_2O_2/MeOH for 1 hour at 4^{o}C, rinsing in MeOH and storing overnight at -20^{o}C. Embryos were rehydrated in 75% MeOH, 50% MeOH then 25% MeOH in PBS and washed in PBT before washing three times in detergent mix (1% IGEPAL, 1% SDS, 0.5% deoxycholate, 50mM Tris-HCl pH8, 1mM EDTA, 150mM NaCl) for 20 minutes each time, re-fixing in 4% PFA/PBS for 20 minutes and rinsing twice in PBT. Equilibration in pre-hybridisation mix (50% formamide, 5x SSC, 2% SDS, 2% BBR, 250µg/ml RNA, 100µg/ml heparin) was conducted for 1 hour at 65^{o}C prior to overnight incubation with hybridisation mix, containing the antisense DIG-labelled RNA probe (10µl/ml), at 65^{o}C. The following day, embryos were rinsed in Solution X (50% formamide, 2x SSC pH4.5, 1% SDS), washed four times with Solution X for 30 minutes each time at 65^{o}C, before rinsing and washing twice in MABT (1x MAB [1 M maleic acid, 1.5 M NaCl], 0.1% Tween-20) for 30 minutes each time. Embryos were left to equilibrate in MABT/2% BBR/20% serum for 1 hour before incubating with anti-DIG alkaline phosphatase (AP)-conjugated antibody (1:2000; Roche 11093274910) in MABT/2% BBR/20% serum for three nights at 4^{o}C. After rinsing three times in MABT, embryos were washed extensively with seven changes of MABT for 1 hour each wash before leaving in MABT overnight at 4^{o}C. The following day, embryos were washed twice in NTMT pH9.5 (0.5mg/ml Levamisole, 100mM NaCl, 100mM Tris-HCl pH9.5, 50mM $MgCl_2$, 1% Tween-20) for 10 minutes each time and staining was initiated by adding the substrate nitro-blue tetrazolium/5-bromo-4-chloro-3'-indolyphosphate (NBT/BCIP; Roche 11681451001) to NTMT (2µl/ml). Once the blue signal was sufficiently strong, staining was stopped by washing in NTMT for 10 minutes and then rinsing and washing twice in PBT for 10 minutes each time before fixing overnight in 4% PFA/PBS at 4^{o}C. Embryos that did not undergo IHC following ISH

were washed in PBS before either embedding in 20% gelatin/PBS for vibratome sectioning or washed in 20% glycerol, 50% glycerol then 80% glycerol in PBS for long-term storage.

2.9 Whole-mount IHC - DAB staining and fluorescence

Embryos undergoing whole-mount IHC following ISH were washed three times in PBS for 10 minutes each time and equilibrated in PBS/5% serum/1% Triton X-100 for 30 minutes, before incubating with the primary antibody in PBS/10% serum/1% Triton X-100/0.02% Na-azide for 4 nights at 4^{o}C. Embryos that had been fixed in 4% PFA/PBS undergoing whole-mount IHC without ISH were instead washed three times in PBS for 1 hour each time, bleached overnight in PBS/5% serum/1% Triton X-100/0.1% H_2O_2 at 4^{o}C then washed three times in PBS/5% serum/1% Triton X-100 for 1 hour each time at 4^{o}C, before incubating with the primary antibody as described above. All embryos were then washed three times in PBS/1% serum/1% Triton X-100 for 1 hour each time at 4^{o}C and incubated with the horseradish peroxidase (HRP)-conjugated secondary antibody in PBS/5% serum/1% Triton X-100 overnight at 4^{o}C. The next day, embryos were again washed at 4^{o}C, three times in PBS/1% serum/1% Triton X-100 for 1 hour each time and twice in 100mM Tris-HCl pH7.5 for half an hour each time, before equilibrating in inactive diaminobenzidine (DAB; ACROS Organics AC328005000, Alfa Aesar J60972) as substrate in 100mM Tris-HCl pH7.5 (10 mg/20 ml) filtered with 0.22µm Millex-GP syringe filter (Merck Millipore) for 3 hours at 4^{o}C in the dark. Staining was initiated by incubating with DAB solution activated with 30% H_2O_2 (0.6µl 30% H_2O_2/ml inactive DAB) at RT in the dark. Once the brown signal was sufficiently strong, staining was stopped by rinsing three time with tap water and washing twice in PBT for 20 minutes each time before fixing overnight in 4% PFA/PBS at 4^{o}C. Embryos were then washed in PBS before either embedding in 20% gelatin/PBS for vibratome sectioning or washed in 20% glycerol, 50% glycerol then 80% glycerol in PBS for long-term storage. Refer to Table 2i for information regarding primary and secondary antibodies.

Table 2i. Primary and secondary antibodies. Antibodies used in ISH, IHC and ISZ experiments are provided together with working concentrations and suppliers.

Antibodies	**Concentration**	**Supplier details**
Primary Antibodies:		
TuJ1	1:2000	R&D Biosystems MAB1195, mouse
Phosphohistone H3	1:500	EMD Millipore 06-570, rabbit
Anti-CD34 (AV138)	1:1000	Bio-Rad MCA5936GA, mouse
Anti-HNK-1/N-CAM (CD57)	1:500	Sigma-Aldrich C6680, mouse
Anti-laminin (avian)	1:500	Hybridoma bank 3H11, mouse
Fibronectin (avian)	1:500	Hybridoma bank B3/D6, mouse
α6 integrin (avian)	1:200	Hybridoma bank P2C62C4, mouse
β1 integrin (avian)	1:500	Hybridoma bank V(2)E(9), mouse
Anti-GFP	1:1000	Invitrogen A6455, rabbit serum
Secondary Antibodies:		
Peroxidase-conjugated AffiniPure goat anti-mouse IgG + IgM	1:100	Jackson ImmunoResearch 115-035-044
Alexa Fluor® 546-conjugated goat anti-mouse IgG	1:200	Invitrogen A-11003
Alexa Fluor® 488-conjugated goat anti-rabbit IgG	1:200	Jackson ImmunoResearch 111-545-003

2.10 Gelatin embedding and vibratome sectioning of *G. gallus* embryos

Embryos in 4% PFA/PBS were washed three times in PBS for 10 minutes each time before equilibrating in 20% gelatin/PBS for 2 hours at 65°C. The embryos were transferred to embedding moulds containing 20% gelatin/PBS and positioned into the correct orientation before the gelatin cooled and solidified. Gelatin blocks containing the embedded embryos were removed from the moulds and fixed in 4% PFA/PBS at 4°C for at least 5 nights before sectioning. Sections of 30μm thickness were cut using a Leica VT1000 S vibratome and mounted on glass slides with 100% glycerol. Sections of 60μm thickness were cut from embryos that underwent fluorescent immunostaining before mounting on glass slides with an aqueous mounting medium.

2.11 LHC on *X. laevis* sections

X. laevis embryos collected from the European Xenopus Resource Centre (EXRC) were de-jellied in 2% cysteine pH7.9 then washed extensively with 1x MBS. Embryos between stages 40 to 50 (Nieuwkoop & Faber, 1956) were collected by anaesthetising in 0.025% tricaine methanesulfonate (MS-222) before fixing in 1x MEMFA (0.1M MOPS pH7.4, 2mM EGTA pH8, 1mM Mg_2SO_4, 3.7% formaldehyde) for 1 hour. Embryos were washed three times in MeOH then stored in MeOH overnight at 20°C. The rehydration of embryos proceeded with successive washes in 75% MeOH, 50% MeOH, 25% MeOH in PBT and a 5-minute PBT wash before bleaching (5% formamide, 0.5x SSC pH4.5, 10% H_2O_2) atop a light box. Embryos were washed twice in PBT for 5 minutes each time before equilibrating in 20% gelatin/PBS for 1 hour at 65°C. The embryos were transferred to embedding moulds containing 20% gelatin/PBS and positioned into the correct orientation before the gelatin cooled and solidified. Gelatin blocks containing the embedded embryos were removed from the moulds and fixed in 4% PFA/PBS at 4°C for at least 5 nights before sectioning. Sections of 100μm thickness were cut using a Leica VT1000 S vibratome and transferred to a 24-well plate containing 4% PFA/PBS. Sections were washed twice in PBS for 5 minutes each time and PBT for 30 minutes then equilibrated in PBT/20% serum for 1 hour prior to overnight incubation with biotinylated *Lycopersicon esculentum* (Tomato) lectin (LEL) 1:200 (Vector

Laboratories B-1175) in PBT/20% serum/0.02% Na-azide at 4°C. The following day, sections were washed extensively with five changes of PBT for 30 minutes each wash and PBT/20% serum for 1 hour. Sections were incubated overnight in HRP-conjugated streptavidin 1:200 (Vector Laboratories SA-5004) in PBT/20% serum at 4°C then washed extensively in PBT the next day, followed by a 30-minute wash in 100mM Tris-HCl pH7.5. After equilibrating in inactive DAB solution for 30 minutes at 4°C in the dark, staining was conducted with active DAB as previously described. Sections were fixed overnight in 4% PFA/PBS at 4°C and washed in PBS the next day before successive washes in 20%, 50% and 80% glycerol/PBS. Sections were then mounted on slides with 80% glycerol/PBS prior to microscope analysis.

2.12 Bead experiments with MMP inhibitors, active MMP-1 and Notch inhibitor, followed by IHC

Bead implantation experiments were conducted on stage HH22 *G. gallus* embryos to investigate the effects of ARP 100 (Santa Cruz Biotechnology sc-203522), SB-3CT (Santa Cruz Biotechnology sc-205847), Batimastat BB-94 (Tocris 2961), active MMP-1 (gifted from Dr. Pickford, University of Portsmouth, dialysed using a Pierce 7K MWCO Slide-A-Lyzer Dialysis Cassette [ThermoFisher Scientific 66372] in 1L of 100mM Tris-HCl pH7.5 as buffer) and DAPT (Insight Biotechnology CAS 208255-80-5) on vascularisation. Acrylic beads were soaked in reagents for at least one hour prior to implantation and all eggs were disinfected with 70% EtOH before removing 1.5ml albumin from each egg and cutting a window from the shell. Embryos were hydrated with 50 units penicillin and 50µg streptomycin/ml PBS. A single bead was implanted *in ovo* into the head mesoderm on the right side of each embryo, positioned just beneath the surface ectoderm adjacent to the ventral midbrain. The shell was placed back into position to cover the exposed embryo and eggs were incubated for a further 29 hours at 38.5°C then harvested in PBS at stage HH26 (Fig. 2ii, A-B). Embryos were fixed overnight in 4% PFA/PBS at 4°C before undergoing IHC with CD34 to detect endothelial cells, followed by embedding in 20% gelatin/PBS, vibratome sectioning and microscope analysis. The number of endothelial cells were then counted on the side containing the bead and was compared with the contra lateral control side of each embryo (Fig. 2ii, C). A paired

t-test was performed for each control and experimental condition using Minitab 17 in order to determine if there was a significant difference in the number of endothelial cells present within the brain in the control side compared to the side exposed to a pharmacological inhibitor or active MMP-1.

MMP inhibitors ARP 100 and SB-3CT were used at a concentration of 8mM in either DMSO or PBS, and Batimastat was used at a concentration of 1mM in DMSO. Active MMP-1 was used at 25nM and 1μM concentrations in 100mM Tris-HCl pH7.5 dialysis equilibration buffer. The Notch inhibitor DAPT was used at a concentration of 10mM in DMSO. Control experiments involved implanting beads soaked in the relevant buffer excluding the inhibitor or active MMP-1.

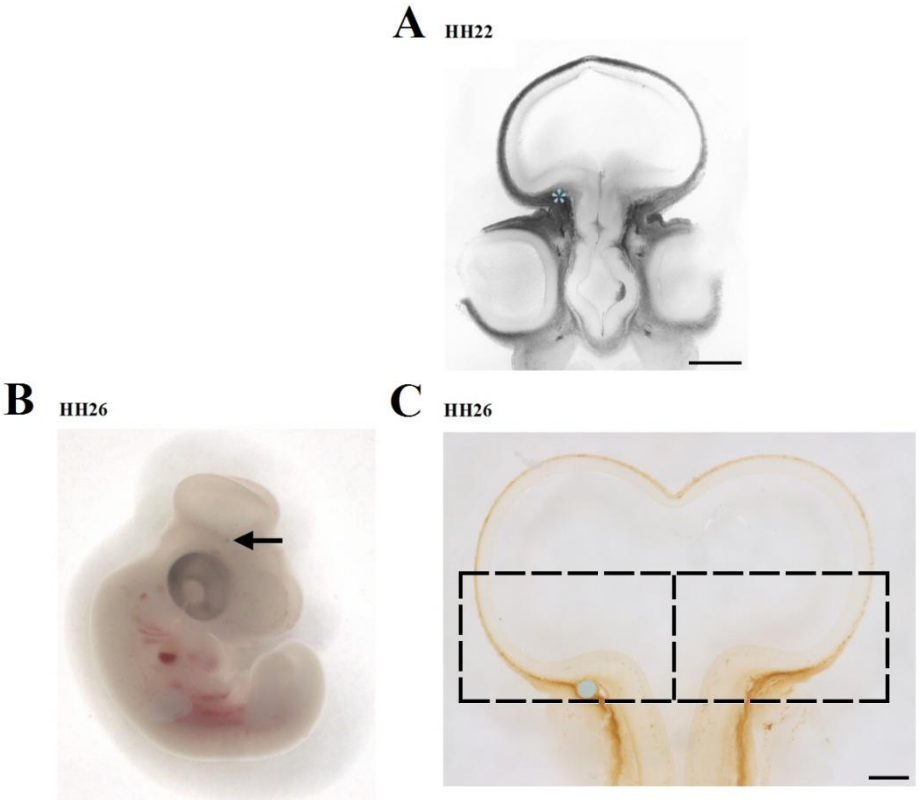

Figure 2ii. Bead placement for bead implantation studies and method for cell counting. The activity of enzymes and signalling molecules is altered by implanting acrylic beads soaked in a pharmacological inhibitor (ARP100, SB-3CT, Batimastat or DAPT) or active MMP-1 into the mesoderm just beneath the surface ectoderm adjacent to the basal plate of the midbrain. The beads are implanted into stage HH22 chick embryos *in ovo* (**A**, blue asterisk), which are then incubated to stage HH26 (**B**). Harvested embryos undergo further analysis, for example, immunostaining with a CD34 antibody to detect endothelial cells. Endothelial cells are counted within the ventral half of the midbrain on the side containing the bead and compared with the contra lateral control side, down to the horizontal line posterior to the bead in all sections in which the bead is detected (**C**). Scale bar = 250μm.

2.13 Roller culture experiments

G. gallus embryos were harvested at stage HH8 and cultured *ex ovo* using a modified Cornish pasty method (Fig. 2iii, MC method, Nagai *et al.*, 2011) in which each embryo is folded along the axis parallel to the primitive streak. Embryos were transferred to L15 medium containing 10% chick serum, gentamicin (30μg/ml) and either 1μM or 10μM ARP 100 and rolled in an incubator for 40 hours at 37^{o}C. Embryos were then removed and fixed overnight in 4% PFA/PBS before conducting whole mount IHC, as previously described, with an anti-HNK-1 antibody. Embryos were then embedded in 20% gelatin/PBS and fixed in 4% PFA/PBS at 4^{o}C for at least 5 nights before cutting 30μm sections with a vibratome. Control embryos were roller cultured in DMSO then underwent IHC with an anti-HNK-1 antibody for comparison with experimental embryos.

2.14 Whole-mount ISZ with DQ gelatin, followed by IHC

G. gallus embryos were harvested at stage HH26 in ice cold PBS, fixed in 4% PFA/PBS for 15 minutes at 4^{o}C then washed in PBS. Incisions were made to the telencephalic vesicles before removing the heads and incubating in 20μg/ml fluorescein-conjugated DQ™ Gelatin (Molecular Probes D12054) in reaction buffer at pH7.5 (150mM NaCl, 5mM $CaCl_2$, 0.02% NaN_3, 50mM Tris-HCl pH7.5) for 24 hours in a dark, humidified chamber at 37^{o}C. Control embryos were either incubated in reaction buffer alone or 10mM EDTA in reaction buffer. Samples were then washed extensively with eight changes of PBS for 30 minutes each wash and fixed overnight in 4% PFA/PBS at 4^{o}C in the dark. Whole-mount fluorescent IHC was conducted with all steps performed at 4^{o}C in the dark. The samples were washed three times in PBS and twice in PBS/5% serum/1% TritonX-100 for 1 hour each time before incubating with CD34 (1:1000) in PBS/10% serum/1% Triton X-100/0.02% Na-azide for 4 nights. The following day, the samples were washed three times in PBS/1% serum/1% TritonX-100 for 1 hour each time then incubated overnight in Alexa Fluor® 546 conjugated-goat anti-mouse secondary antibody (1:200) in PBS/5% serum/1% TritonX-100. Washes were conducted with PBS/1% serum/1% TritonX-100 for 1 hour each time before fixing overnight in 4% PFA/PBS then embedding in 20% gelatin/PBS and cutting 60μm sections with a vibratome.

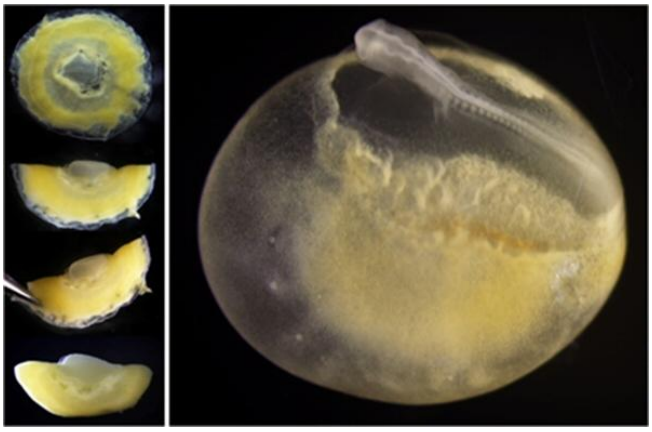

Figure 2iii. MC method for roller culture experiments. The embryo is folded along the axis parallel to the primitive streak to form a half-moon shape. Once in culture medium, fluid transport causes the embryo to inflate and rise to the surface of the medium, whilst maintaining epiblast tension required for early development (Nagai *et al*., 2011; Riken, 2011).

2.15 VEGFA RT-PCR

Total RNA was isolated from whole *G. gallus* embryos between stages HH11-21 of development, or from the head only at stages HH21-28, using an RNeasy Protect Mini Kit (Qiagen 74124) immediately after harvesting. Genomic DNA was removed from RNA preparations with a DNase I digest followed by purification using a SigmaSpin Sequencing Reaction Clean-Up Kit (Sigma-Aldrich) before storing at -70^{o}C. The synthesis of cDNA from total RNA was conducted for each developmental stage using a Transcriptor High Fidelity cDNA Synthesis Kit (Roche 05091284001). The cDNA was then used as template to amplify *VEGFA* in PCR with nested primers by combining 1.0µl of stage-specific cDNA with 10.5µl H_2O, 12.5µl 2x Pwo master mix (Roche) and 0.5µl each of the outer forward primer (cVEGF_F1 GGAGACCCCGAAGAGGAGAC) and outer reverse primer (cVEGF_R1 TGTCCAGGCGAGAAATCAGG) at 100 pmol/µl. The PCR was conducted with the following parameters: 1' 95^{o}C; 5x (15" 95^{o}C, 15" 60^{o}C, 2' 72^{o}C); 25x (15" 95^{o}C, 15" 55^{o}C, 2' 72^{o}C); 15' 72^{o}C. Inner primers that were designed to amplify particular groups of VEGFA isoforms depending on the presence of exons 6 and 7, were then used in three separate reactions by combining 1.0µl of PCR product with 10.5µl H_2O, 12.5µl 2x Pwo master mix and 0.5µl each of the inner forward and reverse primers at 100pmol/µl. The forward primers cVEGFA_Ex4_F AACCCCATCAGAGTCAGCAC and cVEGFA_Ex6_F ATCAAAGCGAGGAAAGGGGA were combined with reverse primers cVEGFA_Ex8_R CTTCTTTTCCGCTGCTCACC and cVEGFA_Ex7_R GCGCTCGTTTAACTCAAGCT in the following three reactions: set A- Exon4_F, Exon8_R (all isoforms), set B- Exon4_F, Exon7_R (isoforms with exon 7) and set C- Exon6_F, Exon7_R (isoforms with both exons 6 and 7). The PCR was conducted with the following parameters: 1' 95^{o}C; 5x (15" 95^{o}C, 15" 60^{o}C, 1' 72^{o}C); 25x (15" 95^{o}C, 15" 57^{o}C, 1' 72^{o}C); 15' 72^{o}C. The PCR2^{A}, PCR2^{B} and PCR2^{C} products were gel purified using a NucleoSpin Gel and PCR Clean-up kit (Macherey-Nagel) or a High Pure PCR Product Purification Kit (Roche) and stored at 4^{o}C.

The purified PCR2 products were then blunt-end cloned in pCR^{TM} Blunt II-TOPO$^{®}$ vector a using a Zero Blunt$^{®}$ TOPO$^{®}$ PCR Cloning Kit (Invitrogen 450245) and were stored on ice prior to transformation of α select chemically competent cells

(Bioline) as previously described. Plating on LB agar/kanamycin, inoculations and minipreps were also conducted as previously described. Screening for recombinants was performed with EcoRI restriction digests or by PCR amplification using M13 primers with the following parameters: 1' 95^{o}C; 5x (15" 95^{o}C, 15" 65^{o}C, 2' 72^{o}C); 25x (15" 95^{o}C, 15" 50^{o}C, 2' 72^{o}C); 8' 72^{o}C. Purified plasmid DNA samples were sequenced and stored at 4^{o}C.

2.16 Electroporation of Shh into the *G. gallus* mesencephalon, followed by IHC

Electroporation experiments were conducted on stage HH11-12 *G. gallus* embryos to investigate the effect of altering neural patterning on brain vascularisation. All eggs were disinfected with 70% EtOH before removing 1.5ml albumin from each egg, cutting a window from the shell and hydrating the embryos with 50 units penicillin and 50µg streptomycin/ml PBS. The vitelline membrane was removed from the anterior end of the embryo and both pXEX-Shh (1mg/ml; gifted from Prof. Cliff Ragsdale; Agarwala *et al*., 2001) and pCAG-GFP (0.5mg/ml; gifted from Dr. Jonathon Gilthorpe; Yaneza *et al*., 2002) expression constructs, together with 0.1% fast green dye loaded in a glass needle (settings: 990, 900, 770; Sutter Instrument P-30 vertical needle puller), were injected into the mesencephalon. The constructs were electroporated into the left side of the mesencephalon using an Intracel TSS20 Ovodyne electroporator with the following settings applied for the current: 12.5V, 3 pulses, 20ms width, 100ms space. Control embryos were either unelectroporated or electroporated with only the GFP construct. Embryos were rehydrated and the shell was placed back into position. Eggs were incubated for a further 72 hours at 38.5^{o}C, harvested in PBS and fixed overnight in 4% PFA/PBS at 4^{o}C (Fig. 2iv).

Fluorescent immunostaining was conducted with CD34 to detect endothelial cells and anti-GFP to identify cells that had successfully taken up the expression constructs. Embryos were then fixed in 4% PFA/PBS for an hour and a half before embedding in 20% gelatin/PBS for 4 nights and sections of 60µm were cut using a vibratome. Sections were mounted on glass slides with aqueous mounting medium.

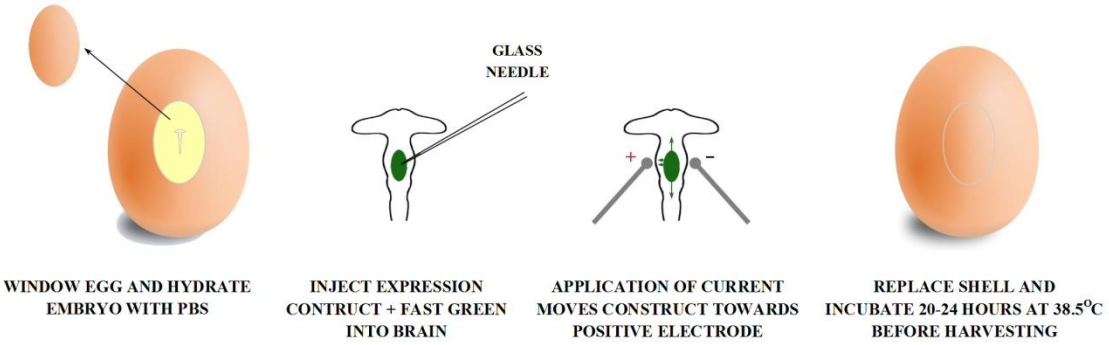

Figure 2iv. Schematic of electroporation experiments. Eggs were windowed and embryos at stage HH11-12 were hydrated with PBS containing penicillin and streptomycin before injecting expression constructs for pXEX-Shh and pCAG-GFP, together with fast green dye, into the mesencephalon. The constructs entered the left side of each embryo upon application of the current. Control embryos were either unelectroporated or electroporated with only the GFP construct. The eggs were then incubated for a further 72 hours at 38.5^{o}C before harvesting.

2.17 Microscope analyses

Whole and sectioned embryos were visualised and analysed following DAB or fluorescent IHC using a Zeiss Axio Zoom.V16 microscope with ZEN imaging software and a Nikon Eclipse E800 microscope. Image editing was performed using Jasc PaintShop Pro 8 photo editing software.

3. ANATOMICAL CHARACTERISATION OF VASCULAR INGRESSION INTO THE EMBRYONIC VERTEBRATE BRAIN

The investigation into vascular ingression in the embryonic vertebrate brain has focused on characterising both the anatomy and molecular control involved in the ingression process. Extensive research into blood vessel patterning events of the neural tube previously conducted in avian embryos, mainly through studies of the spinal cord (Kurz *et al*., 1996; James *et al*., 2009), support the choice of *G. gallus* as the main model organism for analysing events in the brain, with comparative anatomical work conducted in *X. laevis*.

The ingressing endothelial cells are presented with a number of challenges as they enter the brain and subsequently form a new capillary network. The cells must switch to a migratory behaviour, leading to the formation of the PNVP, before penetrating the basal lamina of the brain and navigating radially between the cells in the neuroepithelium. The ependymal layer must then be recognised by the endothelial cells as a signal to branch and fuse to form the INVP. The process of vascularisation has been studied in the spinal cord of avian embryos (Kurz *et al.*, 1996; Hogan *et al*., 2004; James *et al*., 2009) but very little work has been conducted in the rostral brain. A detailed anatomical description of vascular ingression was therefore conducted in order to document the spatial and temporal location of endothelial cells involved in the ingression process of the *G. gallus* brain during early embryonic development.

3.1 Brain vascularisation involves endothelial cell migration, PNVP formation, sprouting and INVP formation

The ETS transcription factors are major regulators of vascular development and almost all endothelial-specific genes contain the ETS DNA binding site. The ETS gene, Ets1, is expressed in endothelial cells and is important for the regulation of angiogenesis as it has been shown to induce the expression of uPA, MMP-1, MMP-3 and MMP-9 and also controls cell migration by regulating the expression of αv integrins, β2 and β3 integrins, ICAMs and VE cadherin (Iwasaka *et al*., 1996; Sato, 1998; Kita *et al*., 2001). Whole-mount ISH was therefore performed in *G. gallus*

embryos to stain endothelial cells blue using an antisense probe against Ets1. ISH was coupled with IHC using a TuJ1 antibody against neuron-specific Class III β-tubulin to stain neurons brown in order to identify if the position of the differentiated neurons correlates with the position of the developing PNVP or the points at which the endothelial sprouts invade the brain. The embryos were then embedded in gelatin and sectioned with a vibratome through the prosencephalon, mesencephalon and rhombencephalon as indicated in Fig. 3i.

Ets1-positive cells were seen migrating above and below the level of the somites towards the left and right sides of the anterior spinal cord at stage HH11 (Fig. 3ii, A). The PNVP began to form at stage HH13 as Ets1-positive cells were identified close to the neural tube and lined up against the mesencephalon as the embryos grew to stage HH15 (Fig. 3ii, B-C, arrows). However, the PNVP did not appear to develop in correlation with the position of the differentiated neurons. The first ingressing endothelial cells were identified as Ets1-positive cells appeared in the formation of narrow individual sprouts that had penetrated the basal lamina of the brain and invaded the ventral mesencephalon and rhombencephalon at stage HH21 (Fig. 3iii, A and C, arrows). The staining of the PNVP appeared dark and thick as numerous endothelial cells were present around the mesencephalon at this stage. The dorsal migration of isolated angioblasts, however, could not be detected using the antisense Ets1 probe between stages HH19 and HH26 of development (Fig. 3iv, C). Sprouting continued throughout the mesencephalon at stage HH26 (Fig. 3iii, A, arrows), whereas sprouting into the diencephalon first began at this developmental stage (Fig. 3iv, B, arrow). The location at which endothelial sprouts invaded the brain did not appear to correlate with the position of the differentiated neurons. Upon reaching the ependymal layer, Ets1-positive cells were not seen to migrate farther towards the ventricular zone. Instead, Ets1-positive cells began to branch and continued to migrate in a different direction, parallel with the ventricular surface of the brain, leading to the initiation of INVP formation through the anastomosis of neighbouring sprouts, which was first observed in both the ventral mesencephalon and rhombencephalon at stage HH24 (Fig. 3iii, B-C, arrows). The sprouting process initiated as a single specialised endothelial cell, referred to as the tip cell, penetrated the basal lamina. Multiple stalk cells were seen aligned behind the tip cell, which leads the endothelial sprout into the brain (Fig. 3v, arrowheads).

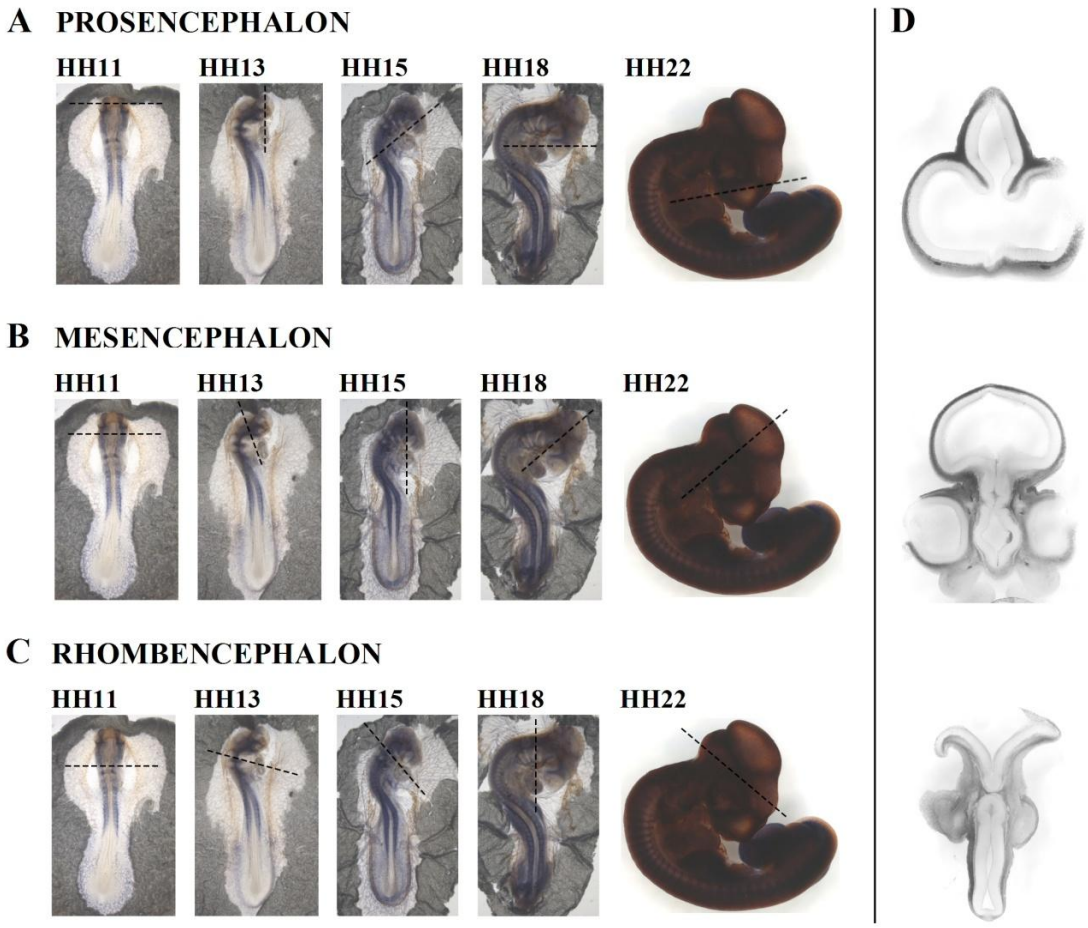

Figure 3i. Planes of sectioning following whole-mount ISH and IHC. Endothelial cells (blue) and neurons (brown) were detected with an antisense Ets1 probe and a TuJ1 antibody against neuron-specific Class III β-tubulin antibody, respectively. Embryos were embedded in 20% gelatin/PBS before cutting 30μm sections through the prosencephalon (**A**), mesencephalon (**B**) and rhombencephalon (**C**) using a vibratome. Typical sections taken through a stage HH22 chick embryo from each plane are displayed on the right (**D**).

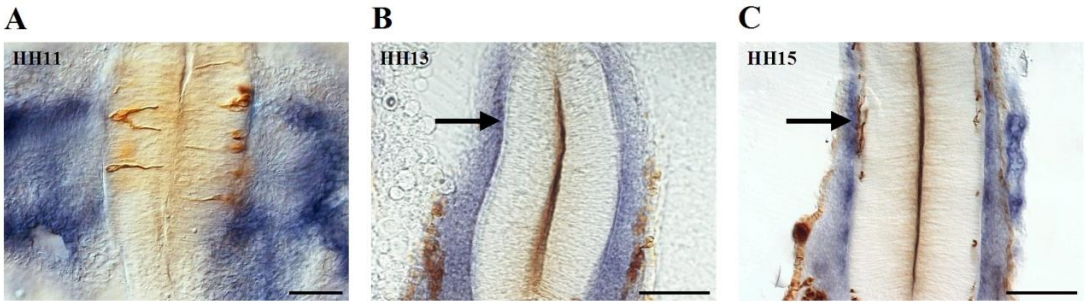

Figure 3ii. Endothelial cell migration and PNVP formation. Endothelial cells (blue) and neurons (brown) were detected with an antisense Ets1 probe and a TuJ1 antibody, respectively. **A**. Endothelial cells can be seen migrating towards the neural tube at stage HH11 of chick development and the formation of the PNVP around the mesencephalon begins thereafter at stage HH13 (**B**, arrow). The PNVP continues to develop around the mesencephalon at stage HH15 (**C**, arrow). Scale bar = 50μm.

Figure 3iii. Vascularisation of the *G. gallus* mesencephalon and rhombencephalon using ISH with an Ets1 antisense probe and IHC with a TuJ1 antibody. Endothelial cells (blue) and neurons (brown) were detected in the basal plate of the mesencephalon (**A**), ventral mesencephalon (**B**) and rhombencephalon (**C**) of stage HH19-26 chicken embryos. Endothelial cell sprouting into the brain is first observed in the ventral mesencephalon and rhombencephalon at stage HH21 (**A** and **C**, arrows), continuing in the basal plate of the mesencephalon at stage HH26 (**A**, arrows). The formation of the INVP is seen to begin in both the ventral mesencephalon and rhombencephalon at stage HH24 (**B-C**, arrows). HH19 n=3; HH21 n=3; HH24 n=8; HH26 n=7. Scale bar = 50µm.

HH26
HH24
HH21
HH19
A
MESENCEPHALON
BASAL PLATE
B
MESENCEPHALON
VENTRAL
C
RHOMBEN-
CEPHALON

Figure 3iv. Vascularisation of the *G. gallus* prosencephalon and mesencephalon using ISH with an Ets1 antisense probe and IHC with a TuJ1 antibody. Endothelial cells (blue) and neurons (brown) were detected in the telencephalon (**A**), diencephalon (**B**), dorsal (**C**) and alar plate (**D**) of the mesencephalon of stage HH19-26 chicken embryos. Endothelial cell sprouting begins in the diencephalon at stage HH26 (**B**, arrow), occurring later than the rest of the brain. Ingression into the alar plate of the mesencephalon can be seen at the same developmental stage (**D**, arrows). HH19 n=3; HH21 n=3; HH24 n=8; HH26 n=7. Scale bar = 50μm.

HH26
HH24
HH21
HH19
A
TELENCEPHALON
B
DIENCEPHALON
C
MESENCEPHALON
DORSAL
D
MESENCEPHALON
ALAR PLATE

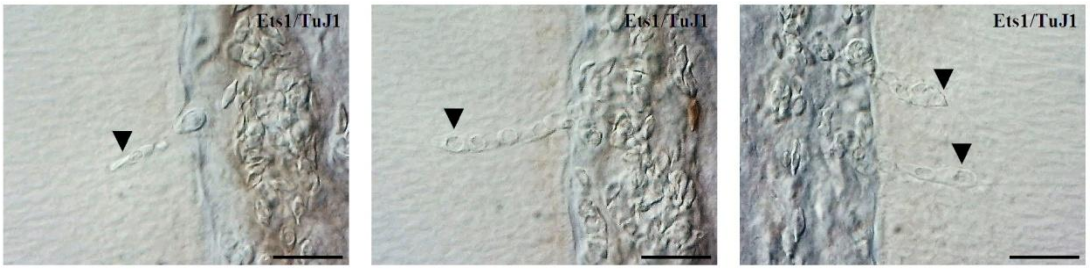

Figure 3v. The arrangement of tip and stalk cells within endothelial sprouts. Endothelial cells in the diencephalon at HH26 were detected with an antisense Ets1 probe using whole-mount ISH and are stained blue. A single specialised endothelial cell, referred to as the tip cell (arrowheads), leads each sprout through the basal lamina into the brain. The tip cell is followed by a number of stalk cells during ingression. Scale bar = 10μm.

3.2 Fibronectin expression occurs in close proximity to invading endothelial cells

Since endothelial cells are known to synthesise fibronectin, which is suggested to mediate the adherence of migrating endothelial cells (Clark *et al*., 1986; Peters *et al*., 1990), Ets1 staining was coupled with IHC to identify the location of fibronectin in relation to vascular ingression (Fig. 3vi). Fibronectin was not detected prior to the initiation of ingression at stage HH19, but as Ets1 was detected in endothelial cells that began to ingress into the ventral mesencephalon at stages HH21 and HH22, the staining patterns indicated the presence of fibronectin in close proximity to the invading sprouts. The co-localisation of endothelial cells and fibronectin within the mesencephalon became more apparent at stage HH24 as staining appeared darker, particularly in the region of the INVP. The staining for fibronectin continued to increase in abundance and strength as the internal capillary network continued to develop at stage HH26.

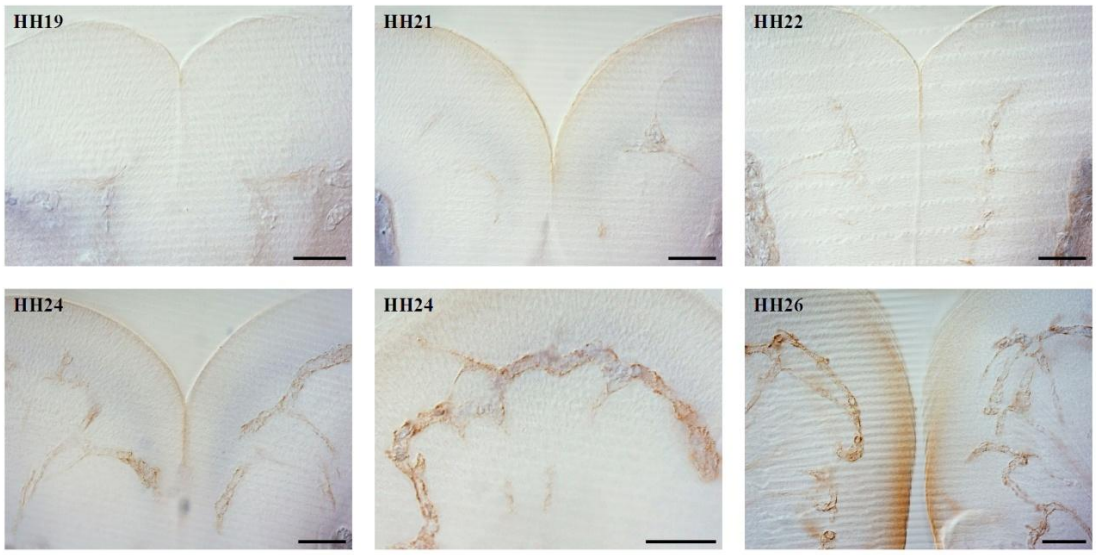

Figure 3vi. Time-course analysis of fibronectin production within the midbrain of stage HH19-26 *G. gallus* embryos. Endothelial cells (blue) are detected using whole-mount ISH with an Ets1 antisense probe, coupled with IHC using the fibronectin antibody B3/D6 (n=1 for each stage). Fibronectin is detected together with the invading sprouts when ingression into the ventral midbrain begins at stage HH21 and is also present in the basal lamina. The ingressing endothelial cells are likely to produce fibronectin as staining is present in close proximity to the location of vessel sprouts and coordinates with the developing INVP as the embryos grow. Scale bar = 50μm.

3.3 The detection of Mef2c and CD34 can also be used to identify the location of endothelial cells during brain vascularisation

Sprouting angiogenesis involves the specific induction of the transcription factor Mef2c by Ets1, which is mediated by A2M, resulting in a strong inhibitory effect on angiogenic sprouting in order to prevent excess angiogenesis when local oxygen concentration is sufficient following neovascularisation (De Val *et al*., 2004; Hickey & Simon, 2006; Sturtzel *et al*., 2014). Whole-mount ISH with an antisense probe against Mef2c was therefore also performed in *G. gallus* embryos to label endothelial cells at stages HH19-26 of development. Following gelatin embedding and sectioning, Mef2c-positive cells were seen migrating into the dorsal prosencephalon at stage HH19 (Fig. 3vii, B, arrows) and in the mesencephalon at stage HH21 (Fig. 3vii, C, arrow). Since Ets1 induces Mef2c expression it is interesting that isolated angioblasts migrating into the dorsal brain were Mef2c-positive but could not be detected with the antisense Ets1 probe. It may be possible that Ets1 was expressed at a level too low for detection using ISH or that Mef2c was induced by an unknown factor at this stage. Similar to the staining achieved with the antisense Ets1 probe, the initiation of sprouting was also detected at stage HH21 as Mef2c-positive cells were seen invading the ventral mesencephalon (Fig. 3viii, A-B, arrows). Sprouting was also seen to begin in the telencephalon at stage HH26 (Fig. 3vii, A, arrow). The branching and fusion of Mef2c-positive sprouts, indicating the formation of the INVP, was clearly visible in the ventral mesencephalon and rhombencephalon at stage HH24 (Fig. 3viii, B-C, arrowheads). Comparing the staining patterns of Ets1 and Mef2c, the expression of Ets1 was more diffuse throughout the PNVP, whereas Mef2c appeared to be expressed more specifically in individual cells that were discernible within the PNVP (Fig. 3ix). A summary of the ingression process is provided in Fig. 3x that documents the earliest stage at which each event was detected, including the formation of the PNVP and endothelial sprouting. The subsequent formation of the INVP was detected at stage HH28 as an extensive capillary network was seen developing throughout the mesencephalon (Fig. 3x, M). A schematic summary showing the progression of vascularisation of the embryonic *G. gallus* brain is also provided in Fig. 3xi.

Figure 3vii. Vascularisation of the *G. gallus* prosencephalon and mesencephalon using ISH with a Mef2c antisense probe. Endothelial cells (blue) were detected in the telencephalon (**A**), diencephalon (**B**), dorsal (**C**) and alar plate (**D**) of the mesencephalon of stage HH19-26 chicken embryos. The formation of the PNVP appears to continue between stages HH19 and HH24 of development. Angioblasts begin to migrate into the diencephalon and dorsal mesencephalon at stages HH19 and HH21, respectively (**B-C**, arrows). Endothelial cell sprouting into the telencephalon is also observed to begin at stage HH26 (**A**, arrow). HH19 n=4; HH21 n=6 ; HH24 n=6 ; HH26 n=3. Scale bar = 50µm.

HH26
HH24
HH21
HH19
A
TELENCEPHALON
B
DIENCEPHALON
C
MESENCEPHALON
DORSAL
D
MESENCEPHALON
ALAR PLATE

Figure 3viii. Vascularisation of the *G. gallus* mesencephalon and rhombencephalon using ISH with a Mef2c antisense probe. Endothelial cells (blue) were detected in the basal plate of the mesencephalon (**A**), ventral mesencephalon (**B**) and rhombencephalon (**C**) of stage HH19-26 chicken embryos. Endothelial cell sprouting is first seen in the ventral half of the mesencephalon at stage HH21 (**A-B**, arrows). The formation of the INVP is clearly visible in both the ventral mesencephalon and rhombencephalon at stage HH24 (**B-C**, arrowheads). HH19 n=4; HH21 n=6 ; HH24 n=6 ; HH26 n=3. Scale bar = 50µm.

HH26
HH24
HH21
HH19
A
MESENCEPHALON
BASAL PLATE
B
MESENCEPHALON
VENTRAL
C
RHOMBEN-
CEPHALON

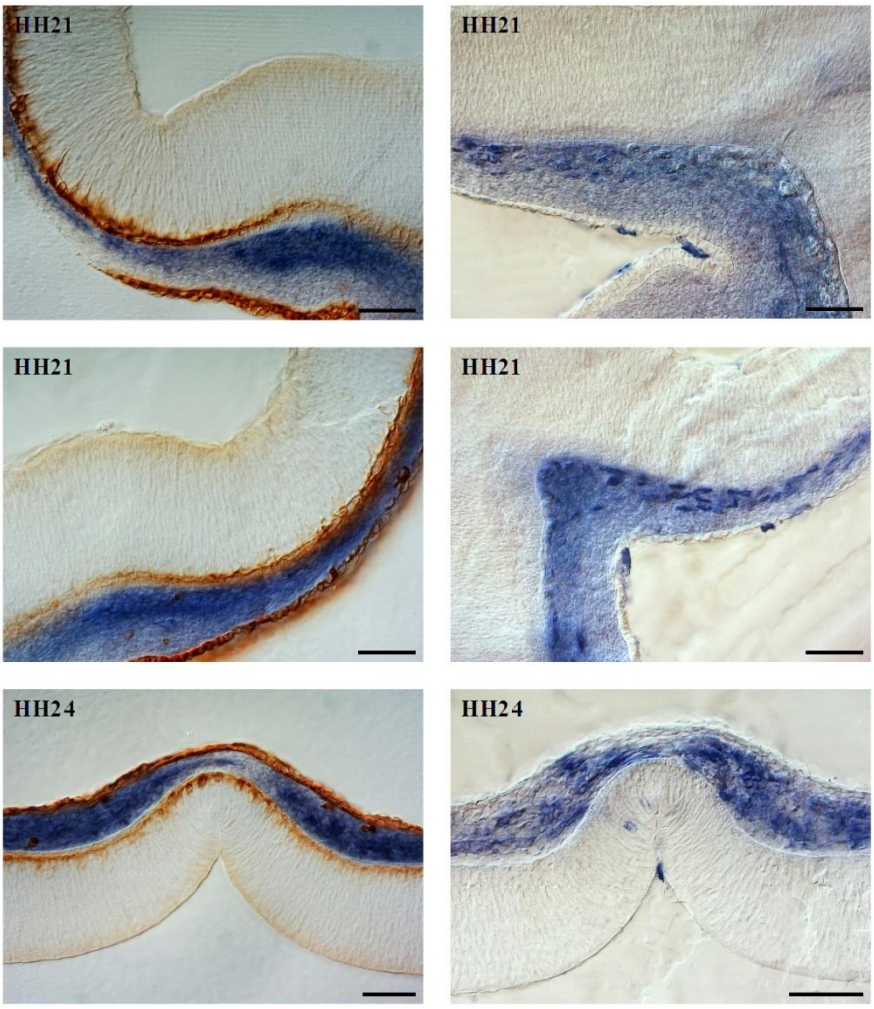

Figure 3ix. Ets1 and Mef2c expression in the PNVP of the mesencephalon. Embryos at stages HH21 and HH24 were stained using ISH to label endothelial cells blue with either an antisense Ets1 probe (left) or Mef2c probe (right). Ets1 staining is coupled with IHC using a TuJ1 antibody to label neurons brown. The dense Ets1 staining marks the location of the PNVP. The expression of Mef2c is detected in individual cells within the PNVP, which is indicated by the discontinuous and more specific staining in this region. Scale bar = 50µm.

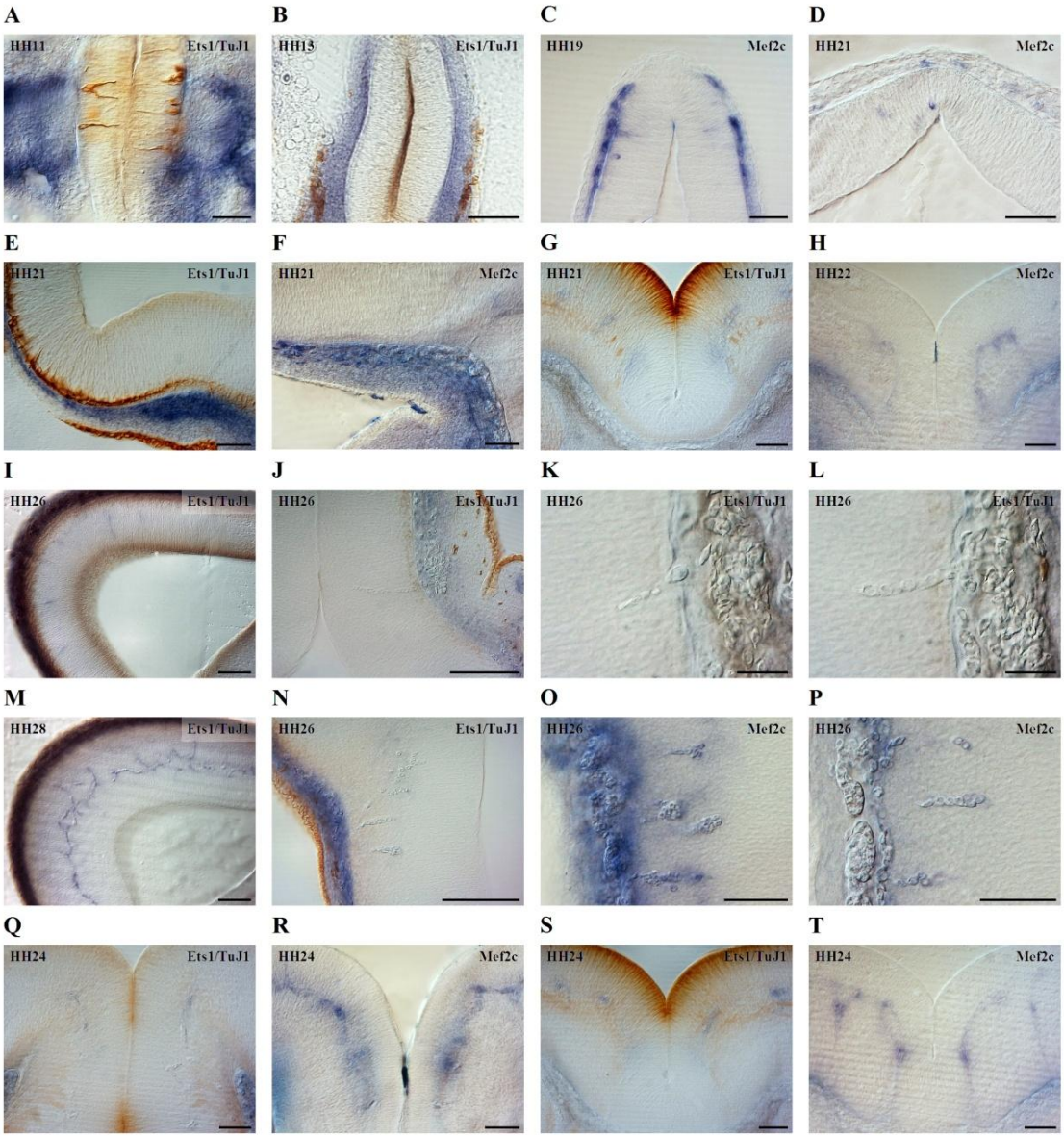

Figure 3x. Summary of events involved in the vascularisation of the *G. gallus* brain. Embryos at stages HH11-28 were stained using ISH to label endothelial cells blue with either an antisense Ets1 or Mef2c probe in order to detect the earliest stage at which each event occurs. Ets1 staining is coupled with IHC using a TuJ1 antibody to label neurons brown. **A**. Endothelial cells are first seen migrating towards the anterior neural tube at HH11, leading to the start of PNVP formation around the mesencephalon by HH13 (**B**). Dorsal migration of angioblasts occurs in the diencephalon at HH19 (**C**) and mesencephalon at HH21 (**D**). Sprouting is first observed in both the ventral mesencephalon (**E-F**) and rhombencephalon (**G-H**) at stage HH21, continuing throughout the tectum at stage HH26 (**I**). Sprouting in the prosencephalon begins later than in the mesencephalon and rhombencephalon, initiating at HH26 in both the diencephalon (**J-L**) and telencephalon (**N-P**). The formation of the INVP begins as neighbouring sprouts anastomose in the ventral mesencephalon (**Q-R**) and rhombencephalon (**S-T**) at HH24, then throughout the tectum at stage HH28 (**M**). Scale bar = 50µm (K-L = 10µm).

Figure 3xi. Schematic summary showing the progression of vascularisation of the embryonic *G. gallus* brain. Lateral and transverse cross sections depict the major vascularisation events between stages HH11 and HH26 of chick development. **A**. Endothelial cells migrate towards the mesencephalon at HH11, leading to the start of PNVP formation by HH13 (**B**). **C**. Dorsal migration of angioblasts occurs in the diencephalon at HH19 and in the mesencephalon at HH21 (**D**), during which sprouting initiates in both the ventral mesencephalon and rhombencephalon. **E**. The INVP begins to form in the ventral mesencephalon and rhombencephalon at HH24 and sprouting continues throughout the tectum at stage HH26 (**F**) when sprouts begin to invade the telencephalon and diencephalon.

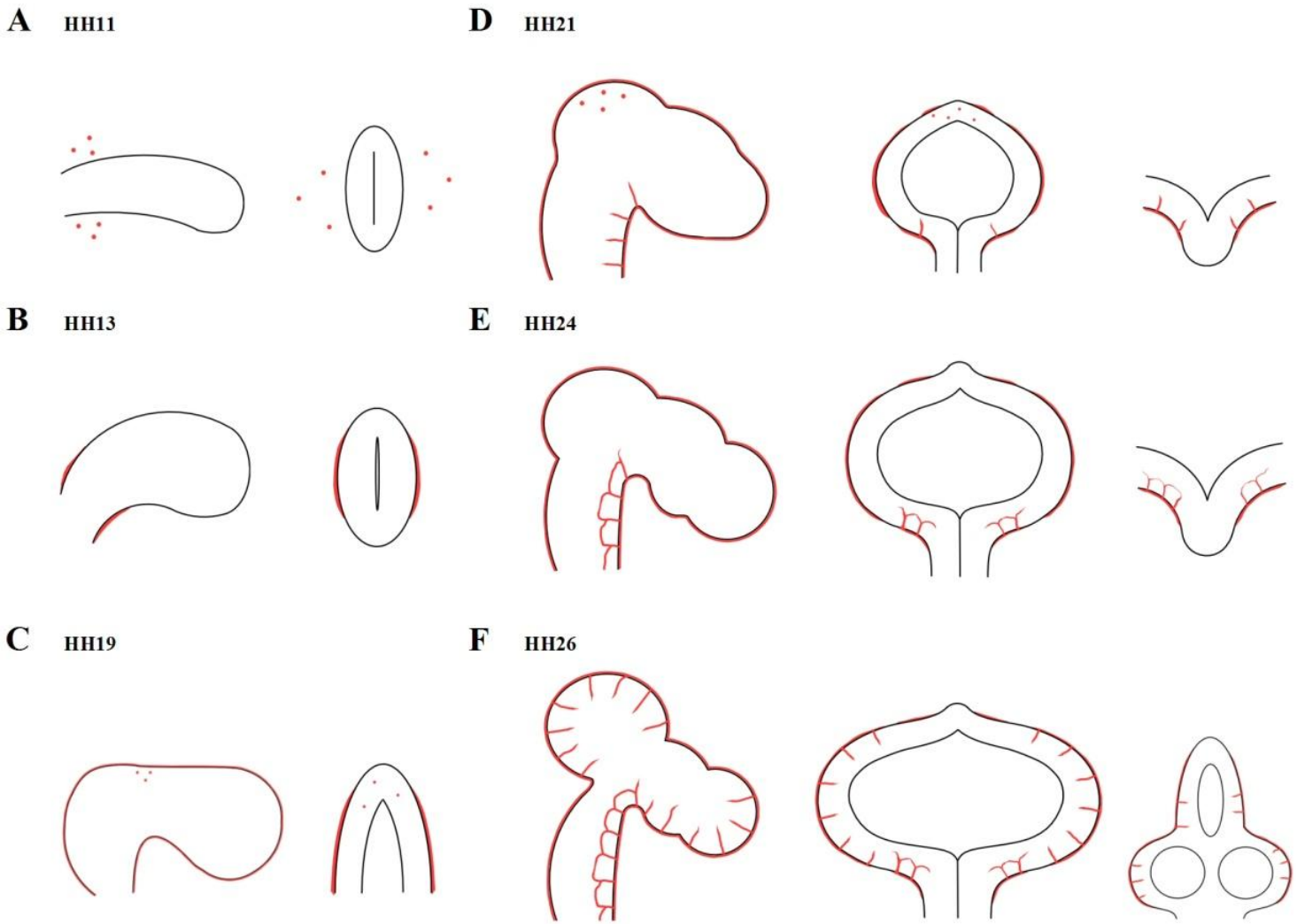
A HH11
B HH13
C HH19
D HH21
E HH24
F HH26

IHC experiments using an anti-CD34 antibody were also used to detect the spatial and temporal location of endothelial cells as an alternative to ISH studies (Fig. 3xii). Ets1-staining appeared to be weaker within the sprouts compared to the PNVP, which may indicate the loss of Ets1 expression during ingression. However, it is also possible that diffusion problems may have occurred in which the probe may not have been able to diffuse as readily through the brain tissue compared to the mesoderm and so access to the RNA by the probe may have been hindered. It is therefore difficult to determine the precise time at which each event occurs during brain vascularisation using the method of ISH, particularly if gene expression levels fluctuate and diffusion problems occur as the embryos develop. The staining of sprouts through the use of Mef2c ISH and CD34 IHC was comparable, although more cells present within the INVP were detected using the anti-CD34 antibody. The reliable identification of endothelial cells can therefore also depend on the chosen method of detection and the progress of vascularisation.

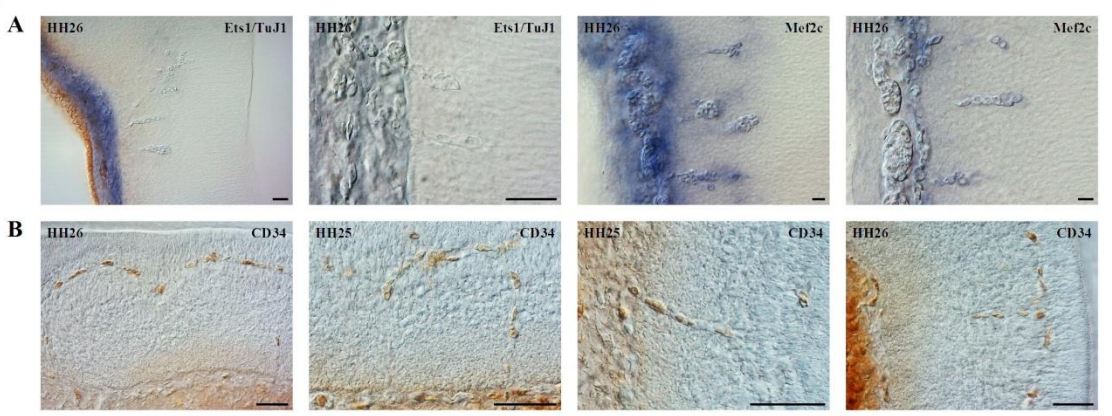

Figure 3xii. The detection of endothelial cells using ISH and IHC methods. A. Chick embryos are stained using ISH to label endothelial cells blue with either an antisense Ets1 probe or Mef2c probe. Ets1 staining is coupled with IHC using a TuJ1 antibody to label neurons brown. Scale = 10μm. **B**. Endothelial cells can be detected using whole-mount IHC with a CD34 antibody as a faster alternative to ISH experiments. Visualisation is achieved with the addition of DAB substrate to the HRP-conjugated secondary antibody, staining endothelial cells brown. The two methods can be used to successfully stain endothelial cells, particularly with the use of Ets1 for the PNVP, Mef2c and CD34 for the invading sprouts, and CD34 for the INVP. Immunostaining experiments provide a versatile method for the spatial and temporal location of biomarkers in embryos and are useful for double-labelling studies involving fluorescent detection. CD34 concentration used at 1:1000. Scale = 50μm.

3.4 Endothelial cell migration and PNVP formation occur earlier in the brain than in the spinal cord

The sequence of events involved in the vascularisation of the avian brain closely follows previous observations in quail and mouse as described in the literature. In concordance with key research previously conducted in the quail spinal cord by Kurz *et al*. (1996) and James *et al*. (2009), the initiation of vascularisation occurs earlier at more anterior levels of the CNS with the PNVP forming around the brain at stage HH13 compared with the thoracic spinal cord at stage HH16. The dorsal migration of angioblasts at HH19 and ventral sprouting at HH21 in both the brain and cervical spinal cord also occur slightly earlier than in the thoracic spinal cord at stage HH22. (Fig. 3xiii).

The observation of these events initiating earlier at more anterior levels of the CNS likely reflects the importance of developing the complex structure and function of the brain, which requires a greater level of molecular control compared with the spinal cord. Furthermore, as development progresses in an anterior to posterior direction, the brain continues to grow in size and may experience tissue hypoxia earlier than the spinal cord. Studies conducted in mouse and rat indicate that angiogenesis is induced by exposure to hypoxia (Harik *et al*., 1995; Masamoto *et al*., 2013), thus supporting the hypothesis that low oxygen concentrations resulting from growth in size of the brain leads to the initiation of angiogenesis. The developing mouse hindbrain is a popular model for studying sprouting angiogenesis and the vascularisation of which appears to proceed in a similar pattern to that observed in the *G. gallus* brain, as sprouts from the PNVP grow radially towards the ventricular zone, migrate at near right angles and extend parallel to the surface of the hindbrain, leading to the formation of the SVP (Fantin *et al.,* 2013).

Figure 3xiii. Comparison of spinal cord and brain vascularisation events in the avian embryo. A. Schematic summary of the major blood vessel patterning events in the spinal cord of quail embryos. A series of steps involved in the vascularisation process are described by the visualisation of endothelial cells through the use of QH1 immunostaining by Kurz *et al.* (1996) at cervical level (**B**) and James *et al*. (2009) at thoracic level (**C**), compared with the vascularisation of the brain achieved through ISH using an Ets1 or Mef2c probe in chick embryos (**D**). The migration of endothelial cells and formation of the PNVP occur earlier in the brain at stages HH11-13. In the spinal cord, the PNVP begins to form along the lateral surface of the neural tube at HH16-18 (**C**) and continues to develop at both cervical and thoracic level as the embryo grows beyond HH20 (**B**) to HH22-24 (**C**). Later events occur at similar stages of embryonic development in both the brain and spinal cord with the dorsal migration of angioblasts and ventral invasion of endothelial sprouts initiating at stages HH19 and the HH21, respectively.

A **SPINAL CORD**

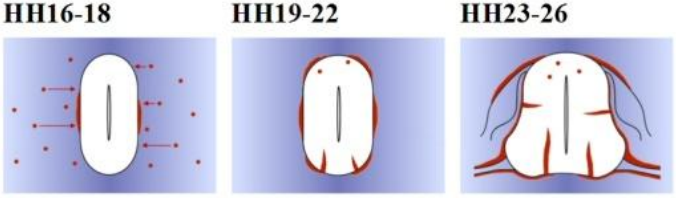

B

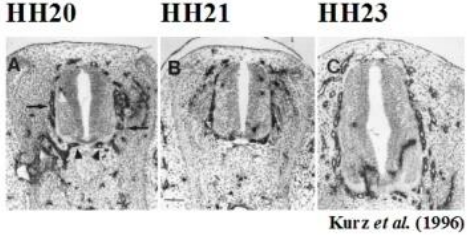

Kurz *et al.* (1996)

C

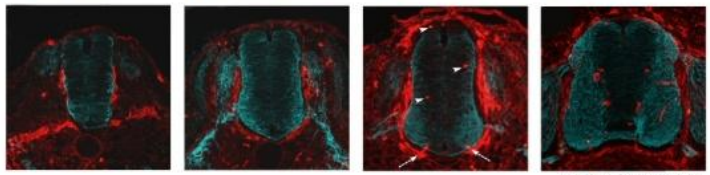

James *et al.* (2009)

D **BRAIN:**

EC MIGRATION TOWARDS BRAIN	**HH11**
PNVP FORMATION	**HH13**
DORSAL MIGRATION	**HH19**
SPROUTING	**HH21 - MIDBRAIN**
	HH21 - HINDBRAIN
	HH26 - FOREBRAIN
INVP FORMATION	**HH24**

3.5 Endothelial cells proliferate throughout the process of vascularisation

Endothelial cells that constitute the blood vessels within the brain were found to originate from the cephalic mesoderm (Couly *et al*., 1995), although cell proliferation during brain vascularisation has not yet been fully documented. The proliferation of endothelial cells is essential for the normal development of blood vessels. Immunostaining was therefore used to investigate cell replication during endothelial ingression into the *G. gallus* brain by labelling mitotic cells with a phosphohistone H3 antibody, following ISH with the Ets1 probe (Fig. 3xiv). Some phosphohistone H3-positive cells were detected within the PNVP and in the sprouts in the prosencephalon, mesencephalon and rhombencephalon during stages HH22 to HH26 of development, indicating that these cells were actively dividing. Mitotic activity was identified within the stalk cells of invading sprouts most clearly at stage HH26 in the prosencephalon and mesencephalon, observed as a line of phosphohistone H3-positive cells extending from the basal lamina towards the ventricular surface of the developing brain (Fig. 3xiv, A-B, arrows). Numerous phosphohistone H3-positive cells in the ventricular zone revealed the position of proliferating neuronal precursor cells. Cell division was also detected in regions where sprouts began to branch and within the nascent INVP (Fig. 3xiv, C-D, arrowheads).

The results provide a novel contribution to the process of brain vascularisation, supporting research conducted in the early postnatal retina by Gerhardt *et al*. (2003) that reported vessel expansion through abundant proliferation in stalk cells of the invading sprouts in response to VEGFA signalling, as well as in the immature capillary plexus. Endothelial tip cell division has also been described in the literature as asymmetric division results in post-mitotic asymmetry of VEGFR. The heterogeneity of daughter cells as tip or stalk cells, independent of Dll4/Notch signalling, integrates proliferation and collective migration in angiogenesis (Costa *et al*., 2016). However, it is unclear whether or not endothelial tip cell proliferation has been identified in this study. Proliferation could be identified by using NF-κB as another potential marker (Mazor *et al*., 2013) or by conducting bromodeoxyuridine (BrdU) labelling. BrdU is a synthetic analog of the nucleoside thymine, which becomes incorporated into DNA during DNA synthesis. Cells in S phase therefore

become labelled, whereas the phosphohistone H3 antibody identifies the mitosis-specific phosphorylation of histone H3.

Previous research by Couly *et al*. (1995) described the recruitment of angiogenic cells from the cephalic mesoderm to provide the brain with its vasculature. Building upon this knowledge, not all endothelial cells within the brain originate from the outside as cell replication was identified at various stages throughout the process of brain vascularisation.

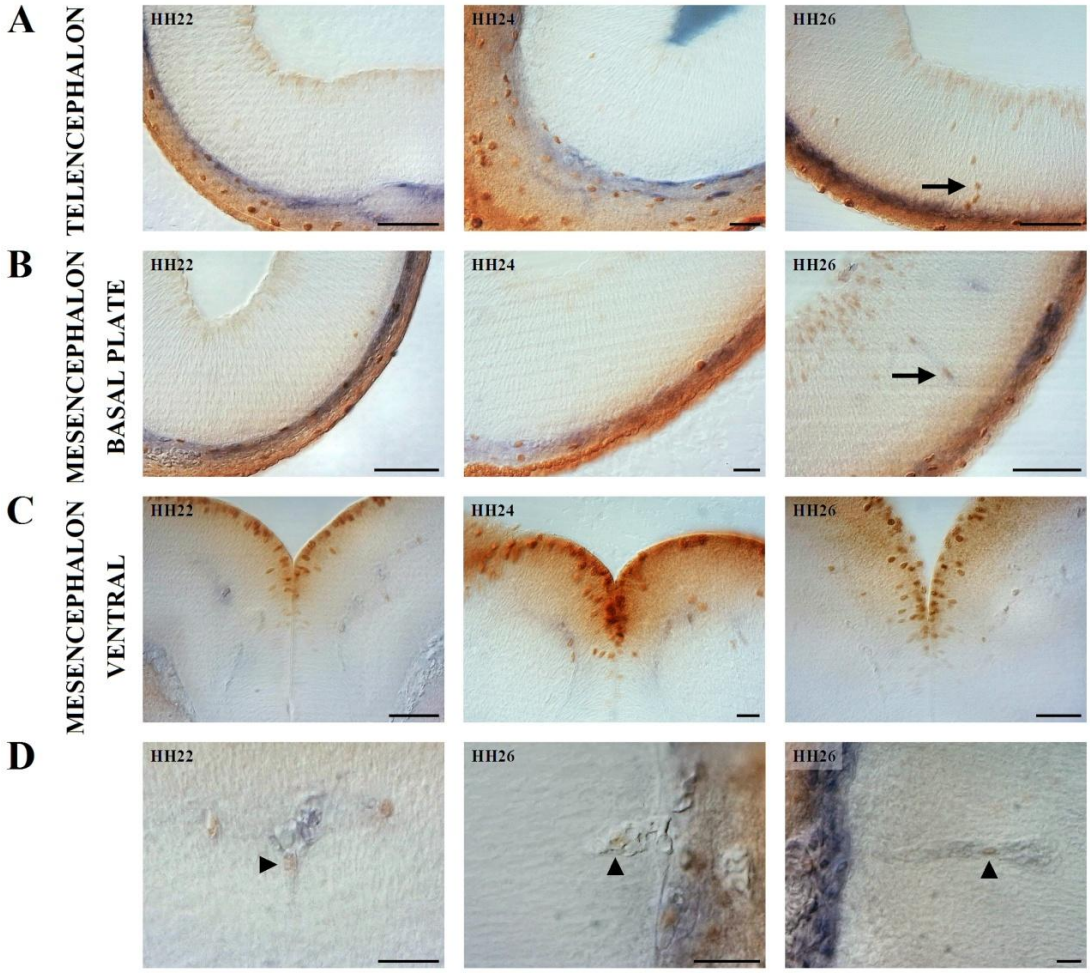

Figure 3xiv. Investigating cell replication during brain vascularisation. Mitotic cells (brown) are labelled using whole-mount IHC with a phosphohistone H3 antibody, following ISH with an antisense Ets1 probe to label endothelial cells (blue) in the prosencephalon (**A**), mesencephalon (**B**) and rhombencephalon (**C**). Endothelial cells are seen dividing within the PNVP across stages HH22-26 throughout the brain and in the stalk cells of invading sprouts (**A-B**, arrows). **D**. Cell division is also detected in regions of vessel branching (arrowheads) and within the developing INVP. Endothelial cells contributing to the brain vasculature initially originate from the mesoderm and replicate throughout the process of vessel ingression. HH22 n=3; HH24 n=4; HH26 n=6. Scale bar A-C = 25µm; D = 10µm.

3.6 The process of brain vascularisation is evolutionarily conserved throughout vertebrate evolution

Investigating the major events involved in the vascularisation of the chick brain provides useful information that builds upon the knowledge previously acquired through studies in both the brain and spinal cord of chick, quail and mouse embryos (Kurz *et al.*, 1996; James *et al.*, 2009; Fantin *et al.*, 2013). Studying these avian and mammalian model organisms is advantageous due to their evolutionary proximity to humans and shared similarities in mechanisms of development. However, research into the vascularisation of the amphibian brain is currently limited and was therefore conducted to identify whether or not the sequence of events by which the brain becomes vascularised is conserved throughout vertebrate evolution.

A method of LHC was established to elucidate the initial vascular patterning events occurring in the brain of *X. laevis* (Fig. 3xv). Lectins are carbohydrate-binding proteins that have previously been useful in microvascular analysis (Thurston *et al.*, 1996; Jilani *et al.*, 2003; Mazzetti *et al.*, 2004) and the *L. esculentum* agglutinin lectin was utilised, which binds specifically to N-acetyl-D-glucosamine-β(1,4)N-acetyl-D-glucosamine oligomers on the surface of endothelial cells. Preliminary experiments revealed the presence of endothelial cells lining up along the mid-level of the lateral surface of the midbrain by stage 42, which was indicative of a developing PNVP. Sprouting was first detected at this stage as endothelial cells formed narrow individual sprouts that invaded the ventral midbrain, similar to the observations in *G. gallus*, which was then followed by medial angiogenic sprouting at stage 46. The pattern of long continuous groups of endothelial cells sprouting into the midbrain at stage 46 and 48 developed into what appeared to be the presence of extensive discontinuous sprouts or scattered groups of endothelial cells within the brain at stage 50. The formation of an internal capillary network was unrecognisable at this stage, although the pattern may differ from that observed in *G. gallus* embryos as ingression may proceed in a number of different angles.

Some similarities in the vascularisation of the *X. laevis* brain and that of the avian and mouse models, specifically the formation of a PNVP and initial sprouting into the ventral brain followed by medial angiogenic sprouting, support the notion that

particular events involved in the process of brain vascularisation is conserved in vertebrate evolution. However, the dorsal migration of angioblasts and the formation of an obvious capillary network within the *Xenopus* brain were undetected by stage 50. A network of capillaries may already be forming within the brain and this could be determined by performing sagittal sections and analysing *X. laevis* embryos beyond stage 50 of development.

Studies conducted in zebrafish also provide extra support for an evolutionarily conserved process across numerous model organisms. Zebrafish embryos are particularly useful for studying vascular development due to their accessibility and optical clarity. Previous studies have described the origin and fates of vessels in the zebrafish trunk (Childs *et al*., 2002) and a number of transgenic lines have been generated as *in vivo* models for the imaging of blood vessels using *Fli1* or *VEGFR2* promoters to drive the expression of GFP (Lawson & Weinstein, 2002; Cross *et al*., 2003). The direct observation of angiogenesis in *TG(fli1:EGFP)* embryos reveals that enhanced GFP (EGFP) is first detected at the three-somite stage. Individual angioblasts have been seen to exit a strip of lateral mesodermal EGFP-positive cells, which then migrate towards the trunk midline and a vascular network is established as tip cells join with neighbouring anterior and posterior cells. Endothelial cells of the segmental arteries and the dorsal longitudinal anastomotic vessel undergo extensive proliferation during the formation of the trunk. Observations in the hindbrain have shown that central arteries are present at 3 days post-fertilisation (dpf), displaying extensive filopodial activity and pathfinding behaviour similar to neuronal growth cones (Lawson & Weinstein, 2002; Blum *et al*., 2008). A more in-depth analysis could however be conducted in order to identify the early events involved in vascular patterning of the embryonic zebrafish brain, from the initial migration of angioblasts to the formation of an internal vessel network.

Figure 3xv. Vascularisation of the *X. laevis* midbrain using LHC on sections. Endothelial cells were detected in stage 42-50 embryos using a biotinylated *L. esculentum* agglutinin lectin. Visualisation was achieved through the addition of HRP-conjugated streptavidin and DAB substrate to stain endothelial cells brown. The PNVP can be seen developing along the mid-level of the lateral surface of the brain by stage 42 of development when sprouting initiates in the ventral midbrain (arrow). Medial angiogenic sprouting is observed at stage 46, which continues as the embryos grow. Extensive sprouting is exhibited by stage 50, although the formation of an internal capillary network remains unrecognisable at this stage. Stage 42 n=6; stage 44 n=8; stage 46 n=7; stage 48 n=5; stage 50 n=6. Scale bar = 10µm.

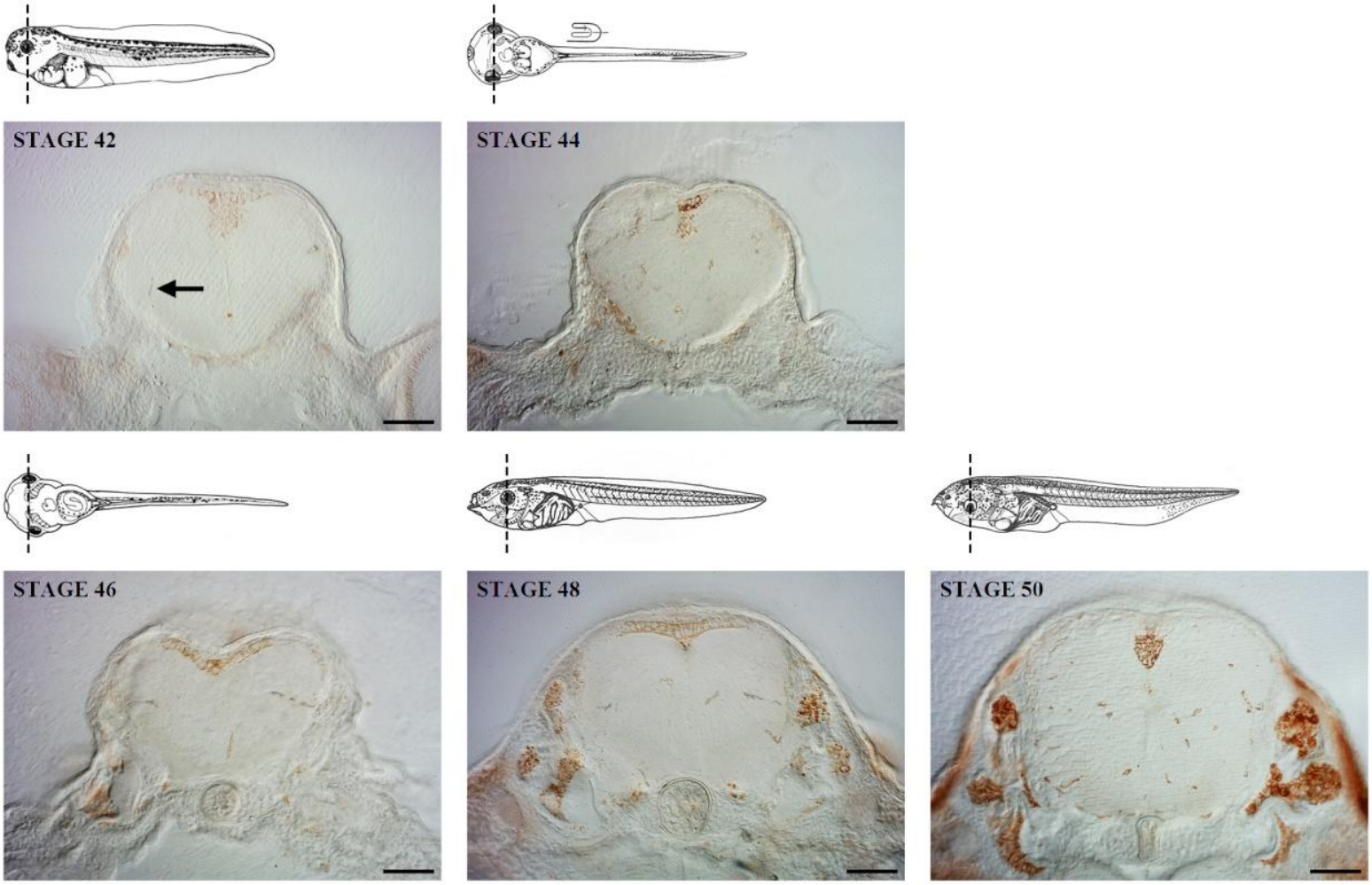
STAGE 42
STAGE 44
STAGE 46
STAGE 48
STAGE 50

3.7 Vascular ingression proceeds in correlation with the pattern of neurogenesis in the early brain

The early axon scaffold in the embryonic vertebrate brain is established from the arrangement of early nerve connections that follow a well-conserved pattern. The development of the early axon scaffold in the *G. gallus* embryo has previously been analysed by Ware & Schubert (2011), revealing that the first neurons in the brain differentiate in the diencephalon at stage HH11 and begin to form the first axon tract known as the medial longitudinal fascicle (MLF). Shortly afterwards, the first neurons of the descending tract of the mesencephalic nucleus of the trigeminal nerve (DTmesV) appear at the dorsal midline of the mesencephalon and neurons of the tract of the postoptic commissure (TPOC) appear in the rostral hypothalamus. A continuous ventral longitudinal tract (VLT) is formed by the TPOC and MLF at HH15 and axons of the DTmesV move towards the alar-basal boundary in the mesencephalon. The DTmesV axons then turn caudally towards the midbrain-hindbrain boundary (MHB) during which axons from the mamillo-tegmental tract (MTT) neurons in the caudal hypothalamus join the VLT. The major axon tracts increase in complexity as the embryo develops and at HH17 additional neurons differentiate in the rostral diencephalon and in the alar plate of the mesencephalon.

Endothelial ingression begins after neurogenesis and proceeds in a fashion that follows the pattern of which neurons and axon tracts first appeared in the brain. Similar to the differentiation of the first neurons in the brain, the migration of angioblasts is also first observed in the diencephalon, albeit dorsally, then in the mesencephalon where axons from the MLF neurons are projected. The progression of vessel sprouting into the brain, which first occurs in the ventral mesencephalon and later continues throughout the tectum, is consistent with neurogenesis as neurons also begin to differentiate in the tegmentum, followed by the tectum. Sprouting initiates at the ventral mesencephalon in which the VLT system has formed and also in the rhombencephalon, following the movement of DTmesV axons from the mesencephalon to the rhombencephalon. Sprouting then continues throughout the alar plate as the embryo grows and initiates in both the diencephalon and telencephalon, after the differentiation of additional neurons in these regions. The vascularisation of the brain therefore appears to progress in a similar pattern to

neurogenesis as endothelial ingression is observed in regions of the brain in the same sequence preceded by neuronal differentiation (Fig. 3xvi). The results demonstrate the cross-talk between neural cells and endothelial cells as neurovascular interaction ensues to regulate the formation of an efficient network of blood vessels required to support the growth and development of the brain.

Figure 3xvi. Vascularisation of the brain progresses in a similar pattern to neurogenesis in the *G. gallus* embryo. **A**. The development of neurons and axon tracts during early development. The first MLF neurons differentiate in the diencephalon at HH11 and project axons caudally. Axons of the TPOC project from the rostral hypothalamus towards the diencephalon-midbrain boundary at HH14. A continuous VLT is then formed by the TPOC and MLF. Axons of the DTmesV move towards the alar-basal boundary in the mesencephalon then turn caudally towards the MHB at HH16. Axons from the MTT neurons join the VLT system and additional neurons differentiate in the prosencephalon and in the mesencephalic alar plate, continuing to rise in number at HH18. **B**. The vascularisation of the brain begins as angioblasts first migrate into the dorsal diencephalon at HH19 then in the mesencephalon at HH21. Sprouting also initiates at this developmental stage into the ventral mesencephalon, where the VLT system has formed, and into the rhombencephalon, leading to the subsequent formation of the INVP in both regions at HH24. Sprouting is then observed at HH26 in the prosencephalon and continues throughout the tectum at stage HH26, following the differentiation of additional neurons within these brain regions. III, oculomotor nerve; DTmesV, descending tract of the mesencephalic nucleus of the trigeminal nerve; LLF, lateral longitudinal fascicle; MLF, medial longitudinal fascicle; MTT mamillo-tegmental tract; TB, tecto-bulbar axons; TN, terminal nerve; TPC, tract of the posterior commissure; TPOC, tract of the postoptic commissure.

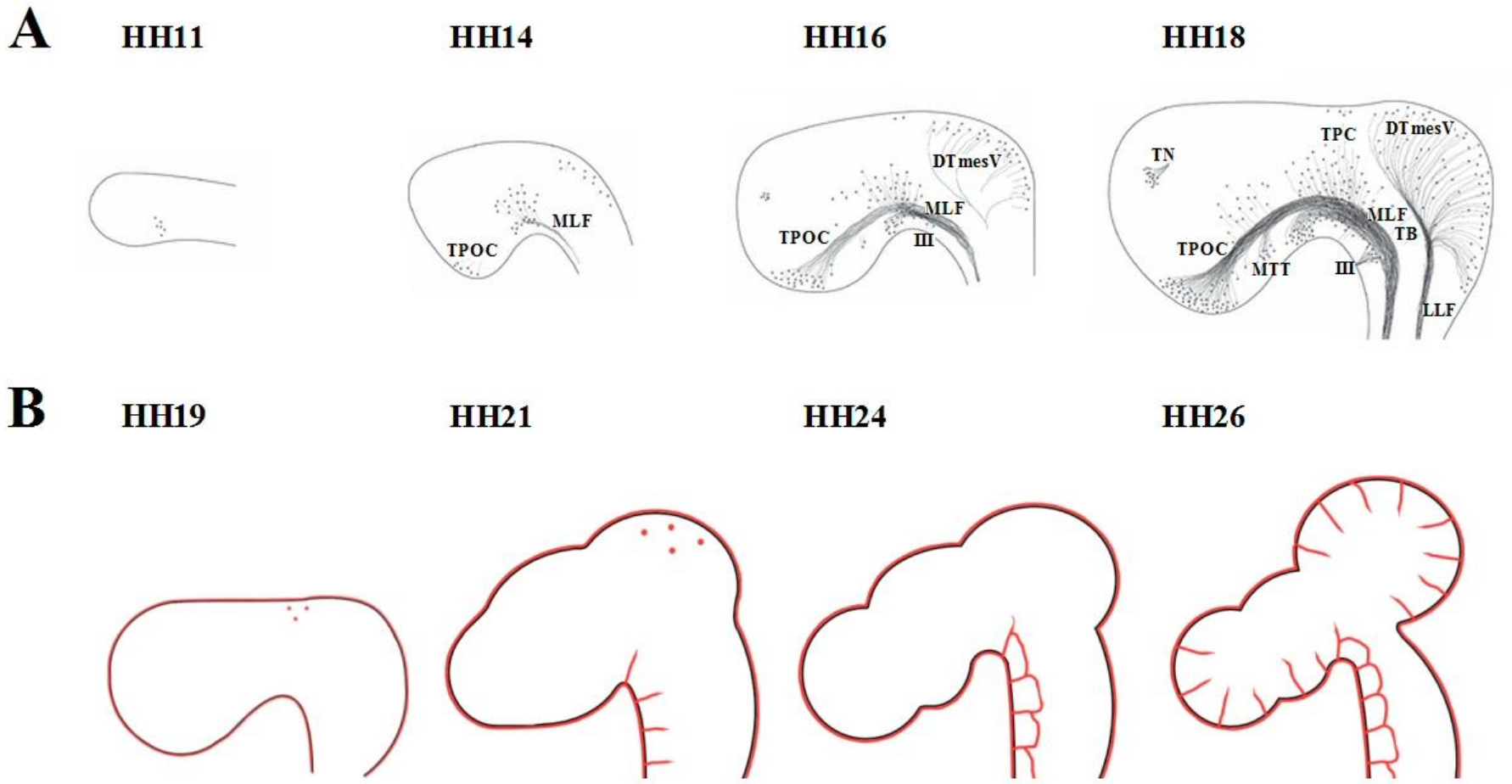
A
HH11
HH14
HH16
HH18
MLF
TPOC
DTmesV
MLF
TPOC
III
TN
TPC
DTmesV
MLF
TB
TPOC
MTT
III
LLF
B
HH19
HH21
HH24
HH26

4. THE INFLUENCE OF MMP ACTIVITY ON ENDOTHELIAL CELL INGRESSION

CNS vascularisation is distinct from general angiogenesis as the neuroectoderm is absent of endothelial cells and is also unable to give rise to angioblastic cells. The vascularisation of the neural tube therefore relies solely on an extraneuroectodermal origin of endothelial cells and angioblasts, which are recruited from the surrounding mesodermal tissue (Couly *et al*., 1995). The remodelling of the ECM is an essential aspect in angiogenesis. In addition to the well-established role of MMPs in matrix degradation, which subsequently liberates cells and growth factors from the matrix, the capabilities of these proteolytic enzymes extend to regulating other proteinases and proteinase inhibitors, latent growth factors, cleaving and activating cell-surface receptors and targeting cell-cell adhesion molecules (Brooks *et al*., 1996; Yu & Stamenkovic, 1999; Nagase & Woessner, 1999; Woessner & Nagase, 2000; Belkin *et al*., 2001; Kajita *et al*., 2001; Egeblad & Werb, 2002; Deryugina *et al*., 2002; Visse & Nagase, 2003; Boire *et al*., 2005). *In vitro* studies suggest that the migration of cultured vascular smooth muscle cells (VSMCs) through basement membrane barriers, of which type IV collagen is a major component, is dependent on MMP-2 activity (Pauly *et al*., 1994). Furthermore, type IV collagen has been shown to promote the activation of proMMP-2 by HT1080 fibrosarcoma cells (Maquoi *et al*., 2000). It is therefore conceivable that MMP activity is likely to be implicated in influencing brain vascularisation as endothelial cells can respond to a variety of signals that may lead to their migration towards the developing brain and penetration of the basal lamina upon the initiation of ingression. Very little is known about MMPs in CNS vascularisation, therefore the expression patterns of MMPs were analysed using ISH as a first step in the analysis of MMP activity during the vascularisation of the embryonic *G. gallus* brain. The primary focus was on MMP-1, which is known to cleave and activate PAR1 leading to the promotion of cell migration, as well as MMPs -2 and -9 that degrade type IV collagen present in the basement membrane. Gelatinase activity was also investigated in the developing brain of *G. gallus* embryos using ISZ studies. The levels of MMP activity were then manipulated by exposing embryos to pharmacological inhibitors and active MMP-1 in order to investigate the role of MMPs in ingression.

4.1 MMPs are expressed in the PNVP and the nascent INVP, with differential expression identified within the invading sprouts

Gene fragments for MMPs -1, -2 and -9 were cloned and used to synthesise antisense probes for whole-mount ISH experiments in *G. gallus* embryos at stages HH19-24 of development in order to identify the spatial and temporal expression patterns of these MMPs immediately prior to ingression, during ingression and as the INVP began to form in the mesencephalon. Specific staining was observed for each MMP at stage HH19 within the PNVP surrounding the ventral half of the mesencephalon, with particularly strong staining for MMP-1 close to the basal lamina of the brain as endothelial cells prepare to ingress (Fig. 4i, arrows). The absence of staining in the dorsal half of the mesencephalon at stage HH19 indicated a lack of obvious expression of MMPs -1, -2 and -9 in this region (Fig. 4ii). The expression of each MMP within the PNVP appeared to become more specific when the embryos developed to stage HH21 as individual cells were visible within the PNVP surrounding both the prosencephalon (Fig. 4iii) and the ventral half of the mesencephalon, with MMP-2 particularly present along the basal lamina of the brain (Fig. 4iv, arrows). Staining for all three MMPs remained absent from the dorsal half of the mesencephalon at this stage, either from a lack of expression in this region or due to levels that remained too low for ISH detection (Fig. 4v). The involvement of other proteases in the dorsal migration of angioblasts, which initiates in the mesencephalon at HH21, is therefore highly likely. The expression of each MMP also occurred within the invading sprouts at stage HH24 (Fig. 4vi, arrows) with strong staining of MMP-2 and MMP-9 observed parallel to the ventricular surface of the brain, indicative of the region where the INVP was being established (Fig. 4vi, B, arrows). Staining was first detected in the mesenchyme surrounding the dorsal mesencephalon at this developmental stage (Fig. 4vii, arrows).

Upon closer observation, the staining patterns seemed to indicate differential expression within the endothelial sprouts. MMP-1 appeared to be expressed more towards the tip of the sprout with lower levels present in the stalk cells. Staining for MMP-9 showed expression within the stalk cells and in the INVP, whereas MMP-2 was present throughout the sprout with strong expression also detected in the INVP (Fig. 4viii). Identifying differential expression patterns of MMPs -1, -2 and -9,

particularly within the ingressing endothelial sprouts, is fundamental in understanding the proteolytic function involved in the focused migration and navigation of sprouts through the ECM and also understanding how MMPs integrate and function within the complex signalling networks involved in brain angiogenesis.

The roles of tip cell migration and stalk cell proliferation resulting from differential gene expression between both cell types likely involves regulation by specific MMPs. The promotion of cell migration through the cleavage and activation of PAR1 by MMP-1 has been described in the literature (Boire *et al*., 2005; Blackburn & Brinckerhoff, 2008) and a stronger expression of MMP-1 identified towards the tip of the endothelial sprout than the base possibly indicates a role in directing the migration of the tip cell. MMP-2 and MMP-9 present in the base of the sprout and in the INVP suggests that these MMPs may influence the structure of the sprout and formation of the internal capillary network. The differential expression of MMPs observed within the invading sprouts is a novel contribution to the knowledge of angiogenesis within the brain and may contribute to the understanding of tumour progression since sprouts are also formed by invading cancer cells. Activated endothelial cells have been shown to express MMP-1, MMP-9 and MT1-MMP during sprouting angiogenesis and the formation of lumina-containing tubules. In a pancreatic cancer model, MMP-9 activity mediates endothelial sprouting and the release of ECM-bound VEGF and FGF2, thus acting to increase the bioavailability of proangiogenic factors *in vitro*. MT1-MMP also plays a key role in angiogenesis and the vascular expression and activity are largely confined to the sprouting tip of neovessels and migrating tumour cells, regulating collagen degradation at the leading edge of developing capillary structures (Bergers *et al*., 2000; Gálvez *et al*., 2005; Saunders *et al*., 2006; Yana *et al*., 2007; Ra & Parks, 2007; van Hinsbergh & Koolwijk, 2008; Packard *et al*., 2009; Deryugina & Quigley, 2010).

Figure 4i. MMP expression in the ventral half of the mesencephalon of stage HH19 *G. gallus* embryos. Whole-mount ISH was used with antisense probes against MMPs -1, -2 and -9, followed by vibratome sectioning (n=1 for each MMP). MMP expression in the basal plate (**A**) and ventral mesencephalon (**B**) compared to Ets1/TuJ1 staining for endothelial cells (blue) and neurons (brown) shown in the left-hand column. MMP-2 and MMP-9 are expressed within the PNVP beside the ventral half of the mesencephalon (arrows). Specific staining for MMP-1 is particularly strong within the PNVP and is present close to the basal lamina. MMP expression appears absent from the dorsal half of the mesencephalon, which is indicated by a lack of staining in this region. Scale bar = 50μm.

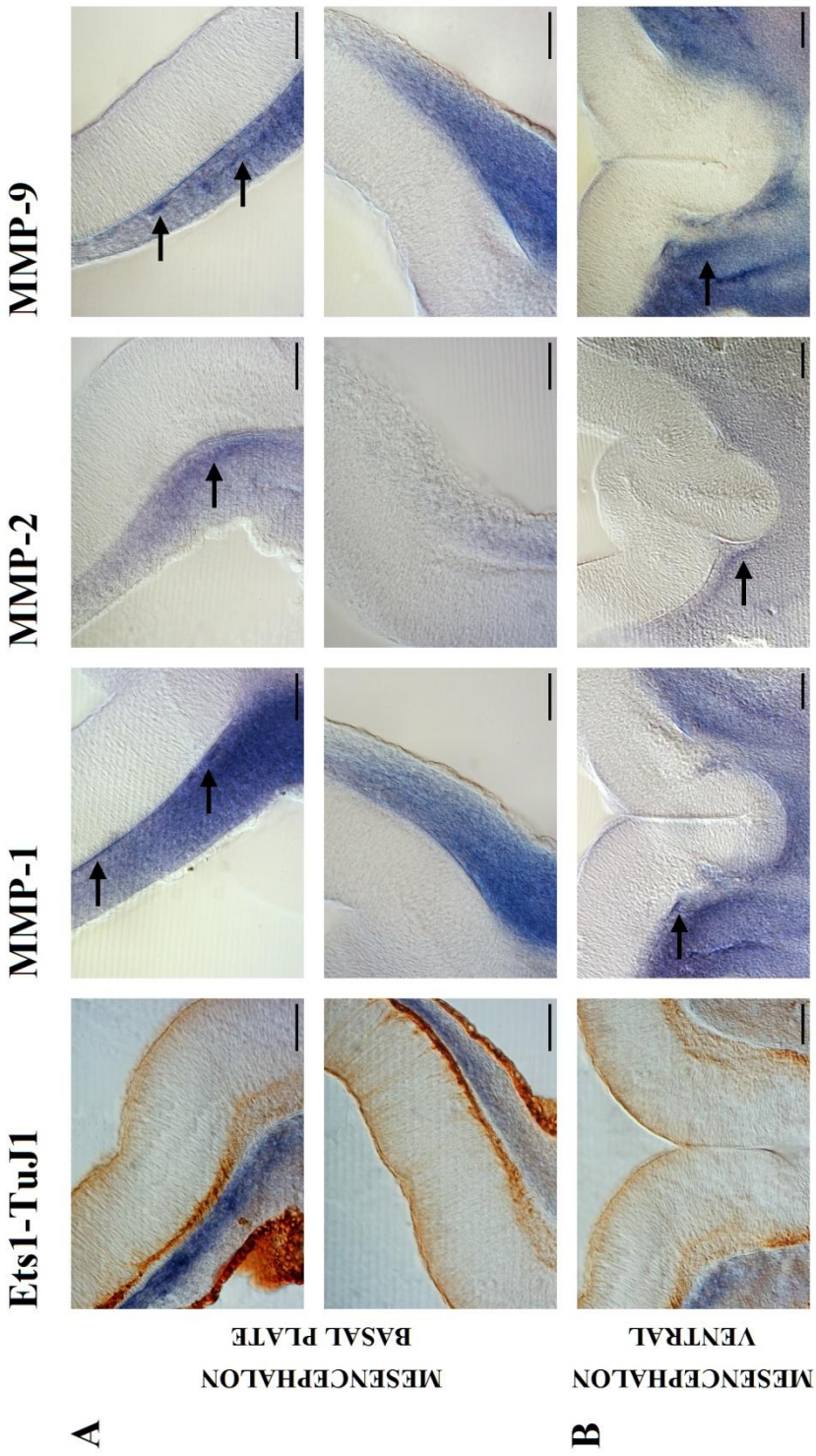
MMP-9
MMP-2
MMP-1
Ets1-TuJ1
MESENCEPHALON
BASAL PLATE
MESENCEPHALON
VENTRAL
A
B

Figure 4ii. MMP expression in the dorsal half of the mesencephalon of stage HH19 *G. gallus* embryos. Whole-mount ISH was used with antisense probes against MMPs -1, -2 and -9, followed by vibratome sectioning (n=1 for each MMP). MMP expression in the dorsal mesencephalon (**A**) and alar plate (**B**) compared to Ets1/TuJ1 staining for endothelial cells (blue) and neurons (brown) shown in the left-hand column. The lack of staining indicates an absence of MMP expression in this region of the brain. Scale bar = 50μm.

MMP-9
MMP-2
MMP-1
Ets1-TuJ1
MESENCEPHALON
DORSAL
A
MESENCEPHALON
ALAR PLATE
B

Figure 4iii. MMP expression in the prosencephalon of stage HH21 *G. gallus* embryos. Whole-mount ISH was used with antisense probes against MMPs -1, -2 and -9, followed by vibratome sectioning (n=2 for each MMP). MMP expression in the telencephalon (**A**) and diencephalon (**B**) of the prosencephalon compared to Ets1/TuJ1 staining for endothelial cells (blue) and neurons (brown) shown in the left-hand column. All three MMPs are expressed in specific cells within the PNVP of the prosencephalon. MMPs -1 and -2 staining patterns appear particularly close to the basal lamina of the brain. Scale bar = 50μm.

MMP-9
MMP-2
MMP-1
Ets1-TuJ1
TELENCEPHALON
DIENCEPHALON
A
B

Figure 4iv. MMP expression in the ventral half of the mesencephalon of stage HH21 *G. gallus* embryos. Whole-mount ISH was used with antisense probes against MMPs -1, -2 and -9, followed by vibratome sectioning (n=2 for each MMP). MMP expression in the basal plate (**A**) and ventral mesencephalon (**B**) compared to Ets1/TuJ1 staining for endothelial cells (blue) and neurons (brown) shown in the left-hand column. The specific staining for each MMP is more apparent compared to the expression patterns observed in the ventral half of the mesencephalon at stage HH19. All three MMPs are expressed in specific cells within the PNVP (arrows) with MMP-2 appearing along the basal lamina of the brain. Scale bar = 50μm.

MMP-9
MMP-2
MMP-1
Ets1-TuJ1
A
MESENCEPHALON
BASAL PLATE
B
MESENCEPHALON
VENTRAL

Figure 4v. MMP expression in the dorsal half of the mesencephalon of stage HH21 *G. gallus* embryos. Whole-mount ISH was used with antisense probes against MMPs -1, -2 and -9, followed by vibratome sectioning (n=2 for each MMP). MMP expression in the dorsal mesencephalon (**A**) and alar plate (**B**) compared to Ets1/TuJ1 staining for endothelial cells (blue) and neurons (brown) shown in the left-hand column. The lack of staining indicates that MMP expression remains absent in this region of the brain. Scale bar = 50μm.

MMP-9
MMP-2
MMP-1
Ets1-TuJ1
A
MESENCEPHALON
DORSAL
B
MESENCEPHALON
ALAR PLATE

Figure 4vi. MMP expression in the ventral half of the mesencephalon of stage HH24 *G. gallus* embryos. Whole-mount ISH was used with antisense probes against MMPs -1, -2 and -9, followed by vibratome sectioning (n=2 for each MMP). MMP expression in the basal plate (**A**) and ventral mesencephalon (**B**) compared to Ets1/TuJ1 staining for endothelial cells (blue) and neurons (brown) shown in the left-hand column. Staining is observed for each MMP within the invading sprouts with notable staining for MMP-2 and MMP-9 in the region where the INVP is being established (**B**, arrows). Scale bar = 50μm.

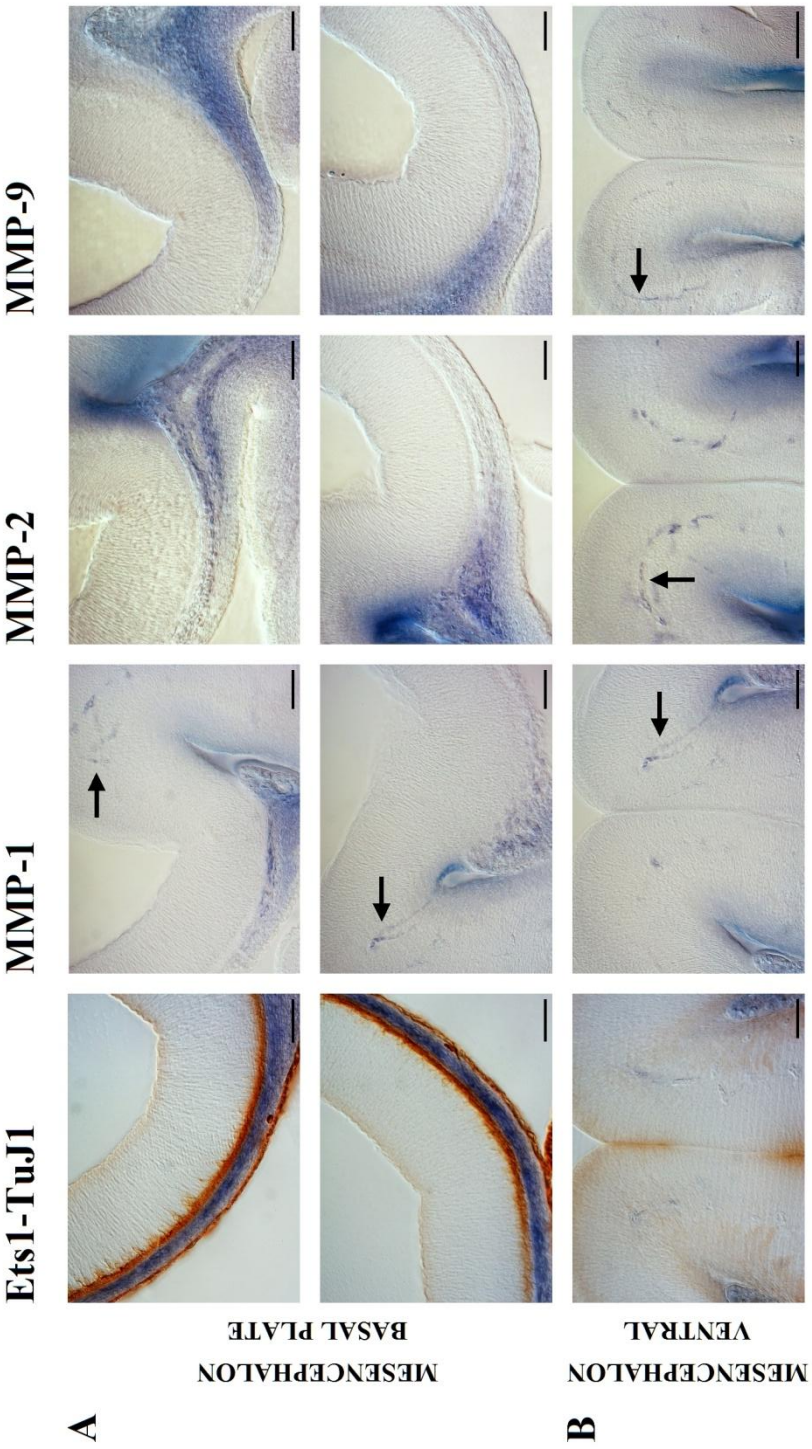
MMP-9
MMP-2
MMP-1
Ets1-TuJ1
A
MESENCEPHALON
BASAL PLATE
B
MESENCEPHALON
VENTRAL

Figure 4vii. MMP expression in the dorsal half of the mesencephalon of stage HH24 *G. gallus* embryos. Whole-mount ISH was used with antisense probes against MMPs -1, -2 and -9, followed by vibratome sectioning (n=2 for each MMP). MMP expression in the dorsal mesencephalon (**A**) and alar plate (**B**) compared to Ets1/TuJ1 staining for endothelial cells (blue) and neurons (brown) shown in the left-hand column. Expression is observed for all three MMPs in the mesenchyme surrounding the dorsal mesencephalon (arrows). Scale bar = 50μm.

MMP-9
MMP-2
MMP-1
Ets1-TuJ1
A
MESENCEPHALON
DORSAL
B
MESENCEPHALON
ALAR PLATE

Figure 4viii. MMP expression within endothelial sprouts. Whole-mount ISH was conducted in stage HH24 embryos with antisense probes against MMP-1 (**A**, n=2), MMP-2 (**B**, n=2) and MMP-9 (**C**, n=2), followed by vibratome sectioning. Staining patterns appear to indicate differential expression within ingressing endothelial sprouts. MMP-1 expression is stronger towards the tip of the sprout with lower levels present in the stalk cells. MMP-9 staining reveals a strong expression in the base of the sprout and in the INVP, while MMP-2 appears to be expressed equally throughout the sprout with a strong expression in the INVP (**D**). Scale bar = 25μm.

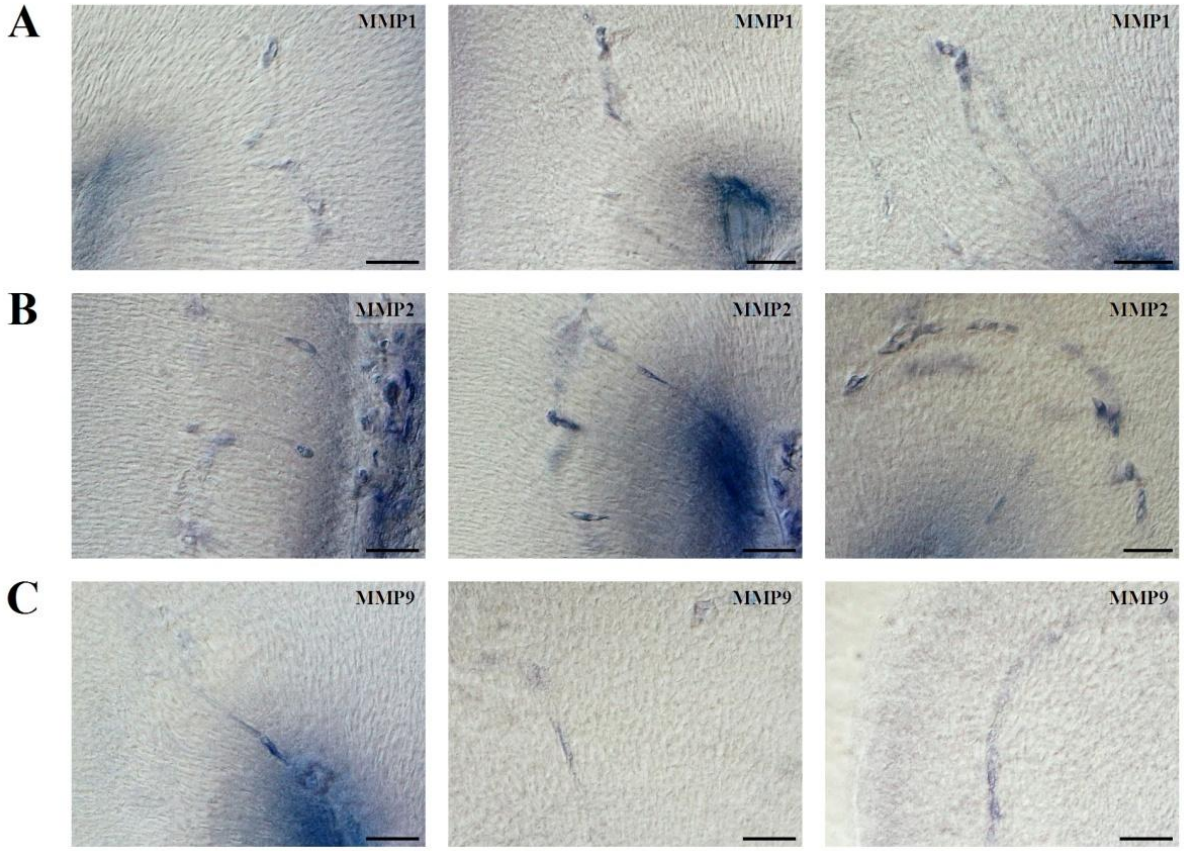
A
MMP1
MMP1
MMP1
B
MMP2
MMP2
MMP2
C
MMP9
MMP9
MMP9

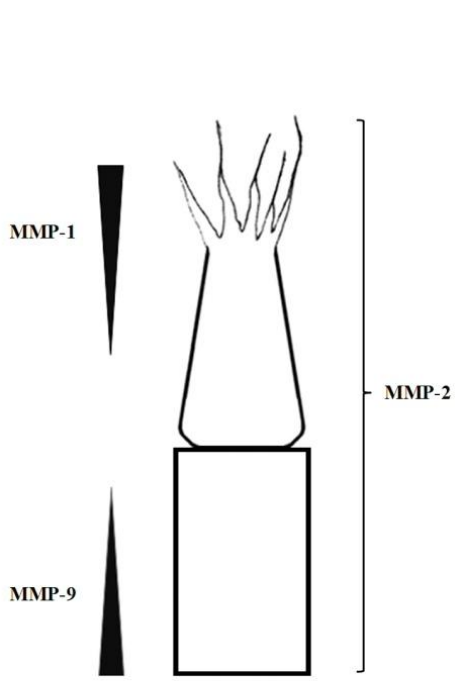
D
MMP-1
MMP-2
MMP-9

4.2 Gelatinase activity is present in specific cells in the PNVP and within the invading sprouts

The method of whole-mount ISH was useful for identifying the spatial and temporal location of MMP mRNA during vascular ingression, although further experiments involving the double staining of endothelial cells and MMPs in the same embryo would be beneficial for a more direct comparison in expression and to aid in determining whether or not the location of MMPs are associated with the ingressing endothelial cells. ISH studies, however, cannot provide information regarding the translation of MMP mRNA into protein and do not allow direct conclusions to be made regarding MMP activity, which is highly regulated at post-translational level. A method for identifying both the location and activity of gelatinases, including MMP-2 and MMP-9, was established in whole *G. gallus* embryos and is referred to as whole-mount ISZ. DQ gelatin was used as a fluorogenic substrate (fluorescein-conjugated gelatin), which is initially self-quenched due to the heavily-packed high concentration of fluorophores interacting with one another. Hydrolysis is catalysed by the presence of active gelatinases, which leads to the proteolysis of the substrate. The compact formation of fluorophores is subsequently disrupted, resulting in the release of fluorescence. Normally, ISZ is conducted on frozen sections of unfixed tissues as tissue fixation is generally believed to inhibit enzyme activity. The exact localisation of activity is therefore difficult to determine as frozen sections present impaired tissue morphology compared with paraffin-embedded tissues fixed with ethanol- or zinc-based fixatives that exhibit stronger signals and better morphology for a more precise detection of gelatinolytic activity (Galis *et al*., 1995; Porto *et al*., 2009; George & Johnson, 2010; Hadler-Olsen *et al*., 2010). However, adapting ISZ to a technique that can be applied to freshly-harvested embryos that are briefly fixed in 4% PFA/PFS prior to experimentation is novel in achieving the precise detection and localisation of gelatinase activity in whole embryo samples of good structural integrity in which the fine morphological details of the tissues were preserved, whilst also maintaining a high level of enzyme activity. Since sprouting was observed to occur throughout the mesencephalon at stage HH26 of development (Fig. 3x, I), embryos at this stage were incubated with DQ-gelatin in order to investigate if gelatinase activity coordinates with the location of the ingressing sprouts. ISZ was then combined with fluorescent immunostaining using a CD34 antibody for the co-

localisation of endothelial cells. Control embryos were either incubated in reaction buffer alone or 10mM EDTA in reaction buffer. Embryos incubated only in reaction buffer did not exhibit any fluorescence relating to gelatinolytic activity following IHC due to the absence of DQ-gelatin (Fig. 4ix, A). The addition of EDTA to the zymography buffer should have resulted in the inhibition of fluorescence generated by DQ-gelatin cleavage as EDTA is a general divalent cation chelator and MMP antagonist. However, in the presence of EDTA, embryos became extremely fragile and tissue morphology was severely lost.

Compared to the data observed using ISH in which MMP expression was identified in specific cells within the PNVP that surrounded the prosencephalon and only the ventral mesencephalon at stage HH21, ISZ revealed the presence of active gelatinases in specific cells within the PNVP surrounding the prosencephalon (Fig. 4ix, B, arrow) and both the tegmentum and tectum of the mesencephalon at stage HH26 of development (Fig. 4x, arrow), which was indicated by the presence of intermittent fluorescence in this region. The intermittent green fluorescence indicates that active gelatinases were not associated with all cells within the PNVP, which would otherwise be identified as continuous fluorescence, but located only to cells that may be in a preparatory phase prior to degradation of collagen IV in the basal lamina by these proteinases upon the initiation of ingression. A similar pattern of intermittent fluorescence associated with MMP gelatinolytic activity has previously been observed in angiogenesis, co-localising with microvessels in the adult mouse brain under VEGF hyperstimulation (Lee *et al*., 2009). Gelatinase activity was also coincident with the location of endothelial sprouts that were seen beginning to invade the prosencephalon as fluorescence was detected extending from the PNVP into the brain (Fig. 4ix, C, arrow). Gelatinase activity was observed throughout the vessel sprouts in the mesencephalon and as the sprouts branched to form the nascent internal capillary network (Fig. 4x, arrowhead). In contrast to the intermittent fluorescence relating to active gelatinases observed within the PNVP, the pattern of fluorescence throughout the sprouts in the mesencephalon appeared to be more continuous, suggesting that active gelatinases were present in the majority of cells within the invading sprouts. Gelatinase activity therefore appeared to correlate with major events of brain vascularisation, possibly functioning in endothelial cell invasion and also in the structure of the vessel sprouts.

Figure 4ix. Whole-mount ISZ in the prosencephalon of stage HH26 embryos. Chick embryos harvested at HH26 were fixed in 4% PFA/PBS prior to incubation with DQ-gelatin to detect gelatinolytic activity (green), which was then combined with fluorescent IHC with a CD34 antibody to detect endothelial cells (red). Sections of 60μm were cut from gelatin-embedded embryos using a vibratome before fluorescence was visualised. **A**. Control buffer at pH7.5 does not detect gelatinolytic activity due to the lack of DQ-gelatin substrate, n=2. **B**. Buffer containing DQ-gelatin substrate reveals the presence of gelatinolytic activity in specific cells within the PNVP as indicated by intermittent green fluorescence (arrow), n=4. **C**. Enlarged region of dorsal diencephalon indicates the expression of active gelatinases by endothelial cells during ingression into the brain (arrow). Scale bar A, B = 100μm; C = 10μm.

ACTIVE GELATINASES
CD34
MERGE
A
CONTROL
B
C
DQ-GELATIN

Figure 4x. Whole-mount ISZ in the mesencephalon of stage HH26 embryos. Chick embryos harvested at HH26 were fixed in 4% PFA/PBS prior to incubation with DQ-gelatin to detect gelatinolytic activity (green), which was then combined with fluorescent IHC with a CD34 antibody to detect endothelial cells (red). Sections of 60μm were cut from gelatin-embedded embryos using a vibratome before fluorescence was visualised. The detection of intermittent green fluorescence indicates the presence of gelatinolytic activity in specific cells within the PNVP (arrow). Gelatinolytic activity is also present within endothelial sprouts that are invading the brain and are branching to form the INVP (arrowhead), n=4. Scale bar = 100μm.

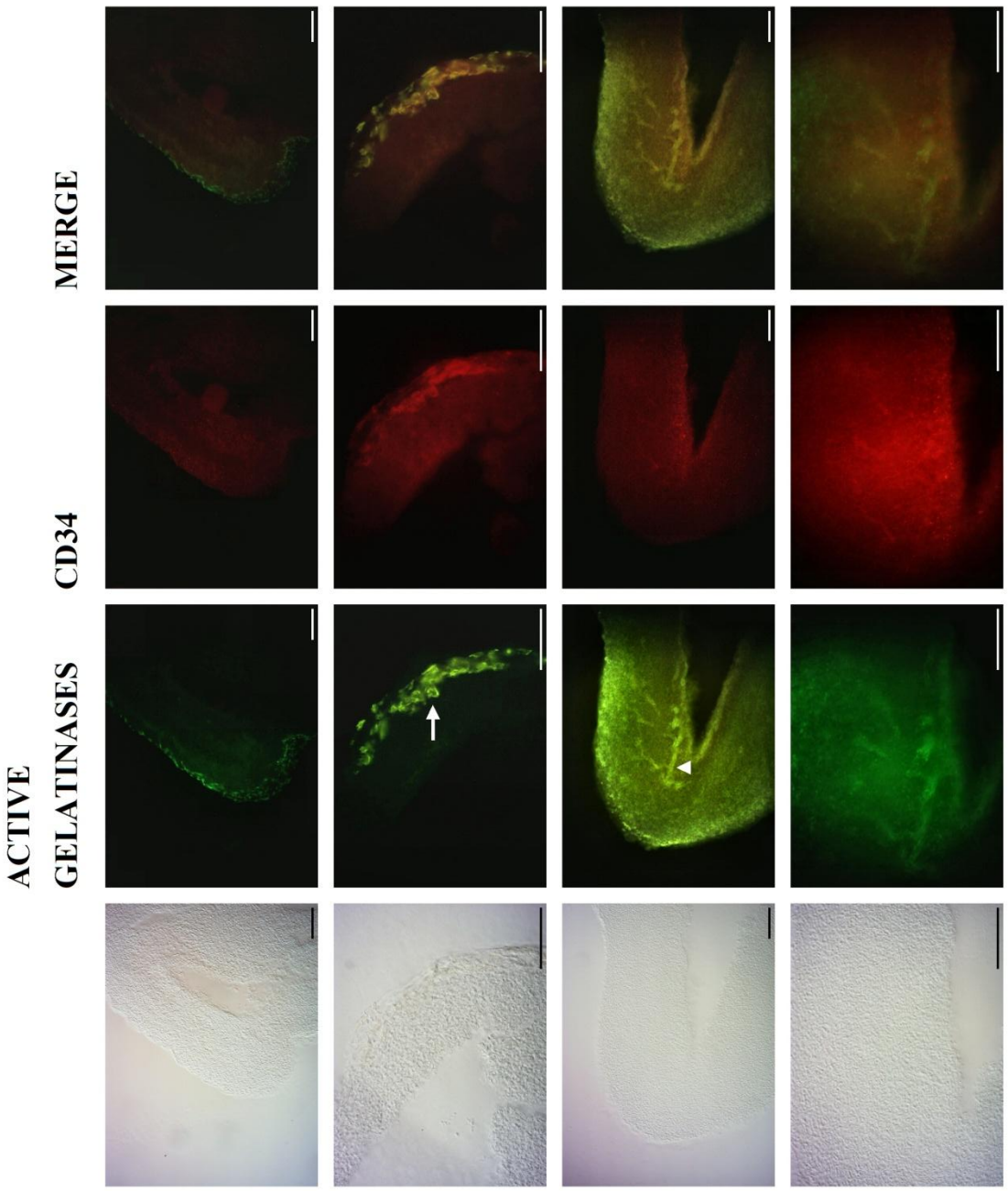
ACTIVE GELATINASES
CD34
MERGE

While ISZ with DQ-gelatin detects and locates gelatinolytic activity *in situ*, it is important to note that this method assesses the net activity of gelatinases, which is regulated by a number of factors such as the presence of ubiquitous proteinase inhibitors including TIMPs. However, the ability to observe protease activity in whole embryos is a powerful technique that can contribute significantly to the understanding of proteolytic activity involved in vascularisation of the brain and also permits the role of gelatinases to be explored in pathobiology. The visualisation of active MMP-1 would be advantageous and if detected and located to invading sprouts similar to the pattern observed with MMP-1 mRNA, particularly at the leading edge, the analysis would support the hypothesis of the involvement of MMP-1 in tip cell migration.

4.3 Altering MMP activity leads to changes in endothelial cell ingression

The analysis of MMP mRNA by ISH and active gelatinases by ISZ provides valuable information that confirms the presence of MMPs during brain vascularisation and is a crucial step prior to elucidating the function of MMPs in endothelial cell ingression. The tip cells that initiate vascular ingression are faced with the specific challenge to penetrate the basal lamina of the brain, which requires the remodelling of the ECM by active proteases. The role of MMPs in brain vascularisation was investigated by manipulating the level of MMP activity to which ingressing endothelial cells were exposed (Fig. 4xi). MMPs play a major role in hydrolysing structural components present in the ECM, therefore a change in the level of MMP activity could result in a change to vessel sprouting into the brain. The local activity of MMPs was altered through the *in ovo* implantation of acrylic beads soaked with pharmacological inhibitors or active MMP-1.

Figure 4xi. Signalling pathways involved in angiogenesis affected by altering MMP levels. The endogenous levels of MMPs are determined by a network of regulatory pathways primarily induced by VEGFA signalling and active uPA. A reduction in the level of MMPs -2 and -9 through exposure to MMP inhibitors ARP 100 and SB-3CT would likely result in a reduction of angiogenesis due to decreased degradation of the ECM leading to the release of fewer proangiogenic factors. Conversely, increasing the level of active MMP-1 may promote angiogenesis by increasing cell migration and enhancing the release of growth factors from the matrix.

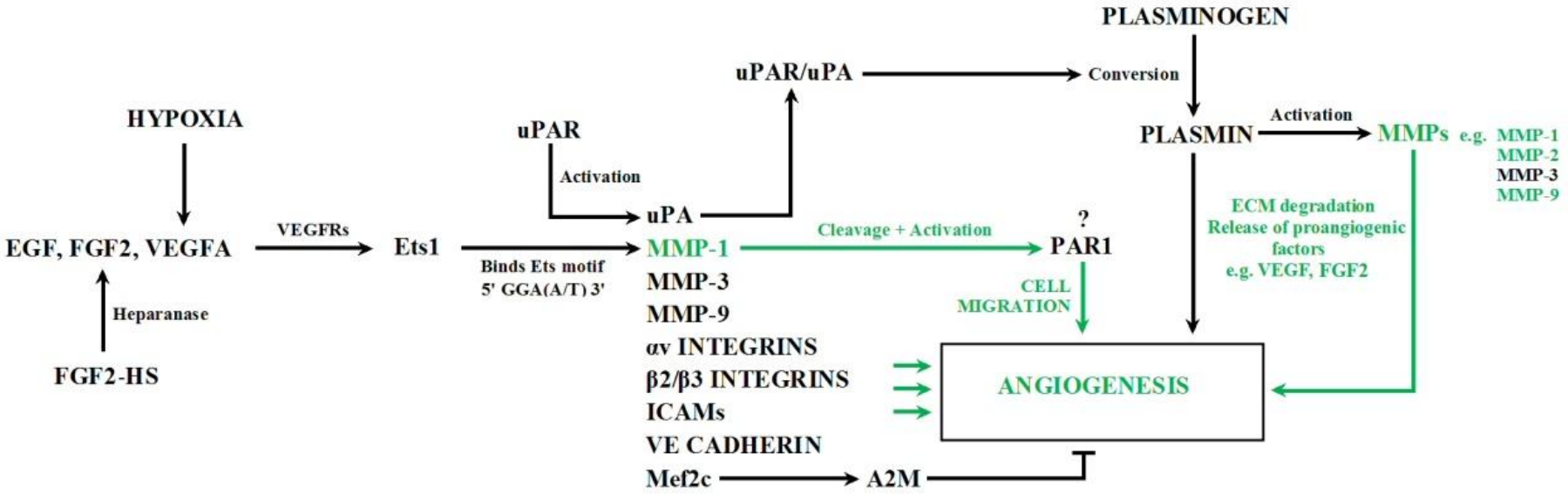
PLASMINOGEN
uPAR/uPA
Conversion
HYPOXIA
uPAR
Activation
PLASMIN
Activation
MMPs
e.g. MMP-1
MMP-2
MMP-3
MMP-9
uPA
ECM degradation
Release of proangiogenic factors
e.g. VEGF, FGF2
EGF, FGF2, VEGFA
VEGFRs
Ets1
Cleavage + Activation
?
PAR1
Binds Ets motif
5' GGA(A/T) 3'
MMP-1
MMP-3
MMP-9
CELL MIGRATION
αv INTEGRINS
β2/β3 INTEGRINS
ICAMs
VE CADHERIN
ANGIOGENESIS
Heparanase
FGF2-HS
Mef2c
A2M

The grafting of beads into the developing embryo is an approach that is widely used to directly test the effects of specific growth factors or inhibitors on gene expression at defined developmental stages. The technique has been employed in a number of studies that include the identification of factors that alter the patterning of the limb, such as Shh and retinoic acid, and in studying the roles of signals involved in regulating muscle development, including BMPs, hepatocyte growth factor (HGF) and FGF18 (Tickle *et al*., 1982; Riddle *et al*., 1993; Brand-Saberi *et al*., 1996; Amthor *et al*., 1998; Mohammed & Sweetman, 2016).

The pharmacological inhibitors ARP 100, SB-3CT and Batimastat were used to alter MMP activity in the developing *G. gallus* embryo. ARP 100 (Santa Cruz Biotechnology; Chetty *et al*., 2010; Miyake *et al*., 2015) is a selective inhibitor of MMP-2 (IC_{50} = 12nM), displaying selectivity over MMP-9 (IC_{50} = 200nM), MMP-3 (IC_{50} = 4.5μM), MMP-1 (IC_{50} = 50μM) and MMP-7 (IC_{50} = >50μM). SB-3CT (Santa Cruz Biotechnology; Bonfil *et al*., 2006; Kim *et al*., 2008) is a selective inhibitor of MMP-2 and MMP-9 that has been shown to directly bind to the catalytic zinc ion on MMP-2 (MMP-1: K_i = 206μM; MMP-3: K_i = 15μM; MMP-7: K_i = 96μM; MMP-2: K_i = 13.9nM; MMP-9: K_i = 600nM; ADAM17/TACE: K_i = 4μM). Batimastat (Tocris Bioscience; Wylie *et al*., 1999; Duong & Erickson, 2004) is a potent, broad spectrum inhibitor of MMPs (IC_{50} values are 3, 4, 4, 6 and 20nM for MMP -1, -2, -9, -7 and -3 respectively). Active MMP-1 (gifted from Dr. Pickford, University of Portsmouth) was synthesised as proMMP-1, which was expressed, purified, activated using APMA and MMP-3 then re-purified. MMP-3 cuts at a specific point between the PRO and CAT domains therefore resulting in a much higher activity compared with auto-activation. APMA interrupts the interaction between Cys92 and the catalytic zinc ion, which leads to the unfolding of the PRO domain and subsequent removal by proteolysis. The MMP inhibitors were tested at concentrations that were much higher than the known IC_{50} concentrations as the extent to which each inhibitor diffuses away from the bead and becomes diluted over time is unknown. The beads were positioned in the mesoderm of stage HH22 *G. gallus* embryos just beneath the surface ectoderm adjacent to the basal plate of the mesencephalon, immediately after the initiation of sprouting in the ventral mesencephalon. The embryos were incubated further and harvested at stage HH26, during which sprouting normally occurs at multiple points throughout the

mesencephalon (Fig. 3x, I). Endothelial cells were then detected with IHC using a CD34 antibody (Fig. 4xii) and counted (Fig. 2ii and Appendix A).

A paired t-test was performed using Minitab 17 in order to determine if there was a significant decrease in the number of endothelial cells present within the brain in the side exposed to a pharmacological inhibitor compared with the contra lateral control side (Appendices B-J). In control embryos that were implanted with beads containing only DMSO, endothelial cells ingressing into both sides of the mesencephalon were similar in number (Fig. 4xii, A, and Appendix B). Two-thirds of the embryos implanted with beads containing 8mM ARP 100 in DMSO, an inhibitor of MMP-2, showed fewer cells ingressing into the mesencephalon on the experimental side compared with the control side. The reduction in the number of ingressing cells was likely to be an effect that arose as a result of the inhibitor rather than from the encapsulation of a foreign body, although this difference was not statistically significant (Fig. 4xii, B, and Appendix C). Furthermore, no significant difference was observed in the number of endothelial cells ingressing into the control and experimental sides in embryos implanted with beads containing either 8mM SB-3CT in DMSO, an inhibitor of MMP-2 and MMP-9 (Fig. 4xii, C, and Appendix D), or the broad spectrum inhibitor, 1mM Batimastat in DMSO (Fig. 4xii D, and Appendix E).

ARP 100 and SB-3CT stock solutions were prepared with DMSO, although additional results were acquired from preliminary experiments in which the inhibitors were diluted in PBS rather than DMSO (Fig. 4xiii). In control embryos that were implanted with beads containing only PBS, endothelial cells ingressing into both sides of the mesencephalon were similar in number (Fig. 4xiii, A, and Appendix F). However, no significant difference was observed in the number of endothelial cells ingressing into the control and experimental sides in embryos implanted with beads containing either 8mM ARP 100, 1mM ARP 100, 8mM SB-3CT or 1mM SB-3CT in PBS (Fig. 4xiii and Appendices G-J).

Figure 4xii. Sections through the mesencephalon of embryos following the implantation of beads containing MMP inhibitors in DMSO. Acrylic beads containing DMSO (blue) are positioned in the mesoderm beneath the surface ectoderm of the mesencephalon in stage HH26 embryos. A similar number of endothelial cells, which are detected using IHC with a CD34 antibody (brown), are seen ingressing into both sides of the mesencephalon at the level of the bead in control embryos (**A**, n=7). In two thirds of embryos implanted with beads containing 8mM ARP 100 in DMSO, fewer endothelial cells are seen ingressing into the mesencephalon on the experimental side containing the bead compared with the control side (**B**, n=6). In embryos implanted with beads containing either 8mM SB-3CT (**C**, n=5) or 1mM Batimastat (**D**, n=6) in DMSO, a difference in the number of endothelial cells ingressing into the experimental and control sides was not detected. Clusters of endothelial cells (arrows) were observed within the mesencephalon in close proximity to the implanted bead in one embryo exposed to 8mM ARP 100 and three embryos exposed to 8mM SB-3CT. Endothelial cell clusters were absent from all control embryos. Scale bar = 100μm.

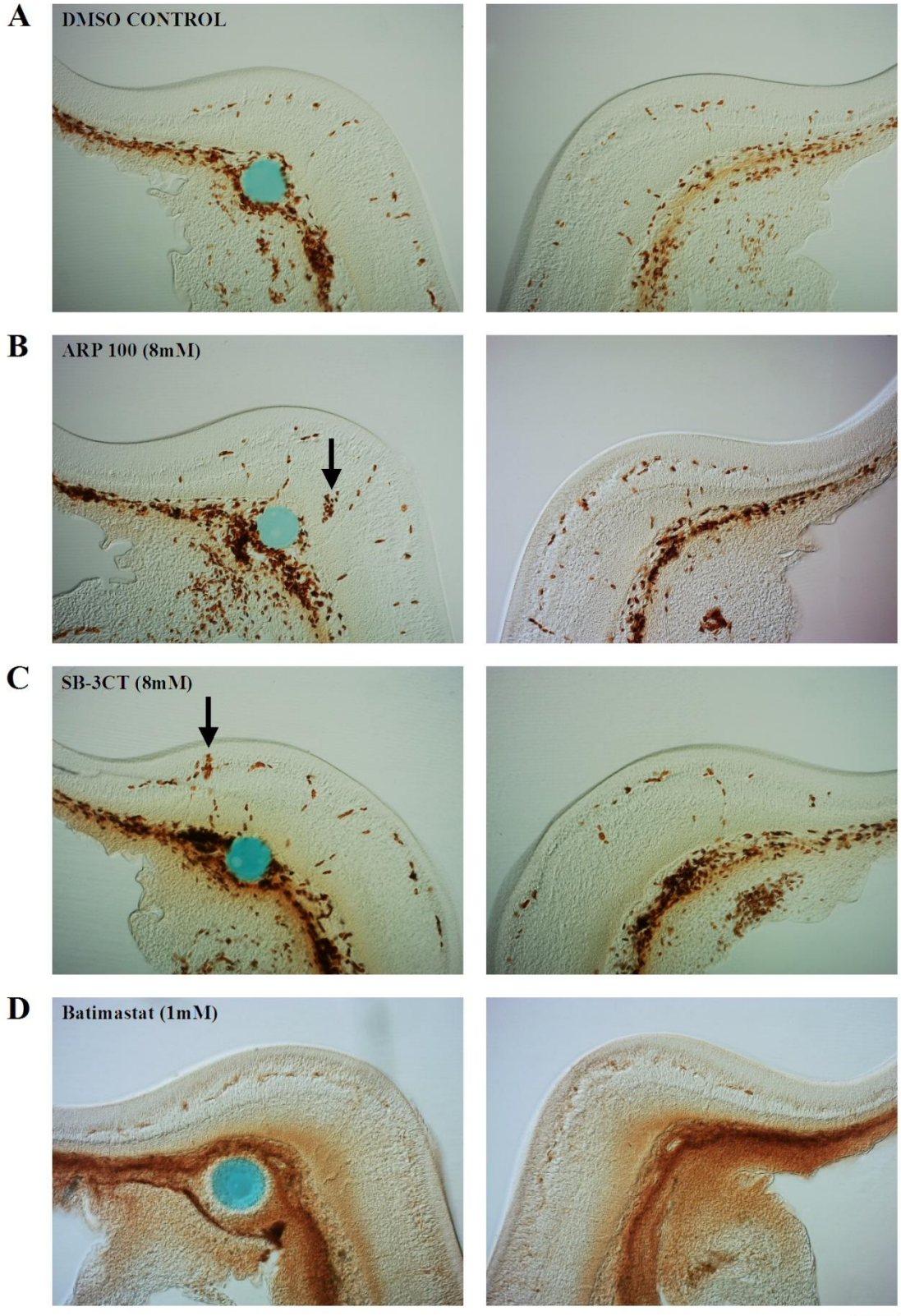
A
DMSO CONTROL
B
ARP 100 (8mM)
C
SB-3CT (8mM)
D
Batimastat (1mM)

Figure 4xiii. Sections through the mesencephalon of embryos following the implantation of beads containing MMP inhibitors in PBS. Acrylic beads containing PBS (blue) are positioned in the mesoderm beneath the surface ectoderm of the mesencephalon in stage HH26 embryos. A similar number of endothelial cells, which are detected using IHC with a CD34 antibody (brown), are seen ingressing into both sides of the mesencephalon at the level of the bead in control embryos (**A**, n=7). In embryos implanted with beads containing either 8mM ARP 100 (**B**, n=5), 1mM ARP 100 (**C**, n=9), 8mM SB-3CT (**D**, n=7) or 1mM SB-3CT (**E**, n=10) in PBS, no significant difference occurs between the mean number of endothelial cells on the control side and the mean number of endothelial cells containing the bead. Similar to an effect seen with MMP inhibitors in DMSO, clusters of endothelial cells (arrows) were observed within the mesencephalon in close proximity to the implanted bead in one embryo exposed to 8mM ARP 100 and three embryos exposed to 8mM SB-3CT. Endothelial cell clusters were absent from all control embryos. Scale bar = 100μm.

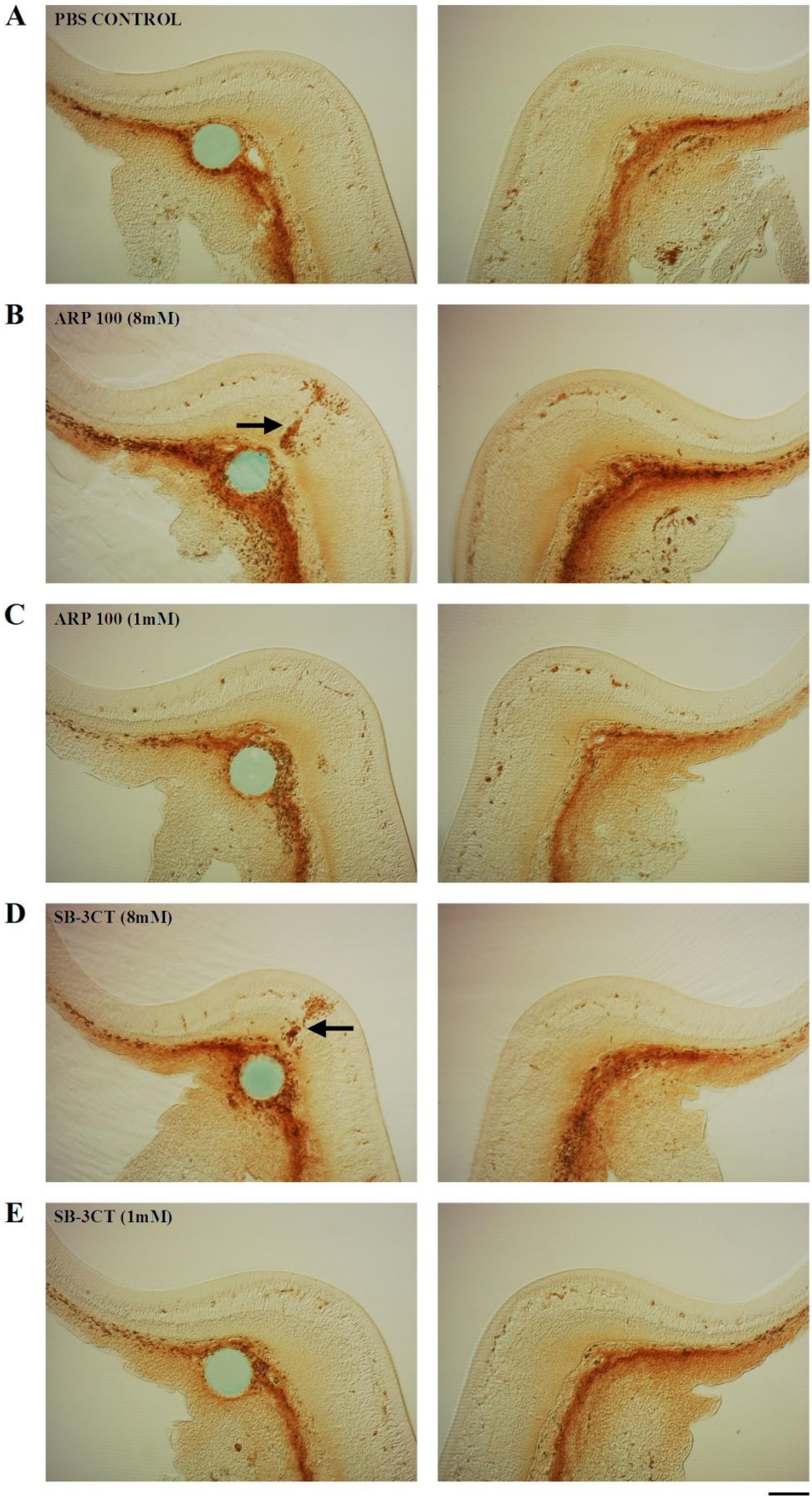
A
PBS CONTROL
B
ARP 100 (8mM)
C
ARP 100 (1mM)
D
SB-3CT (8mM)
E
SB-3CT (1mM)

Decreasing MMP activity was hypothesised to reduce the number of endothelial cells ingressing into the brain as the ability of endothelial cells to penetrate the basal lamina may be hindered. The loss-of-function experiments that were conducted through the application of MMP inhibitors, specifically ARP 100, resulted in a reduction in vascular ingression, although this result was not statistically significant. MMP-2 may be necessary for normal sprouting patterns into the developing brain as it is known to degrade collagen IV in the basement membrane, therefore the decrease in MMP-2 activity may have prevented the ingression of endothelial cells in close contact with the inhibitor. The presence of MMP-9 however may have been sufficient to enable the ingression of cells affected by ARP 100. The inhibition of multiple MMPs through exposure to SB-3CT or Batimastat did not significantly affect the number of endothelial cells invading the experimental side compared with the control side. The results were unexpected as an increase in MMP inhibition would presumably show further reduction in ingression compared with the effect of ARP 100, as less degradation of the ECM would lead to the release of fewer growth factors from the matrix, including VEGFA, which would in turn lead to fewer endothelial cells migrating towards the brain and greatly lowering the ability of these cells to penetrate the basal lamina and migrate once inside the brain. The reason for this is unclear, but as MMPs are involved in complex regulatory networks it is likely that the effect of SB-3CT, for example, could be counteracted by alterations to certain MMP activators and inhibitors such as MT1-MMP, MT3-MMP, TIMP-1 and TIMP-3, in order to re-establish local MMP-2 and MMP-9 activity to the correct levels required for normal endothelial ingression. Furthermore, other matrix-degrading enzymes such as proteases of the ADAM family, cathepsin cysteine proteases and serine proteases, might also compensate for the decrease in MMP activity.

The effect of ARP 100 on inhibiting MMP-2 was previously confirmed *in vivo* through the inhibition of neural crest cell formation (Duong & Erickson, 2004), although studies conducted *in vitro* and *in vivo* have described the effects of ARP 100, SB-3CT and Batimastat more specifically in angiogenesis. The inhibition of MMP-2 using ARP 100 has been shown to decrease MMP-2 interaction with αvβ3 integrin, leading to the decreased expression of VEGF in lung cancer angiogenesis and also significantly inhibited the formation of capillary tube-like structures in

HUVECs (Chetty *et al*., 2010; Miyake *et al*., 2015). Inhibiting both MMP-2 and MMP-9 using SB-3CT reduced intratumoral vascular density in an experimental mouse model of prostate cancer bone metastases and inhibited bone marrow endothelial cell invasion and tubule formation *in vitro* (Bonfil *et al*., 2006). Furthermore, birds treated with SB-3CT displayed a decreased endothelial mitotic index to the adult vocal control centre and the recruitment of neurons was substantially diminished (Kim *et al*., 2008). The effect of the broad spectrum inhibitor, Batimastat, has also been investigated *in vivo* and was shown to limit tumour metastasis in mice by inhibiting angiogenesis through the reduction in vascular volume of liver metastasis (Wylie *et al*., 1999). Continuing the investigation with larger sample numbers for ARP 100, SB-3CT and Batimastat would be advantageous and further investigation into the inhibitory effects of each inhibitor on MMP activity *in vivo* would support the current literature and help to verify the changes observed in endothelial ingression into the brain.

Further to the ISH experiments in which MMP-1 was expressed more towards the tips of endothelial sprouts (Fig. 4viii), a gain-of-function experiment was then conducted in order to investigate if an increase in MMP activity would lead to an increase in the number of endothelial cells ingressing into the brain. Acrylic beads soaked in 1μM or 25nM MMP-1 that was activated using APMA and MMP-3 (gifted from Dr. Andy Pickford, University of Portsmouth; Chung *et al*., 2004; Arnold *et al*., 2011), were implanted just beneath the surface ectoderm adjacent to the mesencephalon using the method described above. The embryos were incubated further and harvested at stage HH26. Endothelial cells were then detected with IHC using a CD34 antibody (Fig. 4xiv) and counted (Fig. 2ii and Appendix A). A paired t-test was performed using Minitab 17 in order to determine if there was a significant increase in the number of endothelial cells present within the brain in the experimental side that was exposed to active MMP-1 compared with the contra lateral control side (Appendices K-N).

Figure 4xiv. Sections through the mesencephalon of embryos following the implantation of beads containing active MMP-1 in Tris-HCl. Acrylic beads containing 100mM Tris-HCl pH7.5 (blue) are positioned in the mesoderm beneath the surface ectoderm of the mesencephalon in stage HH26 embryos. A similar number of endothelial cells, which are detected using IHC with a CD34 antibody (brown), are seen ingressing into both sides of the mesencephalon at the level of the bead in control embryos (**A**, n=4). In embryos exposed to 25nM active MMP-1 (**B**, n=5), more endothelial cells are shown to ingress on the experimental side in 80% of embryos, although this increase was not statistically significant. An increased density of endothelial cells within the INVP can be seen in one embryo on the side containing the bead in comparison to the control side (**B**, arrow). In embryos implanted with beads containing 250nM active MMP-1 (**C**, n=3), no difference was found in the number of endothelial cells ingressing into the experimental and control sides. Embryos implanted with beads containing 1μM active MMP-1 exhibit a larger number of endothelial cells ingressing into the mesencephalon on the experimental side containing the bead compared with the control side (**D**, n=5), although this increase was not statistically significant. Endothelial cells are seen pushing through the ventricular surface of the midbrain in one embryo and a cluster of endothelial cells is detected in close proximity to the bead in another (**D**, arrows). Endothelial cell clusters were absent from all control embryos. One embryo also shows the presence of densely-packed endothelial cells within the INVP (**D**, arrowheads). Scale bar = 100μm.

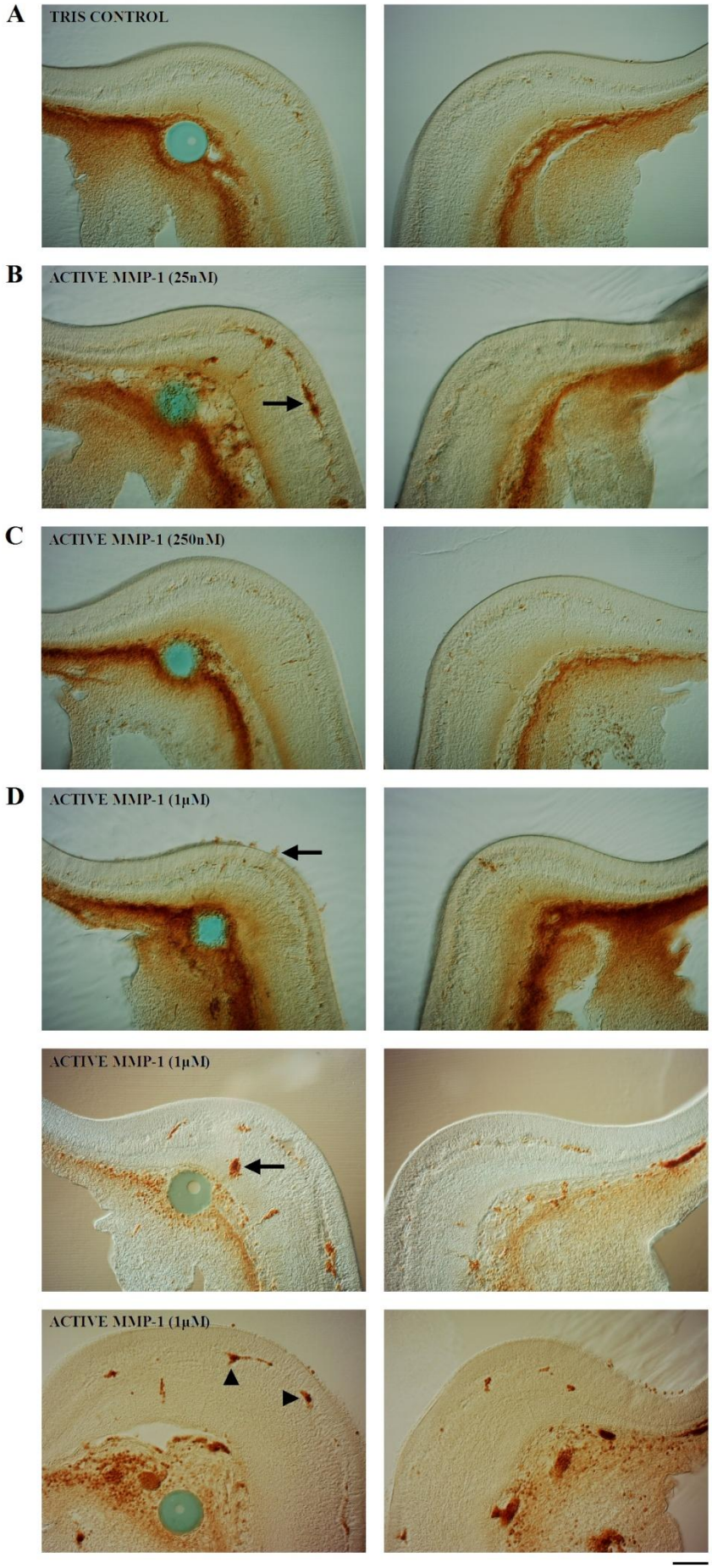
A
TRIS CONTROL
B
ACTIVE MMP-1 (25nM)
C
ACTIVE MMP-1 (250nM)
D
ACTIVE MMP-1 (1µM)
ACTIVE MMP-1 (1µM)
ACTIVE MMP-1 (1µM)

In control embryos that were implanted with beads containing only 100mM Tris-HCl pH7.5, endothelial cells ingressing into both sides of the mesencephalon were similar in number (Fig. 4xiv, A, and Appendix K). The majority of embryos exposed to 25nM active MMP-1 showed an increase in endothelial cell ingression on the experimental side compared with the contra lateral control side, although this increase was not statistically significant (Fig. 4xiv, B, and Appendix L). An increased density of endothelial cells within the INVP was also observed in one embryo on the side containing the bead in comparison to the control side (Fig. 4xiv, B, arrow). In embryos implanted with beads containing 250nM active MMP-1, no difference was observed in the number of endothelial cells ingressing into the control and experimental sides (Fig. 4xiv, C, and Appendix M). Upon exposure to beads containing 1μM active MMP-1 in Tris-HCl, a larger number of endothelial cells were seen on the experimental side compared with the control side, although the increase in number was not statistically significant (Fig. 4xiv, D, Fig. 4xv and Appendix N). A number of effects that did not arise in the control embryos were however detected. Endothelial cells were seen pushing through the ventricular surface of the brain in one embryo and the formation of a cluster of endothelial cells was also present in close proximity to the bead in another embryo (Fig. 4xiv, D arrows), which was similar to the appearance of clusters arising from reduced MMP activity through the application of pharmacological inhibitors. An expansion in the size of the invading sprouts and increased density of endothelial cells within the INVP were also observed (Fig. 4xiv, D arrowheads).

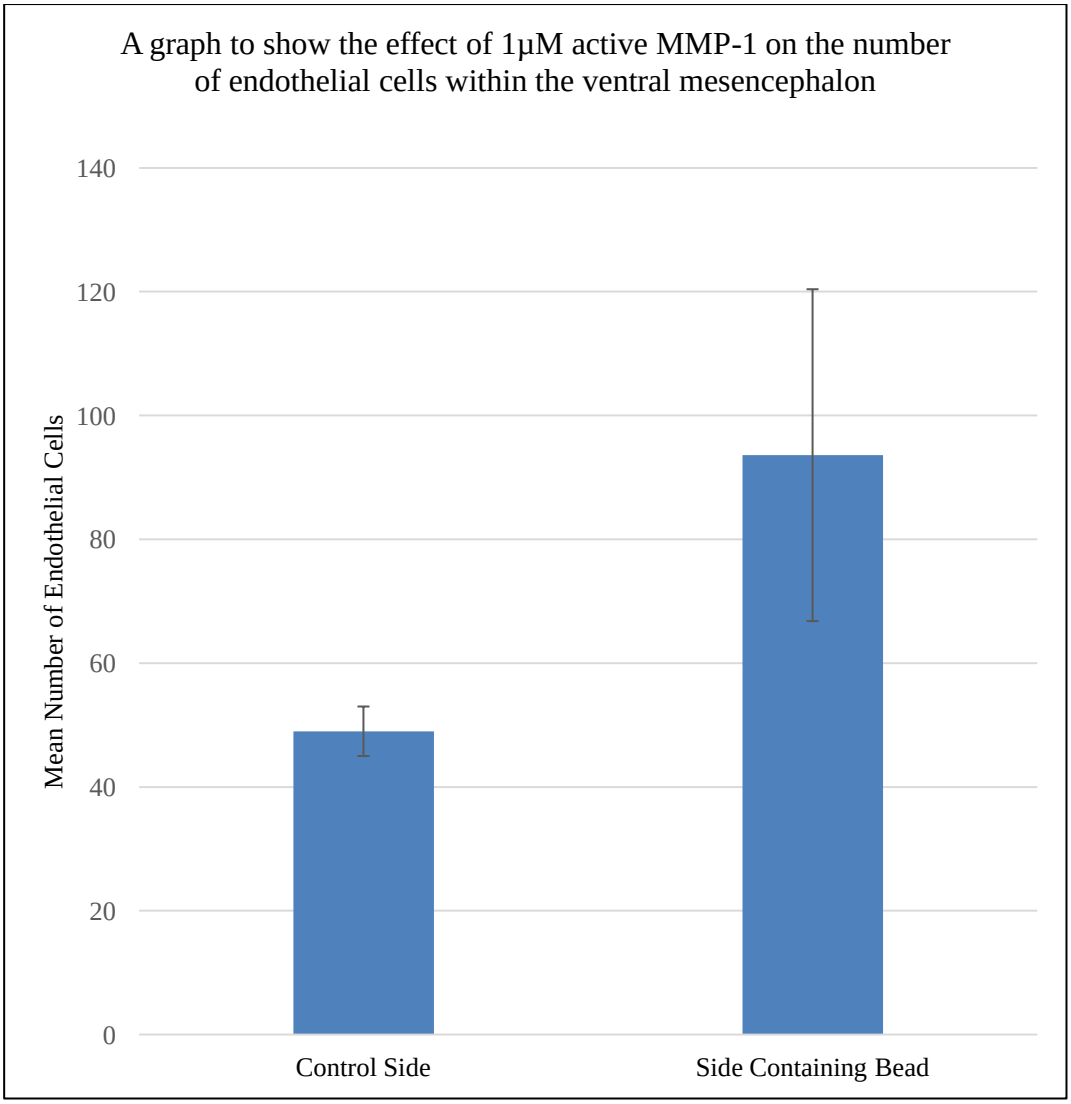

Figure 4xv. The effect of 1uM active MMP-1 on endothelial cell ingression. The mean number of endothelial cells on the side containing the bead (n=5) is compared with the mean number of endothelial cells on the contra lateral control side (n=5) after exposure to 1uM active MMP-1. Error bars represent the standard error of the mean. A larger number of endothelial cells was identified on the experimental side, although this increase was not found to be statistically significant (p value = 0.066, Appendix N).

While increased exposure to the pharmacological inhibitor, ARP 100, lead to a reduction in endothelial cell ingression into the brain, increasing the level of active MMP-1 resulted in an increase in the number of ingressing endothelial cells, however, neither were statistically significant. Since MMP-1 does not degrade collagen IV, it is likely that MMP-2 and MMP-9 have a larger role in penetrating the basal lamina at the initiation of ingression. Any increase in the number of endothelial cells observed on the experimental side of the mesencephalon may therefore have resulted from an increase in cell proliferation, which has been shown to occur throughout the process of brain vascularisation, indicated by few invading sprouts that appeared larger in size and the detection of densely-packed endothelial cells within the developing INVP. The similarity in the size and density of the PNVP on both experimental and control sides suggest that the proposed increase in cell proliferation occurs once the endothelial cells have entered the brain, an effect that may have been promoted by the elevated level of active MMP-1. A study by Mazor *et al.* (2013) conducted *in vitro* suggests a mechanism by which MMP-1 has a role in sensitising endothelial cell functions that are mediated by VEGFR2. Endothelial cells treated with MMP-1 consistently and significantly stimulated an up-regulation of VEGFR2 mRNA and functional protein that enhanced VEGFA signalling and accelerated cell proliferation when compared to controls and cells treated with MMP-8 or MMP-9. The up-regulation of VEGFR2 by MMP-1 was found to be mediated by activation of the NF-κB pathway in endothelial cells, a response that was dependent upon MMP-1 activation of PAR-1 (Zania *et al*., 2006; Mazor *et al*., 2013). Further to the effect on endothelial cell proliferation, MMP-1 has also been described in the upregulation of cell growth and proliferation in various other cell types including lung alveolar epithelial cells (Herrera *et al*., 2013) and breast cancer cells (Liu *et al*., 2012) and is therefore critical in medical research regarding pathogenesis, tumourigenicity and metastatic ability.

The effect of increasing active MMP-1 was more prominent in embryos exposed to 1μM active MMP-1 compared with the lower concentrations as some cells were seen to migrate farther and penetrated the ventricular surface of the mesencephalon. Previous studies have investigated the cleavage and activation of PAR1 by MMP-1, which leads to the induction of proangiogenic genes that promote cell migration in both angiogenesis and tumourigenesis (Boire *et al*., 2005; Blackburn &

Brinckerhoff, 2008). However, it is currently unknown if the same mechanism exists in the migratory stage of brain vascularisation and is therefore yet to be established. Identifying the temporal and spatial location of PAR1 during early brain development would be a good strategy, particularly if the expression patterns are found to coincide with the strong expression of MMP-1 mRNA towards the tips of endothelial sprouts. The analysis would help in providing a deeper insight into the mechanism of ingression, investigating whether or not MMP-1-activated PAR1 is also involved in augmenting endothelial cell proliferation and migration in a new context to those previously studied, specifically, in the process of brain vascularisation.

4.4 Altering MMP activity leads to the formation of endothelial cell clusters

The modification of MMP protein levels, either through the application of active MMP-1 as well as pharmacological inhibitors ARP 100 and SB-3CT, resulted in the distinct formation of densely packed endothelial cell clusters on the experimental side of the mesencephalon. Endothelial cell clusters were absent from all control embryos, suggesting that MMP activity plays an important role in forming or maintaining the structure of the invading sprouts that normally comprises a leading tip cell and follower stalk cells. The study conducted by Mazor *et al.* (2013) in HUVECs and bovine aortic endothelial cells (BAECs), which describes the NF-κB-mediated upregulation of VEGFR2 by MMP-1 leading to enhanced VEGFA signalling and proliferation of endothelial cells, may provide an explanation into the formation of clusters upon exposure to increased active MMP-1. The expression of VEGFR2 is characteristic of endothelial tip cells, yet stalk cells are highly proliferative. It is possible that cells present within the clusters may consist of endothelial cells that either remained unspecialised or have lost the phenotypic specialisation as tip or stalk cells. A more in-depth analysis could therefore be performed using additional staining methods in order to assay for tip and stalk cell markers such as VEGFR1, VEGFR2 and NRP1, in addition to using a phosphohistone H3 antibody to establish whether or not these cells are proliferative. Further investigation could also be conducted to identify if these cells are associated with pericytes that normally associate with endothelial cells during sprout assembly (Gerhardt & Betsholtz, 2003).

The structural integrity of a new sprout is maintained due to the adherent and tight junctions established by the endothelial stalk cells (Dejana *et al*., 2009; Phng & Gerhardt, 2009; Ribatti & Crivellato, 2012) and a number of studies in the literature have shown that the breakdown of tight junctions by MMP activation, particularly MMP-2 and MMP-9, facilitates the permeability of the BBB and blood-retinal barrier (BRB) in pathological conditions by degrading tight junction proteins, occludin and claudin-5 (Giebel *et al*., 2005; Yang *et al*., 2007; Yang & Rosenberg, 2011; Feng *et al*., 2011; Che *et al*., 2014). The decrease in MMP protein levels, achieved by the application of pharmacological inhibitors, was therefore hypothesised to result in the breakdown of fewer tight junction complexes, thus maintaining the stability of the sprout. The unexpected formation of endothelial cell clusters, however, suggests a disruption to the typical arrangement of the sprout that normally consists of a single migratory tip cell followed by highly proliferative stalk cells. Furthermore, the formation of clusters appeared more frequently upon exposure to SB-3CT, which inhibits both MMP-2 and MMP-9, compared with ARP 100 that only inhibits MMP-2. Considering the directional regulation of cell migration in angiogenesis, motility is controlled by chemotaxis driven by growth factors such as VEGFA (Hogan *et al*., 2004; James *et al*., 2009; Kurz *et al*., 1996; Ruhrberg *et al*., 2002), although the ECM also regulates motility by haptotaxis in which cells migrate in response to an increasing concentration of ECM proteins and an associated gradient of cellular adhesion sites (Hsu *et al*., 2005; Rozario & DeSimone, 2010). Investigation into the motility of BAECs has shown that cells exhibit directional motility towards a higher concentration of fibronectin, and BAECs on higher fibronectin concentrations have decreased cell motility due to increased adherence compared to cells in low fibronectin density (Bennett, 2012).

Integrins are transmembrane receptors that mediate the interactions between endothelial cells and the ECM. Endothelial β1 integrins have been shown to regulate sprouting and the formation of complex networks of endothelial tubes in murine ES cells as vessel development in β1 integrin-deficient EBs was strongly defective due to reduced endothelial cell maturation, migration and elongation, together with increased apoptosis (Malan *et al*., 2010). A study conducted on resected invasive colorectal tumours has shown that upregulated MMP-2 expression enhances cell motility by significantly reducing adhesion to collagen and fibronectin through the

increased partial cleavage of β1 integrin to which it associates. Conversely, the degradation of β1 integrin can be abolished by inhibiting MMP-2 activity (Kryczka *et al*., 2012). In the context of brain vascularisation, lowering the level of MMP-2 may lead to a similar effect of reduced migration by preventing the cleavage of β1 integrin and altering intracellular signalling pathways that in turn enhances the adhesion of endothelial cells to the ECM. In addition to MMP-2, MMP-9 has also been shown to associate with β1 integrin and is localised at the surface of cell membranes to promote tumour cell invasion (Radjabi *et al*., 2008). Lowering MMP-9 activity in addition to MMP-2 may initially reduce the invasive capabilities of endothelial cells when passing through the basal lamina and prevent the migration of cells that do ingress into the brain. Reduced levels of MMP-2 and MMP-9 would result in less degradation of ECM components, which could also negatively affect motility. Endothelial cells may be unable to migrate due to the physical restrictions imposed by the matrix, thereby resulting in aberrant angiogenesis and disorganised patterns of vascularisation during the development of the embryonic brain. However, this remains unclear since endothelial cells have previously been shown to migrate into areas containing a higher density of collagen (Hsu *et al*., 2005). Moreover, although MMP-2 correlates with neural crest cell-generation but does not affect the migration of cells that have already detached from the neural epithelium (Duong & Erickson, 2004), it is possible that MMP-2 may have an important role in the initial formation of endothelial sprouts then contribute to the degradation of β1 integrin during the migration of sprouts within the brain. It is therefore important to recognise that different cell types may use different mechanisms in order to migrate.

4.5 Lowering MMP-2 activity leads to reduced breakdown of fibronectin and α6 integrin

Staining patterns have previously revealed the presence of fibronectin in close proximity to endothelial sprouts invading the brain during early development (Fig. 3vi). In order to investigate the effect of MMP-2 activity on ECM remodelling during vascular ingression, preliminary experiments were performed in which beads containing ARP 100 were implanted into the mesoderm beneath the surface ectoderm of the mesencephalon at stage HH22. IHC was then conducted at HH26 to identify if the decrease in MMP-2 activity, brought about by the application of ARP

100, would alter the presence of laminin, fibronectin, α6 integrin and β1 integrin when sprouting normally occurs throughout the mesencephalon (Fig. 4xvi).

The levels of fibronectin and α6 integrin appeared to be higher on the experimental side containing the ARP 100 bead, compared to the control side, suggesting a possible role of MMP-2 in the breakdown of these components within the brain. However, further studies need to be conducted to provide a better understanding of MMP activity on ECM remodelling. Beads containing MMP inhibitors or active MMP-1 could be implanted into the embryo as previously described, followed by ISZ with DQ-gelatin to analyse the effect on MMP activity and IHC to detect the effect on endothelial cell ingression, as well as the expression of integrins, fibronectin and collagen IV *in vivo*.

The inhibitory effect of ARP 100 on MMP-2 was tested as a positive control experiment as MMP-2 is known to be expressed in neural crest cells during detachment from the neural tube (Duong & Erickson, 2004). Stage HH8 embryos were subjected to varying concentrations of ARP 100 in roller cultures then the formation of neural crest cells was analysed using IHC with an anti-HNK-1 antibody after 40 hours of incubation (Fig. 4xvii). The anti-HNK-1 antibody is a reliable marker that thoroughly labels migratory neural crest cells due to the HNK-1 epitope that becomes present in large amounts on the cell surface (Loring & Erickson, 1987; Del Barrio & Nieto, 2004; Giovannone *et al*., 2015). Fewer HNK-1-positive migratory neural crest cells were detected compared with the DMSO control as the concentration of ARP 100 increased, thus supporting the use of ARP100 as an effective inhibitor of MMP-2 in the bead implantation experiments.

Figure 4xvi. Preliminary investigation into the effect of MMP-2 inhibitor, ARP 100, on components of the ECM. The acrylic beads containing 8mM ARP 100 in DMSO (blue) are positioned in the mesoderm beneath the surface ectoderm of the midbrain, delivering the inhibitor to the surrounding tissues. Whole-mount IHC in stage HH26 embryos is used to detect laminin (**A**, n=2), fibronectin (**B**, n=2), α6 integrin (**C**, n=1) and β1 integrin (**D**, n=1), which are stained brown. The presence of fibronectin and α6 integrin is detected at a higher level on the experimental side containing the bead compared to the contra lateral control side, suggesting a possible role of MMP-2 in the breakdown of these two components within the brain. Scale bar = 100μm.

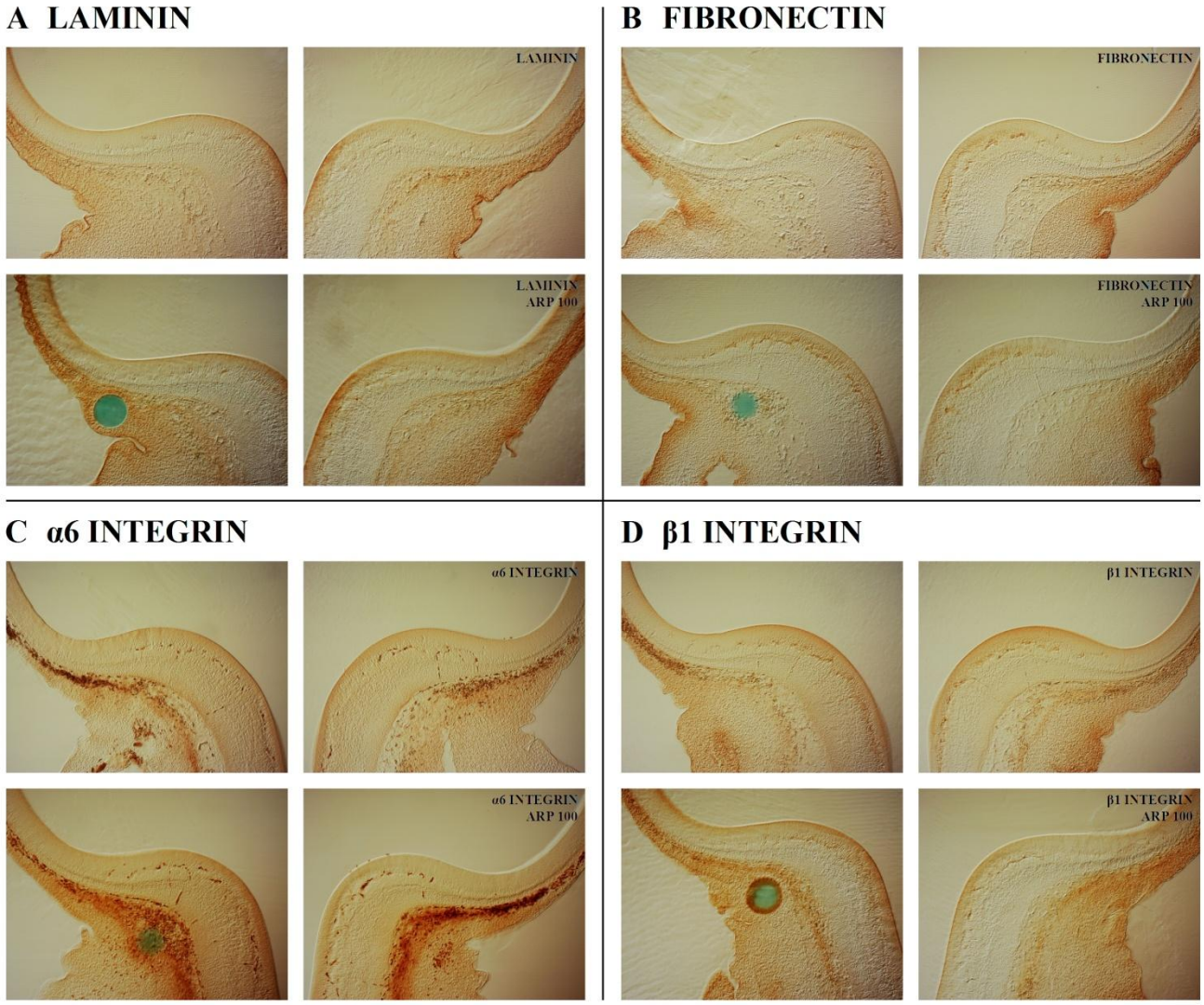
A LAMININ
LAMININ
LAMININ
ARP 100
B FIBRONECTIN
FIBRONECTIN
FIBRONECTIN
ARP 100
C α6 INTEGRIN
α6 INTEGRIN
α6 INTEGRIN
ARP 100
D β1 INTEGRIN
β1 INTEGRIN
β1 INTEGRIN
ARP 100

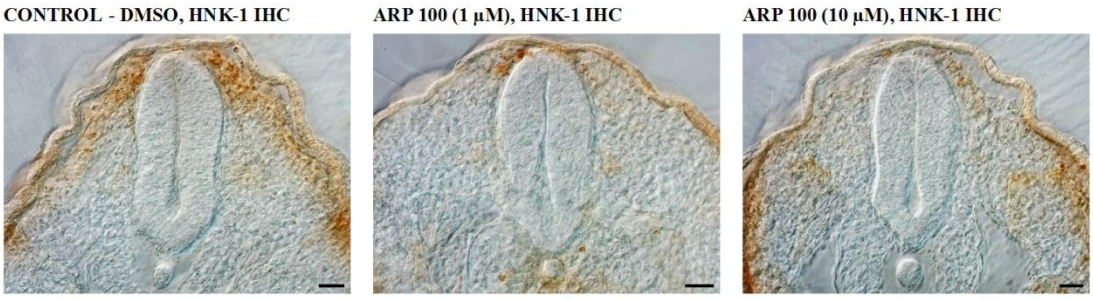

Figure 4xvii. Roller culture experiments with ARP 100 followed by neural crest cell detection using IHC with an anti-HNK-1 antibody. The inhibitory effect of ARP 100 on MMP-2 was tested by incubating stage HH8 embryos with 1µM or 10µM concentrations of ARP 100 in roller cultures for 40 hours during which they grew to stage HH15. The embryos underwent IHC with an anti-HNK-1 antibody to label neural crest cells brown. The DMSO control identifies the normal location of neural crest cells and highlights the migration path away from the neural tube (n=6). Fewer migratory neural crest cells are observed at 1µM concentration of ARP 100 (n=5), an effect that increases with a higher concentration of inhibitor. Only a few cells are exposed to active MMP-2 at 10µM ARP 100, allowing these cells to undergo the EMT required in the formation of neural crest cells (n=7). The results support previous findings by Duong & Erickson (2004) and the selection of ARP100 for use as an effective inhibitor of MMP-2 in bead implantation experiments. Scale bar = 25µm.

The implantation of beads is a valuable but laborious and technically challenging technique in which many variables are difficult to control in order to obtain valid and consistent repeats, including the implantation of beads into the same position in each embryo, the depth of specific staining against the background and cutting sections at the same angle, in addition to the individual differences possessed by each embryo. The substances loaded onto the beads also require further testing to analyse certain properties such as the rate of diffusion from the bead into the surrounding tissues and to identify the vicinity of the brain within which each substance can diffuse. In doing so, concentrations can be optimised in order to reduce any off-target effects that may have occurred as a result of applying high concentrations of inhibitors or active MMP-1 to the beads. The diffusion of the inhibitors from the beads, for example, may also be affected by binding to MMPs therefore the importance of analysing dissociation constants should also be taken into account. Alternative methods involving the detection and analysis of endothelial cells and ECM components in MMP-knockout mice would be extremely valuable for investigating the roles of specific MMPs on endothelial cell ingression into the embryonic brain.

Brain vascularisation is a carefully orchestrated process and changes to local MMP activity not only appeared to result in an effect on endothelial cell ingression but may also lead to defective cell proliferation and migration. The outcome of these experiments develops a more comprehensive understanding of the molecular mechanisms involved in angiogenic sprouting *in vivo*, providing a particularly novel insight into the roles of MMPs -1, -2 and -9 in endothelial cell ingression into the developing brain. The process involves the invasion of the ectoderm by sprouts from the mesoderm with the arrangement of a leading tip cell and follower stalk cells reminiscent of cancer progression and so the mechanism underlying endothelial sprouting in the brain may share similarities with the process of tumour angiogenesis. MMPs have been found to play a major role in the growth and metastasis of malignant tumours due to the large variety of MMP substrates in addition to ECM components. A major element in tumour metastasis is the invasiveness of cancer cells in which MMPs are required for focalised proteolysis as well as integrins for adhesion. The analyses of MMPs and integrins are therefore crucial for clarifying the roles of these proteases and receptors in both angiogenesis

and tumour invasiveness in order to aid in identifying specific targets for therapy, particularly with regards to brain metastasis.

5. THE INFLUENCE OF NEURAL TUBE PATTERNING ON BRAIN VASCULARISATION

5.1 The identification of VEGFA isoforms and VEGFR expression during the vascularisation of the embryonic *G. gallus* brain

The neural tube plays an important role in organising its vasculature and the signalling pathways that govern neural development and patterning are also involved in controlling the development of blood vessels. A substantial amount of work on the influence of brain-derived signals on endothelial ingression focusing on VEGFA has already been described in the literature. The alternative splicing of the VEGFA primary transcript yields distinct isoforms that interact with the ECM and the extent to which each isoform can bind is determined by the presence of exons 6 and 7, which encode heparin-binding domains (Ruhrberg *et al*., 2002; Ambler *et al*., 2003; Hogan *et al*., 2004; James *et al*., 2009; Bautch, 2012). In addition to this research, RT-PCR was conducted in order to identify the VEGFA isoforms present during brain vascularisation and to detect any changes in the expression level of each isoform as the embryos develop. The experiment was designed to utilise different primer sets in separate reactions to amplify either all VEGFA isoforms present, isoforms containing exon 7, or isoforms containing both exons 6 and 7. A total of four VEGFA isoforms were identified in the *G. gallus* brain between stages HH11 and HH28 of development (Fig. 5i-ii).

The expression level of the full VEGFA isoform appears to coincide with endothelial ingression detected using ISH with an antisense Ets1 probe as this isoform was detected in the head at stage HH21 (Fig. 5ii) when ingression into the ventral mesencephalon begins (Fig. 3x, E). The concentration of this isoform increased at stage HH24 when ingression continues and as the INVP begins to develop (Fig. 3x, Q-T), then dramatically decreased at stage HH26 although sprouting throughout the mesencephalon continues (Fig. 3x, I). An increase in the expression of the shorter isoform that lacks both exons 6 and 7 was detected at this stage (Fig. 5ii). The expression of VEGFA isoforms then appears to decrease in the head after stage HH26 when an extensive INVP is detected (Fig. 3x, M). The identification of the full isoform at the initiation of ingression supports previous research in which the

electroporation of heparin-binding isoforms VEGF189 and VEGF165 into the quail neural tube has been shown to induce localised ectopic ingression points (James *et al*., 2009). The full VEGFA isoform therefore appears to be important during the vascularisation of the brain as the heparin-binding properties enable interaction with the matrix, resulting in endothelial ingression from HH21 and as the embryo develops to HH24. However, a decrease in the level of this isoform was detected at stage HH26 during which an increase in the shorter isoform was detected when sprouting continues throughout the mesencephalon. In the quail electroporation study, the ectopic expression of the non-heparin binding isoform VEGF121 into the neural tube resulted in ingressing vessels that became dysmorphogenic but the number of blood vessel ingression points was not affected (James *et al*., 2009). The full isoform may therefore be important during the initial stages of ingression, whereas the shorter isoform could play a role in guiding the migration of tip cells.

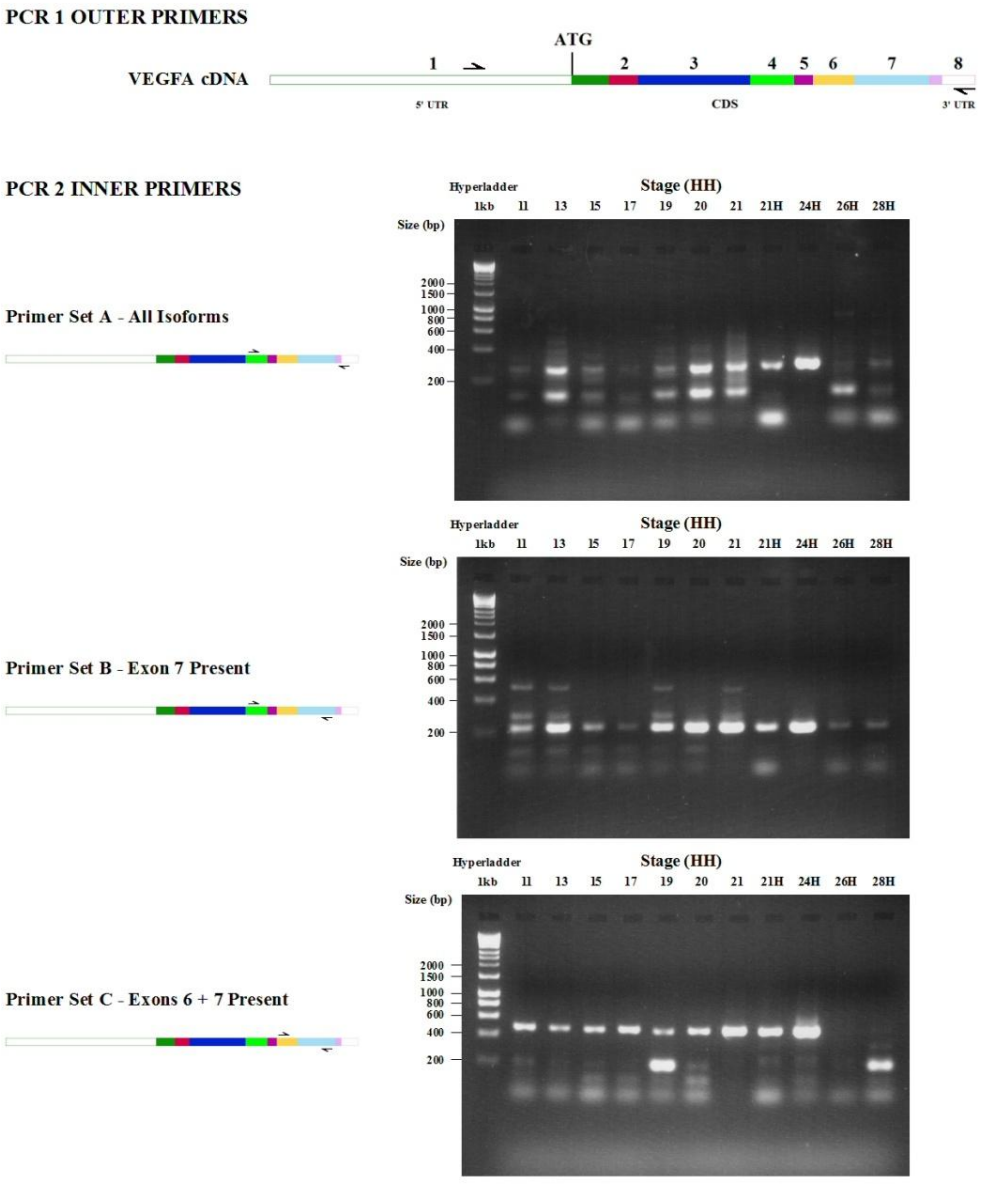

Figure 5i. Nested primers used in RT-PCR for the identification of VEGFA isoforms in *G. gallus* embryos at stages HH11-28 of development. A number of different isoforms of VEGFA are produced from a single gene due to the alternative splicing of the initial VEGFA transcript. The presence of exon 6 and exon 7 determines the distribution of secreted VEGFA as these exons encode heparin-binding domains that confer the ability of each isoform to interact with the ECM. RNA isolated from homogenised chick embryos is reverse-transcribed to form cDNA from each developmental stage for use in PCR with nested primers, which are designed to increase the yield and provide more specific product. Outer primers are used in the first round of PCR and the product of which is used as template in the second round, utilising different primer sets in three separate reactions to amplify certain groups of isoforms: all isoforms (set A), isoforms with exon 7 (set B) and isoforms with both exons 6 and 7 (set C). RT-PCR was conducted using whole embryos at stages HH11-21 and from the head only at stages HH21-28.

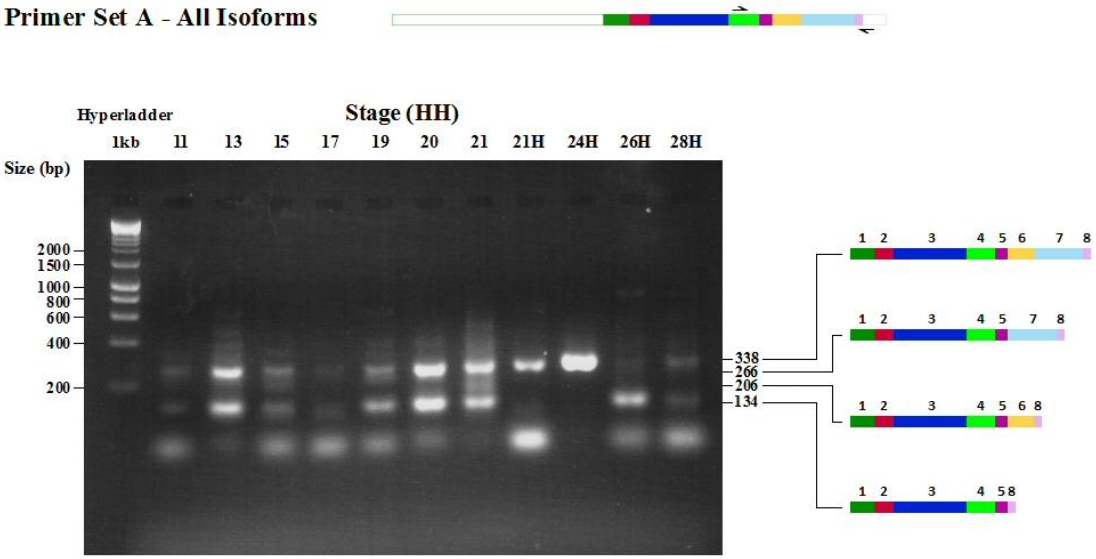

Figure 5ii. VEGFA isoforms present in *G. gallus* embryos identified by RT-PCR. Sequencing results obtained from extracted gel bands identify four different VEGFA isoforms present between stages HH11 and HH28 of chick development. The full isoform is detected at stage HH21 in the head, which is the stage when endothelial ingression into the ventral midbrain begins. The concentration of this isoform increases at stage HH24 when the INVP begins to develop and is indicated by a single bright band of DNA. The level then dramatically decreases at stage HH26 even though sprouting continues throughout the rest of the midbrain, although there is an increased expression of the shorter isoform. The expression of VEGFA isoforms decreases after stage HH26 as the level of ingression falls, which is consistent with ISH results identifying the established INVP.

VEGFA signalling through VEGFRs is involved in the migration of endothelial cells towards the neural tube, the selection of tip cells and the initiation of ingression (Ambler *et al*., 2003; Gerhardt *et al*., 2003; Hogan *et al*., 2004; Roberts *et al*., 2004; James *et al*., 2009). The expression patterns of VEGFRs were therefore investigated in the mesencephalon of stage HH19-28 *G. gallus* embryos using whole-mount ISH (Fig. 5iii-viii). Prior to the initiation of vascular ingression, VEGFR1, VEGFR2 and VEGFR3-positive cells were detected within the PNVP around the mesencephalic basal plate from stage HH19 as the expression of each VEGFR appeared to occur in specific cells that lined up against the basal lamina of the brain (Fig. 5iii, 5v and 5vii, C-D, arrows). In the process of vascular ingression, previous studies have shown that the gene expression profile of tip cells is distinct due to the strong expression of VEGFR2, whereas the expression of VEGFR1 is prominent within the stalk cells (Gerhardt *et al*., 2003). VEGFR1 appeared to be particularly prominent in coordinating with the invading sprouts from stage HH21 (Fig. 5iii, C-D, arrowheads) as the pattern of expression was similar to that observed from the detection of endothelial cells invading the ventral brain (Fig. 3x, E-H). VEGFR1 was then detected in the ventral mesencephalon at stage HH22 in the region where the INVP subsequently develops (Fig. 5iii, D, arrow), with continued expression in the nascent INVP from stage HH24 (Fig. 5iv, C-D, arrows). The dorsal mesencephalon was absent of VEGFR1-positive cells until stage HH24 onward (Fig. 5iv, A). In the alar plate, the pattern of expression at stage HH26 (Fig. 5iv, B, arrowheads) appeared to be similar to the detection of endothelial cells in this region at the same developmental stage (Fig. 3x, I), suggesting that VEGFR1 may continue to coordinate with the invading sprouts throughout the mesencephalon. Strong expression was observed in the established INVP throughout the mesencephalon at stage HH28 of development. In comparison to the VEGFR1 expression pattern, VEGFR2 and VEGFR3-positive cells were observed within the PNVP surrounding the dorsal half of the mesencephalon at stage HH21, lining up against the basal lamina of the brain (Fig. 5v and 5vii, A-B, arrowheads). Few VEGFR2-positive cells were identified within the ventral mesencephalon at this stage (Fig. 5v, D, arrow), although this became more apparent when more sprouts were invading the brain at stage HH22 (Fig. 5v, D, arrowheads). VEGFR2 expression was then observed in the alar plate at stage HH26 (Fig. 5vi, B, arrows), possibly coordinating with the ingressing sprouts. The expression of VEGFR3 was first observed in the

ventral mesencephalon at stage HH22 (Fig. 5vii, D, arrow) in a pattern that also appeared to resemble the ingressing sprouts. Expression was then detected in the alar plate at stage HH28 (Fig. 5viii, B, arrows), occurring a little later in development than VEGFR2. In the ventral mesencephalon at stage HH24, VEGFR2 (Fig. 5vi, D, arrowhead) and VEGFR3 (Fig. 5viii, D, arrowhead) expression was also identified within the developing INVP in addition to VEGFR1 (5iv, C-D, arrows).

Upon comparing the temporal and spatial expression pattern of VEGFR2 with MMP-1 expression, VEGFR2-positive cells were present within the PNVP at the dorsal half of the mesencephalon at stage HH21 (Fig. 5v) prior to the expression of MMP-1, which was not detected in this region until stage HH24 (Fig. 4vii). Before ingression into the brain, endothelial cells may begin to specialise into tip and stalk cells through VEGFA-VEGFR2 and Dll4-Notch signalling as described in the literature, which could be enhanced by the subsequent expression of MMP-1 leading to invasion, then followed by an increase in cell proliferation as identified through phosphohistone H3 immunostaining. The results could offer support to the mechanism proposed by Mazor *et al*. (2013) in which MMP-1 sensitises VEGFR2-mediated functions in endothelial cells although further analysis is required. Identifying the location of active collagenases in the brain using collagen zymography experiments and assaying for endothelial markers, together with MMP-1 gain- and loss-of function experiments, would be particularly useful for investigating the role of MMP-1 in endothelial cell ingression.

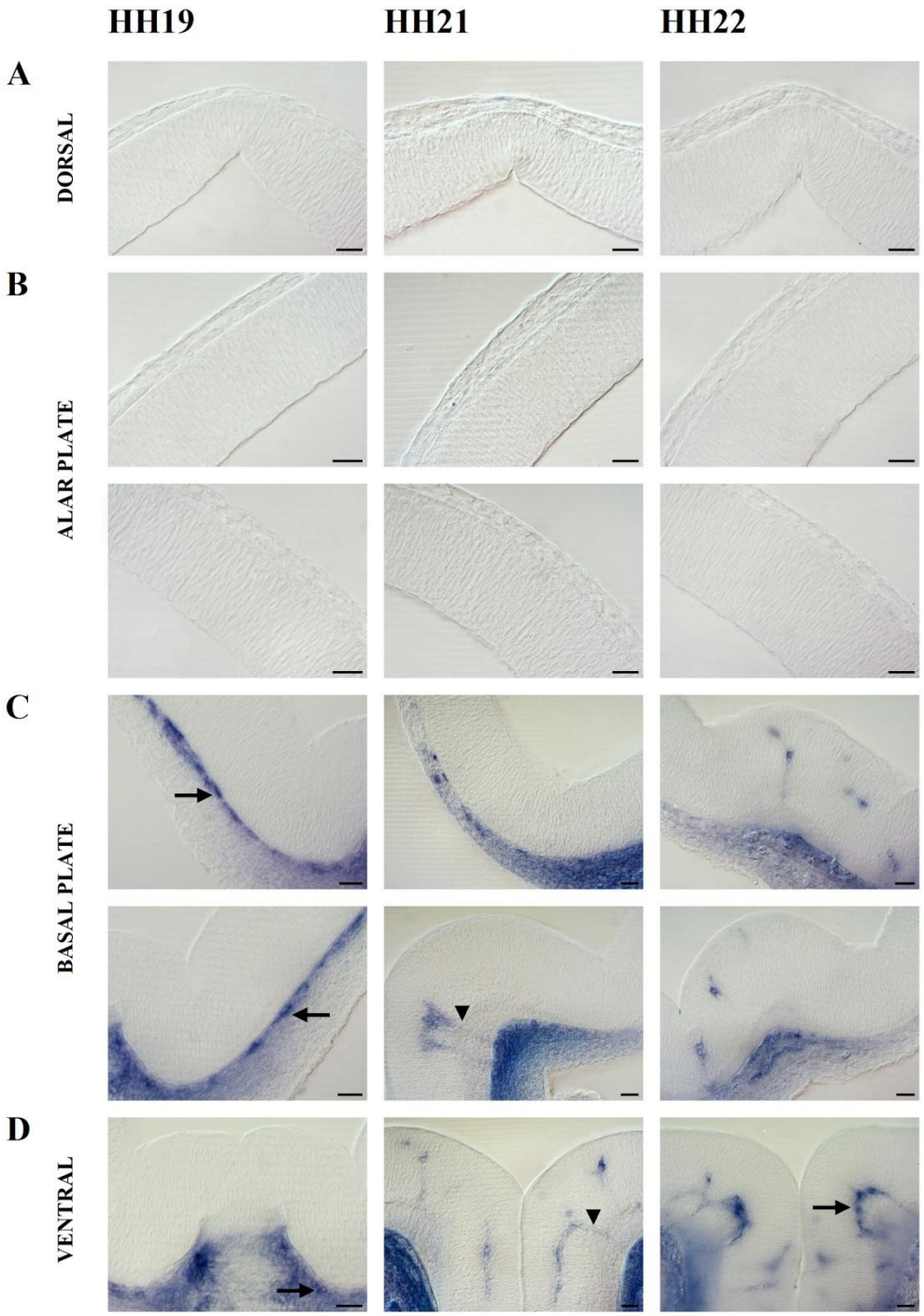

Figure 5iii. VEGFR1 expression in the mesencephalon of stage HH19-22 *G. gallus* embryos. Whole-mount ISH was used with an antisense probe against VEGFR1, followed by vibratome sectioning. VEGFR1 expression levels (blue) are shown in the dorsal (**A**), alar plate (**B**), basal plate (**C**) and ventral (**D**) areas of the mesencephalon. VEGFR1 is present in the PNVP by the basal plate at HH19 (arrows) and the expression pattern appears to coordinate with endothelial sprouting into the ventral mesencephalon at stage HH21 (arrowheads). VEGFR1-positive cells were also detected at stage HH22 in the region where the INVP would subsequently develop (arrow). The receptor was not expressed in the dorsal half of the mesencephalon. Scale bar = 25μm.

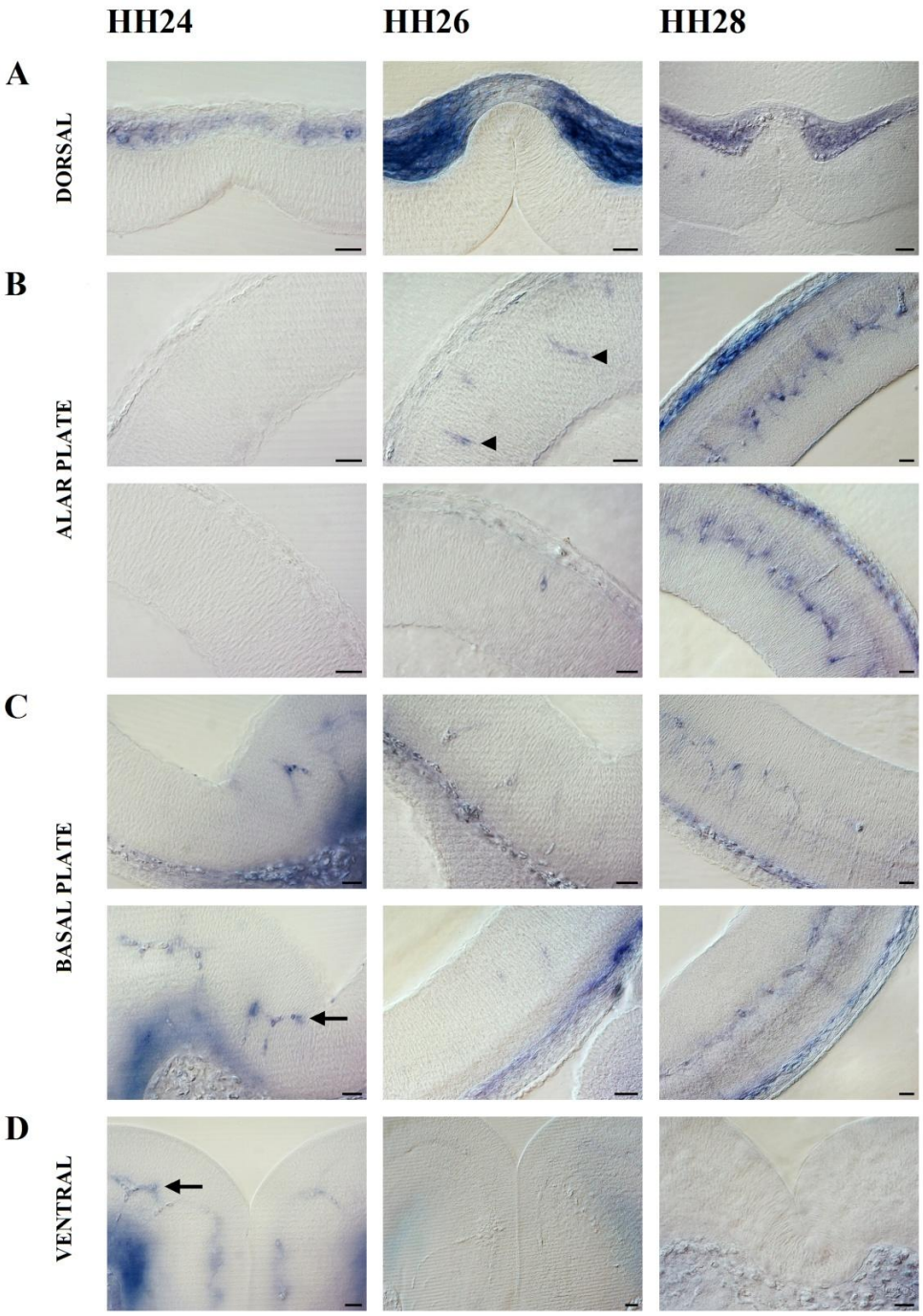

Figure 5iv. VEGFR1 expression in the mesencephalon of stage HH24-28 *G. gallus* embryos. Whole-mount ISH was used with an antisense probe against VEGFR1, followed by vibratome sectioning. VEGFR1 expression levels (blue) are shown in the dorsal (**A**), alar plate (**B**), basal plate (**C**) and ventral (**D**) areas of the mesencephalon. Expression by the dorsal mesencephalon is first observed at stage HH24 and continued expression in the nascent INVP is also detected at this stage (arrows). VEGFR1-positive cells were present in the alar plate at stage HH26 (arrowheads), which appear to coordinate with endothelial sprouting throughout the mesencephalon. VEGFR1 is strongly expressed in the established INVP at stage HH28. Scale bar = 25μm.

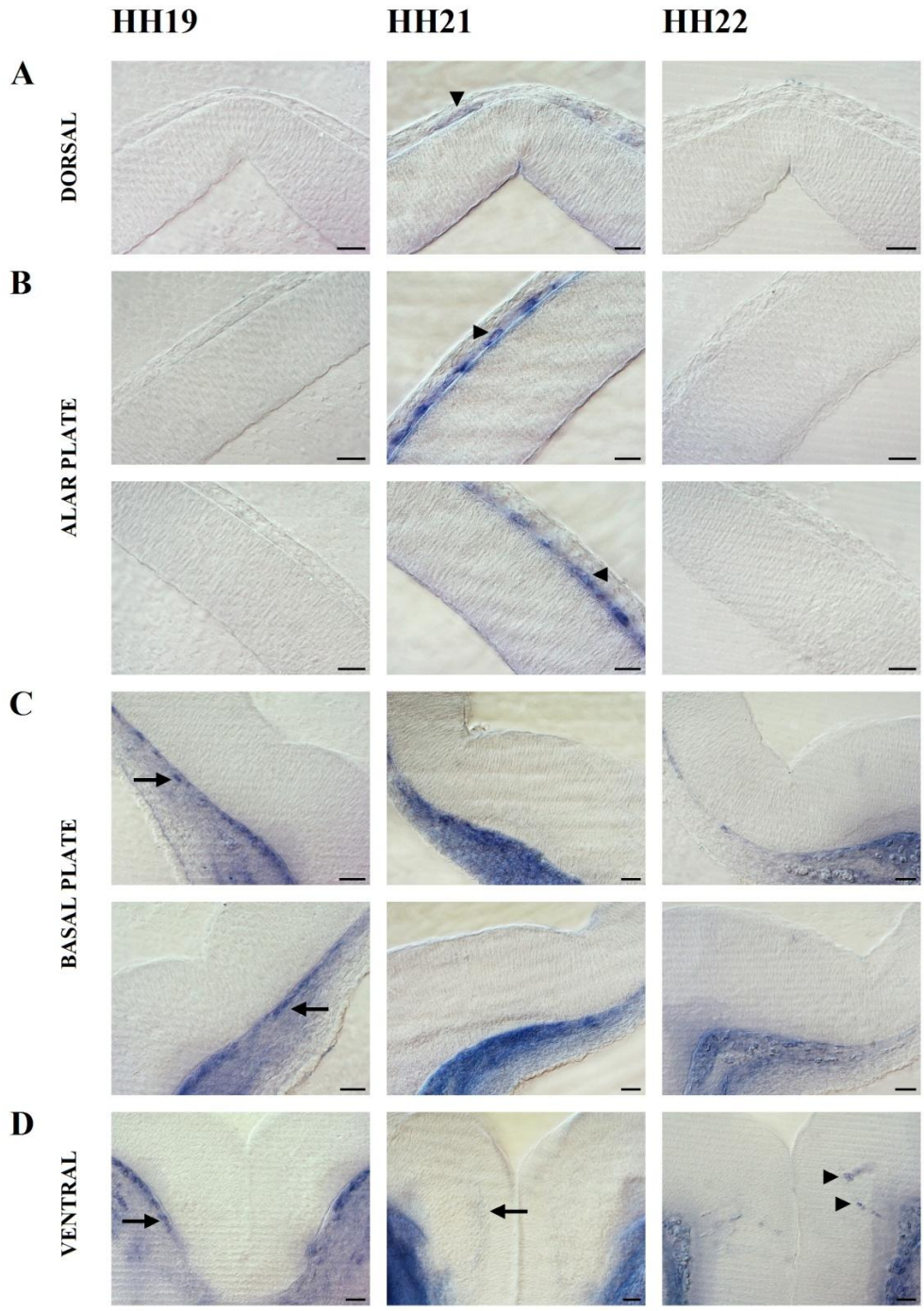

Figure 5v. VEGFR2 expression in the mesencephalon of stage HH19-22 *G. gallus* embryos. Whole-mount ISH was used with an antisense probe against VEGFR2, followed by vibratome sectioning. VEGFR2 expression levels (blue) are shown in the dorsal (**A**), alar plate (**B**), basal plate (**C**) and ventral (**D**) areas of the mesencephalon. VEGFR2 is seen in the PNVP by the basal plate at stage HH19 (arrows). Expression by the dorsal midbrain and in the PNVP by the alar plate is detected at stage HH21 (arrowheads). VEGFR2-positive cells were also detected in the ventral mesencephalon at this stage (arrow), which became more apparent at stage HH22 (arrowheads), appearing to coordinate with the invading sprouts. Scale bar = 25μm.

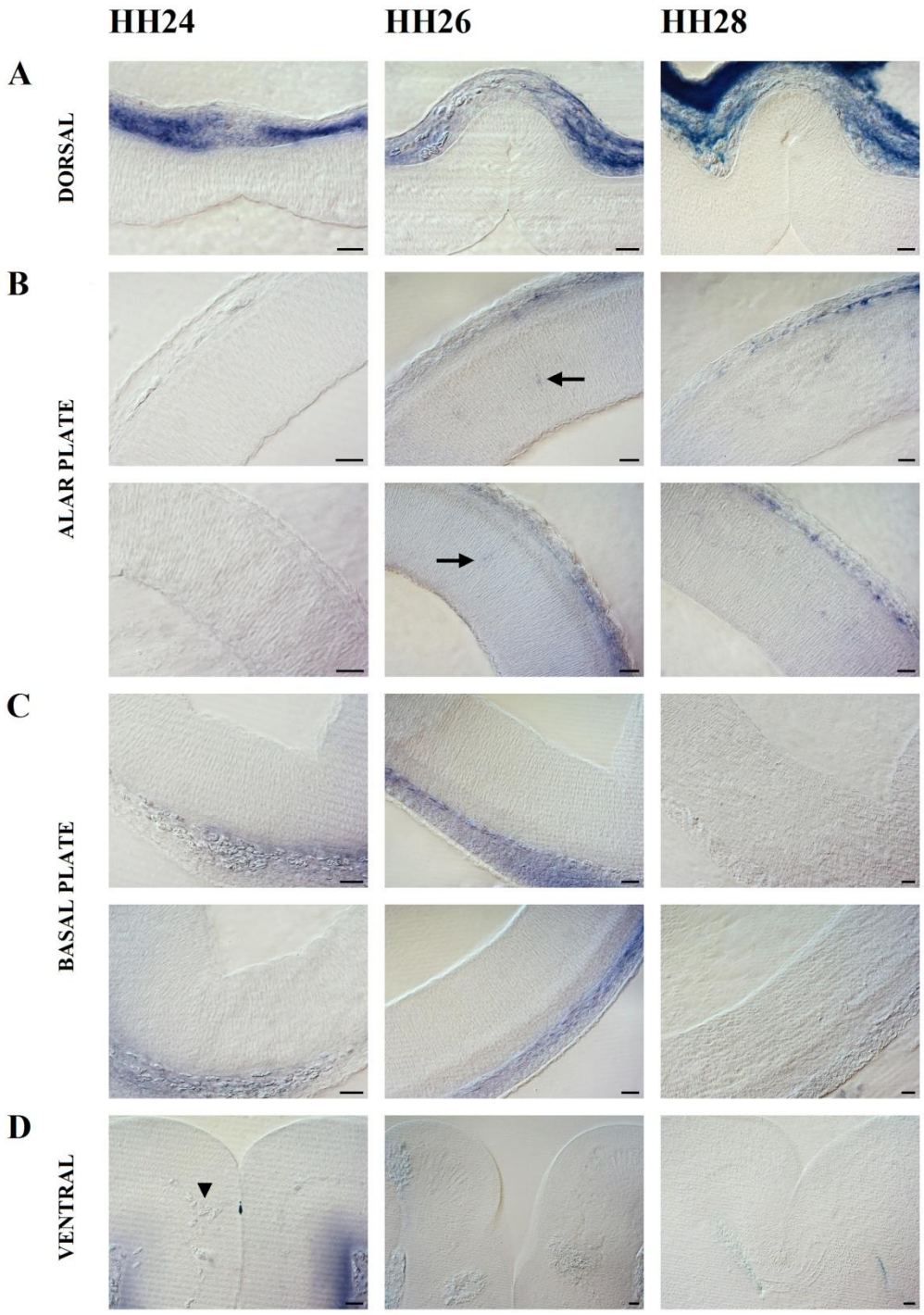

Figure 5vi. VEGFR2 expression in the mesencephalon of stage HH24-28 *G. gallus* embryos. Whole-mount ISH was used with an antisense probe against VEGFR2, followed by vibratome sectioning. VEGFR2 expression levels (blue) are shown in the dorsal (**A**), alar plate (**B**), basal plate (**C**) and ventral (**D**) areas of the mesencephalon. Expression by the dorsal mesencephalon is prominent at stage HH24. The INVP in the ventral mesencephalon is identifiable at this stage but few VEGFR2-positive cells were observed in this region (arrowhead). VEGFR2 expression was detected in the alar plate of the mesencephalon at stage HH26 of development (arrows). Scale bar = 25μm.

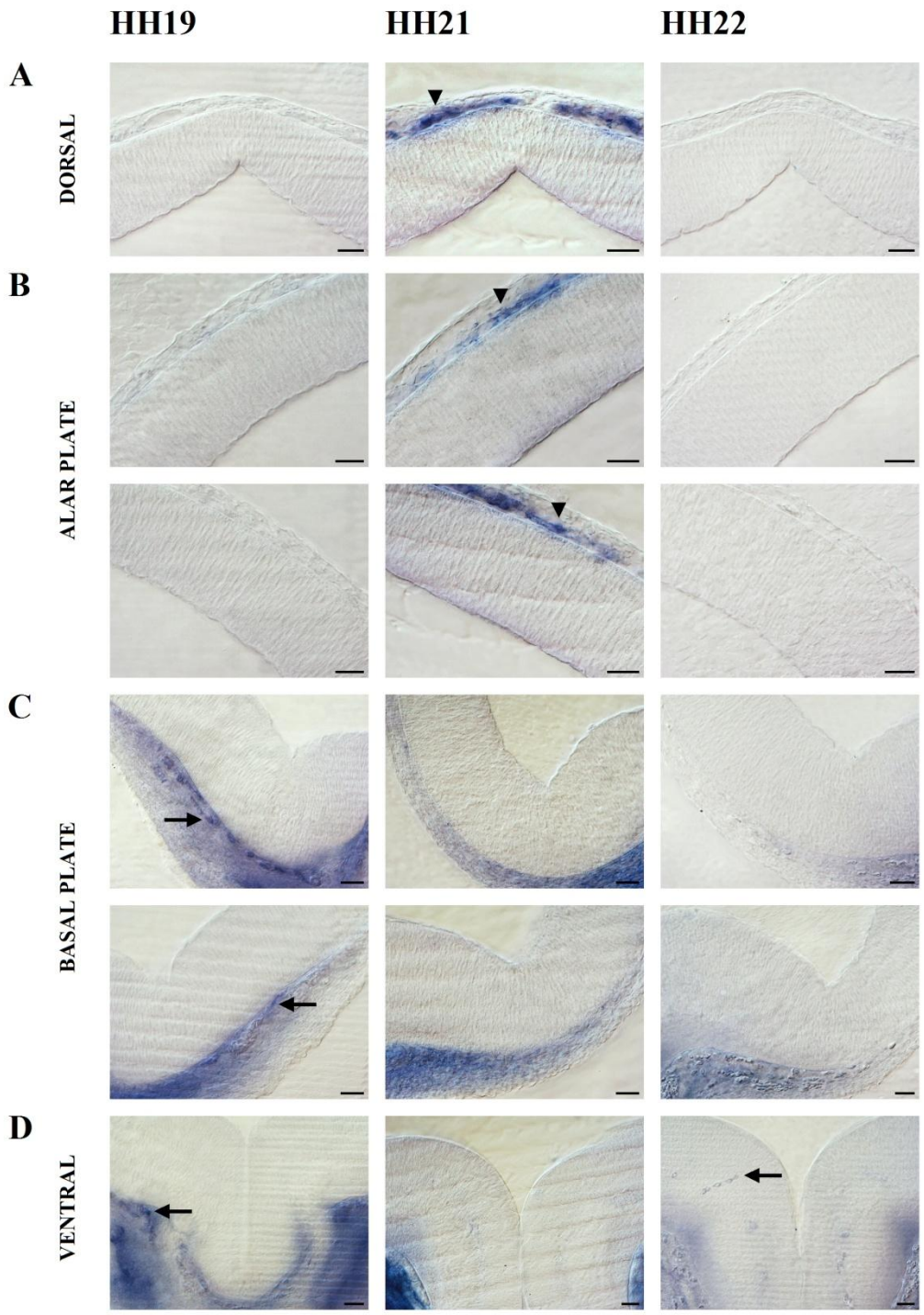

Figure 5vii. VEGFR3 expression in the mesencephalon of stage HH19-22 *G. gallus* embryos. Whole-mount ISH was used with an antisense probe against VEGFR3 (Flt-4), followed by vibratome sectioning. VEGFR3 expression levels (blue) are shown in the dorsal (**A**), alar plate (**B**), basal plate (**C**) and ventral (**D**) areas of the mesencephalon. VEGFR3 is present within the PNVP by the basal plate at stage HH19 (arrows). Expression by the dorsal mesencephalon and in the PNVP by the alar plate is detected at stage HH21 (arrowheads) and subsequently in the ventral mesencephalon at stage HH22 (arrow) in a pattern that appears to coordinate with the ingressing sprouts. Scale bar = 25μm.

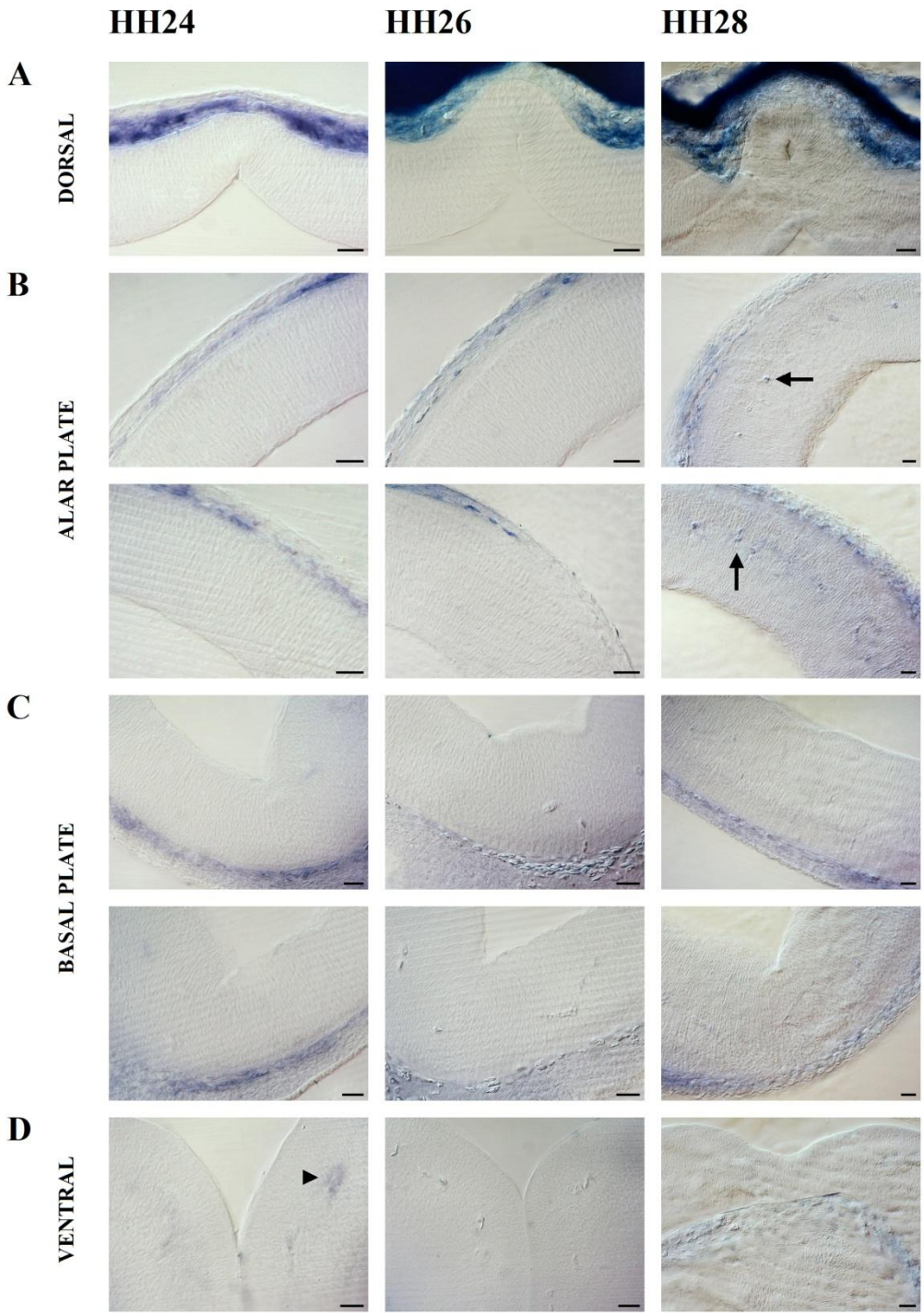

Figure 5viii. VEGFR3 expression in the mesencephalon of stage HH24-28 *G. gallus* embryos. Whole-mount ISH was used with an antisense probe against VEGFR3, followed by vibratome sectioning. VEGFR3 expression levels (blue) are shown in the dorsal (**A**), alar plate (**B**), basal plate (**C**) and ventral (**D**) areas of the mesencephalon. VEGFR3-positive cells are seen in the developing INVP in the ventral mesencephalon at stage HH24 (arrowhead) and in the alar plate at stage HH28 of development (arrow), which appears to coordinate with the ingressing sprouts. Scale bar = 25μm.

5.2 Ectopic expression of Shh leads to PNVP expansion, disrupted sprout formation and ectopic endothelial ingression

The development of blood vessels is preceded by the process of neurogenesis and is regulated in part by molecular signals that are relayed from the neural network to the endothelial cells, resulting in the formation of an elaborate and highly efficient vascular network required for supporting the developing brain. The influence of neural regulation on brain vasculature was explored as regional differences in vascular ingression were identified, particularly along the dorsoventral axis of the brain (refer to chapter 3). In order to investigate if these differences occurred due to the dorsoventral patterning of the brain, electroporation experiments were conducted using an expression construct for Shh. Shh is involved in the spatial organisation of neuronal cell types and is well established as the main ventralising signal for the neural tube. The dorsoventral pattern is established very early on in development (Wilson & Maden, 2005), therefore the Shh construct was electroporated into one side of the mesencephalon of stage HH11-12 *G. gallus* embryos with the aim of transferring the tectum into tegmentum and investigating if the vasculature would respond to the ventralisation by resulting in ectopic sprouting in the alar plate as would normally occur in the basal plate. The embryos were incubated further and then fixed at stages HH26-29.

The electroporation of Shh into the mesencephalon resulted in perturbation to the growth of the developing brain. A distinct phenotype was identified in which the side receiving ectopic Shh was notably smaller compared with the non-electroporated control side and control embryos (Fig. 5ix). Upon comparing the size and shape of the mesencephalon in sections taken from GFP control and Shh-electroporated embryos, a number of malformations were observed in the tectum (Fig. 5x). Instead of the normal expansion that occurs during embryonic development, the tectum on the electroporated side remained compact and an increase in the size of the ventricular zone was also observed on the electroporated side (Fig. 5x, arrow). The detection of endothelial cells by fluorescent IHC with a CD34 antibody identified a thickening that was indicative of the tegmentum in one embryo (Fig. 5xi, arrow), which was consistent with a change in brain patterning resulting from ectopic Shh expression. The ingression of endothelial sprouts into the

restructured mesencephalon was also observed (Fig. 5xi, arrowheads). Experiments involving the misexpression of this dorsoventral patterning molecule have shown that an ectopic source of Shh is sufficient to induce a duplicate set of tegmental arcs, which allocate neurons to distinct nuclear fates (Agarwala *et al*., 2001; Agarwala & Ragsdale, 2002). The results therefore appear to show the ventralisation of the dorsal mesencephalon and abnormal patterning or partial duplication of the mesencephalic arcs. Additional staining using ISH with multiple probes to detect specific transcription factors such as GATA2 and FOXA2 can be performed in order to detect the location of these territories.

Further to the abnormalities in the size and shape of the mesencephalon, altering neural patterning through the electroporation of Shh also resulted in defects to the developing vasculature. An expansion of the PVNP was detected on the electroporated side (Fig. 5xii, arrow) and endothelial cells were observed ingressing into the mesencephalon, although sprout formation appeared to be disrupted and the development of the INVP was disorganised (Fig. 5xii, arrowheads). The described effects resulting from the ectopic expression of Shh were absent from the non-electroporated control side and control embryos (Fig. 5xiii). A study conducted in zebrafish embryos has suggested a signalling cascade in which Shh activates VEGF, leading to the activation of Notch signalling (Lawson *et al*., 2002). Conducting fluorescent IHC for VEGF in addition to CD34 immunostaining would therefore be important to test the proposed cascade. Detecting a higher expression of VEGF on the electroporated side could then provide an explanation to the observed expansion of the PNVP as an increase in VEGF signalling would act to promote endothelial cell migration towards the mesencephalon leading to a larger quantity of endothelial cells present alongside the brain that may further increase in number due to cell division, thus expanding the size of the PNVP. The disruption to the formation of endothelial sprouts may have resulted from the downstream effect of ectopic Shh signalling on promoting Notch activation that would in turn increase the number of tip cells present within the mesencephalon. Abnormal sprout formation would consequently affect the formation of the internal capillary network resulting from changes to normal branching and fusion patterns that occur during normal development.

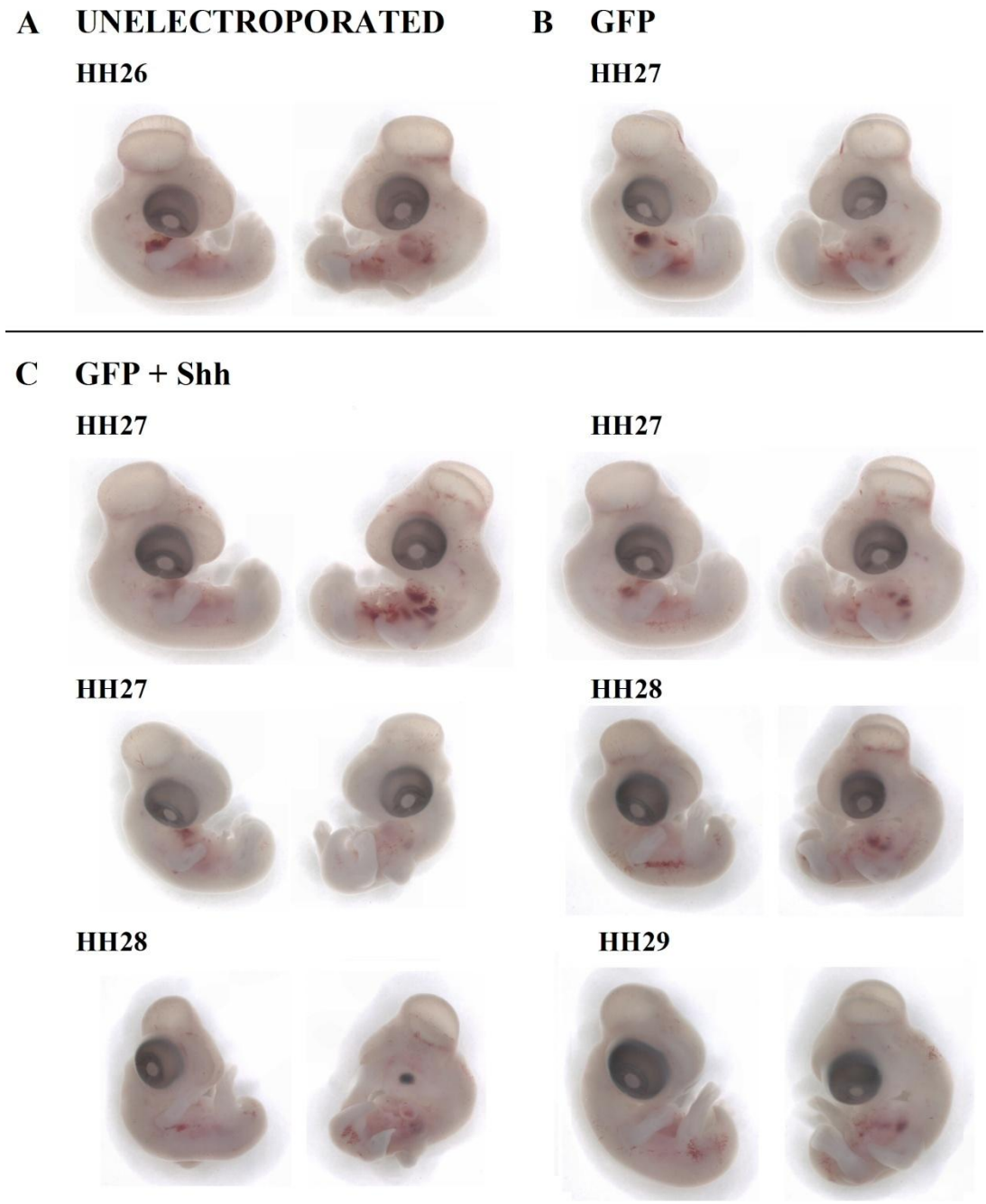

Figure 5ix. ***G. gallus*** **embryos following the electroporation of an expression construct for Shh into the mesencephalon.** The co-electroporation of Shh and GFP expression constructs was performed in the left side of the mesencephalon of stage HH11-12 embryos. The embryos were incubated and fixed in 4% PFA/PBS upon reaching stages HH26-29 of development. The left and right sides of the mesencephalon from control embryos that were either unelectroporated (**A**) or electroporated with the GFP construct (**B**) appear to be similar in morphology. The development of the mesencephalon from embryos electroporated with the Shh and GFP expression constructs (**C**) reveals a phenotype in which the electroporated side appears to be underdeveloped and distinctly smaller compared with the non-electroporated control side and the mesencephalon of control embryos.

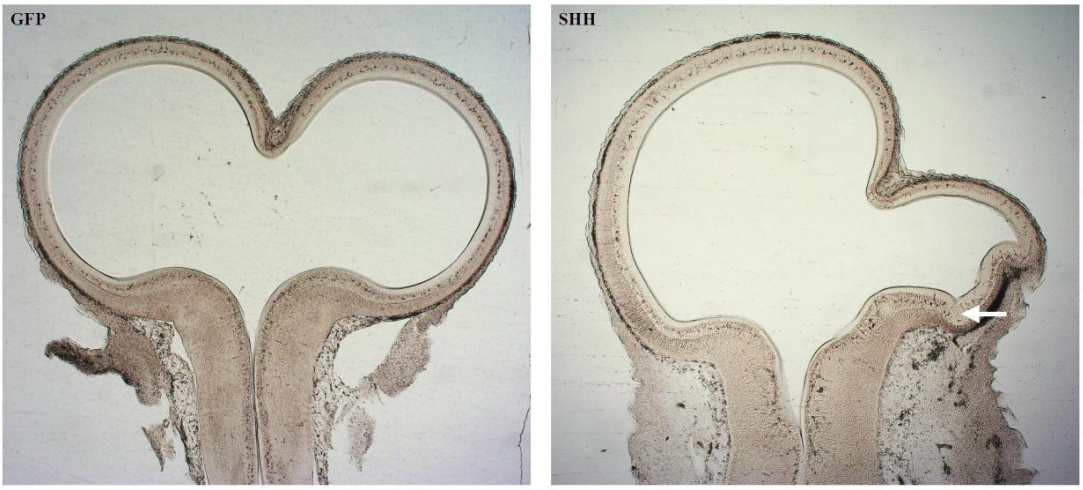

Figure 5x. Sections taken from the mesencephalon of stage HH28 embryos following electroporation of a Shh expression construct compared with the GFP control. The phenotype observed from embryos electroporated with both Shh and GFP expression constructs reveal a malformed mesencephalon on the electroporated side compared with the non-electroporated control side as the tectum appears compact. An increase in the size of the ventricular zone is also detected (arrow). The effect that Shh has on the morphology is substantially different from that of the control embryo electroporated only with the GFP expression construct in which the left and right sides of the mesencephalon appear similar in both shape and size**.**

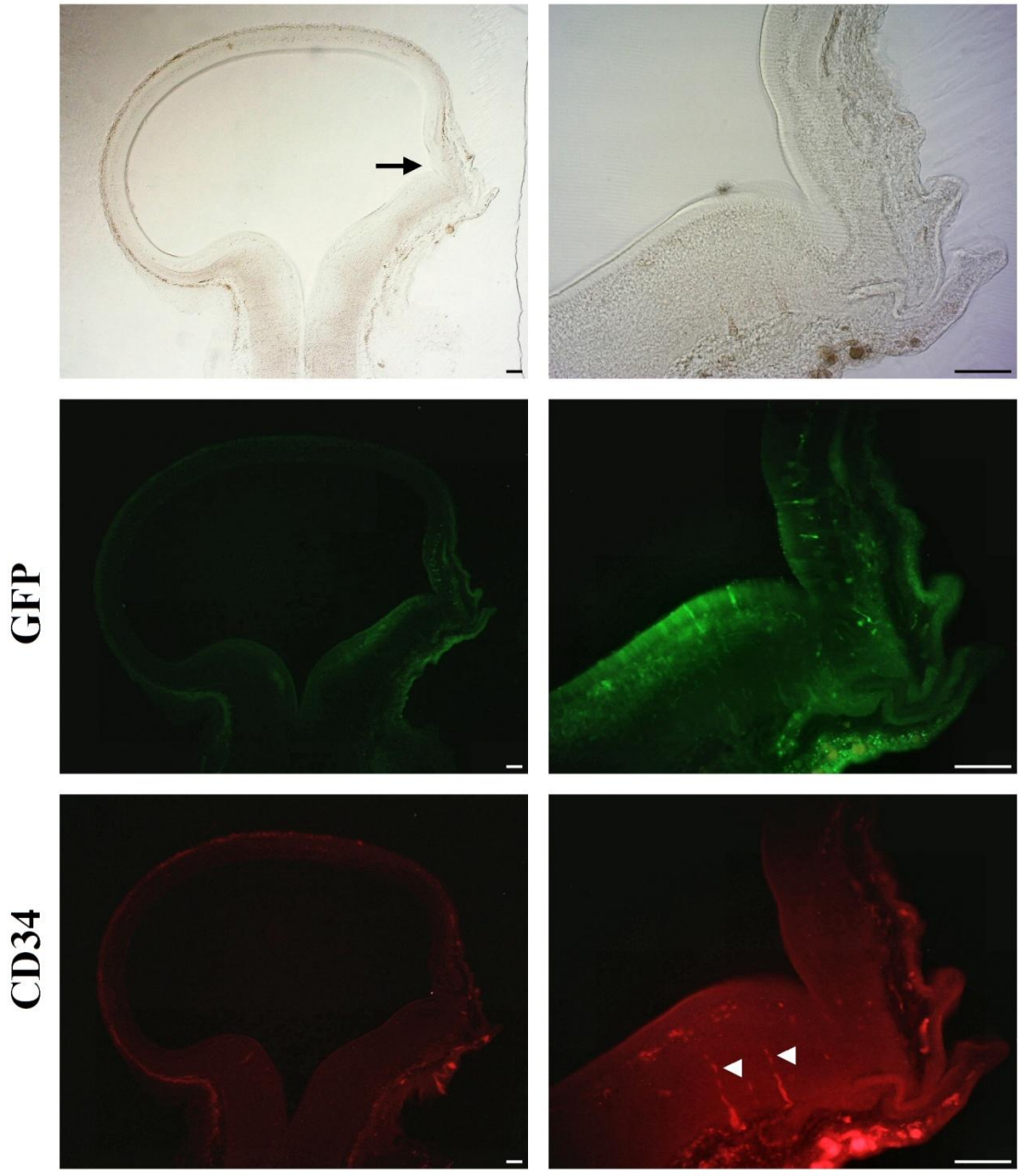

5xi. Abnormal development of the mesencephalon following ectopic expression of Shh. Whole-mount fluorescent IHC was conducted using a CD34 antibody to detect endothelial cells (red) and an anti-GFP antibody to identify cells that successfully took up the expression construct (green). The ectopic expression of Shh results in the aberrant development of the mesencephalon as a thickening was detected on the electroporated side (n=1, arrow) compared to the controls. The invasion of endothelial sprouts into the electroporated region was observed (arrowheads). Scale bar = 100μm.

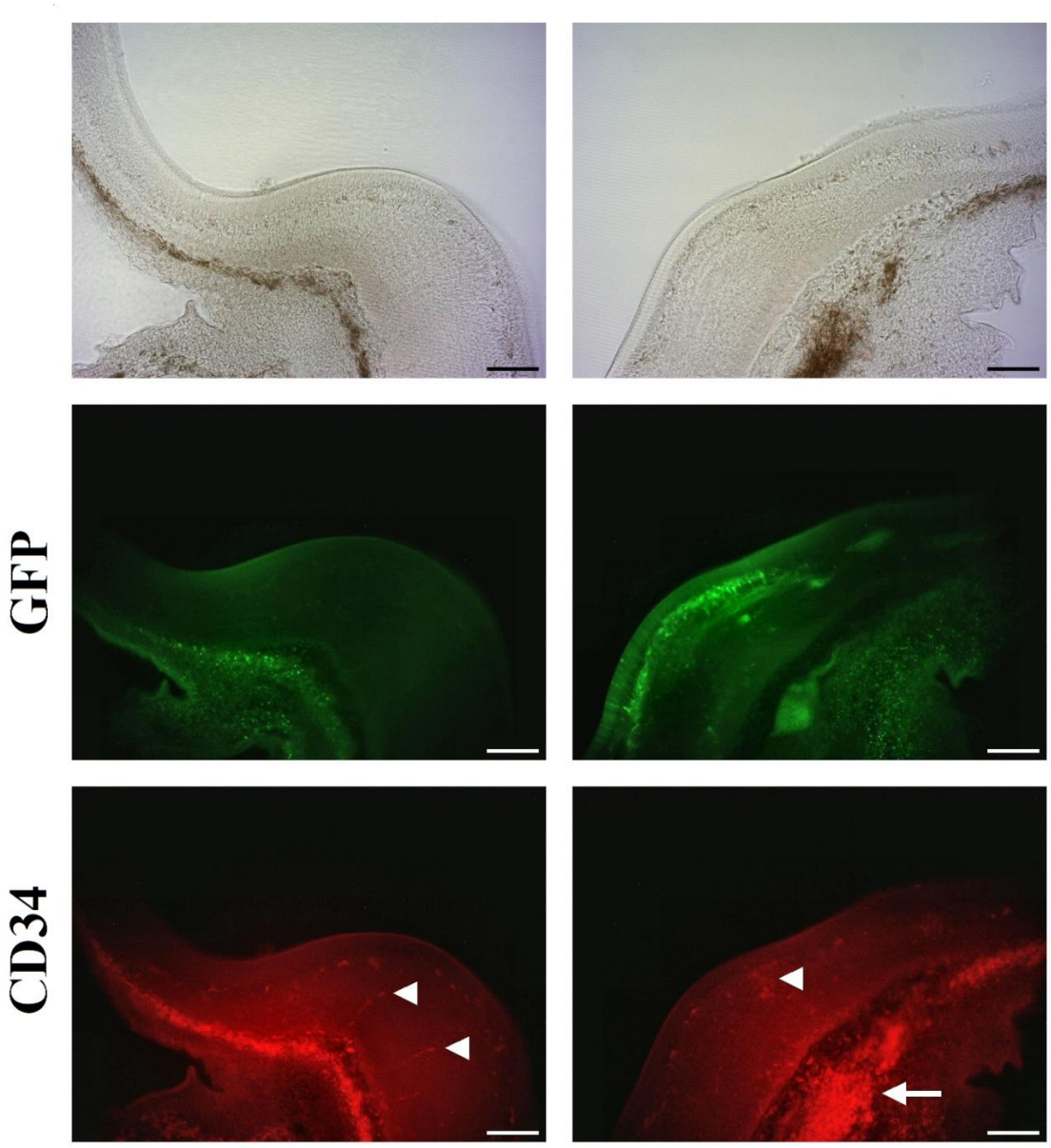

Figure 5xii. Endothelial cell detection using fluorescent IHC following the co-electroporation of Shh and GFP expression constructs into the mesencephalon. Whole-mount fluorescent IHC was conducted using a CD34 antibody to detect endothelial cells (red) and an anti-GFP antibody to identify cells that successfully took up the expression construct (green). The ectopic expression of Shh leads to an expansion in the size of the PNVP by the basal plate, indicated by a large area of red-fluorescing cells (arrow) compared with the control side (6/6 embryos). Endothelial cells have ingressed into the electroporated side of the mesencephalon although the normal formation of vessel sprouts with a leading tip cell and follower stalk cells appears to be disrupted (3/6 embryos) and the development of the INVP is also disorganised compared with the control side (4/6 embryos, arrowheads). Scale bar = 100μm.

Figure 5xiii. Endothelial cell detection using fluorescent IHC in the mesencephalon of control embryos. Embryos were either unelectroporated wild type (**A**, n=1) or electroporated with a GFP expression construct (**B**, n=4). Whole-mount fluorescent IHC was conducted using a CD34 antibody to detect endothelial cells (red) and an anti-GFP antibody to identify cells that successfully took up the GFP construct (green). A low level of auto fluorescence is emitted from the tissues in both controls although a higher intensity of green fluorescence in electroporated embryos on the side receiving GFP (arrow) indicates that these cells have successfully taken up the expression construct. The fluorescence for CD34 indicates the location of endothelial cells and ingressing sprouts, which appears to be similar in the left and right sides of both controls. Scale bar (sections) = 100μm.

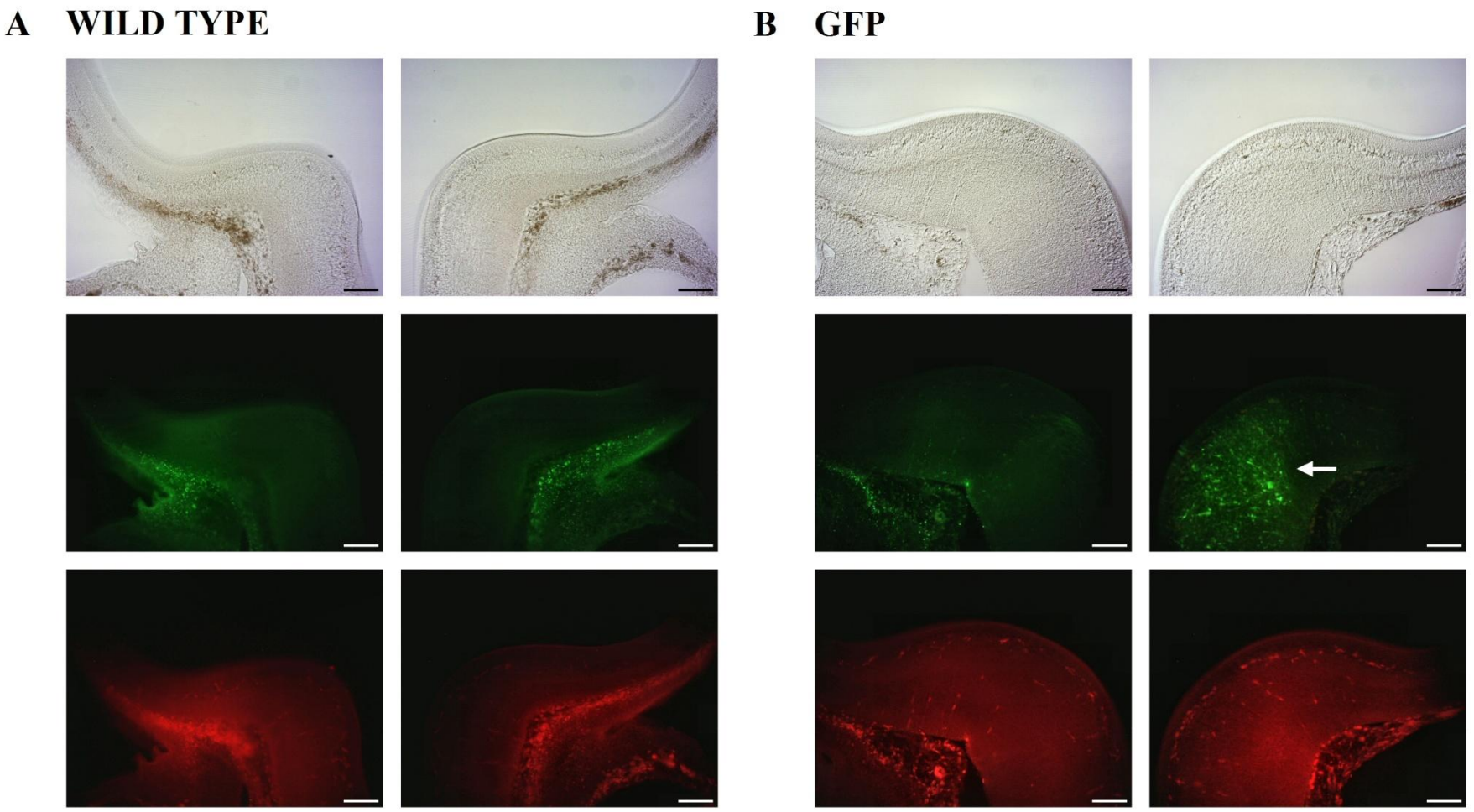
A WILD TYPE
B GFP

The ectopic expression of a single regulatory molecule has been shown to coordinate both size and shape of the brain and to indirectly regulate the intricate pattern of vascular development through changes to the neural patterning of the mesencephalon. However, further analysis is required to identify and understand the cascade of signals existing between Shh expression and endothelial ingression into the embryonic brain. Previous studies have suggested that Shh signalling regulates angiogenic sprouting by establishing populations of motor neurons that express pro-angiogenic Ang-1, which acts to guide vessel ingression in the neural tube. The subsequent stabilisation of the nascent BBB is partly regulated by cross-communication between Shh-secreting astrocytes and associated endothelial cells (Nagase *et al*., 2005; Alvarez *et al*., 2011). However, whether or not a similar process occurs in the embryonic *G. gallus* brain is unclear. The observed effects that Shh had upon brain vasculature nevertheless resulted from the tight coordination of the developing nervous and vascular systems and the complex relay of molecular information existing between the two systems. The exact effect on neural patterning resulting from Shh electroporation should first be analysed by immunostaining for the expression of genes involved in dorsoventral patterning, such as GATA2 and Pax7, in addition to motor neuron and astrocyte markers including Islet1 and GFAP, respectively, in order to provide a more detailed understanding regarding the effect of neural organisation on ingression.

5.3 Notch activity affects endothelial cell ingression and may play a role in maintaining endothelial sprout integrity after ingression

The behaviour of endothelial cells in sprouting angiogenesis is known to be regulated by the Notch pathway, which is induced by VEGFA (Gerhardt *et al*., 2003). Previous research conducted in the mouse retina has shown that the inhibition of Notch signalling promotes an increase in tip cell numbers and vessel branching, whereas Notch activation results in fewer tip cells and vessel branches (Hellström *et al.*, 2007; Suchting *et al*., 2007). The effect of Notch signalling on endothelial sprout invasion was investigated in order to build upon this research and provide a deeper understanding of the process occurring within the brain. The level of Notch signalling to which endothelial cells were exposed was reduced through the *in ovo* implantation of acrylic beads soaked with the Notch inhibitor, DAPT, which

is an inhibitor of γ-secretase that blocks the proteolytic activation of Notch receptors. DAPT has been shown to cause a reduction in amyloid-beta 40 and amyloid-beta 42 levels in human primary neuronal cultures (IC_{50} values are 115nM and 200nM for total amyloid-beta 40 and amyloid-beta 42, respectively) and in brain extract, cerebrospinal fluid and plasma *in vivo* (Insight Biotechnology). DAPT was tested at a concentration much higher than the known IC_{50} values as the extent of diffusion from the bead and dilution across the tissue over time are unknown. The beads were positioned just beneath the surface ectoderm adjacent to the basal plate of the mesencephalon of stage HH22 chick embryos. Embryos were incubated further and harvested at stage HH26, during which sprouting normally occurs at multiple points throughout the mesencephalon (Fig. 3x, I). Endothelial cells were detected with IHC using a CD34 antibody (Fig. 5xiv) and counted (Fig. 2ii and Appendix O).

Research conducted in the mouse retina gave rise to a hypothesis in which a decrease in the level of Notch would increase the number of endothelial cells ingressing into the brain. A paired t-test was performed using Minitab 17 in order to determine if there was a significant increase in the number of endothelial cells present within the brain in the side exposed to DAPT compared with the contra lateral control side. In control embryos that were implanted with beads containing only DMSO or PBS (Fig. 5xiv, A and C) endothelial cells ingressing into both sides of the mesencephalon were similar in number (Appendices P-Q). Embryos implanted with beads containing 10mM DAPT in DMSO showed a significant increase in the quantity of endothelial cells ingressing into the mesencephalon on the experimental side compared with the control side (Fig. 5xiv, B, Fig. 5xv and Appendix R). Clusters of endothelial cells were formed in half of these embryos (Fig. 5xiv, B, arrow), a response that was absent from controls. Similar to the clustering observed when MMP activity was altered, the reduction in Notch signalling produced groups of endothelial cells that varied in size and were detected within the brain only on the experimental side in which the bead containing 10mM DAPT in DMSO was implanted. The presence of cell clusters could result from a disruption to the formation of the endothelial sprouts, suggesting a crucial role for Notch signalling during vascular ingression into the developing brain. No difference was found in the number of endothelial cells ingressing into the experimental and control sides of embryos exposed to 10mM DAPT in PBS (Fig. 5xiv, D, and Appendix S).

Figure 5xiv. Sections through the mesencephalon of *G. gallus* embryos following the implantation of beads containing DAPT. Acrylic beads (blue) containing either DMSO (n=7) or PBS (n=7) are positioned in the mesoderm beneath the surface ectoderm of the mesencephalon in stage HH26 embryos. A similar number of endothelial cells, which are detected using IHC with a CD34 antibody (brown), are seen ingressing into both sides of the mesencephalon at the level of the bead in control embryos (**A**, **C**). A significant increase in the quantity of endothelial cells ingressing into the mesencephalon on the experimental side compared with the control side was detected in embryos implanted with beads containing 10mM DAPT in DMSO (n=5, **B**). Clusters of endothelial cells were also observed in half of these embryos (arrow). No difference was found in the number of endothelial cells ingressing into the experimental and control sides of embryos exposed to 10mM DAPT in PBS (**D**, n=3). Scale bar = 100μm.

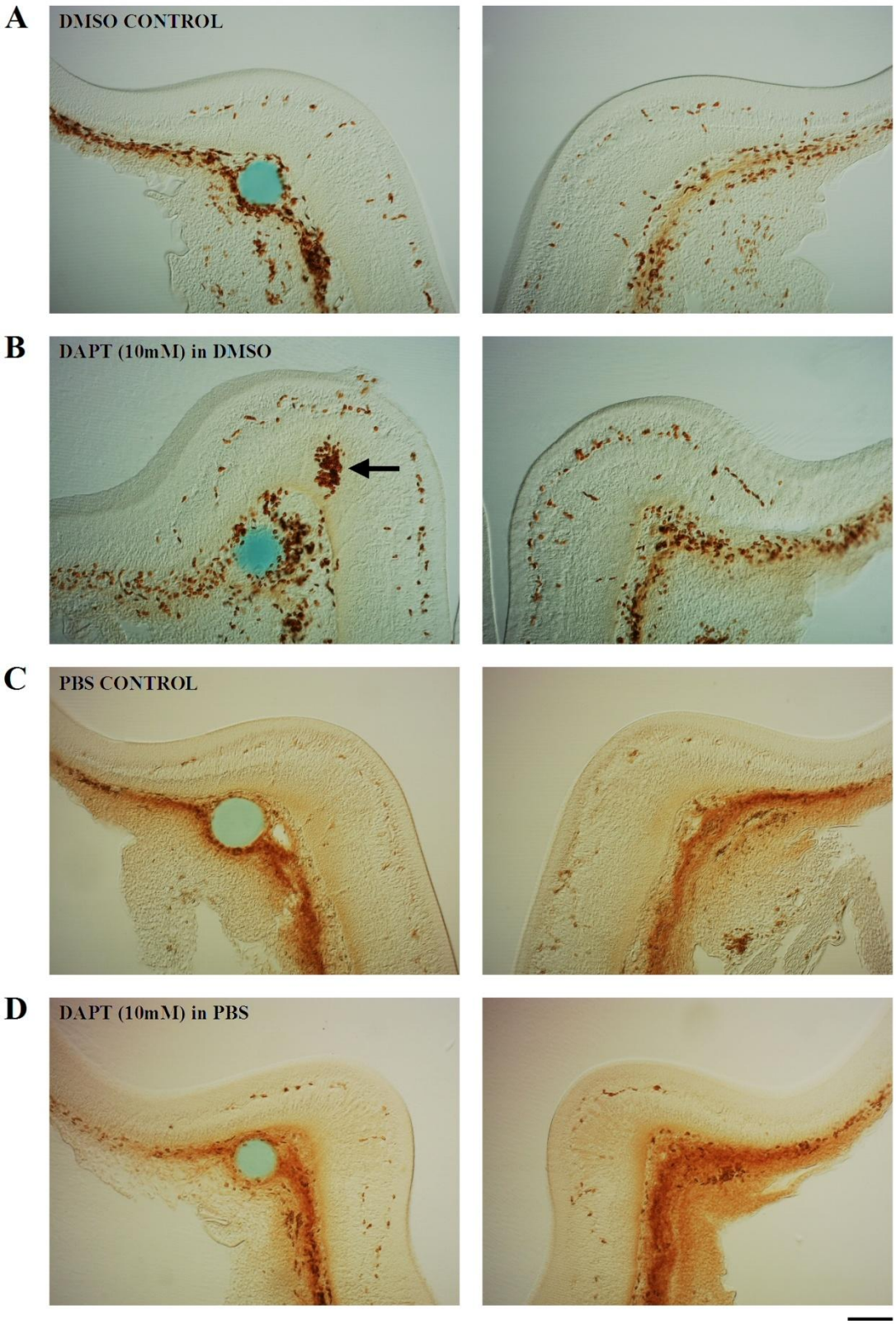
A
DMSO CONTROL
B
DAPT (10mM) in DMSO
C
PBS CONTROL
D
DAPT (10mM) in PBS

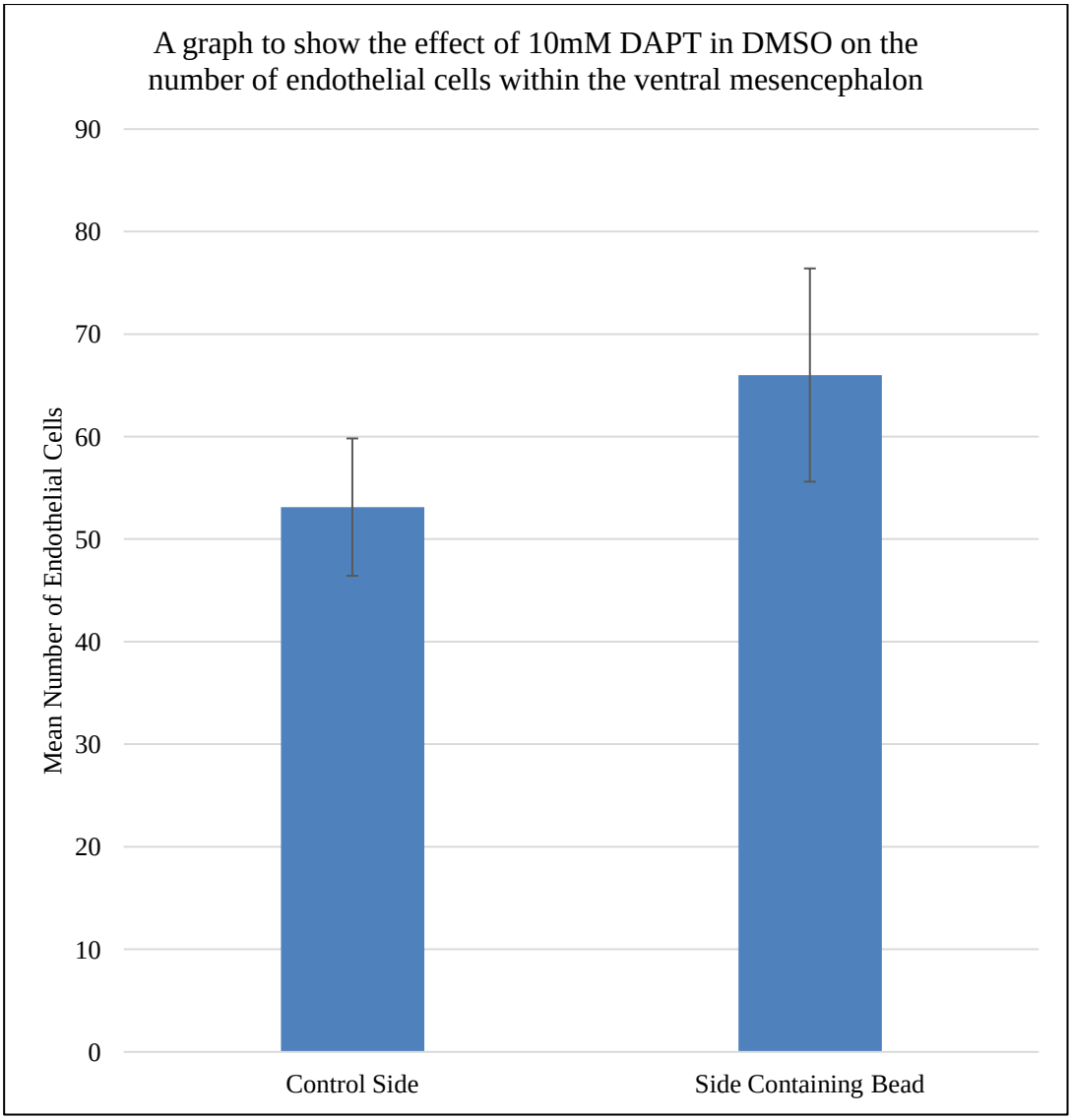

Fig. 5xv. The effect of 10mM DAPT in DMSO on endothelial cell ingression. The mean number of endothelial cells on the side containing the bead (n=5) is compared with the mean number of endothelial cells on the contra lateral control side (n=5) after exposure to 10mM DAPT in DMSO. Error bars represent the standard error of the mean. A statistically significant increase in the number of endothelial cells was identified on the experimental side (p value = 0.036, Appendix R).

The exposure of DAPT to one side of the early embryonic mesencephalon resulted in an increase in the number of endothelial cells ingressing into the experimental side compared with the control side and resulted in the formation of endothelial cell clusters, similar to those detected as a consequence of altering levels of MMPs. Since ingression into the ventral mesencephalon was previously observed at stage HH21, endogenous signalling at the start of brain vascularisation would enable tip and stalk cell selection to take place and ingression to begin as normal. The delivery of DAPT at stage HH22 may therefore have enhanced ingression as the embryos continued to develop. Shortly after the initiation of ingression, the formation of endothelial cell clusters within the mesencephalon suggests either a prevention of or disruption to the structural integrity of the vessel sprout brought about by the Notch inhibitor. The results are among the first to suggest a crucial role for Notch signalling in the formation of sprouts during endothelial ingression into the developing brain. Endothelial cells have been shown to dynamically shuffle and compete for the tip cell position, suggesting that these specialist phenotypes are highly transient and exchangeable. The regular exchange of the leading tip cell occurs as cells interact with new neighbouring cells, and in a Notch-dependent system the differential regulation of VEGFR1 and VEGFR2 in individual cells modulates the expression of Dll4 (Jakobsson *et al*., 2010). The identity of the cells that form the clusters as either tip or stalk cells remain unknown although alterations to the identities of each cell within the ingressing sprout are highly likely. Further analysis should be conducted to determine whether or not these phenotypes are present by staining for tip and stalk cells markers such as VEGFR1 and VEGFR2 and the cells to which they are associated could subsequently be investigated. The implantation of beads could also be performed at an earlier stage to expose cells to the Notch inhibitor prior to tip and stalk cell selection and ingression at stage HH21. The lack of Notch signalling would be hypothesised to enhance sprouting into the mesencephalon due to an increase in the number of tip cells present and the effect this has on ingression can be analysed with an assay for endothelial markers.

The effect on the nascent vessel morphology within the embryonic brain in addition to the selection of tip and stalk cells is likely to be controlled by a plethora of molecular pathways as well as Notch signalling, although a definitive regulatory network underlying brain vascularisation has not yet been established. A primary

focus should be to identify the spatial and temporal expression of Notch during early development, which will be paramount for comparison with the effect on expression following loss- or gain-of-function experiments through DAPT exposure or the electroporation of a Notch construct in the embryonic brain, respectively. The importance of Notch signalling in coordinating VEGFA-VEGFR, SEMA3E-PlexinD1, ALK1 and endothelial Smad1/5 in the promotion or inhibition of tip cell formation has been researched and analysed in various model systems with a particular focus on the mouse retina (Gerhardt *et al*., 2003; Hellström *et al.*, 2007; Suchting *et al*., 2007; Kim *et al*., 2011; Larrivée *et al*., 2012; Moya *et al*., 2012) and is in no doubt crucial in angiogenesis. The same regulatory networks may underlie the formation of endothelial sprouts and ingression into the embryonic brain, although due to the complex function and architecture of the brain it is likely that this process is governed by an even more intricate system of regulation, particularly in orchestrating the establishment of an adequate ratio of tip and stalk cells required for normal sprouting patterns. A more detailed analysis of these factors in addition to the functional analysis of MMPs on endothelial ingression would be worthwhile in providing a better understanding of the process of vascularisation in the early vertebrate brain. Furthermore, the combinatory effects of MMP and VEGFA antagonists and agonists could later help in motivating the development of novel anti-angiogenic strategies that may be useful for reducing tumourigenesis and aiding in establishing proangiogenic treatments for the recovery of stroke.

REFERENCES

Abbott, N. J., Patabendige, A. A., Dolman, D. E., Yusof, S. R., Begley, D. J. (2010). Structure and function of the blood-brain barrier. *Neurobiology of Disease*. 37: 13-25

Agarwala, S. & Ragsdale, C. W. (2002). A role for midbrain arcs in nucleogenesis. *Development*. 129: 5779-5788

Agarwala, S., Sanders, T. A. & Ragsdale, C.W. (2001). Sonic hedgehog control of size and shape in midbrain pattern formation. *Science*. 291: 2147-2150

Aimes, R. T. & Quigley, J. P. (1995). Matrix metalloproteinase-2 is an interstitial collagenase. Inhibitor-free enzyme catalyzes the cleavage of collagen fibrils and soluble native type I collagen generating the specific 3/4- and 1/4-length fragments. *The Journal of Biological Chemistry*. 270: 5872-5876

Airola, K., Karonen, T., Vaalamo, M., Lehti, K., Lohi, J., Kariniemi, A. L., Keski-Oja, J. & Saarialho-Kere, U. K. (1999). Expression of collagenases-1 and -3 and their inhibitors TIMP-1 and -3 correlates with the level of invasion in malignant melanomas. *British Journal of Cancer*. 80: 733-743

Allinson, K. R., Lee, H. S., Fruttiger, M., McCarty, J. H. & Arthur, H. M. (2012). Endothelial expression of TGFβ type II receptor is required to maintain vascular integrity during postnatal development of the central nervous system. *PLoS One*. 7: e39336

Alon, T., Hemo, I., Itin, A., Pe'er, J., Stone, J. & Keshet, E. (1995). Vascular endothelial growth factor acts as a survival factor for newly formed retinal vessels and has implications for retinopathy of prematurity. *Nature Medicine*. 1: 1024-1028

Alvarez, J. I., Dodelet-Devillers, A., Kebir, H., Ifergan, I., Fabre, P. J., Terouz, S., Sabbagh, M., Wosik, K., Bourbonnière, L., Bernard, M., van Horssen, J., de Vries, H. E., Charron, F. & Prat, A. (2011). The Hedgehog pathway promotes blood-brain barrier integrity and CNS immune quiescence. *Science*. 334: 1727-1731

Alvarez-Buylla, A., García-Verdugo, J. M. & Tramontin, A. D. (2001). A unified hypothesis on the lineage of neural stem cells. *Nature Reviews. Neuroscience*. 2: 287-293

Ambati, B. K., Nozaki, M., Singh, N., Takeda, A., Jani, P. D., Suthar, T., Albuquerque, R. J., Richter, E., Sakurai, E., Newcomb, M. T., Kleinman, M. E., Caldwell, R. B., Lin, Q., Ogura, Y., Orecchia, A., Samuelson, D. A., Agnew, D. W., St Leger, J., Green, W. R., Mahasreshti, P. J., Curiel, D. T., Kwan, D., Marsh, H., Ikeda, S., Leiper, L. J., Collinson, J. M., Bogdanovich, S., Khurana, T. S., Shibuya, M., Baldwin, M. E., Ferrara, N., Gerber, H. P., De Falco, S., Witta, J., Baffi, J. Z., Raisler, B. J. & Ambati, J. (2006). Corneal avascularity is due to soluble VEGF receptor-1. *Nature*. 443: 993-997

Ambler, C. A., Nowicki, J. L., Burke, A. C. and Bautch, V. L. (2001). Assembly of trunk and limb blood vessels involves extensive migration and vasculogenesis of somite-derived angioblasts. *Developmental Biology*. 234: 352-364

Ambler, C. A., Schmunk, G. M. & Bautch, V. L. (2003). Stem cell-derived endothelial cells/progenitors migrate and pattern in the embryo using the VEGF signaling pathway. *Developmental Biology*. 257: 205-219

Amin, M., Pushpakumar, S., Muradashvili, N., Kundu, S., Tyagi, S. C., Sen, U. (2016). Regulation and involvement of matrix metalloproteinases in vascular diseases. *Frontiers in Bioscience (Landmark Edition)*. 21: 89-118

Amthor, H., Christ, B., Weil, M. & Patel, K. (1998). The importance of timing differentiation during limb muscle development. *Current Biology*. 8: 642-652

Anand, M., Van Meter, T. E. & Fillmore, H. L. (2011). Epidermal growth factor induces matrix metalloproteinase-1 (MMP-1) expression and invasion in glioma cell lines via the MAPK pathway. *Journal of Neuro-oncology*. 104: 679-687

Anand-Apte, B., Bao, L., Smith, R., Iwata, K., Olsen, B. R., Zetter, B. & Apte, S. S. (1996). A review of tissue inhibitor of metalloproteinases-3 (TIMP-3) and experimental analysis of its effect on primary tumor growth. *Biochemistry and Cell Biology*. 74: 853-862

Anthony, T. E., Klein, C., Fishell, G. & Heintz, N. (2004). Radial glia serve as neuronal progenitors in all regions of the central nervous system. *Neuron*. 41: 881-890

Apte, S. S., Olsen, B. R. & Murphy, G. (1995). The gene structure of tissue inhibitor of metalloproteinases (TIMP)-3 and its inhibitory activities define the distinct TIMP gene family. *The Journal of Biological Chemistry*. 270: 14313-14318

Armulik, A., Genové, G., Mäe, M., Nisancioglu, M. H., Wallgard, E., Niaudet, C., He, L., Norlin, J., Lindblom, P., Strittmatter, K., Johansson, B. R. & Betsholtz, C. (2010). Pericytes regulate the blood-brain barrier. *Nature*. 468: 557-561

Arnold, L. H., Butt, L. E., Prior, S. H., Read, C. M., Fields, G. B. & Pickford, A. R. (2011). The interface between catalytic and hemopexin domains in matrix metalloproteinase-1 conceals a collagen binding exosite. *The Journal of Biological Chemistry*. 286: 45073-45082

Arnold, T. D., Ferrero, G. M., Qiu, H., Phan, I. T., Akhurst, R. J., Huang, E. J. & Reichardt, L. F. (2012). Defective retinal vascular endothelial cell development as a consequence of impaired integrin αVβ8-mediated activation of transforming growth factor-β. *The Journal of Neuroscience*. 32: 1197-1206

Aspalter, I. M., Gordon, E., Dubrac, A., Ragab, A., Narloch, J., Vizán, P., Geudens, I., Collins, R. T., Franco, C. A., Abrahams, C. L., Thurston, G., Fruttiger, M., Rosewell, I., Eichmann, A. & Gerhardt, H. (2015). Alk1 and Alk5 inhibition by Nrp1 controls vascular sprouting downstream of Notch. *Nature Communications*. 6: 7264

Ayadi, A., Suelves, M., Dollé, P. & Wasylyk, B. (2001). Net, an Ets ternary complex transcription factor, is expressed in sites of vasculogenesis, angiogenesis, and chondrogenesis during mouse development. *Mechanisms of Development*. 102: 205-208

Azar, D. T., Casanova, F. H., Mimura, T., Jain, S., Zhou, Z., Han, K. Y. & Chang, J. H. (2010). Corneal epithelial MT1-MMP inhibits vascular endothelial cell proliferation and migration. *Cornea*. 29: 321-330

Bauer, E. A., Stricklin, G. P., Jeffrey, J. J. & Eisen, A. Z. (1975). Collagenase production by human skin fibroblasts. *Biochemical and Biophysical Research Communications*. 64: 232-240

Bauer, H. C., Bauer, H., Lametschwandtner, A., Amberger, A., Ruiz, P. & Steiner, M. (1993). Neovascularization and the appearance of morphological characteristics of the blood-brain barrier in the embryonic mouse central nervous system. *Developmental Brain Research.* 75: 269-278

Bautch, V. L. (2012). VEGF-directed blood vessel patterning: from cells to organism. *Cold Spring Harbour Perspectives in Medicine*. 2: a006452

Behrens, P., Rothe, M., Wellmann, A., Krischler, J. & Wernert, N. (2001). The Ets-1 transcription factor is up-regulated together with MMP 1 and MMP 9 in the stroma of pre-invasive breast cancer. *The Journal of Pathology*. 194: 43-50

Belkin, A. M., Akimov, S. S., Zaritskaya, L. S., Ratnikov, B. I., Deryugina, E. I. & Strongin, A. Y. (2001). Matrix-dependent proteolysis of surface transglutaminase by membrane-type metalloproteinase regulates cancer cell adhesion and locomotion. *The Journal of Biological Chemistry*. 276: 18415-18422

Belotti, D., Paganoni, P., Manenti, L., Garofalo, A., Marchini, S., Taraboletti, G. & Giavazzi, R. (2003). Matrix metalloproteinases (MMP9 and MMP2) induce the release of vascular endothelial growth factor (VEGF) by ovarian carcinoma cells: implications for ascites formation. *Cancer Research*. 63: 5224-5229

Benbow, U., Schoenermark, M. P., Mitchell, T. I., Rutter, J. L., Shimokawa, K., Nagase, H. & Brinckerhoff, C. E. (1999). A novel host/tumor cell interaction activates matrix metalloproteinase 1 and mediates invasion through type I collagen. *The Journal of Biological Chemistry*. 274: 25371-25378

Benedito, R., Rocha, S. F., Woeste, M., Zamykal, M., Radtke, F., Casanovas, O., Duarte, A., Pytowski, B. & Adams, R. H. (2012). Notch-dependent VEGFR3 upregulation allows angiogenesis without VEGF-VEGFR2 signalling. *Nature*. 484: 110-114

Bennett, Breana E., "The Haptotactic Motility of Angiogenic Endothelial Cells" (2012). *Honors College*. 39 [online]. Available at: http://digitalcommons.library.umaine.edu/honors/39

Bergers, G., Brekken, R., McMahon, G., Vu, T. H., Itoh, T., Tamaki, K., Tanzawa, K., Thorpe, P., Itohara, S., Werb, Z. & Hanahan, D. (2000). Matrix metalloproteinase-9 triggers the angiogenic switch during carcinogenesis. *Nature Cell Biology*. 2: 737-744

Bertrand, N., Médevielle, F. & Pituello, F. (2000). FGF signalling controls the timing of Pax6 activation in the neural tube. *Development*. 127: 4837-4843

Bi, W., Drake, C. J. & Schwarz, J. J. (1999). The transcription factor MEF2C-null mouse exhibits complex vascular malformations and reduced cardiac expression of angiopoietin 1 and VEGF. *Developmental Biology*. 211: 255-267

Bibel, M., Richter, J., Schrenk, K., Tucker, K. L., Staiger, V., Korte, M., Goetz, M. & Barde, Y. A. (2004). Differentiation of mouse embryonic stem cells into a defined neuronal lineage. *Nature Neuroscience*. 7: 1003-1009

Birkedal-Hansen, H., Moore, W. G., Bodden, M. K., Windsor, L. J., Birkedal-Hansen, B., DeCarlo, A. & Engler, J. A. (1993). Matrix metalloproteinases: a review. *Critical Reviews in Oral Biology and Medicine*. 4: 197-250

Blackburn, J. S. & Brinckerhoff, C. E. (2008). Matrix metalloproteinase-1 and thrombin differentially activate gene expression in endothelial cells via PAR-1 and promote angiogenesis. *The American Journal of Pathology*. 173: 1736-1746

Blackburn, J. S., Rhodes, C. H., Coon, C. I. & Brinckerhoff, C. E. (2007). RNA interference inhibition of matrix metalloproteinase-1 prevents melanoma metastasis by reducing tumor collagenase activity and angiogenesis. *Cancer Research*. 67: 10849-10858

Blasi, F. & Carmeliet, P. (2002). uPAR: a versatile signalling orchestrator. *Nature Reviews. Molecular Cell Biology*. 3: 932-943

Blum, Y., Belting, H. G., Ellertsdottir, E., Herwig, L., Lüders, F. & Affolter, M. (2008). Complex cell rearrangements during intersegmental vessel sprouting and vessel fusion in the zebrafish embryo. *Developmental Biology*. 316: 312-322

Boire, A., Covic, L., Agarwal, A., Jacques, S., Sherifi, S. & Kuliopulos, A. (2005). PAR1 is a matrix metalloprotease-1 receptor that promotes invasion and tumorigenesis of breast cancer cells. *Cell*. 120: 303-313

Bonfil, R. D., Sabbota, A., Nabha, S., Bernardo, M. M., Dong, Z., Meng, H., Yamamoto, H., Chinni, S. R., Lim, I. T., Chang, M., Filetti, L. C., Mobashery, S., Cher, M. L. & Fridman, R. (2006). Inhibition of human prostate cancer growth, osteolysis and angiogenesis in a bone metastasis model by a novel mechanism-based selective gelatinase inhibitor. *International Journal of Cancer*. 118: 2721-2726

Boocock, C. A., Charnock-Jones, D. S., Sharkey, A. M., McLaren, J., Barker, P. J., Wright, K. A., Twentyman, P. R. & Smith, S. K. (1995). Expression of vascular endothelial growth factor and its receptors flt and KDR in ovarian carcinoma. *Journal of the National Cancer Institute*. 87: 506-516

Bos, P. D., Zhang, X. H., Nadal, C., Shu, W., Gomis, R. R., Nguyen, D. X., Minn, A. J., van de Vijver, M. J., Gerald, W. L., Foekens, J. A. & Massagué, J. (2009). Genes that mediate breast cancer metastasis to the brain. *Nature*. 459: 1005-1009

Brand-Saberi, B., Müller, T. S., Wilting, J., Christ, B. & Birchmeier, C. (1996). Scatter factor/hepatocyte growth factor (SF/HGF) induces emigration of myogenic cells at interlimb level in vivo. *Developmental Biology*. 179: 303-308

Brooks, P. C., Silletti, S., von Schalscha, T. L., Friedlander, M. & Cheresh, D. A. (1998). Disruption of angiogenesis by PEX, a noncatalytic metalloproteinase fragment with integrin binding activity. *Cell*. 92: 391-400

Brooks, P. C., Strömblad, S., Sanders, L.C., von Schalscha, T. L., Aimes, R. T., Stetler-Stevenson, W. G., Quigley, J. P. & Cheresh, D. A. (1996). Localization of matrix metalloproteinase MMP-2 to the surface of invasive cells by interaction with integrin alpha v beta 3. *Cell*. 85: 683-693

Brown, P. D., Bloxidge, R. E., Stuart, N. S., Gatter, K. C. & Carmichael, J. (1993). Association between expression of activated 72-kilodalton gelatinase and tumor spread in non-small-cell lung carcinoma. *Journal of National Cancer Institute*. 85: 574-578

Cao, R., Bråkenhielm, E., Pawliuk, R., Wariaro, D., Post, M. J., Wahlberg, E., Leboulch, P. & Cao, Y. (2003). Angiogenic synergism, vascular stability and improvement of hind-limb ischemia by a combination of PDGF-BB and FGF-2. *Nature Medicine*. 9: 604-613

Carmeliet, P. (2000). Mechanisms of angiogenesis and arteriogenesis. *Nature Medicine.* 6: 389-395

Carmeliet, P., Dor, Y., Herbert, J. M., Fukumura, D., Brusselmans, K., Dewerchin, M., Neeman, M., Bono, F., Abramovitch, R., Maxwell, P., Koch, C. J., Ratcliffe, P., Moons, L., Jain, R. K., Collen, D. & Keshert, E. (1998). Role of HIF-1alpha in hypoxia-mediated apoptosis, cell proliferation and tumour angiogenesis. *Nature*. 394: 485-490

Caronia, G., Wilcoxon, J., Feldman, P. & Grove, E. A. (2010). Bone morphogenetic protein signaling in the developing telencephalon controls formation of the hippocampal dentate gyrus and modifies fear-related behavior. *The Journal of Neuroscience*. 30: 6291-6301

Chang, H., Huylebroeck, D., Verschueren, K., Guo, Q., Matzuk, M. M. & Zwijsen, A. (1999). Smad5 knockout mice die at mid-gestation due to multiple embryonic and extraembryonic defects. *Development*. 126: 1631-1642

Chang, J. Y., Hu, Y., Siegel, E., Stanley, L. & Zhou, Y. H. (2007). PAX6 increases glioma cell susceptibility to detachment and oxidative stress. *Journal of Neuro-oncology*. 84: 9-19

Chapman, H. A. & Wei, Y. (2001). Protease crosstalk with integrins: the urokinase receptor paradigm. *Thrombosis and Haemostasis*. 86: 124-129

Chappell J. C., Mouillesseaux, K. P. & Bautch, V. L. (2013). Flt-1 (vascular endothelial growth factor receptor-1) is essential for the vascular endothelial growth factor-notch feedback look during angiogenesis. *Arteriosclerosis, Thrombosis and Vascular Biology*. 33: 1952-1959

Chappell, J. C., Taylor, S. M., Ferrara, N. & Bautch, V. L. (2009). Local guidance of emerging vessel sprouts requires soluble Flt-1. *Developmental Cell*. 17: 377-386

Chauvet, S., Cohen, S., Yoshida, Y., Fekrane, L., Livet, J., Gayet, O., Segu, L., Buhot, M. C., Jessell, T. M., Henderson, C. E. & Mann, F. (2007). Gating of Sema3E/PlexinD1 signaling by neuropilin-1 switches axonal repulsion to attraction during brain development. *Neuron*. 56: 807-822

Che, X., Fan, X. Q. & Wang, Z. L. (2014). Mechanism of blood-retinal barrier breakdown induced by HIV-1 (Review). *Experimental and Therapeutic Medicine*. 7: 768-772

Chen, H., Chédotal, A., He, Z., Goodman, C. S. & Tessier-Lavigne, M. (1997). Neuropilin-2, a novel member of the neuropilin family, is a high affinity receptor for the semaphorins Sema E and Sema IV but not Sema III. *Neuron*. 19: 547-559

Chetty, C., Lakka, S. S., Bhoopathi, P. & Rao, J. S. (2010). MMP-2 alters VEGF expression via alphaVbeta3 integrin-mediated PI3K/AKT signaling in A549 lung cancer cells. *International Journal of Cancer*. 127: 1081-1095

Childs, S., Chen, J. N., Garrity, D. M. & Fishman, M. C. (2002). Patterning of angiogenesis in the zebrafish embryo. *Development*. 129: 973-982

Chun, T. H., Sabeh, F., Ota, I., Murphy, H., McDonagh, K. T., Holmbeck, K., Birkedal-Hansen, H., Allen, E. D. & Weiss, S. J. (2004). MT1-MMP-dependent neovessel formation within the confines of the three-dimensional extracellular matrix. *The Journal of Cell Biology*. 167: 757-767

Chung, L., Dinakarpandian, D., Yoshida, N., Lauer-Fields, J. L., Fields, G. B., Visse, R. & Nagase, H. (2004). Collagenase unwinds triple-helical collagen prior to peptide bond hydrolysis. *The EMBO Journal*. 23: 3020-3030

Ciani, L. & Salinas, P. C. (2005). WNTs in the vertebrate nervous system: from patterning to neuronal connectivity. *Nature Reviews. Neuroscience*. 6 :351-362

Clark, R. A., Folkvord, J. M. & Nielsen, L. D. (1986). Either exogenous or endogenous fibronectin can promote adherence of human endothelial cells. *Journal of Cell Science*. 82: 263-280

Coffelt, S. B., Lewis, C. E., Naldini, L., Brown, J. M., Ferrara, N. & De Palma, M. (2010). Elusive identities and overlapping phenotypes of proangiogenic myeloid cells in tumors. *The American Journal of Pathology*. 176: 1564-1576

Costa, G., Harrington, K. I., Lovegrove, H. E., Page, D. J., Chakravartula, S., Bentley, K. & Herbert, S. P. (2016). Asymmetric division coordinates collective cell migration in angiogenesis. *Nature Cell Biology*. 18: 1292-1301

Couly, G., Coltey, P., Eichmann, A. & Le Douarin, N. M. (1995). The angiogenic potentials of the cephalic mesoderm and the origin of brain and head blood vessels. *Mechanisms of Development*. 53: 97-112

Cross, L. M., Cook, M. A., Lin, S., Chen, J. N. & Rubinstein, A. L. (2003). Rapid analysis of angiogenesis drugs in a live fluorescent zebrafish assay. *Arteriosclerosis, Thrombosis & Vascular Biology*. 23: 911-912

Cruz-Muñoz, W., Kim, I. & Khokha, R. (2006a). TIMP-3 deficiency in the host, but not in the tumor, enhances tumor growth and angiogenesis. *Oncogene*. 25: 650-655

Cruz-Muñoz, W., Sanchez, O. H., Di Grappa, M., English, J. L., Hill, R. P. & Khokha, R. (2006b). Enhanced metastatic dissemination to multiple organs by melanoma and lymphoma cells in timp-3-/- mice. *Oncogene*. 25: 6489-6496

Dakubo, G. D., Beug, S.T., Mazerolle, C. J., Thurig, S., Wang, Y. & Wallace, V. A. (2008). Control of glial precursor cell development in the mouse optic nerve by sonic hedgehog from retinal ganglion cells. *Brain Research*. 1228: 27-42

Dakubo, G. D., Wang, Y. P., Mazerolle, C., Campsall, K., McMahon, A. P. & Wallace, V. A. (2003). Retinal ganglion cell-derived sonic hedgehog signaling is required for optic disc and stalk neuroepithelial cell development. *Development*. 130: 2967-2980

Daneman, R., Agalliu, D., Zhou, L., Kuhnert, F., Kuo, C. J. & Barres, B. A. (2009). Wnt/beta-catenin signaling is required for CNS, but not non-CNS, angiogenesis. *Proceedings of the National Academy of Sciences of the USA*. 106: 641-646

Daneman, R., Zhou, L., Kebede, A. A. & Barres, B. A. (2010). Pericytes are required for blood-brain barrier integrity during embryogenesis. *Nature*. 468: 562-566

Davies, B., Miles, D. W., Happerfield, L. C., Naylor, M. S., Bobrow, L. G., Rubens, R. D. & Balkwill, F. R. (1993a) Activity of type IV collagenases in benign and malignant breast disease. *British Journal of Cancer*. 67: 1126-1131

Davies, B., Waxman, J., Wasan, H., Abel, P., Williams, G., Krausz, T., Neal, D., Thomas, D., Hanby, A. & Balkwill, F. (1993b). Levels of matrix metalloproteases in bladder cancer correlate with tumor grade and invasion. *Cancer Research*. 53: 5365-5369

Davis, G. E., Pintar Allen, K. A., Salazar, R., Maxwell, S. A. (2001). Matrix metalloproteinase-1 and -9 activation by plasmin regulates a novel endothelial cell-mediated mechanism of collagen gel contraction and capillary tube regression in three-dimensional collagen matrices. *Journal of Cell Science*. 114: 917-930

De Palma, M. & Lewis, C. E. (2013). Macrophage regulation of tumor responses to anticancer therapies. *Cancer Cell*. 23: 277-286

De Val, S., Anderson, J. P., Heidt, A. B., Khiem, D., Xu, S. M. & Black, B. L. (2004). Mef2c is activated directly by Ets transcription factors through an evolutionarily conserved endothelial cell-specific enhancer. *Developmental Biology*. 275: 424-434

De Val, S., Chi, N. C., Meadows, S. M., Minovitsky, S., Anderson, J. P., Harris, I. S., Ehlers, M. L., Agarwal, P., Visel, A., Xu, S. M., Pennacchio, L. A., Dubchak, I., Krieg, P. A., Stainier, D. Y. & Black, B. L. (2008). Combinatorial regulation of endothelial gene expression by ets and forkhead transcription factors. *Cell*. 135: 1053-1064

Dejana, E., Taddei, A. & Randi, A. M. (2007). Foxs and Ets in the transcriptional regulation of endothelial cell differentiation and angiogenesis. *Biochimica et Biophysica Acta*. 1775: 298-312

Dejana, E., Tournier-Lasserve, E. & Weinstein, B. M. (2009). The control of vascular integrity by endothelial cell junctions: molecular basis and pathological implications. *Developmental Cell*. 16: 209-221

Del Barrio, M. G. & Nieto, M. A. (2004). Relative expression of Slug, RhoB, and HNK-1 in the cranial neural crest of the early chicken embryo. *Developmental Dynamics*. 229: 136-139

del Toro, R., Prahst, C., Mathivet, T., Siegfried, G., Kaminker, J. S., Larrivee, B., Breant, C., Duarte, A., Takakura, N., Fukamizu, A., Penninger, J. & Eichmann, A. (2010). Identification and functional analysis of endothelial tip cell-enriched genes. *Blood*. 116: 4025-4033

Deng, C. X., Wynshaw-Boris, A., Shen, M. M., Daugherty, C., Ornitz, D. M. & Leder, P. (1994). Murine FGFR-1 is required for early postimplantation growth and axial organization. *Genes & Development*. 8: 3045-3057

Déry, M. A., Michaud, M. D. & Richard, D. E. (2005). Hypoxia-inducible factor 1: regulation by hypoxic and non-hypoxic activators. *The International Journal of Biochemistry & Cell Biology*. 37: 535-540

Deryugina, E. I. & Quigley, J. P. (2010). Pleiotropic roles of matrix metalloproteinases in tumor angiogenesis: contrasting, overlapping and compensatory functions. *Biochimica et Biophysica Acta*. 1803: 103-120

Deryugina, E. I., Ratnikov, B. I., Postnova, T. I., Rozanov, D. V. & Strongin, A. Y. (2002). Processing of integrin alpha(v) subunit by membrane type 1 matrix metalloproteinase stimulates migration of breast carcinoma cells on vitronectin and enhances tyrosine phosphorylation of focal adhesion kinase. *The Journal of Biological Chemistry*. 277: 9749-9756

Deryugina, E. I., Soroceanu, L., Strongin, A. Y. (2002). Up-regulation of vascular endothelial growth factor by membrane-type 1 matrix metalloproteinase stimulates human glioma xenograft growth and angiogenesis. *Cancer Research*. 62: 580-588

Deryugina, E. I., Zajac, E., Juncker-Jensen, A., Kupriyanova, T. A., Welter, L. & Quigley, J. P. (2014). Tissue-infiltrating neutrophils constitute the major in vivo source of angiogenesis-inducing MMP-9 in the tumor microenvironment. *Neoplasia*. 16: 771-788

Duffy, M. J. & McCarthy, K. (1998). Matrix metalloproteinases in cancer: prognostic markers and targets for therapy (review). *International Journal of Oncology*. 12: 1343-1348

Duong, T. D. & Erickson, C. A. (2004). MMP-2 plays an essential role in producing epithelial-mesenchymal transformations in the avian embryo. *Developmental Dynamics*. 229: 42-43

Echelard, Y., Epstein, D. J., St-Jacques, B., Shen, L., Mohler, J., McMahon, J. A. & McMahon, A. P. (1993). Sonic hedgehog, a member of a family of putative signaling molecules, is implicated in the regulation of CNS polarity. *Cell*. 75: 1417-1430

Eck, S. M., Hoopes, P. J., Petrella, B. L., Coon, C. I. & Brinckerhoff, C. E. (2009). Matrix metalloproteinase-1 promotes breast cancer angiogenesis and osteolysis in a novel in vivo model. *Breast Cancer Research and Treatment*. 116: 79-90

Edwards, M. M., Mammadova-Bach, E., Alpy, F., Klein, A., Hicks, W. L., Roux, M., Simon-Assmann, P., Smith, R. S., Orend, G., Wu, J., Peachey, N. S., Naggert, J. K., Lefebvre, O. & Nishina, P. M. (2010). Mutations in Lama1 disrupt retinal vascular development and inner limiting membrane formation. *The Journal of Biological Chemistry*. 285: 7697-7711

Egeblad, M. & Werb, Z. (2002). New functions for the matrix metalloproteinases in cancer progression. *Nature Reviews. Cancer*. 2:161–174

Eichmann, A., Marcelle, C., Bréant, C. & Le Douarin, N. M. (1993). Two molecules related to the VEGF receptor are expressed in early endothelial cells during avian embryonic development. *Mechanisms of Development.* 42: 33-48

Eliceiri, B. P., Klemke, R., Strömblad, S. & Cheresh, D. A. (1998). Integrin alphavbeta3 requirement for sustained mitogen-activated protein kinase activity during angiogenesis. *The Journal of Cell Biology*. 140: 1255-1263

Eliceiri, B. P., Paul, R., Schwartzberg, P. L., Hood, J. D., Leng, J. & Cheresh, D. A. (1999). Selective requirement for Src kinases during VEGF-induced angiogenesis and vascular permeability. *Molecular Cell*. 4: 915-924

Englund, C., Fink, A., Lau, C., Pham, D., Daza, R. A., Bulfone, A., Kowalczyk, T. & Hevner, R. F. (2005). Pax6, Tbr2, and Tbr1 are expressed sequentially by radial glia, intermediate progenitor cells, and postmitotic neurons in developing neocortex. *The Journal of Neuroscience*. 25: 247-251

Esko, J. D. & Lindahl, U. (2001). Molecular diversity of heparan sulfate. *The Journal of Clinical Investigation.* 108: 169-173

Fan, Y., Shen, F., Frenzel, T., Zhu, W., Ye, J., Liu, J., Chen, Y., Su, H., Young, W. L., Yang, G. Y. (2010). Endothelial progenitor cell transplantation improves long-term stroke outcome in mice. *Annals of Neurology*. 67: 488-497

Fantin, A., Herzog, B., Mahmoud, M., Yamaji, M., Plein, A., Denti, L., Ruhrberg, C. & Zachary, I. (2014). Neuropilin 1 (NRP1) hypomorphism combined with defective VEGF-A binding reveals novel roles for NRP1 in developmental and pathological angiogenesis. *Development*. 141: 556-562

Fantin, A., Lampropoulou, A., Gestri, G., Raimondi, C., Senatore, V., Zachary, I. & Ruhrberg, C. (2015). NRP1 Regulates CDC42 Activation to Promote Filopodia Formation in Endothelial Tip Cells. *Cell Reports*. 11: 1577-1590

Fantin, A., Vieira, J. M., Gestri, G., Denti, L., Schwarz, Q., Prykhozhij, S., Peri, F., Wilson, S. W. & Ruhrberg C. (2010). Tissue macrophages act as cellular chaperones for vascular anastomosis downstream of VEGF-mediated endothelial tip cell induction. *Blood*. 116: 829-840

Fantin, A., Vieira, J. M., Plein, A., Maden, C. H. & Ruhrberg, C. (2013). The embryonic mouse hindbrain as a qualitative and quantitative model for studying the molecular and cellular mechanisms of angiogenesis. *Nature protocols*. 8: 418-429

Feeney, J. F. Jr. & Watterson, R. L. (1946). The development of the vascular pattern within the walls of the central nervous system of the chick embryo. *Journal of Morphology*. 78: 231-303

Feng, S., Cen, J., Huang, Y., Shen, H., Yao, L., Wang, Y. & Chen, Z. (2011). Matrix metalloproteinase-2 and -9 secreted by leukemic cells increase the permeability of blood-brain barrier by disrupting tight junction proteins. *PLoS One*. 6(8): e20599

Flaumenhaft, R., Moscatelli, D. & Rifkin, D. B. (1990). Heparin and heparan sulfate increase the radius of diffusion and action of basic fibroblast growth factor. *The Journal of Cell Biology*. 111: 1651-1659

Flood, E. C. & Hajjar, K. A. (2011). The annexin A2 system and vascular homeostasis. *Vascular Pharmacology*. 54: 59-67

Franco, S. J. & Müller, U. (2011). Extracellular matrix functions during neuronal migration and lamination in the mammalian central nervous system. *Developmental Neurobiology*. 71: 889-900

Frank, S., Hubner, G., Breier, G.. Longaker, M. T., Greenhalgh, D. G. & Werner, S. (1995). Regulation of vascular endothelial growth factor expression in cultured keratinocytes. Implications for normal and impaired wound healing. *Journal of Biological Chemistry*. 270: 12607–12613

Friedlander, M., Brooks, P. C., Shaffer, R. W., Kincaid, C. M., Varner, J. A. & Cheresh, D. A. (1995). Definition of two angiogenic pathways by distinct alpha v integrins. *Science*. 270: 1500-1502

Fridlender, Z. G., Sun, J., Kim, S., Kapoor, V., Cheng, G., Ling, L., Worthen, G. S. & Albelda, S. M. (2009). Polarization of tumor-associated neutrophil phenotype by TGF-beta: "N1" versus "N2" TAN. *Cancer Cell*. 16: 183-194

Fruttiger, M. (2002). Development of the mouse retinal vasculature: angiogenesis versus vasculogenesis. *Investigative Ophthalmology & Visual Science*. 43: 522-527

Fruttiger, M., Calver, A. R., Krüger, W. H., Mudhar, H. S., Michalovich, D., Takakura, N., Nishikawa, S. & Richardson, W. D. (1996). PDGF mediates a neuron-astrocyte interaction in the developing retina. *Neuron*. 17: 1117-1131

Fujisawa, H. (2004). Discovery of semaphorin receptors, neuropilin and plexin, and their functions in neural development. Journal of Neurobiology. 59: 24-33

Fujisawa, H., Ohtsuki, T., Takagi, S. & Tsuji, T. (1989). An aberrant retinal pathway and visual centers in Xenopus tadpoles share a common cell surface molecule, A5 antigen. *Developmental Biology*. 135: 231-240

Funahashi, Y., Shawber, C. J., Vorontchikhina, M., Sharma, A., Outtz, H. H. & Kitajewski, J. (2010). Notch regulates the angiogenic response via induction of VEGFR-1. *Journal of Angiogenesis Research*. 2: 3

Furuta, Y., Piston, D. W. & Hogan, B. L. (1997). Bone morphogenetic proteins (BMPs) as regulators of dorsal forebrain development. *Development*. 124: 2203-2212

Galceran, J., Fariñas, I., Depew, M. J., Clevers, H. & Grosschedl, R. (1999). Wnt3a-/--like phenotype and limb deficiency in Lef1(-/-)Tcf1(-/-) mice. *Genes & Development*. 13: 709-717

Galdiero, M. R., Garlanda, C., Jaillon, S., Marone, G. & Mantovani, A. (2013). Tumor associated macrophages and neutrophils in tumor progression. *Journal of Cellular Physiology*. 228: 1404-1412

Galis, Z. S., Sukhova, G. K. & Libby, P. (1995). Microscopic localization of active proteases by in situ zymography: detection of matrix metalloproteinase activity in vascular tissue. *FASEB J*. 9: 974-980

Gálvez, B. G., Genís, L., Matías-Román, S., Oblander, S. A., Tryggvason, K., Apte, S. S. & Arroyo, A. G. (2005). Membrane type 1-matrix metalloproteinase is regulated by chemokines monocyte-chemoattractant protein-1/ccl2 and interleukin-8/CXCL8 in endothelial cells during angiogenesis. *The Journal of Biological Chemistry*. 280: 1292-1298

Gálvez, B. G., Matías-Román, S., Yáñez-Mó, M., Sánchez-Madrid, F. & Arroyo, A. G. (2002). ECM regulates MT1-MMP localization with beta1 or alphavbeta3 integrins at distinct cell compartments modulating its internalization and activity on human endothelial cells. *The Journal of Cell Biology*. 159: 509-521

Gan, Q., Lee, A., Suzuki, R., Yamagami, T., Stokes, A., Nguyen, B. C., Pleasure, D., Wang, J., Chen, H. W. & Zhou, C. J. (2014). Pax6 mediates ß-catenin signaling for self-renewal and neurogenesis by neocortical radial glial stem cells. *Stem Cell*. 32: 45-58

Gao, F., Sun, M., Gong, Y., Wang, H., Wang, Y. & Hou, H. (2016). MicroRNA-195a-3p inhibits angiogenesis by targeting Mmp2 in murine mesenchymal stem cells. *Molecular Reproduction and Development*. doi: 10.1002/mrd.22638. [Epub ahead of print]

Garbisa, S., Scagliotti, G., Masiero, L., Di Francesco, C., Caenazzo, C., Onisto, M., Micela, M., Stetler-Stevenson, W. G. & Liotta, L. A. (1992). Correlation of serum metalloproteinase levels with lung cancer metastasis and response to therapy. *Cancer Research*. 52: 4548-4549

Gelfand, M. V., Hagan, N., Tata, A., Oh, W. J., Lacoste, B., Kang, K. T., Kopycinska, J., Bischoff, J., Wang, J. H. & Gu, C. (2014). Neuropilin-1 functions as a VEGFR2 co-receptor to guide developmental angiogenesis independent of ligand binding. *Elife*. 3: e03720

George, S. J. & Johnson, J. L. (2010). In situ zymography. *Methods in Molecular Biology*. 622: 271-277

Gerhardt, H. & Betsholtz, C. (2003). Endothelial-pericyte interactions in angiogenesis. *Cell and Tissue Research.* 314: 15-23

Gerhardt, H., Golding, M., Fruttiger, M., Ruhrberg, C., Lundkvist, A., Abramsson, A., Jeltsch, M., Mitchell, C., Alitalo, K., Shima, D. & Betsholtz, C. (2003). VEGF guides angiogenic sprouting utilizing endothelial tip cell filopodia. *The Journal of Cell Biology*. 161: 1163-1177

Gerhardt, H., Ruhrberg, C., Abramsson, A., Fujisawa, H., Shima, D. & Betsholtz, C. (2004). Neuropilin-1 is required for endothelial tip cell guidance in the developing central nervous system. *Developmental Dynamics.* 231: 503-509

Ghilardi, G., Biondi, M. L., Mangoni, J., Leviti, S., DeMonti, M., Guagnellini, E. & Scorza, R. (2001). Matrix metalloproteinase-1 promoter polymorphism 1G/2G is correlated with colorectal cancer invasiveness. *Clinical Cancer Research*. 7: 2344-2346

Giachino, C., Boulay, J. L., Ivanek, R., Alvarado, A., Tostado, C., Lugert, S., Tchorz, J., Coban, M., Mariani, L., Bettler, B., Lathia, J., Frank, S., Pfister, S., Kool, M. & Taylor, V. (2015). A tumor suppressor function for notch signaling in forebrain tumor Subtypes. *Cancer Cell*. 28: 730-742

Giebel, S. J., Menicucci, G., McGuire, P. G. & Das, A. (2005). Matrix metalloproteinases in early diabetic retinopathy and their role in alteration of the blood-retinal barrier. *Laboratory Investigation*. 85: 597-607

Giger, R. J., Urquhart, E. R., Gillespie, S. K., Levengood, D. V., Ginty, D. D. & Kolodkin, A. L. (1998). Neuropilin-2 is a receptor for semaphorin IV: insight into the structural basis of receptor function and specificity. *Neuron*. 21: 1079-1092

Gingras, D., Bousquet-Gagnon, N., Langlois, S., Lachambre, M. P., Annabi, B. & Béliveau, R. (2001). Activation of the extracellular signal-regulated protein kinase (ERK) cascade by membrane-type-1 matrix metalloproteinase (MT1-MMP). *FEBS Letters*. 507: 231-236

Giovane, A., Pintzas, A., Maira, S. M., Sobieszczuk, P. & Wasylyk, B. (1994). Net, a new ets transcription factor that is activated by Ras. *Genes & Development*. 8: 1502-1513

Giovannone, D., Ortega, B., Reyes, M., El-Ghali, N., Rabadi, M., Sao, S., de Bellard, M. E. (2015). Chicken trunk neural crest migration visualized with HNK1. *Acta Histochemica*. 117: 255-266

Gluzman-Poltorak, Z., Cohen, T., Herzog, Y., & Neufeld, G. (2000). Neuropilin-2 is a receptor for the vascular endothelial growth factor (VEGF) forms VEGF-145 and VEGF-165. *The Journal of Biological Chemistry.* 275: 18040-18045

Gnanaguru, G., Bachay, G., Biswas, S., Pinzón-Duarte, G., Hunter, D. D. & Brunken, W. J. (2013). Laminins containing the β2 and γ3 chains regulate astrocyte migration and angiogenesis in the retina. *Development*. 140: 2050-2060

Goldberg, G. I., Wilhelm, S. M., Kronberger, A., Bauer, E. A., Grant, G. A. & Eisen, A. Z. (1986). Human fibroblast collagenase. Complete primary structure and homology to an oncogene transformation-induced rat protein. *The Journal of Biological Chemistry*. 261: 6600-6605

Gomez, D. E., Alonso, D. F., Yoshiji, H. & Thorgeirsson, U. P. (1997). Tissue inhibitors of metalloproteinases: structure, regulation and biological functions. *European Journal of Cell Biology*. 74: 111-122

Gomez-Manzano, C., Fueyo, J., Jiang, H., Glass, T. L., Lee, H. Y., Hu, M., Liu, J. L., Jasti, S. L., Liu, T. J., Conrad, C. A. & Yung, W. K. (2003). Mechanisms underlying PTEN regulation of vascular endothelial growth factor and angiogenesis. *Annals of Neurology*. 53: 109-117

Götz, M. & Huttner, W. B. (2005). The cell biology of neurogenesis. *Nature Reviews. Molecular Cell Biology*. 6: 777-788

Götz, M., Stoykova, A. & Gruss, P. (1998). Pax6 controls radial glia differentiation in the cerebral cortex. *Neuron*. 21: 1031-44

Greenaway, J., Lawler, J., Moorehead, R., Bornstein, P., Lamarre, J. & Petrik, J. (2007). Thrombospondin-1 inhibits VEGF levels in the ovary directly by binding and internalization via the low density lipoprotein receptor-related protein-1 (LRP-1). *Journal of Cellular Physiology*. 210: 807-818

Gross, J., Harper, E., Harris, E. D., McCroskery, P. A., Highberger, J. H., Corbett, C. & Kang, A. H. (1974). Animal collagenases: specificity of action, and structures of the substrate cleavage site. *Biochemical and Biophysical Research Communications*. 61: 605-612

Gross, J. & Lapiere, C. M. (1962). Collagenolytic activity in amphibian tissues: a tissue culture assay. *Proceedings of the National Academy of Sciences of the USA*. 48: 1014-1022

Gu, C., Rodriguez, E. R., Reimert, D. V., Shu, T., Fritzsch, B., Richards, L. J., Kolodkin, A. L. & Ginty, D. D. (2003). Neuropilin-1 conveys semaphorin and VEGF signaling during neural and cardiovascular development. *Developmental Cell*. 5: 45-57

Gu, C., Yoshida, Y., Livet, J., Reimert, D. V., Mann, F., Merte, J., Henderson, C. E., Jessell, T. M., Kolodkin, A. L. & Ginty, D. D. (2005). Semaphorin 3E and plexin-D1 control vascular pattern independently of neuropilins. *Science*. 307: 265-268

Hadler-Olsen, E., Kanapathippillai, P., Berg, E., Svineng, G., Winberg, J. O. & Uhlin-Hansen, L. (2010). Gelatin in situ zymography on fixed, paraffin-embedded tissue: zinc and ethanol fixation preserve enzyme activity. *The Journal of Histochemistry and Cytochemistry*. 58: 29-39

Hamano, Y., Zeisberg, M., Sugimoto, H., Lively, J. C., Maeshima, Y., Yang, C., Hynes, R. O., Werb, Z., Sudhakar, A. & Kalluri, R. (2003). Physiological levels of tumstatin, a fragment of collagen IV alpha3 chain, are generated by MMP-9 proteolysis and suppress angiogenesis via alphaV beta3 integrin. *Cancer Cell*. 3: 589-601

Hamburger, V. & Hamilton, H. L. (1951). A series of normal stages in the development of the chick embryo. *Journal of Morphology*. 88: 49-92

Hamdy, F. C., Fadlon, E. J., Cottam, D., Lawry, J., Thurrell, W., Silcocks, P. B., Anderson, J. B., Williams, J. L. & Rees, R. C. (1994). Matrix metalloproteinase 9 expression in primary human prostatic adenocarcinoma and benign prostatic hyperplasia. *The British Journal of Cancer*. 69: 177-182

Han, K. Y., Dugas-Ford, J., Lee, H., Chang, J. H. & Azar, D. T. (2015). MMP14 Cleavage of VEGFR1 in the Cornea Leads to a VEGF-Trap Antiangiogenic Effect. *Investigative Ophthalmology & Visual Science*. 5450-5456

Harik, S. I., Hritz, M. A. & LaManna, J. C. (1995). Hypoxia-induced brain angiogenesis in the adult rat. *The Journal of Physiology*. 485: 525-530

Harrington, L. S., Sainson, R. C., Williams, C. K., Taylor, J. M., Shi, W., Li, J. L. & Harris, A. L. (2008). Regulation of multiple angiogenic pathways by Dll4 and Notch in human umbilical vein endothelial cells. *Microvascular Research*. 75: 144-154

Hashambhoy, Y. L., Chappell, J. C., Peirce, S. M., Bautch, V. L. & Mac Gabhann, F. (2011). Computational modeling of interacting VEGF and soluble VEGF receptor concentration gradients. *Frontiers in Physiology*. 2: 62

He, Z. & Tessier-Lavigne, M. (1997). Neuropilin is a receptor for the axonal chemorepellent semaphorin III. *Cell*. 90: 739-751

Heins, N., Malatesta, P., Cecconi, F., Nakafuku, M., Tucker, K. L., Hack, M. A., Chapouton, P., Barde, Y. A. & Götz, M. (2002). Glial cells generate neurons: the role of the transcription factor Pax6. *Nature Neuroscience*. 5: 308-315

Hellström, M., Phng, L. K., Hofmann, J. J., Wallgard, E., Coultas, L., Lindblom, P., Alva, J., Nilsson, A. K., Karlsson, L., Gaiano, N., Yoon, K., Rossant, J., Iruela-Arispe, M. L., Kalén, M., Gerhardt, H. & Betsholtz, C. (2007). Dll4 signalling through Notch1 regulates formation of tip cells during angiogenesis. *Nature.* 445: 776-780

Henke, C. A., Roongta, U., Mickelson, D. J., Knutson, J. R., McCarthy, J. B. (1996). CD44-related chondroitin sulfate proteoglycan, a cell surface receptor implicated with tumor cell invasion, mediates endothelial cell migration on fibrinogen and invasion into a fibrin matrix. *The Journal of Clinical Investigation*. 97: 2541-2552

Heo, S. H. & Cho, J. Y. (2014). ELK3 suppresses angiogenesis by inhibiting the transcriptional activity of ETS-1 on MT1-MMP. *International Journal of Biological Sciences*. 10: 438-447

Heo, S. H., Choi, Y. J., Ryoo, H. M. & Cho, J. Y. (2010). Expression profiling of ETS and MMP factors in VEGF-activated endothelial cells: role of MMP-10 in VEGF-induced angiogenesis. *Journal of Cellular Physiology*. 224: 734-742

Herrera, I., Cisneros, J., Maldonado, M., Ramírez, R., Ortiz-Quintero, B., Anso, E., Chandel, N. S., Selman, M. & Pardo, A. (2013). Matrix metalloproteinase (MMP)-1 induces lung epithelial cell migration and proliferation, protects from apoptosis, and represses mitochondrial oxygen consumption. *The Journal of Biological Chemistry*. 288: 25964-25975

Hewitson, K. S. & Schofield, C. J. (2004). The HIF pathway as a therapeutic target. *Drug Discovery Today*. 9: 704-711

Hickey, M. M. & Simon, M. C. (2006). Regulation of angiogenesis by hypoxia and hypoxia-inducible factors. *Current Topics in Developmental Biology*. 76: 217-257

Hiller, O., Lichte, A., Oberpichler, A., Kocourek, A. & Tschesche, H. (2000). Matrix metalloproteinases collagenase-2, macrophage elastase, collagenase-3, and membrane type 1-matrix metalloproteinase impair clotting by degradation of fibrinogen and factor XII. *The Journal of Biological Chemistry*. 275: 33008-33013

Hillman, R. T., Feng, B. Y., Ni, J., Woo, W. M., Milenkovic, L., Hayden Gephart, M. G., Teruel, M. N., Oro, A. E., Chen, J. K. & Scott, M. P. (2011). Neuropilins are positive regulators of Hedgehog signal transduction. *Genes & Development.* 25: 2333-2346

Hinoda, Y., Okayama, N., Takano, N., Fujimura, K., Suehiro, Y., Hamanaka, Y., Hazama, S., Kitamura, Y., Kamatani, N. & Oka, M. (2002). Association of functional polymorphisms of matrix metalloproteinase (MMP)-1 and MMP-3 genes with colorectal cancer. *International Journal of Cancer*. 102: 526-529

Hirota, S., Clements, T. P., Tang, L. K., Morales, J. E., Lee, H. S., Oh, S. P., Rivera, G. M., Wagner, D. S. & McCarty, J. H. (2015). Neuropilin 1 balances β8 integrin-activated TGFβ signaling to control sprouting angiogenesis in the brain. *Development*. 142: 4363-4373

Hirota, S., Liu, Q., Lee, H. S., Hossain, M. G., Lacy-Hulbert, A. & McCarty, J. H. (2011). The astrocyte-expressed integrin αvβ8 governs blood vessel sprouting in the developing retina. *Development*. 138: 5157-5166

Hogan, K. A., Ambler, C. A., Chapman, D. L. & Bautch, V. L. (2004). The neural tube patterns vessels developmentally using the VEGF signaling pathway. *Development*. 131: 1503-1513

Hollenberg, M. D. & Compton, S. J. (2002). International Union of Pharmacology. XXVIII. Proteinase-activated receptors. *Pharmacological Reviews*. 54: 203-217

Hsu, S., Thakar, R., Liepmann, D. & Li, S. (2005). Effects of shear stress on endothelial cell haptotaxis on micropatterned surfaces. *Biochemical and Biophysical Research Communications*. 337: 401-409

Hu, J., Ni, S., Cao, Y., Zhang, T., Wu, T., Yin, X., Lang, Y. & Lu, H. (2016). The Angiogenic Effect of microRNA-21 Targeting TIMP3 through the Regulation of MMP2 and MMP9. *PLoS One*. 11: e0149537

Hu, J. Z., Huang, J. H., Zeng, L., Wang, G., Cao, M. & Lu, H. B. (2013). Anti-apoptotic effect of microRNA-21 after contusion spinal cord injury in rats. *Journal of Neurotrauma*. 30: 1349-1360

Hui, P., Xu, X., Xu, L., Hui, G., Wu, S. & Lan, Q. (2015). Expression of MMP14 in invasive pituitary adenomas: relationship to invasion and angiogenesis. *International Journal of Clinical and Experimental Pathology*. 8: 3556-3567

iKnowledge (2015). Nervous system [online]. Available at: http://clinicalgate.com/nervous-system-7/. Accessed 13-02-17

Inestrosa, N. C. & Arenas, E. (2010). Emerging roles of Wnts in the adult nervous system. *Nature Reviews. Neuroscience*. 11: 77-86

Inoue, T., Yashiro, M., Nishimura, S., Maeda, K., Sawada, T., Ogawa, Y., Sowa, M. & Chung, K. H. (1999). Matrix metalloproteinase-1 expression is a prognostic factor for patients with advanced gastric cancer. *International Journal of Molecular Medicine*. 4: 73-77

Itakura, J., Ishiwata, T., Shen, B. Kornmann, M. & Korc, M. (2000). Concomitant over-expression of vascular endothelial growth factor and its receptors in pancreatic cancer. *International Journal of Cancer*. 85:27-34

Ito, T., Ito, M., Shiozawa, J., Naito, S., Kanematsu, T. & Sekine, I. (1999). Expression of the MMP-1 in human pancreatic carcinoma: relationship with prognostic factor. *Modern Pathology*. 12: 669-674

Iwasaka, C., Tanaka, K., Abe, M. & Sato, Y. (1996). Ets-1 regulates angiogenesis by inducing the expression of urokinase-type plasminogen activator and matrix metalloproteinase-1 and the migration of vascular endothelial cells. *Journal of Cellular Physiology*. 169: 522-531

Jakobsson, L., Franco, C. A., Bentley, K., Collins, R. T., Ponsioen, B., Aspalter, I. M., Rosewell, I., Busse, M., Thurston, G., Medvinsky, A., Schulte-Merker, S. & Gerhardt, H. (2010). Endothelial cells dynamically compete for the tip cell position during angiogenic sprouting. *Nature Cell Biology*. 12: 943-953

James, J. M., Gewolb, C. & Bautch, V. L. (2009). Neurovascular development uses VEGF-A signaling to regulate blood vessel ingression into the neural tube. *Development*. 136: 833-841

James, J. M. & Mukouyama, Y. S. (2011). Neuronal action on the developing blood vessel pattern. *Seminars in Cell & Developmental Biology*. 22: 1019-1027

Jiang, B., Bezhadian, M. A. & Caldwell, R. B. (1995). Astrocytes modulate retinal vasculogenesis: effects on endothelial cell differentiation. *Glia*. 15: 1-10

Jiang, B. H., Zheng, J. Z., Aoki, M. & Vogt, P. K. (2000). Phosphatidylinositol 3-kinase signaling mediates angiogenesis and expression of vascular endothelial growth factor in endothelial cells. *Proceedings of the National Academy of Sciences of the USA*. 97: 1749-1753

Jilani, S. M., Murphy, T. J., Thai, S. N., Eichmann, A., Alva, J. A. & Iruela-Arispe, M. L. (2003). Selective binding of lectins to embryonic chicken vasculature. *The Journal of Histochemistry and Cytochemistry*. 51: 597-604

Johnson, D. E. & Williams, L. T. (1993). Structural and functional diversity in the FGF receptor multigene family. *Advances in Cancer Research*. 60: 1-41

Jozic, D., Bourenkov, G., Lim, N. H., Visse, R., Nagase, H., Bode, W. & Maskos, K. (2005). X-ray structure of human proMMP-1: new insights into procollagenase activation and collagen binding. *The Journal of Biological Chemistry*. 280: 9578-9585

Kajita, M., Itoh, Y., Chiba, T., Mori, H., Okada, A., Kinoh, H. & Seiki, M. (2001). Membrane-type 1 matrix metalloproteinase cleaves CD44 and promotes cell migration. *The Journal of Cell Biology*. 153: 893-904

Kanamori, Y., Matsushima, M., Minaguchi, T., Kobayashi, K., Sagae, S., Kudo, R., Terakawa, N. & Nakamura, Y. (1999). Correlation between expression of the matrix metalloproteinase-1 gene in ovarian cancers and an insertion/deletion polymorphism in its promoter region. *Cancer Research*. 59: 4225-4227

Kanayasu-Toyoda, T., Tanaka, T., Kikuchi, Y., Uchida, E., Matsuyama, A. & Yamaguchi, T. (2016). Cell-surface MMP-9 protein is a novel functional marker to identify and separate pro-angiogenic cells from early endothelial progenitor cells derived from CD133+ cells. *Stem Cells*. doi: 10.1002/stem.2300. [Epub ahead of print]

Kappas, N. C., Zeng, G., Chappell, J. C., Kearney, J. B., Hazarika, S., Kallianos, K. G., Patterson, C., Annex, B. H. & Bautch, V. L. (2008). The VEGF receptor Flt-1 spatially modulates Flk-1 signaling and blood vessel branching. *The Journal of Cell Biology*. 181: 847-858

Kataoka, H., Hayashi, M., Nakagawa, R., Tanaka, Y., Izumi, N., Nishikawa, S., Jakt, M. L., Tarui, H. & Nishikawa, S. (2011). Etv2/ER71 induces vascular mesoderm from Flk1+PDGFRα+ primitive mesoderm. *Blood*. 118: 6975-6986

Kawasaki, T., Kitsukawa, T., Bekku, Y., Matsuda, Y., Sanbo, M., Yagi, T. & Fujisawa, H. (1999). A requirement for neuropilin-1 in embryonic vessel formation. *Development*. 126: 4895-4902

Kim, D. H., Lilliehook, C., Roides, B., Chen, Z., Chang, M., Mobashery, S. & Goldman, S. A. (2008). Testosterone-induced matrix metalloproteinase activation is a checkpoint for neuronal addition to the adult songbird brain. *The Journal of Neuroscience*. 28: 208-216

Kim, J., Oh, W. J., Gaiano, N., Yoshida, Y. & Gu, C. (2011). Semaphorin 3E-Plexin-D1 signaling regulates VEGF function in developmental angiogenesis via a feedback mechanism. *Genes & Development*. 25: 1399-1411

Kim, J. D., Kang, H., Larrivée, B., Lee, M. Y., Mettlen, M., Schmid, S. L., Roman, B. L., Qyang, Y., Eichmann, A. & Jin, S. W. (2012). Context-dependent proangiogenic function of bone morphogenetic protein signaling is mediated by disabled homolog 2. *Developmental Cell*. 23: 441-448

Kim, S. K., Lee, J., Song, M., Kim, M., Hwang, S. J., Jang, H., Park, Y. (2015). Combination of three angiogenic growth factors has synergistic effects on sprouting of endothelial cell/mesenchymal stem cell-based spheroids in a 3D matrix. *Journal of Biomedical Materials Research. Part B, Applied Biomaterials.* doi: 10.1002/jbm.b.33498. [Epub ahead of print]

King, S. E. (2016). Matrix metalloproteinases: new directions toward inhibition in the fight against cancers. *Future Medicinal Chemistry*. 8: 297-309

Kita, D., Takino, T., Nakada, M., Takahashi, T., Yamashita, J. & Sato, H. (2001). Expression of dominant-negative form of Ets-1 suppresses fibronectin-stimulated cell adhesion and migration through down-regulation of integrin alpha5 expression in U251 glioma cell line. *Cancer Research*. 61: 7985-7991

Kolodkin, A. L., Levengood, D. V., Rowe, E. G., Tai, Y. T., Giger, R. J. & Ginty, D. D. (1997). Neuropilin is a semaphorin III receptor. *Cell*. 90: 753-762

Korem, S., Resnick, M. B. & Kraiem, Z. (1999). Similar and divergent patterns in the regulation of matrix metalloproteinase-1 (MMP-1) and tissue inhibitor of MMP-1 gene expression in benign and malignant human thyroid cells. *The Journal of Clinical Endocrinology and Metabolism*. 84: 3322-3327

Kraut, J. (1977). Serine proteases: structure and mechanism of catalysis. *Annual Review of Biochemistry*. 46: 331-358

Kriegstein, A. & Alvarez-Buylla, A. (2009). The glial nature of embryonic and adult neural stem cells. *Annual Review of Neuroscience*. 32: 149-184

Kryczka, J., Stasiak, M., Dziki, L., Mik, M., Dziki, A. & Cierniewski, C. (2012). Matrix metalloproteinase-2 cleavage of the β1 integrin ectodomain facilitates colon cancer cell motility. *The Journal of Biological Chemistry*. 287: 36556-36566

Kühl, S. J. & Kühl, M. (2013). On the role of Wnt/β-catenin signaling in stem cells. *Biochimica et Biophysica Acta*. 1830: 2297-2306

Kurz, H. (2009). Cell lineages and early patterns of embryonic CNS vascularization. *Cell Adhesion & Migration*. 3: 205-210

Kurz, H., Gärtner, T., Eggli, P. S. & Christ, B. (1996). First blood vessels in the avian neural tube are formed by a combination of dorsal angioblast immigration and ventral sprouting of endothelial cells. *Developmental Biology*. 173: 133-147

Kuwabara T. (1975). Development of the optic nerve of the rat. *Investigative Ophthalmology*. 14: 732-745

Kwak, H. I., Kang, .H, Dave, J. M., Mendoza, E. A., Su, S. C., Maxwell, S. A. & Bayless, K. J. (2012). Calpain-mediated vimentin cleavage occurs upstream of MT1-MMP membrane translocation to facilitate endothelial sprout initiation. *Angiogenesis*. 15: 287-303

Labastie, M. C., Poole, T. J., Péault, B. M. & Le Douarin, N. M. (1986). MB1, a quail leukocyte-endothelium antigen: partial characterization of the cell surface and secreted forms in cultured endothelial cells. *Proceedings of the National Academy of Sciences of the USA*. 83: 9016-9020

Lafleur, M. A., Forsyth, P. A., Atkinson, S. J., Murphy, G. & Edwards, D. R. (2001). Perivascular cells regulate endothelial membrane type-1 matrix metalloproteinase activity. *Biochemical and Biophysical Research Communications*. 282: 463-473

Lambert, E., Dassé, E., Haye, B. & Petitfrère, E. (2004). TIMPs as multifacial proteins. *Critical Reviews in Oncology/Hematology*. 49: 187-198

Lan, F., Pan, Q., Yu, H. & Yue, X. (2015). Sulforaphane enhances temozolomide-induced apoptosis because of down-regulation of miR-21 via Wnt/β-catenin signaling in glioblastoma. *Journal of Neurochemistry*. 134: 811-818

Lange, C., Storkebaum, E., de Almodóvar, C. R., Dewerchin, M. & Carmeliet, P. (2016). Vascular endothelial growth factor: a neurovascular target in neurological diseases. *Nature Reviews. Neurology*. 12: 439-454

Larrivée, B., Prahst, C., Gordon, E., del Toro, R., Mathivet, T., Duarte, A., Simons, M. & Eichmann, A. (2012). ALK1 signaling inhibits angiogenesis by cooperating with the Notch pathway. *Development Cell*. 22: 489-500

Lawson, N, D., Vogel, A. M. & Weinstein, B. M. (2002). Sonic hedgehog and vascular endothelial growth factor act upstream of the Notch pathway during arterial endothelial differentiation. *Developmental Cell*. 3: 127-136

Lawson, N. D. & Weinstein, B. M. (2002). In vivo imaging of embryonic vascular development using transgenic zebrafish. *Developmental Biology*. 248: 307-318

Lee, C. Z., Xue, Z., Hao, Q., Yang, G. Y. & Young, W. L. (2009). Nitric oxide in vascular endothelial growth factor-induced focal angiogenesis and matrix metalloproteinase-9 activity in the mouse brain. *Stroke*. 40: 2879-2881

Lee, D., Park, C., Lee, H., Lugus, J. J., Kim, S. H., Arentson, E., Chung, Y. S., Gomez, G., Kyba, M., Lin, S., Janknecht, R., Lim, D. S. & Choi, K. (2008). ER71 acts downstream of BMP, Notch, and Wnt signaling in blood and vessel progenitor specification. *Cell Stem Cell*. 2: 497-507

Lee, S., Jilani, S. M., Nikolova, G. V., Carpizo, D. & Iruela-Arispe, M. L. (2005). Processing of VEGF-A by matrix metalloproteinases regulates bioavailability and vascular patterning in tumors. *The Journal of Cell Biology*. 169: 681-691

Lee, S. H., Schloss, D. J. & Swain, J. L. (2000). Maintenance of vascular integrity in the embryo requires signaling through the fibroblast growth factor receptor. *The Journal of Biological Chemistry*. 275: 33679-33687

Lee, S. M., Tole, S., Grove, E. & McMahon, A. P. (2000). A local Wnt-3a signal is required for development of the mammalian hippocampus. *Development*. 127: 457-467

Leto, G., Gebbia, N., Rausa, L., Tumminello, F. M. (1992). Cathepsin D in the malignant progression of neoplastic diseases (review). *Anticancer Research*. 12: 235-240

Li, F., Lan, Y., Wang, Y., Wang, J., Yang, G., Meng, F., Han, H., Meng, A., Wang, Y. & Yang, X. (2011). Endothelial Smad4 maintains cerebrovascular integrity by activating N-cadherin through cooperation with Notch. *Developmental Cell*. 20: 291-302

Li, Z. B., Li, Z. Z., Li, L., Chu, H. T. & Jia, M. (2015). MiR-21 and miR-183 can simultaneously target SOCS6 and modulate growth and invasion of hepatocellular carcinoma (HCC) cells. *European Review for Medical and Pharmacological Sciences*. 19: 3208-3217

Liabakk, N. B., Talbot, I., Smith, R. A., Wilkinson, K. & Balkwill, F. (1996). Matrix metalloprotease 2 (MMP-2) and matrix metalloprotease 9 (MMP-9) type IV collagenases in colorectal cancer. *Cancer Research*. 56: 190-196

Liebner, S., Kniesel, U., Kalbacher, H. & Wolburg, H. (2000). Correlation of tight junction morphology with the expression of tight junction proteins in blood-brain barrier endothelial cells. *European Journal of Cell Biology*. 79: 707-717

Lindahl, P., Johansson, B. R., Levéen, P. & Betsholtz, C. (1997). Pericyte loss and microaneurysm formation in PDGF-B-deficient mice. *Science.* 277: 242-245

Ling, T. L., Mitrofanis, J. & Stone, J. (1989). Origin of retinal astrocytes in the rat: evidence of migration from the optic nerve. *The Journal of Comparative Neurology*. 286: 345-352

Liu, F., Li, D., Yu, Y. Y., Kang, I., Cha, M. J., Kim, J. Y., Park, C., Watson, D. K., Wang, T. & Choi, K. (2015). Induction of hematopoietic and endothelial cell program orchestrated by ETS transcription factor ER71/ETV2. *EMBO Reports*. 16: 654-669

Liu, H., Kato, Y., Erzinger, S. A., Kiriakova, G. M., Qian, Y., Palmieri, D., Steeg, P. S. & Price, J. E. (2012). The role of MMP-1 in breast cancer growth and metastasis to the brain in a xenograft model. *BMC Cancer*. 12: 583

Liu, Y., Carson-Walter, E. B., Cooper, A., Winans, B. N., Johnson, M. D., Walter, K. A. (2010). Vascular gene expression patterns are conserved in primary and metastatic brain tumors. *Journal of Neuro-oncology*. 99: 13-24

Loring, J. F. & Erickson, C. A. (1987). Neural crest cell migratory pathways in the trunk of the chick embryo. *Developmental Biology*. 121: 220-236

Lowe, L. A., Yamada, S. & Kuehn, M. R. (2001). Genetic dissection of nodal function in patterning the mouse embryo. *Development*. 128: 1831-1843

Ma, X., Conklin, D. J., Li, F., Dai, Z., Hua, X., Li, Y., Xu-Monette, Z. Y., Young, K. H., Xiong, W., Wysoczynski, M., Sithu, S. D., Srivastava, S., Bhatnagar, A. & Li, Y. (2015). The oncogenic microRNA miR-21 promotes regulated necrosis in mice. *Nature Communications*. 6: 7151

Malan, D., Wenzel, D., Schmidt, A., Geisen, C., Raible, A., Bölck, B., Fleischmann, B. K. & Bloch, W. (2010). Endothelial beta1 integrins regulate sprouting and network formation during vascular development. *Development*. 137: 993-1002

Mantovani, A., Sozzani, S., Locati, M., Allavena, P. & Sica, A. (2002). Macrophage polarization: tumor-associated macrophages as a paradigm for polarized M2 mononuclear phagocytes. *Trends in Immunology*. 23: 549-555

Manuel, M. N., Mi, D., Mason, J. O. & Price, D. J. (2015). Regulation of cerebral cortical neurogenesis by the Pax6 transcription factor. *Frontiers in Cellular Neuroscience*. 9:70

Maquoi, E., Frankenne, F., Noël, A., Krell, H. W., Grams, F. & Foidart, J. M. (2000). Type IV collagen induces matrix metalloproteinase 2 activation in HT1080 fibrosarcoma cells. *Experimental Cell Research*. 261: 348-359

Marcelo, K. L., Goldie, L. C. & Hirschi, K. K. (2013). Regulation of endothelial cell differentiation and specification. *Circulation Research*. 112: 1272-1287

Marom, K., Levy, V., Pillemer, G. & Fainsod, A. (2005). Temporal analysis of the early BMP functions identifies distinct anti-organizer and mesoderm patterning phases. *Developmental Biology*. 282: 442-454

Masamoto, K., Takuwa, H., Tomita, Y., Toriumi, H., Unekawa, M., Taniguchi, J., Kawaguchi, H., Itoh, Y., Suzuki, N., Ito, H. & Kanno, I. (2013). Hypoxia-induced cerebral angiogenesis in mouse cortex with two-photon microscopy. *Advances in Experimental Medicine and Biology*. 789: 15-20

Matrisian, L. M. (1990). Metalloproteinases and their inhibitors in matrix remodeling. *Trends in Genetics: TIG*. 6: 121-125

Matrisian, L. M. (1992). The matrix-degrading metalloproteinases. *BioEssays*. 14: 455-463

Mayes, D. A., Hu, Y., Teng, Y., Siegel, E., Wu, X., Panda, K., Tan, F., Yung, W. K., Zhou, Y. H. (2006). PAX6 suppresses the invasiveness of glioblastoma cells and the expression of the matrix metalloproteinase-2 gene. *Cancer Research*. 66: 9809-9817

Mazor, R., Alsaigh, T., Shaked, H., Altshuler, A. E., Pocock, E. S., Kistler, E. B., Karin, M. & Schmid-Schönbein, G. W. (2013). Matrix metalloproteinase-1-mediated up-regulation of vascular endothelial growth factor-2 in endothelial cells. *The Journal of Biological Chemistry*. 288: 598-607

Mazzetti, S., Frigerio, S., Gelati, M., Salmaggi, A. & Vitellaro-Zuccarello, L. (2004). Lycopersicon esculentum lectin: an effective and versatile endothelial marker of normal and tumoral blood vessels in the central nervous system. *European Journal of Histochemistry*. 48: 423-428

McCready, J., Broaddus, W. C., Sykes, V. & Fillmore, H. L. (2005). Association of a single nucleotide polymorphism in the matrix metalloproteinase-1 promoter with glioblastoma. *International Journal of Cancer*. 117: 781-785

Mercier, S., David, V., Ratié, L., Gicquel, I., Odent, S. & Dupé, V. (2013). NODAL and SHH dose-dependent double inhibition promotes an HPE-like phenotype in chick embryos. *Disease Models & Mechanisms*. 6: 537-543

Miao, H. Q., Soker, S., Feiner, L., Alonso, J. L., Raper, J. A. & Klagsbrun, M. (1999). Neuropilin-1 mediates collapsin-1/semaphorin III inhibition of endothelial cell motility: functional competition of collapsin-1 and vascular endothelial growth factor-165. *The Journal of Cell Biology*. 146: 233-242

Miller, E. J., Harris, E. D. Jr., Chung, E., Finch, J. E. Jr., McCroskery, P. A. & Butler, W. T. (1976). Cleavage of Type II and III collagens with mammalian collagenase: site of cleavage and primary structure at the NH2-terminal portion of the smaller fragment released from both collagens. *Biochemisty*. 15: 787-792

Miquerol, L., Langille, B. L. & Nagy, A. (2000). Embryonic development is disrupted by modest increases in vascular endothelial growth factor gene expression. *Development*. 127: 3941-3946

Miyake, M., Goodison, S., Lawton, A., Gomes-Giacoia, E. & Rosser, C. J. (2015). Angiogenin promotes tumoral growth and angiogenesis by regulating matrix metallopeptidase-2 expression via the ERK1/2 pathway. *Oncogene*. 34: 890-901

Mohammed, R. H. & Sweetman, D. (2016). Grafting of Beads into Developing Chicken Embryo Limbs to Identify Signal Transduction Pathways Affecting Gene Expression. *Journal of Visualized Experiments*. 107: e53342

Morancho, A., Ma, F., Barceló, V., Giralt, D., Montaner, J. & Rosell, A. (2015). Impaired vascular remodeling after endothelial progenitor cell transplantation in MMP9-deficient mice suffering cortical cerebral ischemia. *Journal of Cerebral Blood Flow and Metabolism.* 35: 1547-1551

Mori, H., Tomari, T., Koshikawa, N., Kajita, M., Itoh, Y., Sato, H., Tojo, H., Yana, I., Seiki, M. (2002). CD44 directs membrane-type 1 matrix metalloproteinase to lamellipodia by associating with its hemopexin-like domain. *The EMBO Journal*. 21: 3949-3959

Mott, J. D. & Werb, Z. (2004). Regulation of matrix biology by matrix metalloproteinases. *Current Opinion in Cell Biology*. 16: 558-564

Moubarik, C., Guillet, B., Youssef, B., Codaccioni, J. L., Piercecchi, M. D., Sabatier, F., Lionel, P., Dou, L., Foucault-Bertaud, A., Velly, L., Dignat-George, F. & Pisano, P. (2011). Transplanted late outgrowth endothelial progenitor cells as cell therapy product for stroke. *Stem Cell Reviews*. 7: 208-220

Moya, I. M., Umans, L., Maas, E., Pereira, P. N., Beets, K., Francis, A., Sents, W., Robertson, E. J., Mummery, C. L., Huylebroeck, D. & Zwijsen, A. (2012). Stalk cell phenotype depends on integration of Notch and Smad1/5 signaling cascades. *Developmental Cell*. 22: 501-514

Müller, F., Albert, S., Blader, P., Fischer, N., Hallonet, M. & Strähle, U. (2000). Direct action of the nodal-related signal cyclops in induction of sonic hedgehog in the ventral midline of the CNS. *Development*. 127: 3889-3897

Muraguchi, T., Takegami, Y., Ohtsuka, T., Kitajima, S., Chandana, E. P., Omura, A., Miki, T., Takahashi, R., Matsumoto, N., Ludwig, A., Noda, M. & Takahashi, C. (2007). RECK modulates Notch signaling during cortical neurogenesis by regulating ADAM10 activity. *Nature Neuroscience*. 10: 838-845

Murray, G. I., Duncan, M. E., O'Neil, P., McKay, J. A., Melvin, W. T. & Fothergill, J. E. (1998). Matrix metalloproteinase-1 is associated with poor prognosis in oesophageal cancer. *The Journal of Pathology*. 185: 256-261

Murray, G. I., Duncan, M. E., O'Neil, P., Melvin, W. T. & Fothergill, J. E. (1996). Matrix metalloproteinase-1 is associated with poor prognosis in colorectal cancer. *Nature Medicine*. 2: 461-462

Nagai, H., Lin, M. C. & Sheng, G. (2011). A modified cornish pasty method for ex ovo culture of the chick embryo. *Genesis*. 49: 46-52

Nagai, Y., Lapiere, C. M. & Gross, J. (1966). Tadpole collagenase. Preparation and purification. *Biochemistry*. 5: 3123-3130

Nagase, H., Visse, R. & Murphy, G. (2006). Structure and function of matrix metalloproteinases and TIMPs. *Cardiovascular Research*. 69: 562-573

Nagase, H. & Woessner, J. F. Jr. (1999). Matrix metalloproteinases. *The Journal of Biological Chemistry*. 274: 21491-21494

Nagase, T., Nagase, M., Yoshimura, K., Fujita, T. & Koshima, I. (2005). Angiogenesis within the developing mouse neural tube is dependent on sonic hedgehog signaling: possible roles of motor neurons. *Genes to Cells*. 10: 595-604

Nakajima, M., Welch, D. R., Belloni, P. N. & Nicolson, G. L. (1987). Degradation of basement membrane type IV collagen and lung subendothelial matrix by rat mammary adenocarcinoma cell clones of differing metastatic potentials. *Cancer Research*. 47: 4869-4876

Nakopoulou, L., Giannopoulou, I., Gakiopoulou, H., Liapis, H., Tzonou, A., Davaris, P. S. (1999). Matrix metalloproteinase-1 and -3 in breast cancer: correlation with progesterone receptors and other clinicopathologic features. *Human Pathology*. 30: 436-442

Nam, H. S., Kwon, I., Lee, B. H., Kim, H., Kim, J., An, S., Lee, O. H., Lee, P. H., Kim, H. O., Namgoong, H., Kim, Y. D. & Heo, J. H. (2015). Effects of Mesenchymal Stem Cell Treatment on the Expression of Matrix Metalloproteinases and Angiogenesis during Ischemic Stroke Recovery. *PLoS One*. 10: e0144218

Nieuwkoop, P.D. & Faber, J. (Eds.) (1956). *Normal Table of Xenopus laevis (Daudin): A systematical and chronological survey of the development from the fertilized egg till the end of metamorphosis*. Amsterdam: North-Holland Publ. Co.

Nishioka, Y., Kobayashi, K., Sagae, S., Ishioka, S., Nishikawa, A., Matsushima, M., Kanamori, Y., Minaguchi, T., Nakamura, Y., Tokino, T. & Kudo, R. (2000). A single nucleotide polymorphism in the matrix metalloproteinase-1 promoter in endometrial carcinomas. *Japanese Journal of Cancer Research*. 91: 612-615

Noda, M., Oh, J., Takahashi, R., Kondo, S., Kitayama, H. & Takahashi, C. (2003). RECK: a novel suppressor of malignancy linking oncogenic signaling to extracellular matrix remodeling. *Cancer Metastasis Reviews*. 22: 167-175

O'Rahilly, R. & Müller, F. (1987). *Developmental Stages in Human Embryos*. Washington, DC: Carnegie Institution of Washington. Publication 637

Ohuchi, E., Imai, K., Fujii, Y., Sato, H., Seiki, M. & Okada, Y. (1997). Membrane type 1 matrix metalloproteinase digests interstitial collagens and other extracellular matrix macromolecules. *The Journal of Biological Chemistry*. 272: 2446-2451

Ornitz, D. M. (2000). FGFs, heparan sulfate and FGFRs: complex interactions essential for development. *BioEssays*. 22: 108-112

Ornitz, D. M. & Itoh, N. (2001). Fibroblast growth factors**.** *Genome Biology*. 2: REVIEWS3005

Ossovskaya, V. S. & Bunnett, N. W. (2004). Protease-activated receptors: contribution to physiology and disease. *Physiological Reviews*. 84: 579-621

Packard, B. Z., Artym, V. V., Komoriya, A. & Yamada, K. M. (2009). Direct visualization of protease activity on cells migrating in three-dimensions. *Matrix Biology*. 28: 3-10

Pan, Q., Chathery, Y., Wu, Y., Rathore, N., Tong, R. K., Peale, F., Bagri, A., Tessier-Lavigne, M., Koch, A. W. & Watts, R. J. (2007). Neuropilin-1 binds to VEGF121 and regulates endothelial cell migration and sprouting. *The Journal of Biological Chemistry*. 282: 24049-24056

Pardanaud, L., Altmann, C., Kitos, P., Dieterlen-Lievre, F. & Buck, C. A. (1987). Vasculogenesis in the early quail blastodisc as studied with a monoclonal antibody recognizing endothelial cells. *Development.* 100: 339-349

Park, J. E., Keller, G. A. & Ferrara, N. (1993). The vascular endothelial growth factor (VEGF) isoforms: differential deposition into the subepithelial extracellular matrix and bioactivity of extracellular matrix-bound VEGF. *Molecular Biology of the Cell*. 4: 1317-1326

Parker, M. W., Xu, P., Li, X. & Vander Kooi, C. W. (2012). Structural basis for selective vascular endothelial growth factor-A (VEGF-A) binding to neuropilin-1. *The Journal of Biological Chemistry*. 287: 11082-11089

Pauly, R. R., Passaniti, A., Bilato, C., Monticone, R., Cheng, L., Papadopoulos, N., Gluzband, Y. A., Smith, L., Weinstein, C., Lakatta, E. G. & Crow, M. T. (1994). Migration of cultured vascular smooth muscle cells through a basement membrane barrier requires type IV collagenase activity and is inhibited by cellular differentiation. *Circulation Research*. 75: 41-54

Péault B. (1987). MB1, a quail leukocyte/vascular endothelium antigen: characterization of the lymphocyte-surface form and identification of its secreted counterpart as alpha 2-macroglobulin. *Cell Differentiation*. 21: 175-187

Péault, B. M., Thiery, J. P. & Le Douarin N. M. (1983). Surface marker for hemopoietic and endothelial cell lineages in quail that is defined by a monoclonal antibody. *Proceedings of the National Academy of Sciences of the USA*. 80: 2976-2980

Peretz, T., Antebi, S. U., Beller, U., Horowitz, A. T., Fuks, Z. & Vlodavsky, I. (1990). Maintenance on extracellular matrix and expression of heparanase activity by human ovarian carcinoma cells from biopsy specimens. *International Journal of Cancer*. 45: 1054-1060

Peters, J. H., Sporn, L. A., Ginsberg, M. H. & Wagner, D. D. (1990). Human endothelial cells synthesize, process, and secrete fibronectin molecules bearing an alternatively spliced type III homology (ED1). *Blood*. 75: 1801-1808

Pham, V. N., Lawson, N. D., Mugford, J. W., Dye, L., Castranova, D., Lo, B. & Weinstein, B. M. (2007). Combinatorial function of ETS transcription factors in the developing vasculature. *Developmental Biology*. 303: 772-783

Phng, L. K. & Gerhardt, H. (2009). Angiogenesis: a team effort coordinated by notch. *Developmental Cell*. 16: 196-208

Phng, L. K., Stanchi, F. & Gerhardt, H. (2013). Filopodia are dispensable for endothelial tip cell guidance. *Development*. 140: 4031-4040

Pickett, K. L., Harber, G. J., DeCarlo, A. A., Louis, P., Shaneyfelt, S., Windsor, L. J., Bodden, M. K. (1999). 92K-GL (MMP-9) and 72K-GL (MMP-2) are produced in vivo by human oral squamous cell carcinomas and can enhance FIB-CL (MMP-1) activity in vitro. *Journal of Dental Research*. 78: 1354-1361

Pierce, E. A., Foley, E. D. & Smith, L. E. (1996). Regulation of vascular endothelial growth factor by oxygen in a model of retinopathy of prematurity. *Archives of Ophthalmology*. 114: 1219-1228

Plotnikov, A. N., Schlessinger, J., Hubbard, S. R. & Mohammadi, M. (1999). Structural basis for FGF receptor dimerization and activation. *Cell*. 98: 641-650

Plouët, J., Schilling, J. & Gospodarowicz, D. (1989). Isolation and characterization of a newly identified endothelial cell mitogen produced by AtT-20 cells. *The EMBO Journal*. 8: 3801-3806

Polleux, F., Morrow, T. & Ghosh, A. (2000). Semaphorin 3A is a chemoattractant for cortical apical dendrites. *Nature*. 404: 567-573

Poola, I., DeWitty, R. L., Marshalleck, J. J., Bhatnagar, R., Abraham, J. & Leffall, L. D. (2005). Identification of MMP-1 as a putative breast cancer predictive marker by global gene expression analysis. *Nature Medicine*. 11: 481-483

Porto, I. M., Rocha, L. B., Rossi, M. A. & Gerlach, R. F. (2009). In situ zymography and immunolabeling in fixed and decalcified craniofacial tissues. *The Journal of Histochemistry and Cytochemistry*. 57: 615-622

Provis, J. M., Leech, J., Diaz, C. M., Penfold, P. L., Stone, J. & Keshet, E. (1997). Development of the human retinal vasculature: cellular relations and VEGF expression. *Experimental Eye Research*. 65: 555-568

Przybylowska, K., Kluczna, A., Zadrozny, M., Krawczyk, T., Kulig, A., Rykala, J., Kolacinska, A., Morawiec, Z., Drzewoski, J. & Blasiak, J. (2006). Polymorphisms of the promoter regions of matrix metalloproteinases genes MMP-1 and MMP-9 in breast cancer. *Breast Cancer Research and Treatment*. 95: 65-72

Pullen, N. A., Anand, M., Cooper, P. S. & Fillmore, H. L. (2012). Matrix metalloproteinase-1 expression enhances tumorigenicity as well as tumor-related angiogenesis and is inversely associated with TIMP-4 expression in a model of glioblastoma. *Journal of Neuro-oncology*. 106: 461-471

Pulukuri, S. M. & Rao, J. S. (2008). Matrix metalloproteinase-1 promotes prostate tumor growth and metastasis. *International Journal of Oncology*. 32: 757-765

Purushothaman, A., Uyama, T., Kobayashi, F., Yamada, S., Sugahara, K., Rapraeger, A. C. & Sanderson, R. D. (2010). Heparanase-enhanced shedding of syndecan-1 by myeloma cells promotes endothelial invasion and angiogenesis. *Blood*. 115: 2449-2457

Pyke, C., Ralfkiaer, E., Huhtala, P., Hurskainen, T., Danø, K. & Tryggvason, K. (1992). Localization of messenger RNA for Mr 72,000 and 92,000 type IV collagenases in human skin cancers by in situ hybridization. *Cancer Research*. 52: 1336-1341

Pyke, C., Ralfkiaer, E., Tryggvason, K. & Danø, K. (1993). Messenger RNA for two type IV collagenases is located in stromal cells in human colon cancer. *The American Journal of Pathology*. 142: 359-365

Qi, J. H., Ebrahem, Q., Moore, N., Murphy, G., Claesson-Welsh, L., Bond, M., Baker, A. & Anand-Apte, B. (2003). A novel function for tissue inhibitor of metalloproteinases-3 (TIMP3): inhibition of angiogenesis by blockage of VEGF binding to VEGF receptor-2. *Nature Medicine*. 9: 407-415

Qin, L., Liao, L., Redmond, A., Young, L., Yuan, Y., Chen, H., O'Malley, B. W. & Xu, J. (2008). The AIB1 oncogene promotes breast cancer metastasis by activation of PEA3-mediated matrix metalloproteinase 2 (MMP2) and MMP9 expression. *Molecular and Cellular Biology*. 28: 5937-5950

Quigley, J. P., Gold, L. I., Schwimmer, R. & Sullivan, L. M. (1987). Limited cleavage of cellular fibronectin by plasminogen activator purified from transformed cells. *Proceedings of the National Academy of Sciences of the USA*. 84: 2776-2780

Ra, H. J. & Parks, W. C. (2007). Control of matrix metalloproteinase catalytic activity. *Matrix Biology*. 26: 587-596

Radjabi, A. R., Sawada, K., Jagadeeswaran, S., Eichbichler, A., Kenny, H. A., Montag, A., Bruno, K. & Lengyel, E. (2008). Thrombin induces tumor invasion through the induction and association of matrix metalloproteinase-9 and beta1-integrin on the cell surface. *The Journal of Biological Chemistry*. 283: 2822-2834

Raimondi, C., Fantin, A., Lampropoulou, A., Denti, L., Chikh, A. & Ruhrberg, C. (2014). Imatinib inhibits VEGF-independent angiogenesis by targeting neuropilin 1-dependent ABL1 activation in endothelial cells. *The Journal of Experimental Medicine*. 211: 1167-1183

Randi, A. M., Sperone, A., Dryden, N. H. & Birdsey, G. M. (2009). Regulation of angiogenesis by ETS transcription factors. *Biochemical Society Transactions*. 37: 1248-1253

Rao, J. S., Steck, P. A., Mohanam, S., Stetler-Stevenson, W. G., Liotta, L. A. & Sawaya, R. (1993). Elevated levels of M(r) 92,000 type IV collagenase in human brain tumors. *Cancer Research*. 53: 2208-2211

Ribatti, D. & Crivellato, E. (2012). "Sprouting angiogenesis", a reappraisal. *Developmental Biology*. 372: 157-165

Riddle, R. D., Johnson, R. L., Laufer, E. & Tabin, C. (1993). Sonic hedgehog mediates the polarizing activity of the ZPA. *Cell*. 75: 1401-1416

Riken Center for Developmental Biology (CDB) (2011). *New twist on ex ovo culture in bird* [online]. Available at: http://www.cdb.riken.jp/eng/04_news/articles/11/110104_newtwist.html. Accessed 01/08/16

Risau, W. & Wolburg, H. (1990). Development of the blood-brain barrier. *Trends in Neurosciences.* 13: 174-178

Rivera, C. G., Mellberg, S., Claesson-Welsh, L., Bader, J. S. & Popel, A. S. (2011). Analysis of VEGF--a regulated gene expression in endothelial cells to identify genes linked to angiogenesis. *PLoS One*. 6: e24887

Roberts, D. M., Kearney, J. B., Johnson, J. H., Rosenberg, M. P., Kumar, R. & Bautch, V. L. (2004). The vascular endothelial growth factor (VEGF) receptor Flt-1 (VEGFR-1) modulates Flk-1 (VEGFR-2) signaling during blood vessel formation. *The American Journal of Pathology*. 164: 1531-1535

Rosell, A., Morancho, A., Navarro-Sobrino, M., Martínez-Saez, E., Hernández-Guillamon, M., Lope-Piedrafita, S., Barceló, V., Borrás, F., Penalba, A., García-Bonilla, L. & Montaner, J. (2013). Factors secreted by endothelial progenitor cells enhance neurorepair responses after cerebral ischemia in mice. *PLoS One*. 8: e73244

Rosenstein, J. M., Krum, J. M. & Ruhrberg, C. (2010). VEGF in the nervous system. *Organogenesis*. 6: 107-114

Rozario, T. & DeSimone, D. W. (2010). The extracellular matrix in development and morphogenesis: a dynamic view. *Developmental Biology*. 341: 126-140

Ruffell, B., Affara, N. I. & Coussens, L. M. (2012). Differential macrophage programming in the tumor microenvironment. *Trends in Immunology*. 33: 119-126

Ruhrberg, C., Gerhardt, H., Golding, M., Watson, R., Ioannidou, S., Fujisawa, H., Betsholtz, C. & Shima, D. T. (2002). Spatially restricted patterning cues provided by heparin-binding VEGF-A control blood vessel branching morphogenesis. *Genes & Development*. 16: 2684-2698

Rutter, J. L., Mitchell, T. I., Butticè, G., Meyers, J., Gusella, J. F., Ozelius, L. J. & Brinckerhoff, C. E. (1998). A single nucleotide polymorphism in the matrix metalloproteinase-1 promoter creates an Ets binding site and augments transcription. *Cancer Research*. 58: 5321-5325

Salanga, M. C., Meadows, S. M., Myers, C. T. & Krieg, P. A. (2010). ETS family protein ETV2 is required for initiation of the endothelial lineage but not the hematopoietic lineage in the Xenopus embryo. *Developmental Dynamics*. 239: 1178-1187

Sandercoe, T. M., Madigan, M. C., Billson, F. A., Penfold, P. L. & Provis, J. M. (1999). Astrocyte proliferation during development of the human retinal vasculature. *Experimental Eye Research*. 69: 511-523

Santhosh, D. & Huang, Z. (2015). Regulation of the nascent brain vascular network by neural progenitors. *Mechanisms of Development*. 138 Pt 1: 37-42

Sato, H., Takino, T., Okada, Y., Cao, J., Shinagawa, A., Yamamoto, E., & Seiki, M. (1994). A matrix metalloproteinase expressed on the surface of invasive tumour cells. *Nature*. 370: 61-65

Sato, Y. (1998). Transcription factor ETS-1 as a molecular target for angiogenesis inhibition. *Human Cell*. 11: 207-2014

Saunders, W. B., Bohnsack, B. L., Faske, J. B., Anthis, N. J., Bayless, K. J., Hirschi, K. K. & Davis, G. E. (2006). Coregulation of vascular tube stabilization by endothelial cell TIMP-2 and pericyte TIMP-3. *The Journal of Cell Biology*. 175: 179-191

Saxton, T. M. & Pawson, T. (1999). Morphogenetic movements at gastrulation require the SH2 tyrosine phosphatase Shp2. *Proceedings of the National Academy of Sciences of the USA*. 96: 3790-3795

Schapira, M. & Patston. P. A. (1991). Serine protease inhibitors (serpins). *Trends in Cardiovascular Medicine*. 1: 146-151

Schmidt, T. & Carmeliet, P. (2010). Blood-vessel formation: Bridges that guide and unite. *Nature*. 465: 697-699

Schubert, F. R., Fainsod, A., Gruenbaum, Y. & Gruss, P. (1995). Expression of the novel murine homeobox gene Sax-1 in the developing nervous system. *Mechanisms of Development*. 51: 99-114

Schweighofer, B., Testori, J., Sturtzel, C., Sattler, S., Mayer, H., Wagner, O., Bilban, M. & Hofer, E. (2009). The VEGF-induced transcriptional response comprises gene clusters at the crossroad of angiogenesis and inflammation. *Thrombosis and Haemostasis*. 102: 544-554

Seeley, S., Covic, L., Jacques, S. L., Sudmeier, J., Baleja, J. D. & Kuliopulos, A. (2003). Structural basis for thrombin activation of a protease-activated receptor: inhibition of intramolecular liganding. *Chemistry & Biology*. 10: 1033-1041

Sementchenko, V. I. & Watson, D. K. (2000). Ets target genes: past, present and future. *Oncogene*. 19: 6533-6548

Shawber, C. J., Funahashi, Y., Francisco, E., Vorontchikhina, M., Kitamura, Y., Stowell, S. A., Borisenko, V., Feirt, N., Podgrabinska, S., Shiraishi, K., Chawengsaksophak, K., Rossant, J., Accili, D., Skobe, M. & Kitajewski, J. (2007). Notch alters VEGF responsiveness in human and murine endothelial cells by direct regulation of VEGFR-3 expression. *The Journal of Clinical Investigation*. 117: 3369-3382

Shou, J., Rim, P. C. & Calof, A. L. (1999). BMPs inhibit neurogenesis by a mechanism involving degradation of a transcription factor. *Nature Neuroscience*. 2: 339-345

Silletti, S., Kessler, T., Goldberg, J., Boger, D. L. & Cheresh, D. A. (2001). Disruption of matrix metalloproteinase 2 binding to integrin alpha vbeta 3 by an organic molecule inhibits angiogenesis and tumor growth in vivo. *Proceedings of the National Academy of Sciences of the USA*. 98: 119-124

Sirard, C., de la Pompa, J. L., Elia, A., Itie, A., Mirtsos, C., Cheung, A., Hahn, S., Wakeham, A., Schwartz, L., Kern, S. E., Rossant, J. & Mak, T. W. (1998). The tumor suppressor gene Smad4/Dpc4 is required for gastrulation and later for anterior development of the mouse embryo. *Genes & Development*. 12: 107-119

Soker, S., Takashima, S., Miao, H. Q., Neufeld, G. & Klagsbrun, M. (1998). Neuropilin-1 is expressed by endothelial and tumor cells as an isoform-specific receptor for vascular endothelial growth factor. *Cell*. 92: 735-745

Song, H., Pan, D., Sun, W., Gu, C., Zhang, Y., Zhao, P., Qi, Z. & Zhao, S. (2015). SiRNA directed against annexin II receptor inhibits angiogenesis via suppressing MMP2 and MMP9 expression. *Cellular Physiology and Biochemistry*. 35: 875-884

Sounni, N. E., Devy, L., Hajitou, A., Frankenne, F., Munaut, C., Gilles, C., Deroanne, C., Thompson, E. W., Foidart, J. M. & Noel, A. (2002). MT1-MMP expression promotes tumor growth and angiogenesis through an up-regulation of vascular endothelial growth factor expression. *FASEB Journal*. 16: 555-564

Sounni, N. E., Roghi, C., Chabottaux, V., Janssen, M., Munaut, C., Maquoi, E., Galvez, B. G., Gilles, C., Frankenne, F., Murphy, G., Foidart, J. M. & Noel, A. (2004). Up-regulation of vascular endothelial growth factor-A by active membrane-type 1 matrix metalloproteinase through activation of Src-tyrosine kinases. *The Journal of Biological Chemistry*. 279: 13564-13574

Sreenath, T., Matrisian, L. M., Stetler-Stevenson, W., Gattoni-Celli, S. & Pozzatti, R. O. (1992). Expression of matrix metalloproteinase genes in transformed rat cell lines of high and low metastatic potential. *Cancer Research*. 52: 4942-4947

Staveley, B. E. Vertebrate development III: Patterning the early nervous system and the somites [online]. Available at: http://www.mun.ca/biology/desmid/brian/BIOL3530/DEVO_05/devo_05.html Accessed 13-02-17

Stenman, J. M., Rajagopal, J., Carroll, T. J., Ishibashi, M., McMahon, J. & McMahon, A. P. (2008). Canonical Wnt signaling regulates organ-specific assembly and differentiation of CNS vasculature. *Science*. 322: 1247-1250

Stiles, J. & Jernigan, T. L. (2010). The basics of brain development. *Neuropsychology Review*. 20: 327-348

Stone, J. & Dreher, Z. (1987). Relationship between astrocytes, ganglion cells and vasculature of the retina. *The Journal of Comparative Neurology*. 255: 35-49

Stone, J., Itin, A., Alon, T., Pe'er, J., Gnessin, H., Chan-Ling, T. & Keshet, E. (1995). Development of retinal vasculature is mediated by hypoxia-induced vascular endothelial growth factor (VEGF) expression by neuroglia. *The Journal of Neuroscience*. 15: 4738-4747

Stoykova, A., Treichel, D., Hallonet, M. & Gruss, P. (2000). Pax6 modulates the dorsoventral patterning of the mammalian telencephalon. *The Journal of Neuroscience*. 20: 8042-8050

Streeter, G. L. (1942). *Developmental horizons in human embryos. Description of age group XI, 13 to 20 somites, and age group XII, 21 to 29 somites*. Washington DC: Carnegie Institution of Washington. Publication 541; Contributions to Embryology. 30: 211-245

Stricklin, G. P., Bauer, E. A., Jeffrey, J. J. & Eisen, A. Z. (1977). Human skin collagenase: isolation of precursor and active forms from both fibroblast and organ cultures. *Biochemistry*. 16: 1607-1615

Sturtzel, C., Testori, J., Schweighofer, B., Bilban, M., Hofer, E. (2014). The transcription factor MEF2C negatively controls angiogenic sprouting of endothelial cells depending on oxygen. *PLoS One*. 9: e101521

Suchting, S., Freitas, C., le Noble, F., Benedito, R., Bréant, C., Duarte, A. & Eichmann, A. (2007). The Notch ligand Delta-like 4 negatively regulates endothelial tip cell formation and vessel branching. *Proceedings of the National Academy of Sciences of the USA.* 104: 3225-3230

Sumanas, S., Gomez, G., Zhao, Y., Park, C., Choi, K. & Lin, S. (2008). Interplay among Etsrp/ER71, Scl, and Alk8 signaling controls endothelial and myeloid cell formation. *Blood*. 111: 4500-4510

Sumanas, S. & Lin, S. (2006). Ets1-related protein is a key regulator of vasculogenesis in zebrafish. *PLoS Biology*. 4: e10

Sunderkotter, C., Steinbrink, K., Goebeler, M. Bhardwaj R. & Sorg C. *et al*. (1994). Macrophages and angiogenesis. *Journal of Leukocyte Biology*. 55: 410-422

Tabouret, E., Boudouresque, F., Farina, P., Barrié, M., Bequet, C., Sanson, M. & Chinot, O. (2015). MMP2 and MMP9 as candidate biomarkers to monitor bevacizumab therapy in high-grade glioma. *Neuro-oncology*. 1174-1176.

Takagi, S., Hirata, T., Agata, K., Mochii, M., Eguchi, G. & Fujisawa, H. (1991). The A5 antigen, a candidate for the neuronal recognition molecule, has homologies to complement components and coagulation factors. *Neuron*. 7: 295-307

Takagi, S., Kasuya, Y., Shimizu, M., Matsuura, T., Tsuboi, M., Kawakami, A. & Fujisawa, H. (1995). Expression of a cell adhesion molecule, neuropilin, in the developing chick nervous system. *Developmental Biology*. 170: 207-222

Takagi, S., Tsuji, T., Amagai, T., Takamatsu, T. & Fujisawa, H. (1987). Specific cell surface labels in the visual centers of Xenopus laevis tadpole identified using monoclonal antibodies. *Developmental Biology*. 122: 90-100

Takahashi, T., Fournier, A., Nakamura, F., Wang, L. H., Murakami, Y., Kalb, R. G., Fujisawa, H. & Strittmatter, S. M. (1999). Plexin-neuropilin-1 complexes form functional semaphorin-3A receptors. *Cell*. 99: 59-69

Take-uchi, M., Clarke, J. D. & Wilson, S. W. (2003). Hedgehog signalling maintains the optic stalk-retinal interface through the regulation of Vax gene activity. *Development*. 130: 955-968

Tamakoshi, K., Kikkawa, F., Nawa, A., Maeda, O., Kawai, M., Sugamuma, N., Yamagata, S., Tomoda, Y. (1994). Different pattern of zymography between human gynecologic normal and malignant tissues. *American Journal of Obstetrics and Gynecology*. 171: 478-484

Tammela, T., Zarkada, G., Wallgard, E., Murtomäki, A., Suchting, S., Wirzenius, M., Waltari, M., Hellström, M., Schomber, T., Peltonen, R., Freitas, C., Duarte, A., Isoniemi, H., Laakkonen, P., Christofori, G., Ylä-Herttuala, S., Shibuya, M., Pytowski, B., Eichmann, A., Betsholtz, C. & Alitalo, K. (2008). Blocking VEGFR-3 suppresses angiogenic sprouting and vascular network formation. *Nature*. 454: 656-660

Tang, S. J., Hoodless, P. A., Lu, Z., Breitman, M. L., McInnes, R. R., Wrana, J. L. & Buchwald, M. (1998). The Tlx-2 homeobox gene is a downstream target of BMP signalling and is required for mouse mesoderm development. *Development*. 125: 1877-1887

Tazzyman, S., Niaz, H. & Murdoch, C. (2013). Neutrophil-mediated tumour angiogenesis: subversion of immune responses to promote tumour growth. *Seminars in Cancer Biology*. 23: 149-158

Thurston, G., Baluk, P., Hirata, A.& McDonald, D. M. (1996). Permeability-related changes revealed at endothelial cell borders in inflamed venules by lectin binding. *The American Journal of Physiology*. 271(6 Pt 2): H2547-2562

Tickle, C., Alberts, B., Wolpert, L. & Lee, J. (1982). Local application of retinoic acid to the limb bond mimics the action of the polarizing region. *Nature*. 296: 564-566

Tillo, M., Erskine, L., Cariboni, A., Fantin, A., Joyce, A., Denti, L. & Ruhrberg, C. (2015). VEGF189 binds NRP1 and is sufficient for VEGF/NRP1-dependent neuronal patterning in the developing brain. *Development*. 142: 314-319

Trost, A., Lange, S., Schroedl, F., Bruckner, D., Motloch, K. A., Bogner, B., Kaser-Eichberger, A., Strohmaier, C., Runge, C., Aigner, L., Rivera, F. J. & Reitsamer, H. A. (2016). Brain and Retinal Pericytes: Origin, Function and Role. *Frontiers in Cellular Neuroscience*. 10: 20

Turk, V., Turk, B., Guncar, G., Turk, D. & Kos, J. (2002). Lysosomal cathepsins: structure, role in antigen processing and presentation, and cancer. *Advances in Enzyme Regulation*. 42:285-303

Turk, V., Turk, B. & Turk, D. (2001). Lysosomal cysteine proteases: facts and opportunities. *The EMBO Journal*. 20: 4629-4633

van Hinsbergh, V. W., Engelse, M. A. & Quax, P. H. (2006). Pericellular proteases in angiogenesis and vasculogenesis. *Arteriosclerosis, Thrombosis and Vascular Biololgy*. 26: 716-728

van Hinsbergh, V. W. & Koolwijk, P. (2008). Endothelial sprouting and angiogenesis: matrix metalloproteinases in the lead. *Cardiovascular Research*. 78: 203-212

Vasudevan, A., Long, J. E., Crandall, J. E., Rubenstein, J. L. & Bhide, P. G. (2008). Compartment-specific transcription factors orchestrate angiogenesis gradients in the embryonic brain. *Nature Neuroscience*. 11: 429-439

Vaupel, P. (2004). The role of hypoxia-induced factors in tumor progression. *The Oncologist*. 9 Suppl 5: 10-7

Vempati, P., Popel, A. S. & Mac Gabhann, F. (2011). Formation of VEGF isoform-specific spatial distributions governing angiogenesis: computational analysis. *BMC Systems Biology*. 5: 59

Verheul, H. M., Hoekman, K., Luykx-de Bakker, S., Eekman, C. A., Folman, C. C., Broxterman, H. J. & Pinedo, H. M. (1997). Platelet: Transporter of vascular endothelial growth factor. *Clinical Cancer Research*. 3: 2187-2190

Vieira, J. M., Schwarz, Q. & Ruhrberg, C. (2007). Selective requirements for NRP1 ligands during neurovascular patterning. *Development*. 134: 1833-1843

Vincenti, M. P., White, L. A., Schroen, D. J., Benbow, U. & Brinckerhoff, C. E. (1996). Regulating expression of the gene for matrix metalloproteinase-1 (collagenase): mechanisms that control enzyme activity, transcription, and mRNA stability. *Critical Reviews in Eukaryotic Gene Expression*. 6: 391-411

Vintonenko, N., Pelaez-Garavito, I., Buteau-Lozano, H., Toullec, A., Lidereau, R., Perret, G. Y., Bieche, I. & Perrot-Applanat, M. (2011). Overexpression of VEGF189 in breast cancer cells induces apoptosis via NRP1 under stress conditions. *Cell Adhesion & Migration*. 5: 332-343

Visse, R. & Nagase, H. (2003). Matrix metalloproteinases and tissue inhibitors of metalloproteinases: structure, function, and biochemistry. *Circulation Research*. 92: 827-839

Vlodavsky, I., Bar-Shavit, R., Ishai-Michaeli, R., Bashkin, P. & Fuks, Z. (1991). Extracellular sequestration and release of fibroblast growth factor: a regulatory mechanism? *Trends in Biochemical Sciences*. 16: 268-271

Vlodavsky, I., Korner, G., Ishai-Michaeli, R., Bashkin, P., Bar-Shavit, R. & Fuks, Z. (1990). Extracellular matrix-resident growth factors and enzymes: possible involvement in tumor metastasis and angiogenesis. *Cancer Metastasis Reviews*. 9: 203-226

Voellenkle, C., Rooij, Jv., Guffanti, A., Brini, E., Fasanaro, P., Isaia, E., Croft, L., David, M., Capogrossi, M. C., Moles, A., Felsani, A. & Martelli, F. (2012). Deep-sequencing of endothelial cells exposed to hypoxia reveals the complexity of known and novel microRNAs. *RNA*. 18: 472-484

Wang, L. J., He, C. C., Sui, X., Cai, M. J., Zhou, C. Y., Ma, J. L., Wu, L., Wang, H., Han, S. X. & Zhu, Q. (2015). MiR-21 promotes intrahepatic cholangiocarcinoma proliferation and growth in vitro and in vivo by targeting PTPN14 and PTEN. *Oncotarget*. 6: 5932-5946

Wang, N., Zhang, C. Q., He, J. H., Duan, X. F., Wang, Y. Y., Ji, X., Zang, W. Q., Li, M., Ma, Y. Y., Wang, T. & Zhao, G. Q. (2013). MiR-21 down-regulation suppresses cell growth, invasion and induces cell apoptosis by targeting FASL, TIMP3, and RECK genes in esophageal carcinoma. *Digestive Diseases and Sciences*. 58: 1863-1870

Ware, M. & Schubert, F. R. (2011). Development of the early axon scaffold in the rostral brain of the chick embryo. *Journal of Anatomy*. 219: 203-216

Watanabe, T. & Raff, M. C. (1988). Retinal astrocytes are immigrants from the optic nerve. *Nature*. 332: 834-837

Wei, Y., Lukashev, M., Simon, D. I., Bodary, S. C., Rosenberg, S., Doyle, M. V. & Chapman, H. A. (1996). Regulation of integrin function by the urokinase receptor. *Science*. 273: 1551-1555

West, H., Richardson, W. D. & Fruttiger, M. (2005). Stabilization of the retinal vascular network by reciprocal feedback between blood vessels and astrocytes. *Development*. 132: 1855-1862

Wiley, D. M., Kim, J. D., Hao, J., Hong, C. C., Bautch, V. L. & Jin, S. W. (2011). Distinct signalling pathways regulate sprouting angiogenesis from the dorsal aorta and the axial vein. *Nature Cell Biology*. 13: 686-692

Wilson, L. & Maden, M. (2005). The mechanisms of dorsoventral patterning in the vertebrate neural tube. *Developmental Biology*. 282: 1-13

Wilting, J., Brand-Saberi, B., Huang, R., Zhi, Q., Köntges, G., Ordahl, C. P. & Christ, B. (1995). Angiogenic potential of the avian somite. *Developmental Dynamics.* 202: 165-171

Woessner, J. F. & Nagase, H. *Matrix Metalloproteinases and TIMPs*. Oxford: Oxford University Press, 2000

Wolf, K., Wu, Y. I., Liu, Y., Geiger, J., Tam, E., Overall, C., Stack, M. S. & Friedl, P. (2007). Multi-step pericellular proteolysis controls the transition from individual to collective cancer cell invasion. *Nature Cell Biology*. 9: 893-904

Wolfsberg, T. G., Straight, P. D., Gerena, R. L., Huovila, A. P., Primakoff, P., Myles, D. G. & White, J. M. (1995). ADAM, a widely distributed and developmentally regulated gene family encoding membrane proteins with a disintegrin and metalloprotease domain. *Developmental Biology*. 169: 378-383

Wu, K., Fukuda, K., Xing, F., Zhang, Y., Sharma, S., Liu, Y., Chan, M. D., Zhou, X., Qasem, S. A., Pochampally, R., Mo, Y. Y. & Watabe, K. (2015). Roles of the cyclooxygenase 2 matrix metalloproteinase 1 pathway in brain metastasis of breast cancer. *The Journal of Biological Chemistry*. 290: 9842-9854

Wylie, S., MacDonald, I. C., Varghese, H. J., Schmidt, E. E., Morris, V. L., Groom, A. C. & Chambers, A. F. (1999). The matrix metalloproteinase inhibitor batimastat inhibits angiogenesis in liver metastases of B16F1 melanoma cells. *Clinical & Experimental Metastasis*. 17: 111-117

Xiang, T., Xia, X. & Yan, W. (2016). Expression of Matrix Metalloproteinases-2/-9 is Associated With Microvessel Density in Pancreatic Cancer. *American Journal of Therapeutics*. [Epub ahead of print]

Xie, J., Aszterbaum, M., Zhang, X., Bonifas, J. M., Zachary, C., Epstein, E. & McCormick, F. (2001). A role of PDGFRalpha in basal cell carcinoma proliferation. *Proceedings of the National Academy of Sciences of the USA*. 98: 9255-9259

Yamaguchi, T. P., Harpal, K., Henkemeyer, M. & Rossant, J. (1994). fgfr-1 is required for embryonic growth and mesodermal patterning during mouse gastrulation. *Genes & Development*. 8: 3032-3044

Yana, I., Sagara, H., Takaki, S., Takatsu, K., Nakamura, K., Nakao, K., Katsuki, M., Taniguchi, S., Aoki, T., Sato, H., Weiss, S. J. & Seiki, M. (2007). Crosstalk between neovessels and mural cells directs the site-specific expression of MT1-MMP to endothelial tip cells. *Journal of Cell Science*. 120: 1607-1614

Yaneza, M., Gilthorpe, J. D., Lumsden, A. & Tucker, A. S. (2002). No evidence for ventrally migrating neural tube cells from the mid- and hindbrain. *Developmental Dynamics*. 223: 163-167

Yang, J. S., Lin, C. W., Su, S. C. & Yang, S. F. (2016). Pharmacodynamic considerations in the use of matrix metalloproteinase inhibitors in cancer treatment. *Expert Opinion on Drug Metabolism & Toxicology*. 12: 191-200

Yang, Y., Estrada, E. Y., Thompson, J. F., Liu, W. & Rosenberg, G. A. (2007). Matrix metalloproteinase-mediated disruption of tight junction proteins in cerebral vessels is reversed by synthetic matrix metalloproteinase inhibitor in focal ischemia in rat. *Journal of Cerebral Blood Flow and Metabolism*. 27: 697-709

Yang, Y. & Rosenberg, G. A. (2011). MMP-mediated disruption of claudin-5 in the blood-brain barrier of rat brain after cerebral ischemia. *Methods in Molecular Biology*. 762: 333-345

Yoshida, S. & Shiosaka, S. (1999). Plasticity-related serine proteases in the brain (review). *International Journal of Molecular Medicine*. 3: 405-409

Yu, Q. & Stamenkovic, I. (1999). Localization of matrix metalloproteinase 9 to the cell surface provides a mechanism for CD44-mediated tumor invasion. *Genes & Development*. 13: 35-48

Zania, P., Kritikou, S., Flordellis, C. S., Maragoudakis, M. E. & Tsopanoglou, N. E. (2006). Blockade of angiogenesis by small molecule antagonists to protease-activated receptor-1: association with endothelial cell growth suppression and induction of apoptosis. *The Journal of Pharmacology and Experimental Therapeutics*. 318: 246-254

Zeng, Z. S., Cohen, A. M. & Guillem, J. G. (1999). Loss of basement membrane type IV collagen is associated with increased expression of metalloproteinases 2 and 9 (MMP-2 and MMP-9) during human colorectal tumorigenesis. *Carcinogenesis*. 20: 749-755

Zeng, Z. S. & Guillem, J. G. (1995). Distinct pattern of matrix metalloproteinase 9 and tissue inhibitor of metalloproteinase 1 mRNA expression in human colorectal cancer and liver metastases. *British Journal of Cancer*. 72: 575-582

Zhang, A., Liu, Y., Shen, Y., Xu, Y. & Li, X. (2011). miR-21 modulates cell apoptosis by targeting multiple genes in renal cell carcinoma. *Urology*. 78: 474.e13-9

Zhang, Y. & Stone, J. (1997). Role of astrocytes in the control of developing retinal vessels. *Investigative Ophthalmology & Visual Science*. 38: 1653-1666

Zhang, Z., Song, T., Jin, Y., Pan, J., Zhang, L., Wang, L. & Li, P. (2009). Epidermal growth factor receptor regulates MT1-MMP and MMP-2 synthesis in SiHa cells via both PI3-K/AKT and MAPK/ERK pathways. *International Journal of Gynecological Cancer*. 19: 998-1003

Zhao, X., Yue, W., Zhang, L., Ma, L., Jia, W., Qian, Z., Zhang, C. & Wang, Y. (2014). Downregulation of PAX6 by shRNA inhibits proliferation and cell cycle progression of human non-small cell lung cancer cell lines. PLoS One. 9: e85738

Zhao, Y., Xu, Y., Luo, F., Xu, W., Wang, B., Pang, Y., Zhou, J., Wang, X. & Liu, Q. (2013). Angiogenesis, mediated by miR-21, is involved arsenite-induced carcinogenesis. *Toxicology Letters*. 223: 35-41

Zhou, Y. H., Hu, Y., Mayes, D., Siegel, E., Kim, J. G., Mathews, M. S., Hsu, N., Eskander, D., Yu, O., Tromberg, B. J. & Linskey, M. E. (2010). PAX6 suppression of glioma angiogenesis and the expression of vascular endothelial growth factor A. *Journal of Neuro-oncology*. 96: 191-200

Zhou, Y. H., Tan, F., Hess, K. R. & Yung, W. K. (2003). The expression of PAX6, PTEN, vascular endothelial growth factor, and epidermal growth factor receptor in gliomas: relationship to tumor grade and survival. *Clinical Cancer Research*. 9: 3369-3375

Zhou, Y. H., Wu, X., Tan, F., Shi, Y. X., Glass, T., Liu, T. J., Wathen, K., Hess, K. R., Gumin, J., Lang, F. & Yung, W. K. (2005). PAX6 suppresses growth of human glioblastoma cells. *Journal of Neuro-oncology*. 71: 223-229

Ziche, M., Morbidelli, L., Choudhuri, R., Zhang, H. T., Donnini, S., Granger, H. J. & Bicknell, R. (1997). Nitric oxide synthase lies downstream from vascular endothelial growth factor-induced but not basic fibroblast growth factor-induced angiogenesis. *The Journal of Clinical Investigation*. 99: 2625-2634

Ziello, J. E., Jovin, I. S. & Huang, Y. (2007). Hypoxia-Inducible Factor (HIF)-1 regulatory pathway and its potential for therapeutic intervention in malignancy and ischemia. *The Yale Journal of Biology and Medicine*. 80: 51-60

APPENDICES

Appendix A

Endothelial cell counts from bead implantation experiments with MMP inhibitors and active MMP-1. Embryos were implanted with beads containing pharmacological inhibitors ARP 100, SB-3CT or Batimastat, or active MMP-1, just beneath the surface ectoderm adjacent to the basal plate of the mesencephalon. Endothelial cells were detected using a CD34 antibody and counted as described in Figure 2ii. Control embryos were implanted with beads containing DMSO or PBS for the inhibitors, or 100mM Tris-HCl pH7.5 for active MMP-1.

	AVERAGE NUMBER OF ENDOTHELIAL CELLS	
CONDITION	**Side without Bead**	**Side with Bead**
DMSO Control	39.00	43.00
	55.50	50.00
	35.00	37.00
	65.50	69.50
	52.00	42.00
	23.33	27.00
	66.00	39.00
ARP 100, 8mM in DMSO	72.50	72.00
	70.00	50.00
	102.00	68.00
	108.00	71.00
	32.50	45.50
	28.00	29.00
SB-3CT, 8mM in DMSO	50.00	95.00
	76.00	91.00
	64.00	81.00
Batimastat, 1mM in DMSO	43.00	61.00
	81.00	46.00
	87.00	80.00
	87.00	49.00
	59.00	45.50
(*continue on next page*)		

	AVERAGE NUMBER OF ENDOTHELIAL CELLS	
CONDITION	**Side without Bead**	**Side with Bead**
PBS Control	59.33	39.67
	72.67	74.33
	32.50	38.00
	33.00	27.00
	27.67	25.00
	52.00	54.00
	27.50	27.50
ARP 100, 8mM in PBS	78.00	55.00
	69.00	247.00
	41.00	50.00
	55.67	39.67
	26.00	54.00
ARP 100, 1mM in PBS	49.67	68.33
	46.67	32.67
	14.00	33.33
	40.33	43.33
	60.50	91.50
	68.00	49.50
	63.00	59.33
	28.67	33.00
	49.00	46.00
SB-3CT, 8mM in PBS	57.00	86.00
	144.00	50.33
	74.33	83.67
	60.75	43.50
	52.00	41.50
	105.00	67.00
	38.00	19.50
(*continue on next page*)		

	AVERAGE NUMBER OF ENDOTHELIAL CELLS	
CONDITION	**Side without Bead**	**Side with Bead**
SB-3CT, 1mM in PBS	20.00	24.00
	27.00	19.33
	46.50	44.75
	31.00	30.50
	54.50	40.50
	21.33	31.00
	50.33	44.33
	55.00	43.00
	57.50	46.00
	17.50	68.00
100mM Tris-HCl pH7.5 Control	38.00	41.00
	28.50	60.50
	45.00	43.00
	60.00	56.50
Active MMP-1, 25nM in Tris	41.00	75.00
	48.00	73.00
	49.00	140.00
	57.00	79.00
	62.00	50.50
Active MMP-1, 250nM in Tris	52.67	35.00
	43.00	38.00
	53.00	53.00
Active MMP-1, 1μM in Tris	36.00	39.00
	50.50	67.50
	44.50	59.00
	56.50	113.50
	57.50	189.00

Appendix B

Paired t-test and histogram for DMSO control bead experiments. Embryos were implanted with beads containing DMSO, just beneath the surface ectoderm adjacent to the basal plate of the mesencephalon. CD34-stained endothelial cells were counted on the control side (**A**) and compared with the contra lateral side containing the bead (**B**). No significant difference was found between the mean number of endothelial cells on the control side and on the side containing the bead.

A

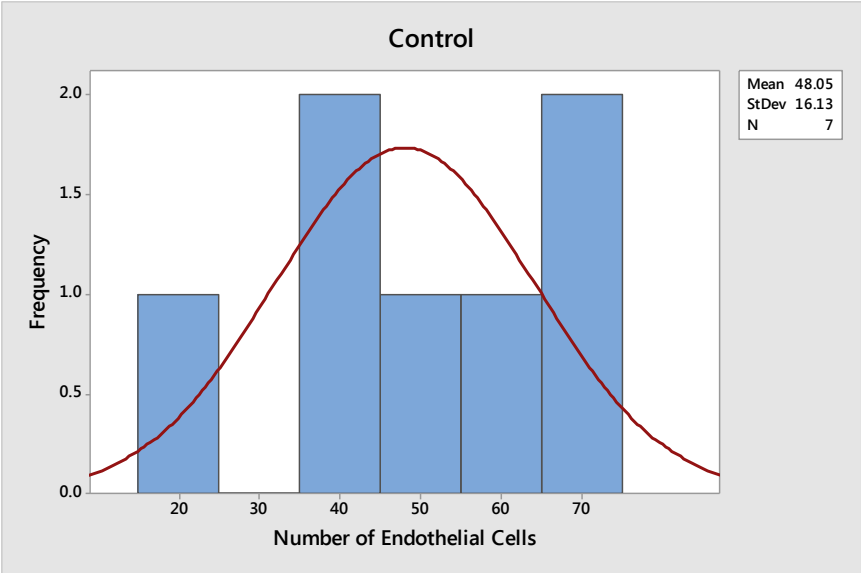

B

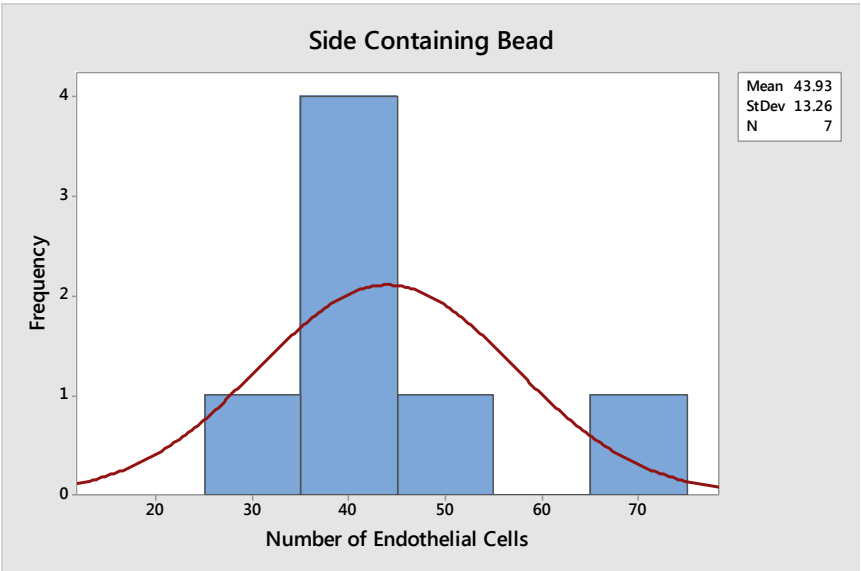

	N	Mean	StDev	SE Mean
Control	7	48.05	16.13	6.10
Bead	7	43.93	13.26	5.01
Difference	7	4.12	11.47	4.34

95% CI for mean difference: (-6.49, 14.73)
T-Test of mean difference = 0 (vs≠0): T-Value = 0.95 P-Value = 0.379

Appendix C

Paired t-test and histogram for bead experiments with 8mM ARP 100 in DMSO. Embryos were implanted with beads containing 8mM ARP 100 in DMSO, just beneath the surface ectoderm adjacent to the basal plate of the mesencephalon. CD34-stained endothelial cells were counted on the control side (**A**) and compared with the contra lateral side containing the bead (**B**). The mean number of endothelial cells on the side containing the bead was found to be lower than that of the control side, although the difference was not statistically significant.

A

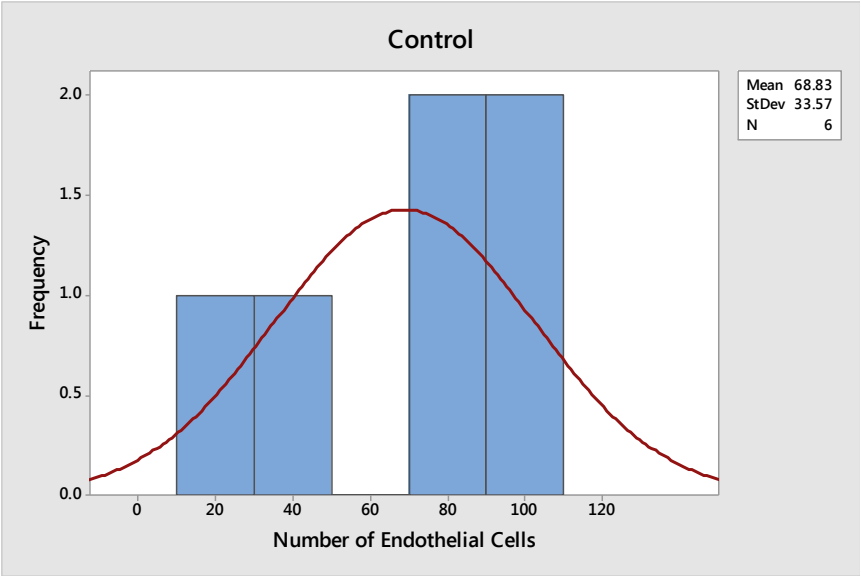

B

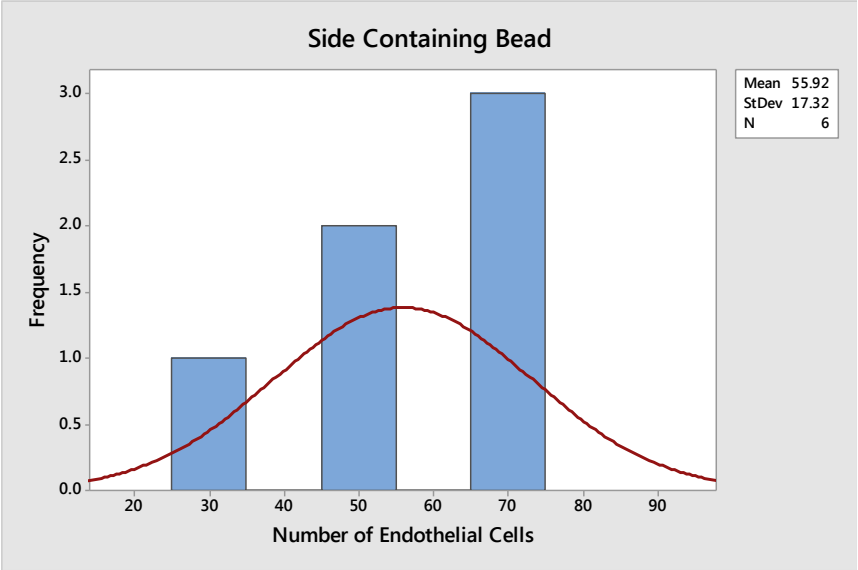

	N	Mean	StDev	SE Mean
Bead	6	55.9	17.3	7.1
Control	6	68.8	33.6	13.7
Difference	6	-12.92	20.47	8.36

95% upper bound for mean difference: 3.92
T-Test of mean difference = 0 (vs<0): T-Value = -1.55 P-Value = 0.091

Appendix D

Paired t-test and histogram for bead experiments with 8mM SB-3CT in DMSO. Embryos were implanted with beads containing 8mM SB-3CT in DMSO, just beneath the surface ectoderm adjacent to the basal plate of the mesencephalon. CD34-stained endothelial cells were counted on the control side (**A**) and compared with the contra lateral side containing the bead (**B**). No significant difference was found between the mean number of endothelial cells on the control side and on the side containing the bead.

A

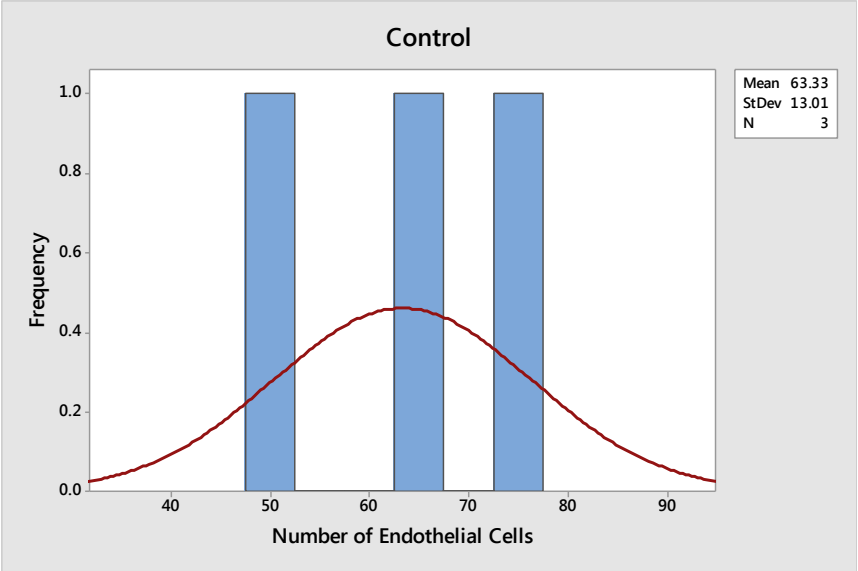

B

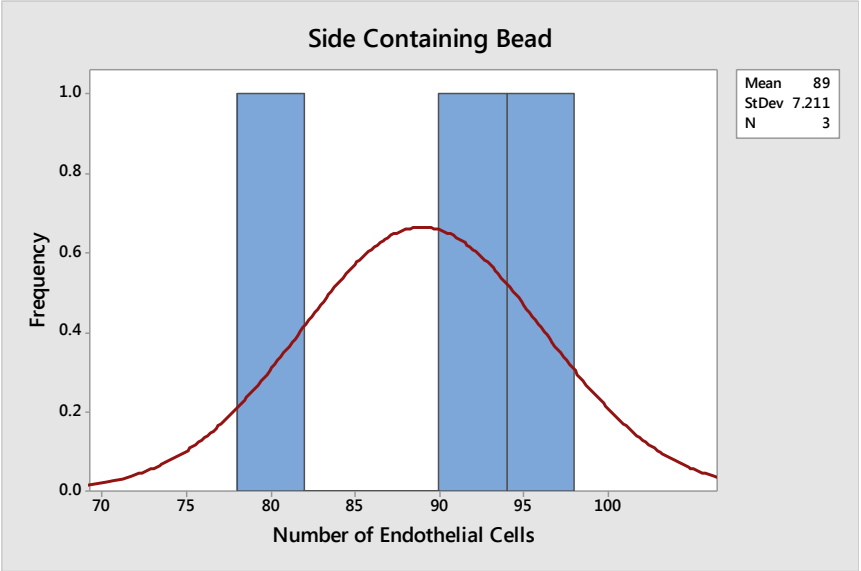

	N	Mean	StDev	SE Mean
Bead	3	89.00	7.21	4.16
Control	3	63.33	13.01	7.51
Difference	3	25.67	16.77	9.68

95% upper bound for mean difference: 53.94
T-Test of mean difference = 0 (vs<0): T-Value = 2.65 P-Value = 0.941

Appendix E

Paired t-test and histogram for bead experiments with 1mM Batimastat in DMSO. Embryos were implanted with beads containing 1mM Batimastat in DMSO, just beneath the surface ectoderm adjacent to the basal plate of the mesencephalon. CD34-stained endothelial cells were counted on the control side (**A**) and compared with the contra lateral side containing the bead (**B**). No significant difference was found between the mean number of endothelial cells on the control side and on the side containing the bead.

A

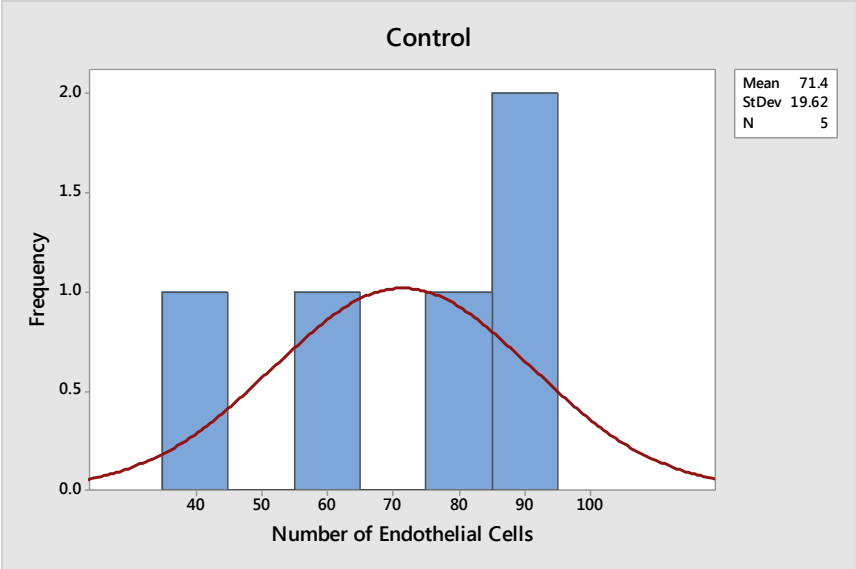

B

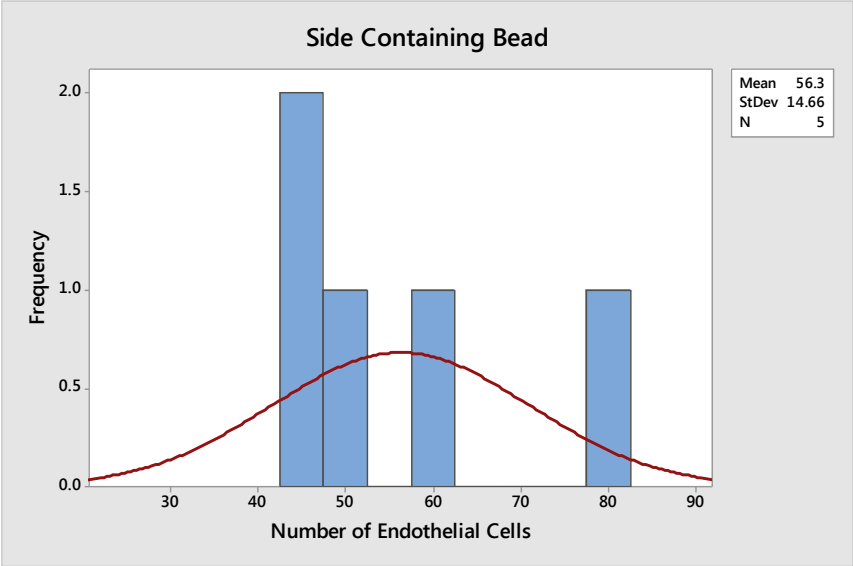

	N	Mean	StDev	SE Mean
Bead	5	56.30	14.66	6.56
Control	5	71.40	19.62	8.77
Difference	5	-15.1	22.8	10.2

95% upper bound for mean difference: 6.7
T-Test of mean difference = 0 (vs<0): T-Value = -1.48 P-Value = 0.107

Appendix F

Paired t-test and histogram for PBS control bead experiments. Embryos were implanted with beads containing PBS, just beneath the surface ectoderm adjacent to the basal plate of the mesencephalon. CD34-stained endothelial cells were counted on the control side (**A**) and compared with the contra lateral side containing the bead (**B**). No significant difference was found between the mean number of endothelial cells on the control side and on the side containing the bead.

A

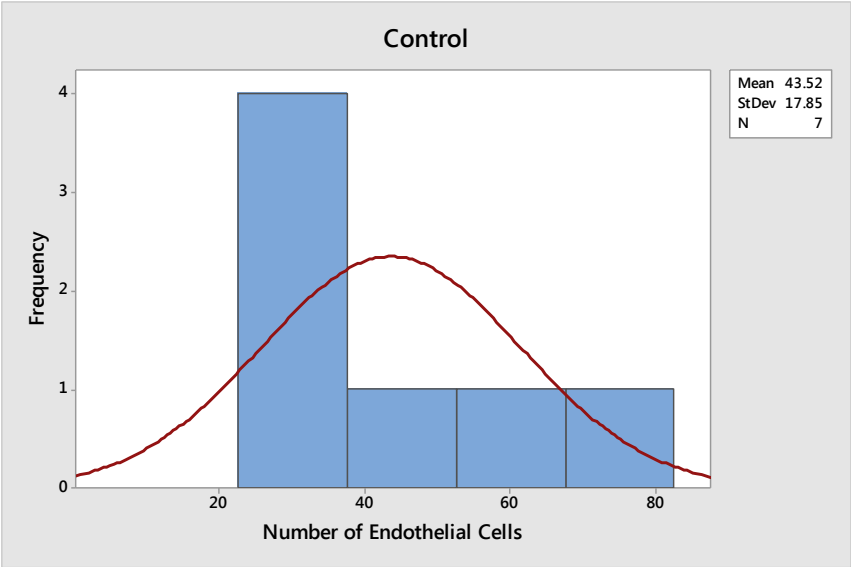

B

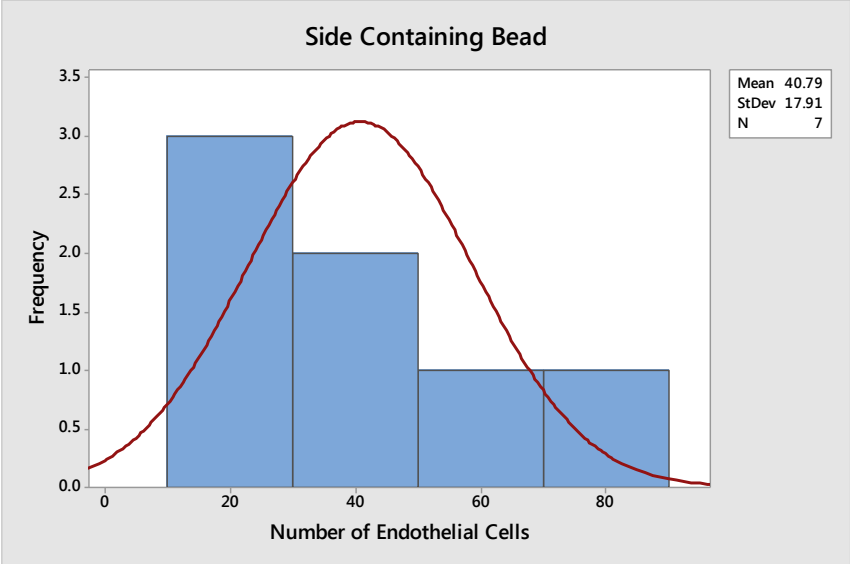

	N	Mean	StDev	SE Mean
Control	7	43.52	17.85	6.75
Bead	7	40.79	17.91	6.77
Difference	7	2.74	8.31	3.14

95% CI for mean difference: (-4.95, 10.42)
T-Test of mean difference = 0 (vs≠0): T-Value = 0.87 P-Value = 0.417

Appendix G

Paired t-test and histogram for bead experiments with 8mM ARP 100 in PBS. Embryos were implanted with beads containing 8mM ARP 100 in PBS, just beneath the surface ectoderm adjacent to the basal plate of the mesencephalon. CD34-stained endothelial cells were counted on the control side (**A**) and compared with the contra lateral side containing the bead (**B**). No significant difference was found between the mean number of endothelial cells on the control side and on the side containing the bead.

A

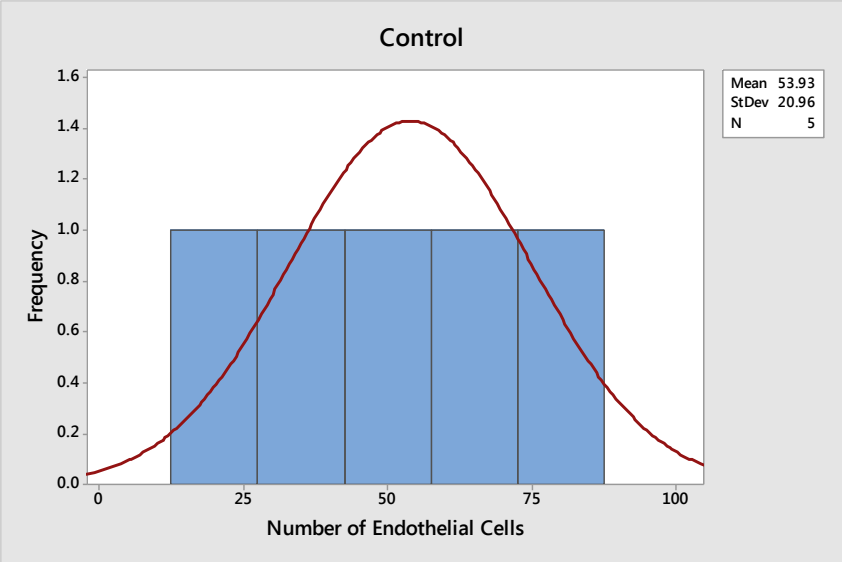

B

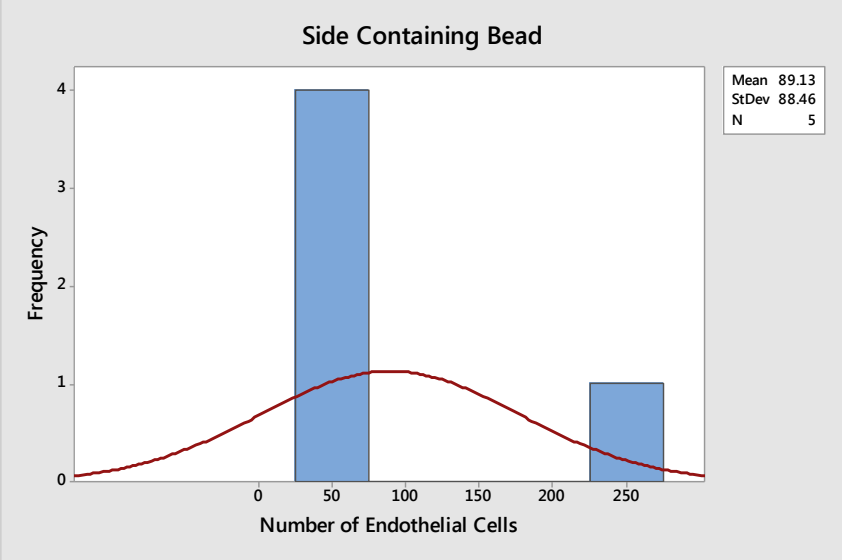

	N	Mean	StDev	SE Mean
Bead	5	89.1	88.5	39.6
Control	5	53.9	21.0	9.4
Difference	5	35.2	82.4	36.8

95% upper bound for mean difference: 113.7
T-Test of mean difference = 0 (vs<0): T-Value = 0.96 P-Value = 0.803

Appendix H

Paired t-test and histogram for bead experiments with 1mM ARP 100 in PBS. Embryos were implanted with beads containing 1mM ARP 100 in PBS, just beneath the surface ectoderm adjacent to the basal plate of the mesencephalon. CD34-stained endothelial cells were counted on the control side (**A**) and compared with the contra lateral side containing the bead (**B**). No significant difference was found between the mean number of endothelial cells on the control side and on the side containing the bead.

A

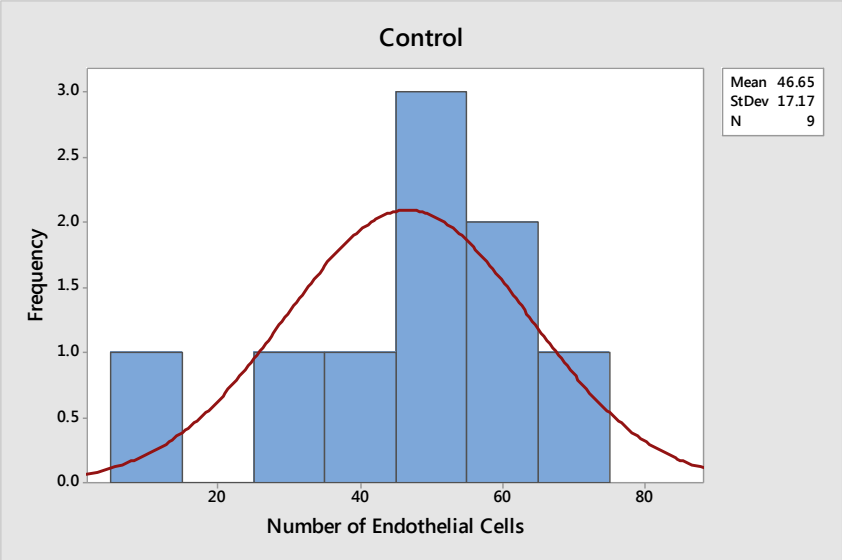

B

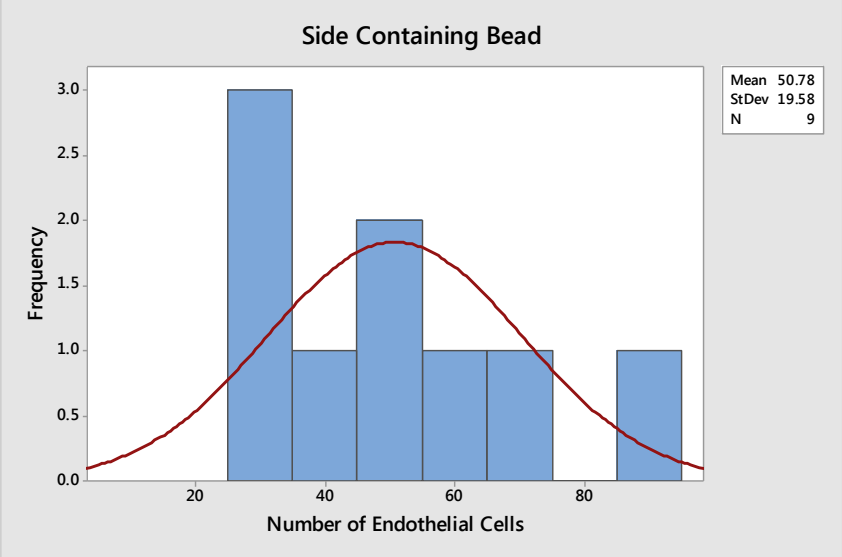

	N	Mean	StDev	SE Mean
Bead	9	50.78	19.58	6.53
Control	9	46.65	17.17	5.72
Difference	9	4.13	16.27	5.42

95% upper bound for mean difference: 14.21
T-Test of mean difference = 0 (vs<0): T-Value = 0.76 P-Value = 0.766

Appendix I

Paired t-test and histogram for bead experiments with 8mM SB-3CT in PBS. Embryos were implanted with beads containing 8mM SB-3CT in PBS, just beneath the surface ectoderm adjacent to the basal plate of the mesencephalon. CD34-stained endothelial cells were counted on the control side (**A**) and compared with the contra lateral side containing the bead (**B**). No significant difference was found between the mean number of endothelial cells on the control side and on the side containing the bead.

A

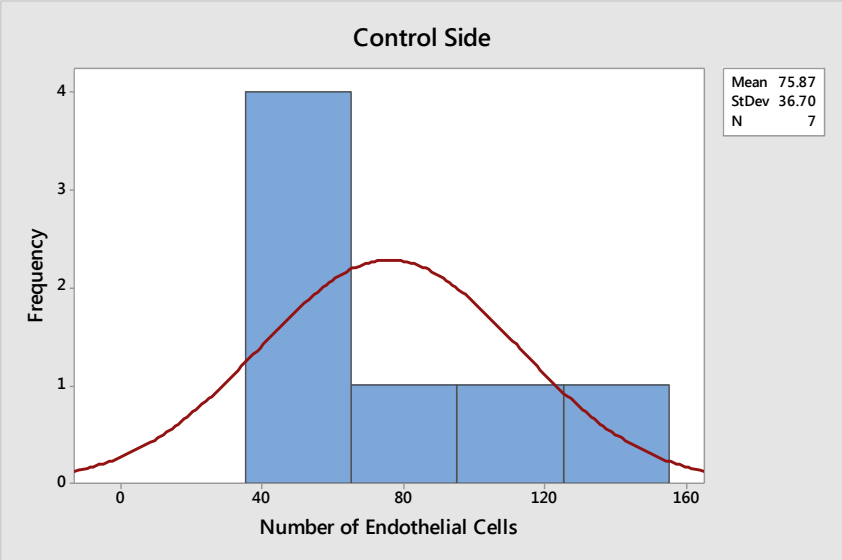

B

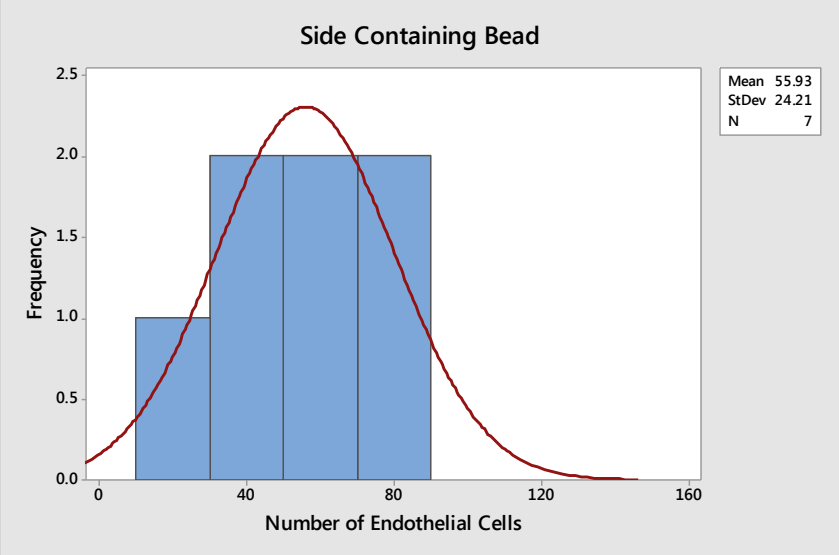

	N	Mean	StDev	SE Mean
Bead	7	55.9	24.2	9.2
Control	7	75.9	36.7	13.9
Difference	7	-19.9	39.0	14.7

95% upper bound for mean difference: 8.7
T-Test of mean difference = 0 (vs<0): T-Value = -1.35 P-Value = 0.112

Appendix J

Paired t-test and histogram for bead experiments with 1mM SB-3CT in PBS. Embryos were implanted with beads containing 1mM SB-3CT in PBS, just beneath the surface ectoderm adjacent to the basal plate of the mesencephalon. CD34-stained endothelial cells were counted on the control side (**A**) and compared with the contra lateral side containing the bead (**B**). No significant difference was found between the mean number of endothelial cells on the control side and on the side containing the bead.

A

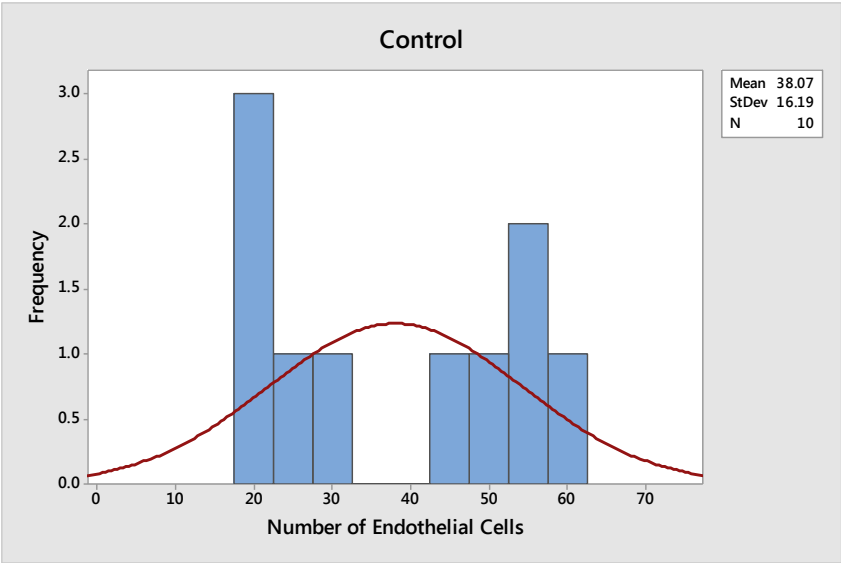

B

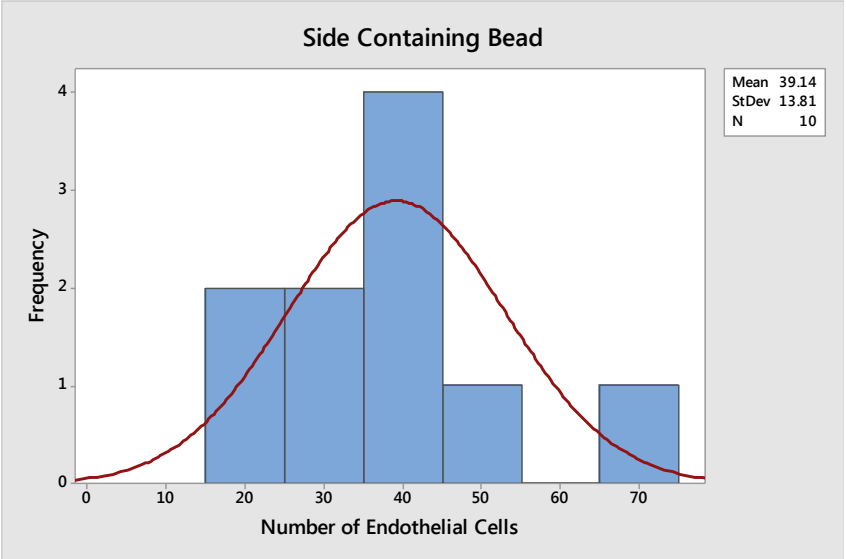

	N	Mean	StDev	SE Mean
Bead	10	39.14	13.81	4.37
Control	10	38.07	16.19	5.12
Difference	10	1.08	18.91	5.98

95% upper bound for mean difference: 12.04
T-Test of mean difference = 0 (vs<0): T-Value = 0.18 P-Value = 0.569

Appendix K

Paired t-test and histogram for 100mM Tris-HCl pH7.5 control bead experiments. Embryos were implanted with beads containing 100mM Tris-HCl pH7.5, just beneath the surface ectoderm adjacent to the basal plate of the mesencephalon. CD34-stained endothelial cells were counted on the control side (**A**) and compared with the contra lateral side containing the bead (**B**). No significant difference was found between the mean number of endothelial cells on the control side and on the side containing the bead.

A

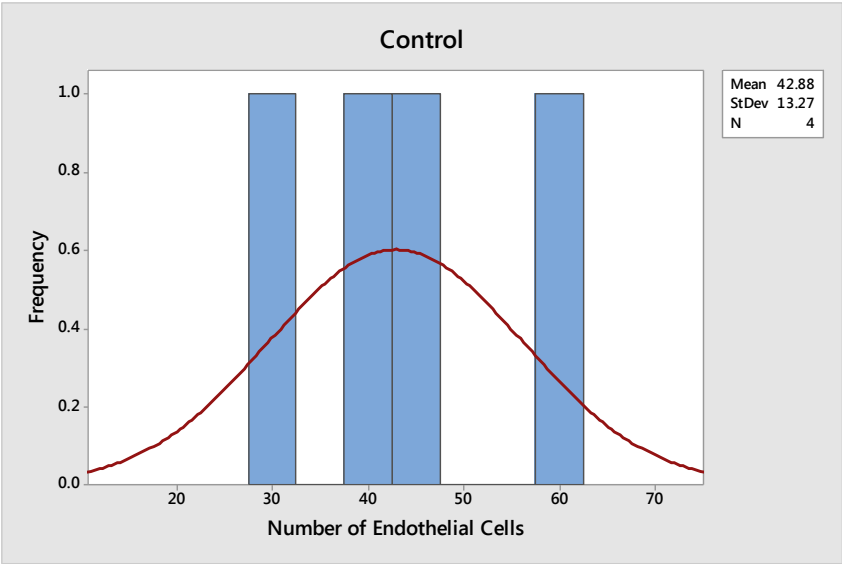

B

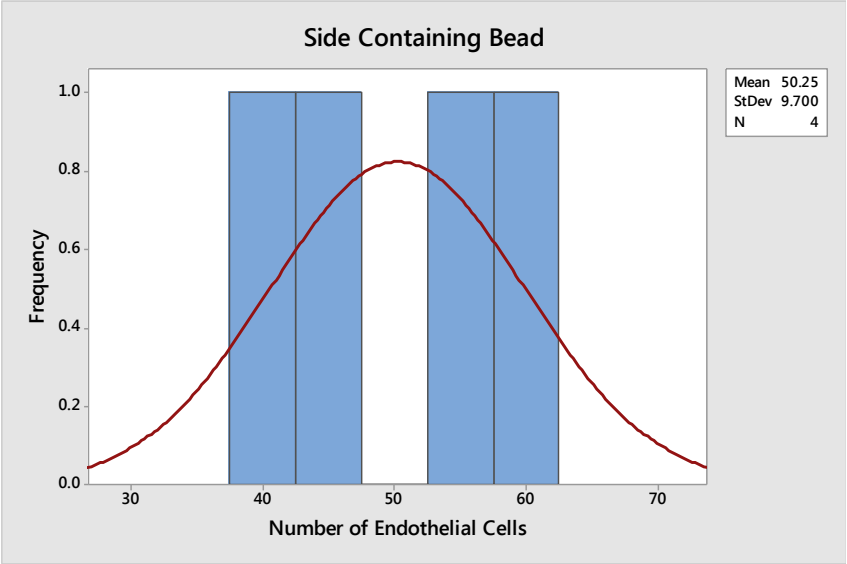

	N	Mean	StDev	SE Mean
Control	4	42.88	13.27	6.63
Bead	4	50.25	9.70	4.85
Difference	4	-7.38	16.65	8.33

95% CI for mean difference: (-33.87, 19.12)
T-Test of mean difference = 0 (vs≠0): T-Value = -0.89 P-Value = 0.441

Appendix L

Paired t-test and histogram for bead experiments with 25nM active MMP-1 in Tris-HCl. Embryos were implanted with beads containing 25nM active MMP-1 in Tris-HCl, just beneath the surface ectoderm adjacent to the basal plate of the mesencephalon. CD34-stained endothelial cells were counted on the control side (**A**) and compared with the contra lateral side containing the bead (**B**). The mean number of endothelial cells on the side containing the bead was higher than that of the control side, although the difference was not statistically significant.

A

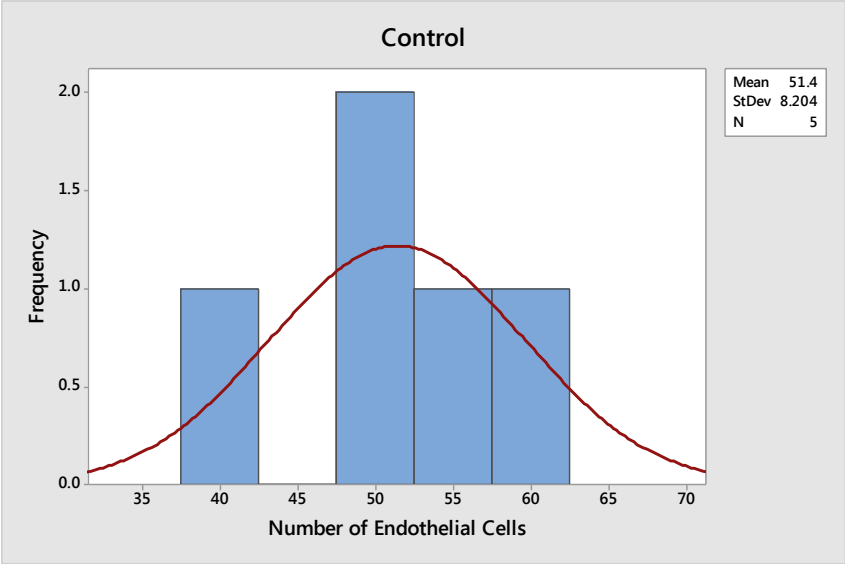

B

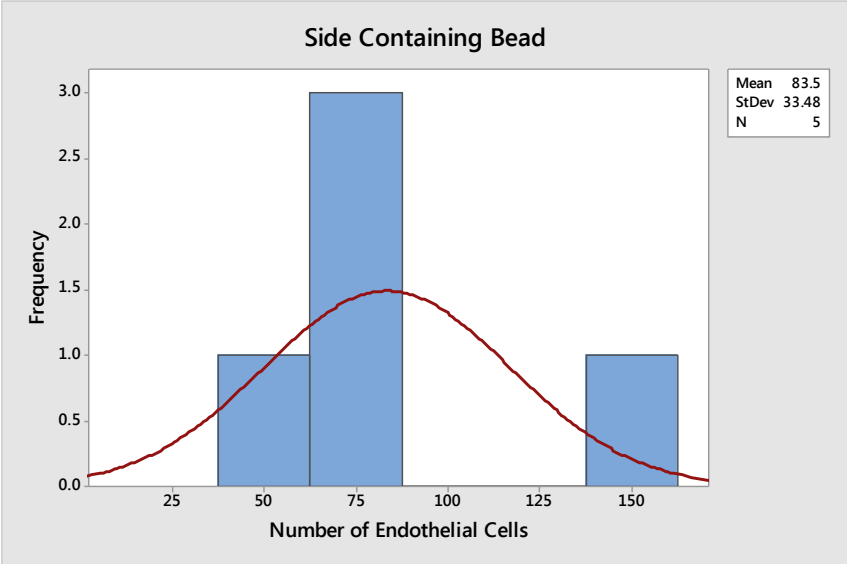

	N	Mean	StDev	SE Mean
Bead	5	83.5	33.5	15.0
Control	5	51.4	8.2	3.7
Difference	5	32.1	37.2	16.6

95% lower bound for mean difference: -3.3
T-Test of mean difference = 0 (vs>0): T-Value = 1.93 P-Value = 0.063

Appendix M

Paired t-test and histogram for bead experiments with 250nM active MMP-1 in Tris-HCl. Embryos were implanted with beads containing 250nM active MMP-1 in Tris-HCl, just beneath the surface ectoderm adjacent to the basal plate of the mesencephalon. CD34-stained endothelial cells were counted on the control side (**A**) and compared with the contra lateral side containing the bead (**B**). No significant difference was found between the mean number of endothelial cells on the control side and on the side containing the bead.

A

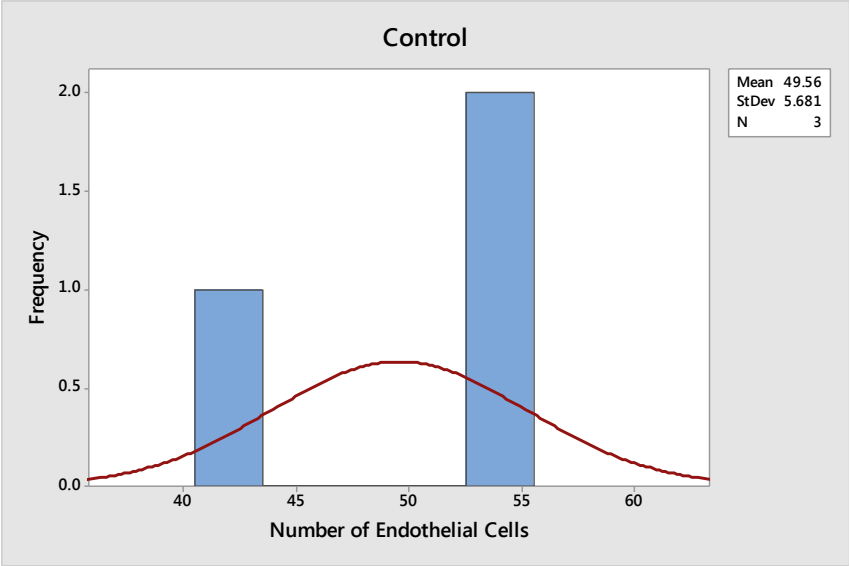

B

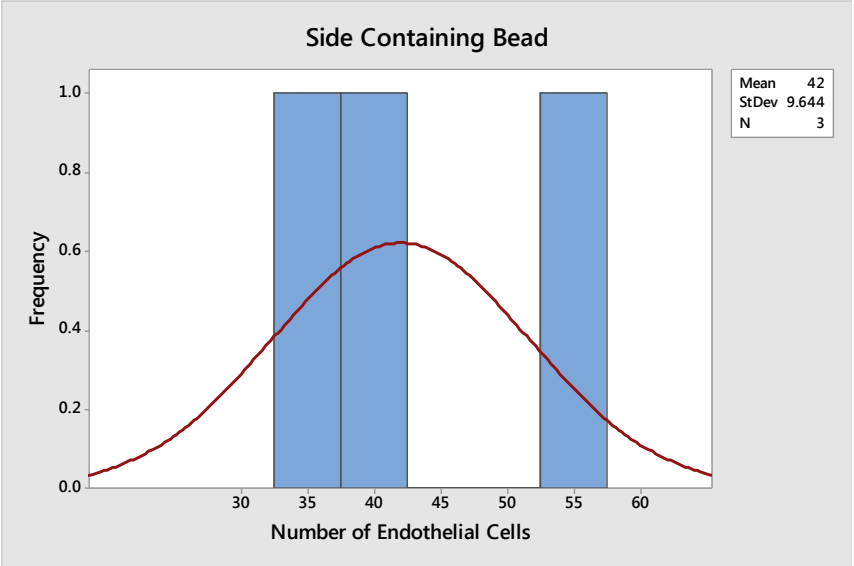


```
N    Mean   StDev   SE Mean
Bead          3   42.00    9.64      5.57
Control       3   49.56    5.68      3.28
Difference    3   -7.56    9.11      5.26

95% lower bound for mean difference: -22.91
T-Test of mean difference = 0 (vs>0): T-Value = -1.44  P-Value = 0.856
```

Appendix N

Paired t-test and histogram for bead experiments with 1µM active MMP-1 in Tris-HCl. Embryos were implanted with beads containing 1µM active MMP-1 in Tris-HCl, just beneath the surface ectoderm adjacent to the basal plate of the mesencephalon. CD34-stained endothelial cells were counted on the control side (**A**) and compared with the contra lateral side containing the bead (**B**). The mean number of endothelial cells on the side containing the bead was found to be higher than that of the control side although this increase was not statistically significant.

A

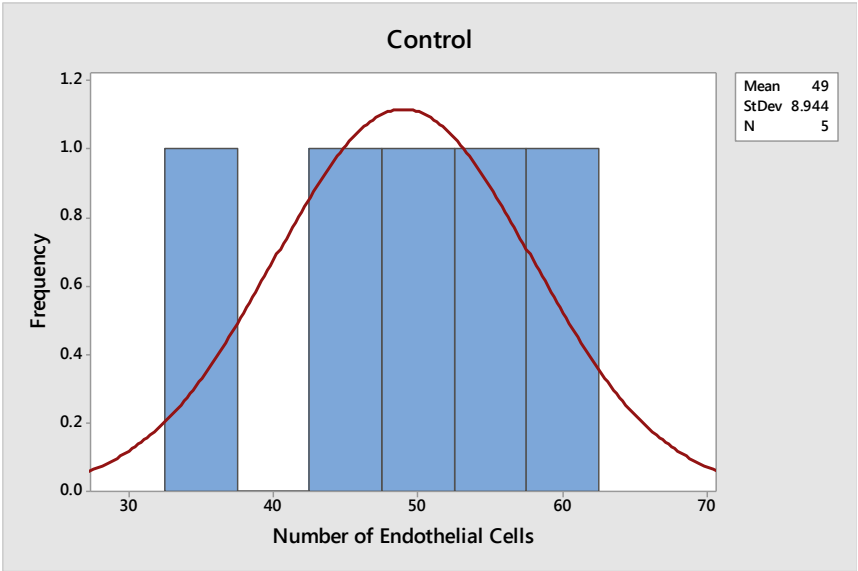

B

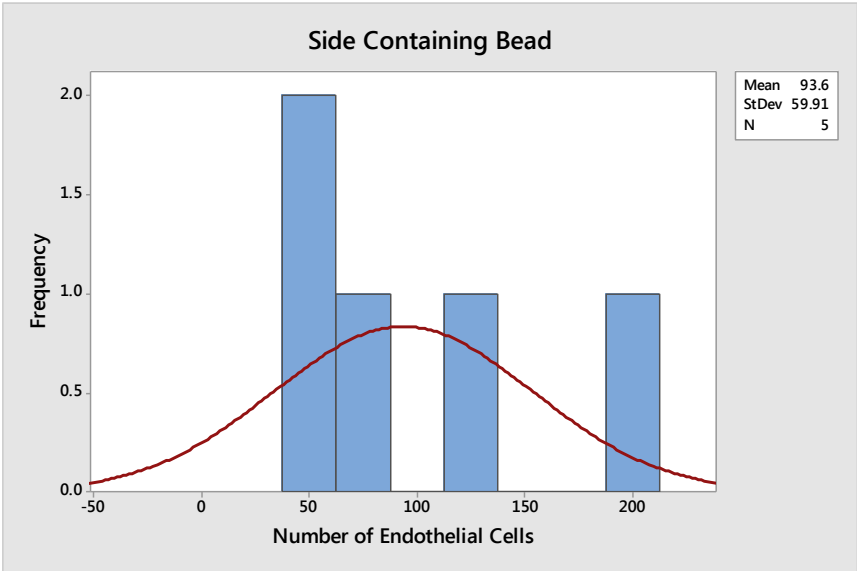

	N	Mean	StDev	SE Mean
Bead	5	93.6	59.9	26.8
Control	5	49.0	8.9	4.0
Difference	5	44.6	52.7	23.6

95% lower bound for mean difference: -5.6
T-Test of mean difference = 0 (vs>0): T-Value = 1.89 P-Value = 0.066

Appendix O

Endothelial cell counts from bead implantation experiments with DAPT. Embryos were implanted with beads containing DAPT in either DMSO or PBS, just beneath the surface ectoderm adjacent to the basal plate of the mesencephalon. Endothelial cells were detected using a CD34 antibody and counted as described in Figure 2ii. Control embryos were implanted with beads containing either DMSO or PBS.

	AVERAGE NUMBER OF ENDOTHELIAL CELLS	
CONDITION	**Side without Bead**	**Side with Bead**
DMSO Control	39.00	43.00
	55.50	50.00
	35.00	37.00
	65.50	69.50
	52.00	42.00
	23.33	27.00
	66.00	39.00
DAPT, 10mM in DMSO	58.50	85.50
	34.33	46.00
	63.00	67.67
	40.50	39.00
	69.33	91.67
PBS Control	59.33	39.67
	72.67	74.33
	32.50	38.00
	33.00	27.00
	27.67	25.00
	52.00	54.00
	27.50	27.50
DAPT, 10mM in PBS	80.00	37.00
	41.00	30.00
	37.00	31.67

Appendix P

Paired t-test and histogram for DMSO control bead experiments. Embryos were implanted with beads containing DMSO, just beneath the surface ectoderm adjacent to the basal plate of the mesencephalon. CD34-stained endothelial cells were counted on the control side (**A**) and compared with the contra lateral side containing the bead (**B**). No significant difference was found between the mean number of endothelial cells on the control side and on the side containing the bead.

A

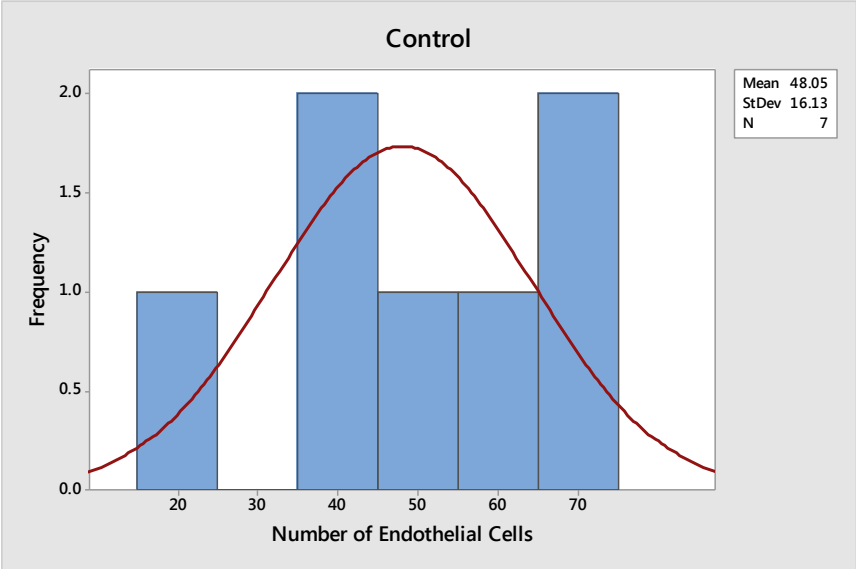

B

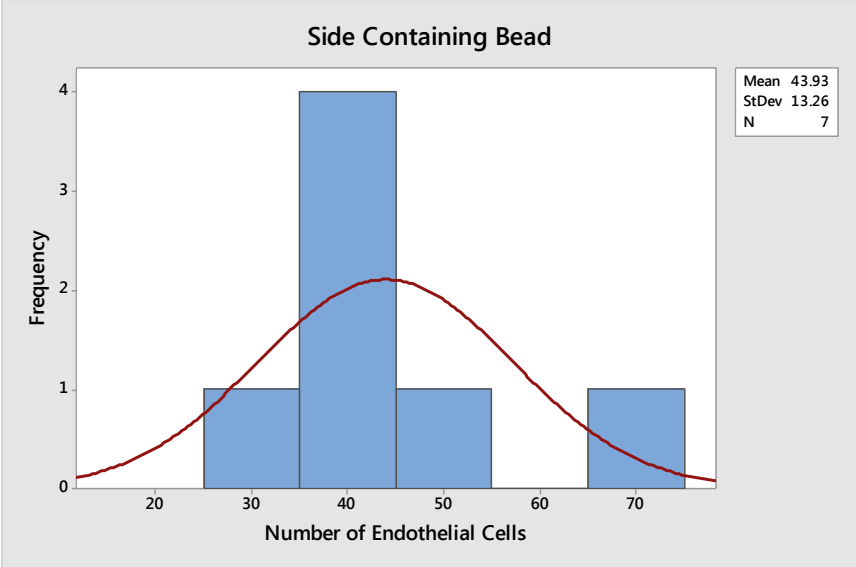

	N	Mean	StDev	SE Mean
Control	7	48.05	16.13	6.10
Bead	7	43.93	13.26	5.01
Difference	7	4.12	11.47	4.34

95% CI for mean difference: (-6.49, 14.73)
T-Test of mean difference = 0 (vs≠0): T-Value = 0.95 P-Value = 0.379

Appendix Q

Paired t-test and histogram for PBS control bead experiments. Embryos were implanted with beads containing PBS, just beneath the surface ectoderm adjacent to the basal plate of the mesencephalon. CD34-stained endothelial cells were counted on the control side (**A**) and compared with the contra lateral side containing the bead (**B**). No significant difference was found between the mean number of endothelial cells on the control side and on the side containing the bead.

A

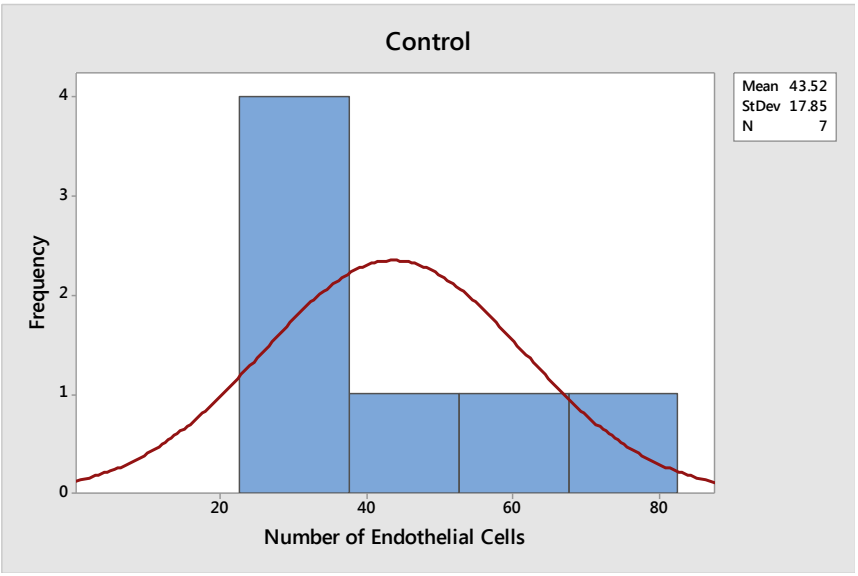

B

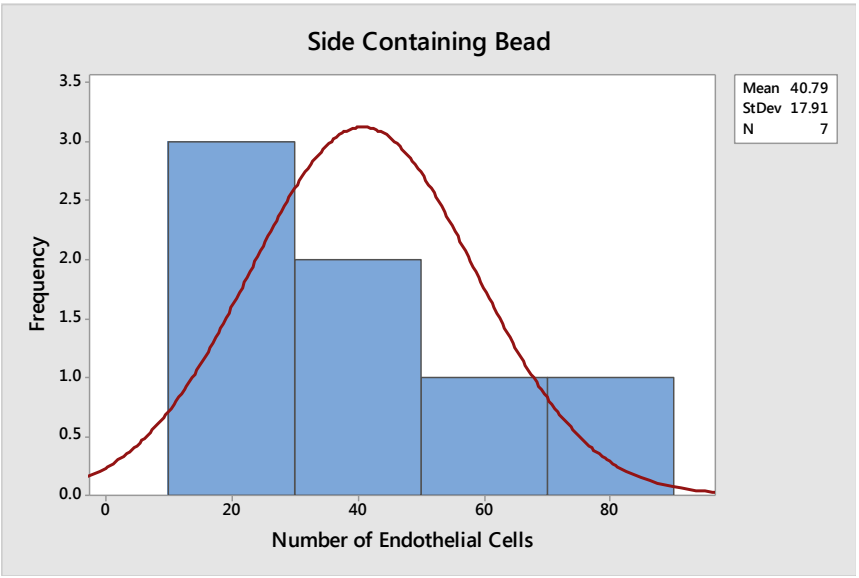

	N	Mean	StDev	SE Mean
Control	7	43.52	17.85	6.75
Bead	7	40.79	17.91	6.77
Difference	7	2.74	8.31	3.14

95% CI for mean difference: (-4.95, 10.42)
T-Test of mean difference = 0 (vs≠0): T-Value = 0.87 P-Value = 0.417

Appendix R

Paired t-test and histogram for bead experiments with 10mM DAPT in DMSO. Embryos were implanted with beads containing 10mM DAPT in DMSO, just beneath the surface ectoderm adjacent to the basal plate of the mesencephalon. CD34-stained endothelial cells were counted on the control side (**A**) and compared with the contra lateral side containing the bead (**B**). The mean number of endothelial cells on the side containing the bead was found to be significantly higher than that of the control side.

A

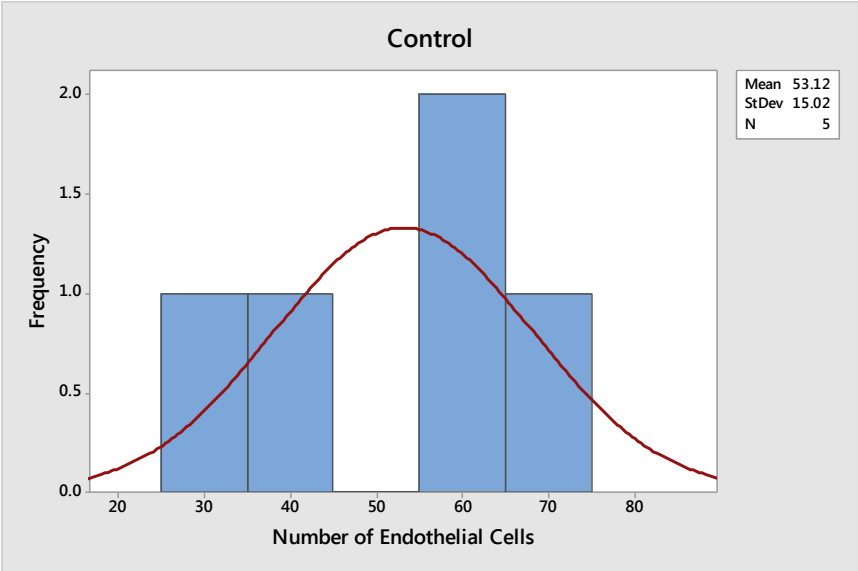

B

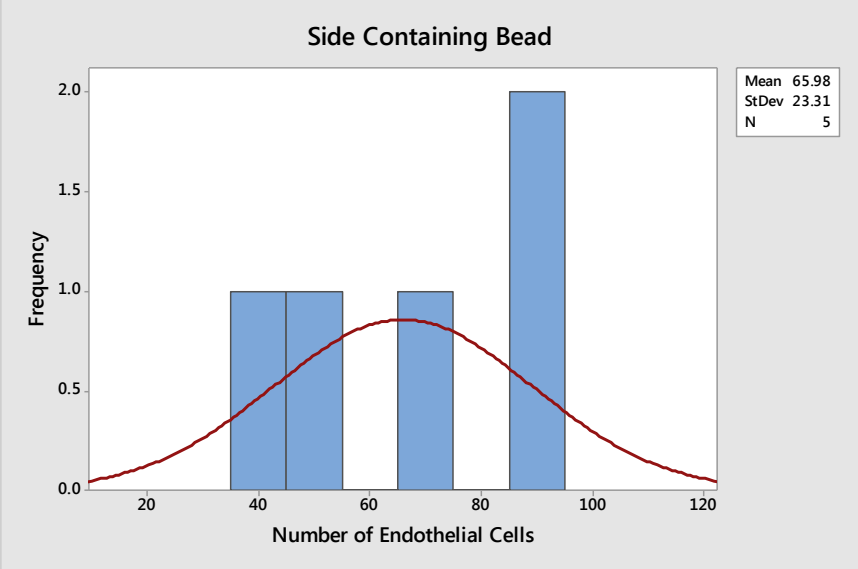

	N	Mean	StDev	SE Mean
Bead	5	66.0	23.3	10.4
Control	5	53.1	15.0	6.7
Difference	5	12.86	11.89	5.32

95% lower bound for mean difference: 1.53
T-Test of mean difference = 0 (vs>0): T-Value = 2.42 P-Value = 0.036

Appendix S

Paired t-test and histogram for bead experiments with 10mM DAPT in PBS. Embryos were implanted with beads containing 10mM DAPT in PBS, just beneath the surface ectoderm adjacent to the basal plate of the mesencephalon. CD34-stained endothelial cells were counted on the control side (**A**) and compared with the contra lateral side containing the bead (**B**). No significant difference was found between the mean number of endothelial cells on the control side and on the side containing the bead.

A

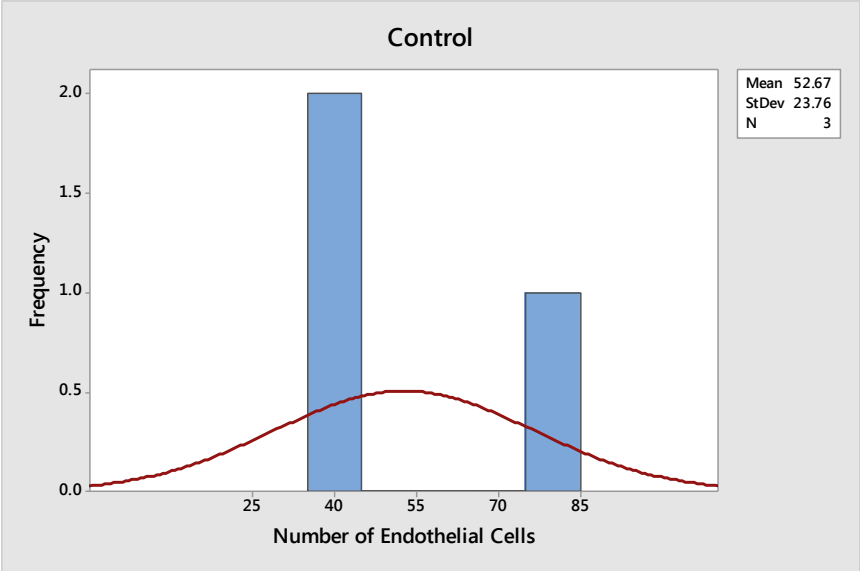

B

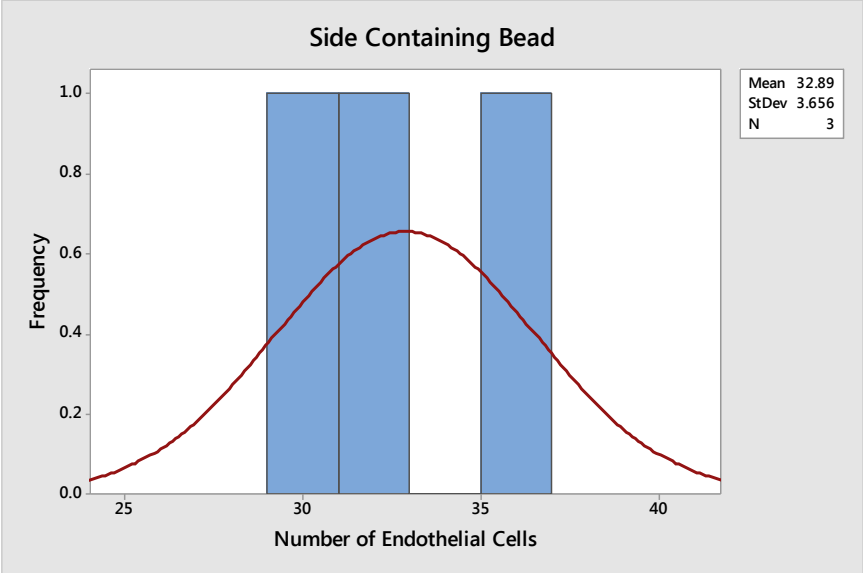

	N	Mean	StDev	SE Mean
Bead	3	32.9	3.7	2.1
Control	3	52.7	23.8	13.7
Difference	3	-19.8	20.3	11.7

95% lower bound for mean difference: -54.0
T-Test of mean difference = 0 (vs>0): T-Value = -1.69 P-Value = 0.883

FORM UPR16

Research Ethics Review Checklist

Please include this completed form as an appendix to your thesis (see the Postgraduate Research Student Handbook for more information

Postgraduate Research Student (PGRS) Information				**Student ID:**	484677
PGRS Name:	Amanda Rose Corla				
Department:	Biology	**First Supervisor:**	Dr. Frank Schubert		
Start Date: (or progression date for Prof Doc students)		**1st October 2013**			
Study Mode and Route:	Part-time ☐	MPhil ☐	MD ☐		
	Full-time ☒	PhD ☐	Professional Doctorate ☐		

Title of Thesis:	The anatomical and molecular characterisation of vascular ingression in the embryonic vertebrate brain
Thesis Word Count: (excluding ancillary data)	31,641 words

If you are unsure about any of the following, please contact the local representative on your Faculty Ethics Committee for advice. Please note that it is your responsibility to follow the University's Ethics Policy and any relevant University, academic or professional guidelines in the conduct of your study

Although the Ethics Committee may have given your study a favourable opinion, the final responsibility for the ethical conduct of this work lies with the researcher(s).

UKRIO Finished Research Checklist:
(If you would like to know more about the checklist, please see your Faculty or Departmental Ethics Committee rep or see the online version of the full checklist at: http://www.ukrio.org/what-we-do/code-of-practice-for-research/)

a) Have all of your research and findings been reported accurately, honestly and within a reasonable time frame?	YES ☒ NO ☐
b) Have all contributions to knowledge been acknowledged?	YES ☒ NO ☐
c) Have you complied with all agreements relating to intellectual property, publication and authorship?	YES ☒ NO ☐
d) Has your research data been retained in a secure and accessible form and will it remain so for the required duration?	YES ☒ NO ☐
e) Does your research comply with all legal, ethical, and contractual requirements?	YES ☒ NO ☐

Candidate Statement:

I have considered the ethical dimensions of the above named research project, and have successfully obtained the necessary ethical approval(s)

Ethical review number(s) from Faculty Ethics Committee (or from NRES/SCREC):	510A

If you have *not* submitted your work for ethical review, and/or you have answered 'No' to one or more of questions a) to e), please explain below why this is so:

Signed *(PGRS)*:	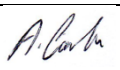	**Date:** 23-02-2018